

**Suppressions and Cascades:
Insights from Gauge/Gravity Dualities**

by

Qudisia Jabeen Ejaz

Submitted to the Department of Physics
in partial fulfillment of the requirements for the degree of

Doctor of Philosophy

at the

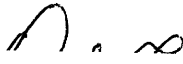
MASSACHUSETTS INSTITUTE OF TECHNOLOGY

June 2008

© Qudisia Jabeen Ejaz, MMVIII. All rights reserved.

The author hereby grants to MIT permission to reproduce and
distribute publicly paper and electronic copies of this thesis document
in whole or in part.

Author



.....

Department of Physics

May 23, 2008

Certified by.....



.....

Hong Liu

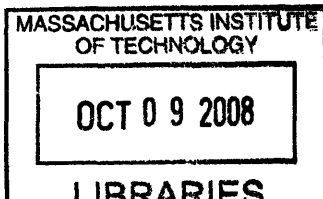
Associate Professor

Thesis Supervisor

Accepted by

.....
Thomas J. Greytak

Associate Department Head for Education



ARCHIVES

Suppressions and Cascades: Insights from Gauge/Gravity Dualities

by

Qudsia Jabeen Ejaz

Submitted to the Department of Physics
on May 23, 2008, in partial fulfillment of the
requirements for the degree of
Doctor of Philosophy

Abstract

At present, there are no non-perturbative analytic methods available for investigating gauge theories at large couplings. Consequently, it is desirable to explore more avenues to gain qualitative and quantitative insights. The gauge/gravity (AdS/CFT) correspondences provides a unique opportunity to study gauge theories both at finite and zero temperatures in the strong coupling regime, potentially leading to insights into QCD. In this regime, where both the 't Hooft coupling and the number of colors is large, the dynamics of the gauge theory is described by supergravity solutions, which describe the low-energy limit of systems of D-branes. In this dissertation, I use the AdS/CFT correspondence to study the dispersion relations of mesons in a particular hot, strongly coupled, supersymmetric gauge theory plasma. This plasma arises by placing a probe D7-brane in the near-horizon geometry of non-extremal D3-branes. I find the large momentum dispersion relations of scalar mesons and extract from them their limiting velocity v_0 , which depends only on the ratio of the temperature to the quark mass. I use v_0 to find that the temperature above which no meson bound states with velocity v exist is $T_{\text{diss}}(v) \simeq (1 - v^2)^{1/4} T_{\text{diss}}(v = 0)$. This agrees with results inferred indirectly via analysis of the screening length between a static quark and antiquark in a moving plasma. Although these calculations are not done in QCD, I argue that the qualitative features of my results may apply to bottomonium and charmonium mesons propagating in the strongly coupled QCD plasma. To aid further investigations of the effect of fundamental matter on hot gauge theory plasmas I find the non-extremal, localized D2/D6-brane solution in its linear limit. Pursuing a different direction, I consider a stack of N D3-branes and M D5-branes wrapped at the apex of a cone over Sasaki-Einstein spaces $Y^{p,q}$. Replacing the D-branes by their fluxes, I construct asymptotic solutions for all p and q in the form of warped products of the cone and $\mathbb{R}^{1,3}$. These theories are not conformal, and the solutions describe cascading renormalization group flows.

Thesis Supervisor: Hong Liu
Title: Associate Professor

Acknowledgments

I dedicate this dissertation to the memory of my Mother-in-law, *Maan ji*. Without her love, support, and trust I never would have made it this far.

I am greatly indebted to my advisor Hong Liu for all he has taught me with profound patience, kindness and diligence. His guidance has had a profound impact on my development as a physicist.

It is a privilege for me to thank Krishna Rajagopal from whom I have learned much about research and writing. I would also like to thank Edward Farhi for his guidance and support throughout my time here as a graduate student.

It is an honor for me to acknowledge my friend and collaborator Thomas Faulkner for all his help, support and very useful discussions while working together and otherwise. I would also like to express my gratitude to Chris P. Herzog, Igor R. Klebanov and Urs A. Wiedemann for all they have taught me during my collaboration with them.

With deep gratitude, I would like to acknowledge my academic advisor John Negele for his help and advice in navigating my journey here at MIT as well as for being available to help and offer his support whenever I requested it.

I would also like to thank all my friend in Women in Physics and CTP for their support and companionship, especially Bonna Newman, Jessie Shelton, Carlos Nuñez, Guido Festuccia, Mauro Brigante and Sean P. Robinson.

Last but not least, I would like to thank Ejaz Nasser for all his love, support and patience, without which this work would never have been completed, and my friend and mentor, Pervez Hoodbhoy for all he has taught and shared with me.

Contents

1	An Overview of the Gauge/Gravity Correspondence	1
1.1	Introduction	1
1.2	$AdS_5 \times S^5$ and $\mathcal{N} = 4$ SYM	4
1.3	A Review of Field Theory Models for Quarkonia in QGP	9
1.4	Calculating the Screening Length using AdS/CFT	15
1.5	Adding Flavors using the Probe Approximation	21
1.5.1	D7-brane Embedding at Zero Temperature	22
1.5.2	D7-brane Embedding at Finite Temperature	25
2	A Limiting Velocity for Quarkonium Propagation in a Strongly Coupled Plasma via AdS/CFT	31
2.1	Introduction	31
2.2	D3/D7-brane Construction of Mesons	34
2.2.1	Zero Temperature	34
2.2.2	Nonzero Temperature	36
2.3	Meson Fluctuations at Nonzero Temperature	40
2.4	Dispersion Relations	49
2.4.1	Low Temperature	50
2.4.2	Large- k Dispersion Relation at Generic Temperature	55
2.4.3	Numerical Results	60
2.4.4	Summary, Limiting Velocity and Dissociation Temperature	60
2.5	Discussion and Open Questions	68

3	Finite Temperature Solution for Fully Localized D2/D6-brane System	77
3.1	Introduction	77
3.2	The Localized D2/D6-brane Solution	79
3.3	The Non-extremal Solution	85
3.3.1	Solutions for q_1 and q_2	87
3.3.2	Solutions for q_3 and q_4	88
3.3.3	Solution for μ_1	90
3.3.4	$N_6 \gg 1$ Limit	93
3.3.5	$N_6 \ll 1$ Limit	95
3.4	The 11-dimensional Solution	97
3.5	Conclusions	100
4	Cascading Renormalization Group Flows from Sasaki-Einstein Manifolds	101
4.1	Introduction	101
4.2	Conifold Theories	103
4.3	The Geometry of $Y^{p,q}$ Spaces.	109
4.4	The Conformal Surface of $Y^{p,q}$ Gauge Theories	112
4.5	Dibaryons and New 3-Cycles	115
4.6	Warped Solutions with (2,1) Flux	118
4.6.1	Derivation of 5-form Flux	120
4.6.2	Solving for the Warp Factor	122
4.7	Matching the β -Function	126
4.8	Cascades in the Dual Gauge Theories	128
4.8.1	Cascades for $Y^{p,p-1}$	128
4.8.2	Cascades for $Y^{p,1}$	131
4.9	Discussions and Conclusions	134
A	Discussion of Brane Embedding and Fluctuations	137
A.1	General Discussion	137

A.2	D7-branes in $AdS_5 \times S^5$ Black Hole	141
A.3	Gauss-Codazzi Relations for Co-dimension 2	142
B	Dp/Dq-brane Theories	145
C	Generating the M2-brane Solution	151
D	Related Special Functions	155
D.1	Generalized Confluent Hypergeometric Equation	155
D.2	A Special Confluent Heun Equation	156
D.3	Some Properties of Special Functions	157
D.4	Useful Integrals	158
E	Aspects of Seiberg Duality	161
E.1	SQCD and Seiberg Duality	161
E.2	Quartic Operators and Seiberg Duality	167
E.3	When is Seiberg Duality Exact?	169
E.4	$N_f = 2N$ and Exactly Marginal Operators	172
E.5	Klebanov-Witten Theory and Seiberg Duality	173
E.6	Klebanov-Strassler Theory and the Duality Cascade	175

List of Figures

1-1 The upper plane is the D3-brane at the boundary of AdS_5 ($r = \infty$) and the lower plane is the black hole horizon. (a) The Wilson loop \mathcal{C} with the string world sheet hanging down from the D3-brane at infinity. (b) At $L = L_s$, the string joining the quark-antiquark pair falls into the black hole horizon and the “meson” in the gauge theory dissociates. 16

1-2 Some possible D7-brane embeddings $y(\rho)$. The quark mass to temperature ratio is determined by $y(\infty) = L$. Specifically, $\sqrt{8}m_q/(T\sqrt{\lambda}) = y(\infty)/u_0 \equiv 1/\sqrt{\epsilon_\infty}$. The top three curves are Minkowski embeddings, with $y(\rho)$ extending from $\rho = 0$ to $\rho = \infty$. The bottom three curves are black hole embeddings, in which the D7-brane begins at the black hole horizon at $y^2 + \rho^2 = u_0^2$. The middle curve is the critical embedding. The seven curves, ordered from top to bottom as they occur in the left part of the figure, are drawn for temperatures specified by $\epsilon_\infty = 0.249, 0.471, 0.5865, 0.5948, 0.5863, 0.647$ and 1.656 . Note that the $\epsilon_\infty = 0.5863$ black hole embedding crosses both the $\epsilon_\infty = 0.5948$ critical embedding and the $\epsilon_\infty = 0.5865$ Minkowski embedding. . . . 28

1-3 This figure shows a different slicing of the D7-brane embedding from the one shown in Figure 1-2. The left-hand panel shows the Minkowski embedding while the right-hand panel shows the black hole embedding. Here T is the temperature, $r = \sqrt{y^2 + \rho^2}$ and x is a direction along the D3-brane. The axis labeled as 5-sphere refers to the angle between y/u_0 and ρ/u_0 in Figure 1-2 where it ranges from 0 to $\frac{\pi}{2}$ in the clockwise direction. In this figure it ranges from $-\frac{\pi}{2}$ to $\frac{\pi}{2}$. Unlike Figure 1-2, the shape of embeddings in this figure are not the exact solutions to the equations of motion, but have the correct qualitative feature. . . . 29

2-1 ϵ_∞ (determined by the embedding y at infinity) versus ϵ (determined either by $y(0)$, for Minkowski embeddings with $\epsilon < 1$, or by where the embedding intersects the horizon, for $\epsilon > 1$). The right panel zooms in on the vicinity of the critical embedding at $\epsilon = 1$. The stable embeddings and the first order phase transition are indicated by the thick curve; the metastable embeddings are indicated by the thin curves. 38

2-2 The squared “masses” of the two orthonormal geometric modes of the D7-brane fluctuations for Minkowski embeddings (left panel) and black hole embeddings (right panel). In each figure, m_1^2 (m_2^2) is plotted as a solid (dashed) line for three values of ϵ_∞ . The Minkowski embeddings have $\epsilon_\infty = 0.587, 0.471$ and 0.249 (top to bottom) and the black hole embeddings have $\epsilon_\infty = 1.656, 0.647$ and 0.586 (again top to bottom, this time with temperature increasing from top to bottom.) The Minkowski embedding is plotted as a function of ρ and the black hole embedding as a function of u with the horizon on the left at $u = 1$. . . 44

2-3 Potentials $V_s(z)$ for Minkowski embeddings at various temperatures, all with $k = \ell = 0$. The left (right) panel is for $s = 1$ ($s = 2$). In each panel, the potentials are drawn for $\epsilon_\infty = 0.249, 0.471, 0.586$ and 0.5948 , with the potential widening as the critical embedding is approached, i.e. as ϵ_∞ is increased. The $\epsilon_\infty = 0.586$ potential is that for the Minkowski embedding at the first order transition; the widest potential shown describes the fluctuations of a metastable Minkowski embedding very close to the critical embedding. The potential becomes infinitely wide as the critical embedding is approached, but it does so only logarithmically in $\epsilon_\infty^c - \epsilon_\infty$. Note that the tip of the D7-brane is at $z = 0$, on the left side of the figure, whereas $\rho = \infty$ has been mapped to a finite value of the tortoise coordinate $z = z_{\max}$, corresponding to the “wall” on the right side of each of the potentials in the figure. . . 46

2-4 Potentials $V_s(z_{bh})$ for black hole embeddings at various temperatures, all with $k = \ell = 0$. The left (right) panel is for $s = 1$ ($s = 2$). In each panel, the potentials are drawn for $\epsilon_\infty = 3584., 0.647, 0.586, 0.586, 0.5940$ and 0.5948 , from narrower to wider, with the potential widening as the critical embedding is approached from the right along the curve in Figure 2-1. Note that z_{bh} is defined such that the horizon is at $z_{bh} = \infty$, and $\rho = \infty$ is at $z_{bh} = 0$. The narrower (wider) of the two potentials with $\epsilon_\infty = 0.586$ is that for the stable (unstable) black hole embedding: at this ϵ_∞ , there is a first order transition (see Figure 2-1) between the stable Minkowski embedding (whose potential is found in Figure 2.3) and the stable black hole embedding. The potentials at $\epsilon_\infty = 0.5940$ and 0.5948 describe fluctuations of metastable black hole embeddings, with the latter being a black hole embedding very close to the critical embedding. 47

- 2-5 The potential (2.56) with $\varepsilon = 0.756$ and $k = 5, 20$ and 100 . We see that as $\Lambda = \varepsilon^2 k^2$ increases, the minimum of the potential moves towards $z = 0$, the potential deepens, and the curvature around the minimum increases. 53
- 2-6 Potential and ground state wave function for ψ_1 (left three panels) and ψ_2 (right three panels) for k given by $5, 20$ and 100 (top to bottom). All plots have $\varepsilon = 0.756$, corresponding to the Minkowski embedding at the dissociation transition. $V(z)$ and the ground state ($n = \ell = 0$) solutions to the Schrödinger equation in the potentials V are both shown as solid lines, and the ground state energies are indicated by the horizontal (red) lines. The dashed lines show the approximation (2.81) to the wave functions. 61
- 2-7 Dispersion relations for the ground state ψ_1 meson with $n = \ell = 0$ at various values of ε (i.e. at various temperatures). The top (red) curve is the zero temperature dispersion relation $\omega = \sqrt{k^2 + m^2}$ with m given by (2.7) and with a group velocity that approaches 1 at large k , as required in vacuum by Lorentz invariance. The next three solid (black) curves are the dispersion relations for $\varepsilon = 0.25, 0.5$ and 0.756 , top to bottom, the latter corresponding to the Minkowski embedding at the temperature T_{diss} at which the first order phase transition occurs. The dashed (red) lines are the large- k approximation discussed in Section 2.4.4, given by $\omega(k) = v_0 k + \Omega \varepsilon L_0 / (v_0 R^2)$ with Ω specified by (2.93). We see that the dispersion relations approach their large- k linear behavior from below. The limiting velocity v_0 decreases with increasing temperature. Had I plotted dispersion relations for $0.756 < \varepsilon < 1$ corresponding to metastable Minkowski embeddings with $T > T_{\text{diss}}$, I would have seen $v_0 \rightarrow 0$ as $\varepsilon \rightarrow 1$, approaching the critical embedding. 62

2-8	Group velocities $v_g = d\omega/dk$ for the dispersion relations from Fig. 2-7, with $\varepsilon = 0.25, 0.5$ and 0.756 (top to bottom). We see that the group velocity approaches its large- k value v_0 from above. And, we see v_0 decreasing with increasing temperature. (Again, v_0 would approach zero if we included the metastable Minkowski embeddings with $T > T_{\text{diss}}$.)	63
2-9	The asymptotic velocity v_0 from (2.87) as a function of ε . The low temperature approximation (2.90) is plotted as a dashed line. Recall that the dissociation transition occurs at $\varepsilon = 0.756$	65
2-10	The k -independent spacing $\Omega\varepsilon L_0/2v_0 R^2$ between the dispersion relations for any two mesons whose n quantum numbers differ by 1, in units of T_{diss} . See (2.93).	66
2-11	Left panel: The solid curve is the limiting velocity v_0 as a function of T/T_{diss} , where T_{diss} is the temperature of the dissociation transition at zero velocity. The dissociation transition occurs at the dot, where $v_0 \approx 0.273$. The dashed curve is the approximation obtained by setting $f(v) = 1$ in (2.94). Right panel: $f(v)$, the ratio of the solid and dashed curves in the left panel at a given v . We see that $f(v)$ is within a few percent of 1 at all velocities.	67
4-1	This figure shows Seiberg duality in Klebanov-Strassler theory with gauge group $SU(N + M) \times SU(N + 2M)$ (i.e. $k = 2$) using quiver diagrams. The vertices of the quiver denote gauge groups while the lines indicate bifundamental fields, their number being given by the number of arrows. Under Seiberg duality, the fundamental fields become anti-fundamental and vice versa, indicated by the reversal in the direction of arrows. The \cong symbol indicates that the second and third quiver are identical, as can be seen by interchanging the two vertices ($\tilde{N} = N - M$). The duality has a self-similar structure under $N \rightarrow \tilde{N} \equiv N - M$, which allows a cascade to occur.	108

4-2	Shown are a) the unit cell σ ; b) the unit cell τ ; and c) the quiver for $Y^{4,3}, \sigma\tilde{\tau}\sigma\tilde{\sigma}$	113
4-3	The quiver for $Y^{4,3}$, which is identical to Figure 4-2c.	129
4-4	The quiver theory for $Y^{4,1}$, involving three τ unit cells and one σ unit cell.	132
4-5	Seiberg duality for the $Y^{p,1}$ quiver: $(\cdots\tau\tilde{\tau}\sigma\tilde{\tau}\cdots) \rightarrow (\cdots\tau\tilde{\sigma}\tau\tilde{\tau}\cdots)$	133
E-1	The beta function and the IR conformal fixed point $g = g_*$ of SQCD when N_f is very close to but less than $3N$, with $N, N_f \gg 1$	164
E-2	The dimension of M , $D(M)$, is 2 in an IR free gauge theory ($N_f > 3N$), is bounded from below by unitarity and in the conformal window is proportional to the sum of the R -charges of q and \tilde{q}	165
E-3	According to Seiberg duality, the fixed point g_* of SQCD (top panel) is identical to the fixed point (g'_*, y_*) of SQCD+M (bottom panel) in the IR. Although the symbol g is used for the gauge coupling in both SQCD and SQCD+M, they are couplings of different gauge groups with generically different values.	166
E-4	Seiberg duality can be extended beyond just a duality at a single conformal fixed point in IR by taking the scales $\Lambda_A, \Lambda_B \gg m \sim \sqrt{\tilde{m}}$	170
E-5	This figure shows the flows of couplings in the presence of a quartic superpotential in SQCD in the range $\frac{3}{2}N < N_f < 2N$. The point C in the top panel is SQCD with N colors and N_f flavors. This theory is Seiberg dual to the point C in the bottom panel which is SQCD+M with \tilde{N} colors and N_f flavors. The duality holds everywhere along the flow from C to C' . Notice that the horizontal axis/plane is just Figure E-3.	171

E-6	The left hand panel shows the conformal surface in Klebanov-Witten and the right-hand panel shows the conformal surface in $\mathcal{N} = 2$ theory which can be thought of as the UV completion of Klebanov-Witten. The left right arrows are the action of Seiberg duality or $\tau_- \rightarrow \tau_- + 2\tau_+$ while the top bottom arrows indicate the action of $SL(2, \mathbb{Z})$ transformation.	174
E-7	The top panel shows the flow along the boundary of the conformal surface, with the Seiberg fixed points shown when one of the gauge couplings and the quartic coupling is zero. The flow connecting g_k to g_{k-2} indicates switching to the Seiberg dual description. The bottom panel shows the same flow with the vertical axes for the quartic couplings suppressed.	176
E-8	This figure is a generalization of E-7 and shows the flow for more generic values of the couplings which do not lie on the conformal surface, i.e. $\delta_0 \sim \frac{1}{2}$	177

List of Tables

E.1	Assignment of Representations and Charges in SQCD	162
E.2	Assignment of Representations and Charges in SQCD+M	165

Chapter 1

An Overview of the Gauge/Gravity Correspondence

“But what ... is it good for?” - Engineer at the Advanced Computing Systems Division of IBM, commenting on the microchip (1968)

1.1 Introduction

Finding a theory of gravity that incorporates quantum effects is an important and exceptionally difficult problem in high energy theoretical physics. A leading candidate that has been extensively studied is string theory. While the historical discovery of string theory arose from studying spectra of nuclear bound states at high spin, J , it was eventually replaced by quantum chromodynamics (QCD), the theory of strong interactions. However, all string theories contain a spin two, massless particle for which the only consistent interaction is gravity. This means that all string theories contain gravity, in addition to being finite in the ultra-violet (UV).

An important element of the string theory story is the existence of D-branes [1]. These D-branes are solitonic solutions of the low-energy equations of motion in closed string theory where they can be considered as solutions of supergravity with fluxes turned on. They can alternatively be thought of as objects in open string theory on which open strings can end. They have a world-volume gauge theory living on them,

which can be thought of as arising from the open string fluctuations. Additionally they preserve half the supersymmetries of the original bulk theory. These solutions help formulate an exact duality between gauge theories and string theories on certain backgrounds, thus providing an exciting opportunity to do calculations at strong gauge couplings via the “gauge/gravity correspondence”, also called AdS/CFT¹, which can be considered one of the most important results arising from string theory. In this dissertation I will use the AdS/CFT correspondence to study gauge theories at finite and zero temperatures.

The simplest example of the AdS/CFT correspondence is provided by the duality between $\mathcal{N} = 4$, $SU(N)$ super-Yang-Mills (SYM) theory and classical gravity on $AdS_5 \times S^5$ [2, 3, 4, 5]. Here AdS_5 is the 5-dimensional anti-de Sitter space which is the Einstein manifold with negative cosmological constant and S^5 is the 5-sphere. On the other hand, the $\mathcal{N} = 4$ super-Yang-Mills (SYM) theory is a superconformal theory with two parameters: the rank of the gauge group N and the gauge coupling g_{YM} (which is replaced in the $N \gg 1$ limit by the 't Hooft coupling $\lambda = g_{YM}^2 N$). The $\mathcal{N} = 4$ means that the theory has 32 supercharges, which is the maximal supersymmetry allowed in 1+3-dimensions. This large amount of symmetry uniquely determines the lagrangian, allows only fields transforming in the adjoint representation of $SU(N)$ (which form the $\mathcal{N} = 4$ gauge hypermultiplet) and sets the β -function to zero making the theory exactly conformally invariant. In the large N and large λ limit, gauge theory problems can be solved using classical supergravity in $AdS_5 \times S^5$.

This gauge/gravity correspondence provides an opportunity to understand properties of finite temperature gauge theories via a dual gravity description. In the appropriate decoupling limit, which will be discussed in Section 1.2, the dual description is just a black hole in some background generated by D-branes [2, 6]. Computations of important thermodynamic and hydrodynamic quantities like the value of entropy density s , the shear viscosity η and the ratio η/s have been carried out for $\mathcal{N} = 4$

¹The term AdS/CFT initially meant that the field theory was conformal and the gravity solution involved the anti-de Sitter space. However the correspondence has been generalized for cases where the field theory is no longer conformal, in which case it is more appropriate to call it a gauge/gravity correspondence. But the two terms are used synonymously in the literature, as in this dissertation.

SYM, using both perturbation theory and using the dual gravity description at strong coupling.

An important direction in studying gauge theories at both finite and zero temperatures using AdS/CFT is to ask what happens in the presence fundamental matter, which is present in QCD. The question of how to introduce fundamental matter is more involved. When the number of flavors (the number of matter fields) is much smaller than the number of colors, one can use a probe approximation. This means that the back-reaction of the branes- that is the warping of spacetime by branes' mass- that provide the flavors is ignored. Placing D7-branes in a background of D3-branes adds fundamental $\mathcal{N} = 2$ hypermultiplets into the $\mathcal{N} = 4$ SYM at finite temperatures. I will study the meson spectrum of this theory at finite temperature and find evidence supporting the proposal that quarkonia propagating in the moving quark-gluon plasma (QGP) observed in the PHENIX experiment at RHIC [7] must be suppressed in a velocity dependent manner. These results will be discussed in Chapter 2 and were published in [8].

It is possible to go beyond the probe approximation and take into account the full gravitational back-reaction of the D7-branes at zero temperature [9]. This solution however is very complicated and there exists another simpler system involving D2-branes localized on D6-branes which is dual to an $\mathcal{N} = 2$, 1+2-dimensional SYM [10]. In Chapter 3, I present the finite temperature solution to this system in its linear limit which is work not previously published.

At zero temperature both the $\mathcal{N} = 4$ SYM in 1+3-dimensions and the $\mathcal{N} = 2$ SYM in 1+2-dimensions are obtained by placing D-branes in a flat background, which warp the spacetime, and taking a near-horizon limit². One can also consider placing the D-branes in a singular background. In such a case, the number of supersymmetries is reduced. An example of this is the solution obtained by I. R. Klebanov and A. A. Tseytlin [11], in which they study string theory on an $AdS_5 \times T^{1,1}$ background- this is obtained by placing a stack of D3-branes at the singularity of a Calabi-Yau

²In the coordinate system in (1.2) for the extremal D-brane solution the horizon is located at $r = 0$.

cone with base $T^{1,1}$, where $T^{1,1}$ is a 5-dimensional, positive curvature, Sasaki-Einstein manifold with an $S^2 \times S^3$ topology. This solution is dual to a certain $\mathcal{N} = 1$ SYM with gauge group $SU(N) \times SU(N+M)$ [12]. After studying a related class of theories that involve the manifolds called $Y^{p,q}$'s, which can be thought of as generalizations of $T^{1,1}$, I will demonstrate how some of the features of $AdS_5 \times T^{1,1}$ are replicated in these theories, such as “duality cascades,” while other features, such as questions about confinement and chiral symmetry breaking, remain open problems. These topics will be covered in Chapter 4 and my work presented therein has been published in [13].

The rest of this chapter is organized as follows: Section 1.2 contains a short discussion of the AdS/CFT conjecture for $\mathcal{N} = 4$ SYM and some of its applications at finite and zero temperatures; Section 1.3 contains a review of the status of field theory based models for understanding the QGP; Section 1.4 contains a review of the potential between a quark-antiquark pair in a moving hot plasma and the velocity-dependence of its screening length; Section 1.5 contains a demonstration of how to add fundamental matter in $\mathcal{N} = 4$ SYM by introducing probe D7-branes. This will be used in Chapter 2 to explore the dispersion relation of mesons. These topics serve as background material for Chapter 2. The introductory material for Chapter 3 is contained in Section 3.2 and for Chapter 4 is presented in Section 4.2.

1.2 $AdS_5 \times S^5$ and $\mathcal{N} = 4$ SYM

I begin this section by giving a concise description of the AdS/CFT correspondence for the simplest and most thoroughly studied example without any proof. The anti-de Sitter/conformal field theory (AdS/CFT) correspondence, as conjectured by J. M. Maldacena [2], states that there are two apparently different theories, that are completely equivalent to one another, in the sense that their operators, states, correlation function and full dynamics agree according to an established dictionary. This equivalence is called a “duality”. One of these theories (AdS side of the duality) is the 10-dimensional type IIB string theory defined on the background $AdS_5 \times S^5$, with a self-dual 5-form flux, where N integral units of this flux are turned on. The radius of

the AdS_5 is equal to the S^5 radius R whose value is given by $R^4 = 4\pi g_s N \alpha'^2$, where g_s is the dimensionless string coupling in which perturbative expansion is carried out; and α' is the square of the string length l_s . Thus α' sets the scale for stringy effects. On the other side (the CFT side) is the $\mathcal{N} = 4$ super-Yang-Mills theory (SYM) in 1+3-dimensions, with gauge group $SU(N)$ and coupling g_{YM} . The string coupling constant g_s is related to the gauge theory parameters, in its conformal phase by

$$4\pi g_s = g_{YM}^2 = \frac{\lambda}{N}, \quad (1.1)$$

where g_{YM}^2 is defined according to standard field theory conventions and is twice as large as the Yang-Mills gauge coupling defined according to standard string theory conventions, and λ is the 't Hooft coupling. It is important to note that this is called the strong form of the conjecture, i.e. this equivalence is true for all possible values of N and $g_{YM}^2 = 4\pi g_s$. In this dissertation, I assume the strong form of the conjecture.

There is a very special and remarkable limit that can be taken. In this limit one first takes $N \rightarrow \infty$ with the 't Hooft coupling $\lambda = g_{YM}^2 N = 4\pi g_s N$ fixed. On the gauge theory side, this corresponds to keeping only the planar graphs. On the string theory side, this gives the classical limit of string theory, i.e. $g_s \rightarrow 0$ with no string loop corrections. Then one takes $\lambda \rightarrow \infty$, which reduces the classical string theory to just type IIB supergravity. On the SYM side however, this corresponds to the highly non-perturbative regime. In particular, in the large N , large λ limit this is a correspondence between the fields on the supergravity side and operators in the SYM. Note that I will work in this limit through out this dissertation.

A way to obtain type IIB string theory on $AdS_5 \times S^5$ is to consider a stack of N D3-branes in 10-dimensional Minkowski space. The D3-branes couple to the 4-form RR-potential, C_4 , in the theory which gives rise to the five form flux, $F_5 = dC_4$ (the

rank of a form is indicated as a subscript). The supergravity solution is given by

$$ds^2 = \left(1 + \frac{R^4}{r^4}\right)^{-1/2} [-dt^2 + dx_1^2 + dx_2^2 + dx_3^2] + \left(1 + \frac{R^4}{r^4}\right)^{1/2} (dr^2 + r^2 d\Omega_5^2), \quad (1.2)$$

$$F_5 = (1 + *_{10})d \left(1 + \frac{R^4}{r^4}\right)^{-1} \wedge dt \wedge dx_1 \wedge dx_2 \wedge dx_3, \quad (1.3)$$

where $t, x_{1,2,3}$ are the brane directions, $r^2 = \sum_{i=4}^9 x_i^2$, $d\Omega_5^2$ is the metric on a 5-sphere and $*_{10}$ denotes the 10-dimensional Hodge dual. R is related to the Yang-Mills theory 't Hooft coupling by

$$\frac{R^2}{\alpha'} = \sqrt{\lambda}. \quad (1.4)$$

In the near-horizon limit where $R \gg r$, the unit term in the warp factors is negligible, leaving us with $AdS_5 \times S^5$ whose metric can be expressed as

$$\begin{aligned} ds^2 &= \frac{r^2}{R^2} (-dt^2 + dx_1^2 + dx_2^2 + dx_3^2) + \frac{R^2}{r^2} dr^2 + R^2 d\Omega_5^2 \\ &= \frac{r^2}{R^2} (-dt^2 + dx_1^2 + dx_2^2 + dx_3^2) + \frac{R^2}{r^2} \sum_{i=4}^9 dx_i^2, \end{aligned} \quad (1.5)$$

The AdS_5 factor on the gravity side of the correspondence has an additional direction r compared to the gauge theory, which is interpreted as a renormalization group scale. A hint of this interpretation comes from the fact that a massless scalar field and r both transform the same way under dilatations $x \longrightarrow e^\alpha x$, where x represents the four dimensional coordinates³. These dilatations are part of both the isometry group of AdS_5 and the global symmetries of the SYM. However a concrete derivation of the interpretation of r as an energy scale was carried out by L. Susskind and E. Witten [14]. They introduced a small distance δ from the boundary to regulate the infinite area of the AdS_5 boundary. They showed that this δ then appears as a UV-cutoff in a 2-point correlation function. Hence larger r corresponds to higher scales in the field theory description.

³Under dilatations, the action of a massless scalar $S = \int d^4x (\partial\phi)^2$ is invariant if $\phi \longrightarrow e^{-\alpha}\phi$. On the other hand $r \longrightarrow e^{-\alpha}r$.

It is important to emphasize that AdS/CFT can be used as a strong/weak coupling duality. That is a calculation in the large N , large λ limit on the AdS side gives a computation in the strong coupling limit of the SYM, which is not always computable. Similarly a perturbative calculation in SYM gives a result on the string theory side where supergravity is no longer applicable and no computational methods are known. While this is a huge challenge in checking the claims of AdS/CFT, if one believes the correspondence, this provides a powerful way of calculating strong coupling effects in SYM by just using classical supergravity.

There have been many checks carried out for the correspondence, some of which I will now briefly mention and are independent of the coupling λ . The global symmetries of the two theories match. The isometry group of AdS_5 is $SO(2,4)$ which is precisely the conformal group in 1+3-dimensions and gives part of the global symmetries of the SYM. The isometries of the S^5 are $SO(6) \sim SU(4)$, which corresponds to the R -symmetries of the SYM. Some other checks carried out for this example include matching the spectrum of chiral primary operators and matching of correlation functions and anomalies that are protected by non-renormalization theorems.

The correspondence can also be used at finite temperature [2, 6]. In this case the D3-black-brane solution is used in the supergravity description in the near horizon limit:

$$ds^2 = -f(r)dt^2 + \frac{r^2}{R^2}d\vec{x}^2 + \frac{1}{f(r)}dr^2 + R^2d\Omega_5^2, \quad (1.6)$$

$$f(r) \equiv \frac{r^2}{R^2} \left(1 - \frac{r_0^4}{r^4} \right), \quad (1.7)$$

where $d\vec{x}^2 = dx_1^2 + dx_2^2 + dx_3^2$ and the horizon of the black hole is located at $r = r_0$. The temperature of the gauge theory in the canonical ensemble is equal to the Hawking temperature of the black hole, which is

$$T = \frac{r_0}{\pi R^2}. \quad (1.8)$$

This is the one addition at nonzero temperature to the dictionary that relates the

parameters of the (now hot) gauge theory to those of its dual gravity description.

This dual gravity description has been used to calculate thermodynamic and hydrodynamic properties of the hot $\mathcal{N} = 4$ gauge theory plasma. A very early result was the calculation of the entropy \mathcal{S} [15]. Under the correspondence, the world-volume V_3 of the gauge theory and the D3-branes is identified. The entropy density, $s \equiv \mathcal{S}/V_3$, is given by

$$s = \frac{2\pi}{3} N^2 T^3 f(\lambda), \quad (1.9)$$

where

$$f(\lambda) = \begin{cases} 1 - \frac{3}{2\pi^2} \lambda + \dots, & \text{when } \lambda \ll 1 \\ \frac{3}{4} + \frac{45}{32} \zeta(3) (2\lambda)^{-3/2} + \dots, & \text{when } \lambda \gg 1, \end{cases} \quad (1.10)$$

where $\zeta(3) \approx 1.2020569$ is Apéry's constant. The above value for $f(\lambda)$ when $\lambda \ll 1$ is calculated in the field theory with standard diagrammatic techniques [16]. On the other hand, the value when $\lambda \gg 1$ is calculated in the supergravity solution by calculating the free energy $F = \beta I$, where I is the Euclidean action of the gravitational solution [17], and then using $\mathcal{S} = -\frac{\partial F}{\partial T}$. The $\lambda^{-3/2}$ correction comes from the $\mathcal{O}(\alpha'^3)$ correction in the lagrangian, which is determined by a quadratic contraction of the Weyl tensor. Note that to lowest order, the entropy in the weak and strong coupling regimes agree to within a factor of $\frac{3}{4}$. Additionally, as at zero temperature, it is possible to calculate various two point correlation functions. As an application of this, the expectation value of the two point retarded correlation function of the energy-momentum tensor has been used to calculate various hydrodynamic coefficients using the Green-Kubo formulas. For example, this procedure gives the value for the shear viscosity η [18]

$$\eta = \frac{\pi}{3} N^2 T^3 \left(1 + \frac{75}{4} \zeta(3) (2\lambda)^{-3/2} + \dots \right). \quad (1.11)$$

The results for η and s can be combined to obtain the ratio

$$\frac{\eta}{s} = \frac{1}{4\pi} \left(1 + \frac{135}{8} \zeta(3) (2\lambda)^{-3/2} + \dots \right). \quad (1.12)$$

On the other hand, the weak coupling value of $\frac{\eta}{s}$ diverges as $1/(g^4 \log(1/g^2))$ (see e.g. [19] and references therein). This leads to the conjecture that $\eta/s \geq 1/4\pi$ at strong coupling for theories with a gravity dual description [20]. Additionally, from conformal invariance it follows that the speed of sound $c_s^2 = 1/3$ and the bulk viscosity $\zeta = 0$ for the $\mathcal{N} = 4$ SYM plasma.

Hydrodynamic models used to describe elliptic flows of QGP at RHIC suggest that the ratio of η/s in the non-perturbative regime is small and close to $1/4\pi$ (see for e.g. [21]). In Chapter 2, I will use the AdS/CFT correspondence to calculate dispersion relations of mesons in a hot plasma and discuss its potential implications for QGP. As a motivation, I will now present a status review of field theory models available at present for understanding QGP.

1.3 A Review of Field Theory Models for Quarkonia in QGP

Before discussing applications of the AdS/CFT correspondence to understand plasmas of hot gauge theories, I will review in this section some of the field theory models currently used for understanding QGP.

The radii of the tightly bound heavy quark-antiquark systems of the charmonium (J/Ψ , Ψ' , χ_c , ...) and bottomonium (Υ , Υ' , ...) families provide a unique set of decreasing length scales in strong interaction physics. On general grounds, it is expected that the attraction between a heavy quark and an anti-quark is sensitive to the medium in which the bound state is embedded, and that this attraction weakens with increasing temperature. In the context of ultra-relativistic nucleus-nucleus collisions, the radii of some quarkonia states correspond to fractions of the natural length scale displayed by the medium produced in heavy ion collisions, namely fractions of

its inverse temperature $1/T$. Such scale considerations support the idea that measurements of the medium-modification or dissociation of quarkonia can characterize properties of the QCD matter produced in heavy ion collisions.

Matsui and Satz were the first to highlight the role of quarkonium in the study of hot QCD matter [22]. They suggested that J/Ψ -suppression is a signature for the formation of deconfined QGP. More precisely, they argued that in comparison to proton-proton or proton-nucleus collisions, the production of J/Ψ mesons should be suppressed if QGP is formed in sufficiently energetic nucleus-nucleus collisions, since the screened interaction of a c and a \bar{c} in QGP would not bind them [22]. The theoretical basis for this argument has been clarified considerably within the last two decades [23]. Model-independent calculations of the static potential between a heavy quark and anti-quark have been performed in lattice-regularized QCD, valid at strong coupling [24, 25, 26, 27, 28, 29, 30, 31, 32]. In lattice calculations without dynamical quarks, at temperature $T = 0$ and large separation L this potential rises linearly with L , consistent with confinement. At nonzero temperature, the potential weakens and levels off at large distances; with increasing temperature, the distance at which this screening occurs decreases. This behavior of the static potential has been mapped out for hot QCD matter both without [28] and with [29, 30] dynamical quarks. However, the physical interpretation of static potentials at finite temperature rests on additional assumptions. For instance, even if a potential supports a bound state with several MeV binding energy, it remains unclear which physics can be attributed to such a state in a heat bath of ~ 200 MeV temperature. Such issues do not arise in a discussion of quarkonium mesons based directly on their Minkowski space spectral functions or dispersion relations. In recent years, the spectral functions have been characterized by lattice calculations of the Euclidean correlation functions to which they are analytically related, again in hot QCD matter both without [33, 34, 35, 36, 37, 38, 39] and with [40, 41, 42, 43] dynamical quarks. The use of these calculations of finitely many points on a Euclidean correlator to constrain the Minkowski space spectral function of interest via the Maximum Entropy Method requires further inputs — for example smoothness assumptions or information on the

analytic properties of the spectral function [33, 34, 35, 36, 37, 38, 39, 40, 41, 42, 43]. At high enough temperatures that QGP becomes weakly coupled, a complementary analytical approach based upon resummed hard-thermal-loop perturbation theory becomes available [44, 45, 46, 47]. These calculations have the advantage that analytical continuation from Euclidean to Minkowski space does not introduce additional uncertainties, but it remains unclear to what extent they can treat a strongly coupled QGP. In broad terms, all these calculations support the qualitative picture behind the original suggestion of Matsui and Satz that color screening in the QGP is an efficient mechanism for quarkonium dissociation. In addition, these studies support the picture of a sequential dissociation pattern [48], in which loosely bound, large, quarkonia such as the Ψ' and χ_c cease to exist close to T_c , the temperature of the crossover between hadronic matter and QGP, whereas more tightly bound, smaller, states dissociate only at significantly higher temperatures. In particular, J/Ψ mesons continue to exist for a range of temperatures above the QCD phase transition and dissociate only above a temperature that lies between $1.5 T_c$ and $2.5 T_c$ [48]. The observation of bound-state-specific quarkonia suppression patterns could thus provide detailed information about the temperature attained in heavy ion collisions.

On the experimental side, there are by now data from the NA50 and NA60 experiments at the CERN SPS and from the PHENIX experiment at RHIC demonstrating that the production of J/Ψ mesons is suppressed in ultra-relativistic nucleus-nucleus collisions compared to proton-proton or proton-nucleus collisions at the same center of mass energy [49, 50, 7]. However, due to lack of statistics and resolution, an experimental characterization of other charmonium states (Ψ' , χ_c , ...) has not yet been possible at RHIC, and bottomonium states have not yet been characterized in any nucleus-nucleus collisions. Moreover, the observed yield of J/Ψ mesons is expected to receive significant decay contributions from Ψ' and χ_c , meaning that the observed suppression of J/Ψ mesons may originate only in the suppression of the larger Ψ' and χ_c states [48], or may indicate a suppression in the number of primary J/Ψ mesons themselves in addition. Thus, at present an experimental test of the sequential quarkonium suppression pattern is not in hand. It is expected that the LHC

heavy ion program will furnish such a test, since two LHC experiments [51, 52, 53] have demonstrated capabilities for discriminating between the different states of the charmonium and bottomonium families.

From the existing data in ultra-relativistic heavy ion collisions and their phenomenological interpretation, it has become clear that an unambiguous characterization of color screening effects in the quarkonium systems requires good experimental and theoretical control of several confounding factors. These include in particular control over the spatio-temporal evolution of the medium, control over the time scale and mechanism of quarkonium formation, as well as control over the effects of quarkonium propagation through the medium. These three sources of uncertainty are commented on below in more detail:

First, there is ample evidence by now that the systems produced in ultra-relativistic heavy ion collisions display effects of position-momentum correlated motion (a.k.a. flow), which are as important as the effects of random thermal motion [54, 55, 56, 57]. Moreover, the energy density achieved in these collisions drops rapidly with time as the matter expands and falls apart after approximately 10 fm/c. As a consequence, the modeling of quarkonium formation in heavy ion collisions cannot be limited to a description of heavy quark bound states in a heat bath at constant temperature (which is the information accessible in *ab initio* calculations in lattice-regularized QCD). The effects of a rapid dynamical evolution during which the relevant degrees of freedom in the medium change from partonic to hadronic must be taken into account.

Second, regarding the formation process, the conversion of a heavy quark pair produced in a hard collision into a bound quarkonium state is not fully understood, even in the absence of a medium. There are different production models, which all have known limitations and for which a systematic calculation scheme remains to be fully established (for a short review of these issues, see [58]). The need for further clarification of the vacuum case has even led to suggestions that nuclear matter could serve as a filter to distinguish between different production mechanisms [59, 60]. However, it has also been pointed out that there may be a novel quarkonium production mechanism operating only in ultra-relativistic heavy ion collisions at RHIC and at

the LHC [61, 62, 63]: charm quarks may be so abundant in these collisions that c and \bar{c} quarks produced separately in different primary hard scattering interactions may find each other and combine, contributing significantly to charmonium production at soft and intermediate transverse momentum. To a lesser extent, this mechanism may also contribute to the production of Upsilon mesons. Identifying and characterizing such a novel formation process is of considerable interest, since recombination is likely to be quadratically sensitive to the phase space density of charm and thus to properties of the produced matter. On the other hand, if realized in nature recombination also implies that quarkonium spectra at soft and intermediate transverse momenta are determined predominantly during the late hadronization stage and cannot be viewed as probes which test color screening in the QGP. This would indicate that the high transverse momentum regime (say above 5-8 GeV) of quarkonium spectra, which should not be significantly affected by recombination, is better suited for tests of the fundamental color screening effects predicted by QCD. However, the sensitivity of high transverse momentum spectra to properties of the medium remains to be established. In particular, quarkonium formation or dissociation proceeds on a time scale comparable to the size of the bound state in its rest frame, meaning that quark-antiquark pairs with very high transverse velocity may escape the finite-sized droplet of hot matter produced in a heavy ion collision before they have time to form a meson, meaning in turn that screening effects cease to play a role in quarkonium production above some very high transverse momentum [64]. At lower transverse momenta, where screening does play a role, one must nevertheless understand for how long quarkonium is exposed to the medium and how readily it dissociates if moving relative to that medium. For quarkonium at high transverse momentum, the time of exposure to the medium depends on the geometry of the collision region, which determines the in-medium path length, and it depends on the propagation velocity. The results contained in Chapter 2 give novel input to modeling this process by demonstrating that the real part of the finite temperature quarkonium dispersion relation can differ significantly from the vacuum one, and can imply a limiting quarkonium propagation velocity which is much smaller than c , the velocity of light in vacuum.

Our results indicate that at temperatures close to but below that at which a given quarkonium state dissociates, these mesons move through a strongly coupled QGP at a velocity that is much smaller than c even if they have arbitrarily high transverse momentum. Certainly this means that the formation time arguments of [64] will need rethinking before they can be applied quantitatively.

Third, let us turn to the question of how the relative motion of quarkonium with respect to the local rest frame of the medium affects quarkonium production. As discussed above, the standard vacuum relation between the momentum of a quarkonium state and its velocity can be altered in the presence of a medium and this effect may be phenomenologically relevant. In addition, it is expected that a finite relative velocity between the medium and the bound state enhances the probability of dissociation [65]. In a recent strong coupling calculation of hot $\mathcal{N} = 4$ supersymmetric QCD, H. Liu, K. Rajagopal and U. A. Wiedemann have shown [66, 67] that the screening length L_s for a heavy quark-antiquark pair decreases with increasing velocity as $L_s(v, T) \sim L_s(0, T)/\sqrt{\gamma}$, with $\gamma = 1/\sqrt{1-v^2}$ the Lorentz boost factor. This suggests that a quarkonium state that is bound at $v = 0$ at a given temperature could dissociate above some transverse momentum due to the increased screening, providing a significant additional source of quarkonium suppression at finite transverse momentum. The present work started from the motivation to establish how this velocity scaling manifests itself in a description of mesons at finite temperature, rather than via drawing inferences from a calculation of the screening length that characterizes the quark-antiquark potential. This motivation is analogous to that behind going from lattice QCD calculations of the static potential in QCD to calculations of the Minkowski space meson spectral function. The calculation will be done in a different strongly coupled gauge theory plasma, in which it is possible to do this investigation for mesons with nonzero velocity. I shall see in Chapter 2 that the critical velocity for the dissociation of quarkonium inferred from the velocity scaling of the screening length in Section 1.4 also appears as a limiting velocity for high-momentum quarkonium propagation in the hot non-abelian plasma.

Finally, the characterization of color screening also depends on the experimental

and theoretical ability to separate its effects on quarkonium production from effects arising during the late time hadronic phase of the heavy ion collision. In particular, it has been noted early on that significant charmonium suppression may also occur in confined hadronic matter [68, 69, 70]. However, it has been argued on the basis of model estimates for the hadronic J/Ψ dissociation cross section [71, 72, 73] that dissociation in a hadronic heat bath is much less efficient than in a partonic one. The operational procedure for separating such hadronic phase effects is to measure them separately in proton-nucleus collisions [74], and to establish then to what extent the number of J/Ψ mesons produced in nucleus-nucleus collisions drops below the yield extrapolated from proton-nucleus collisions [49, 50, 7, 75].

The absence of a conclusive field-theoretic model to understand QGP makes it worthwhile to pursue every opportunity one is afforded in understanding such media at finite temperature. AdS/CFT is uniquely positioned in terms of giving a completely different perspective on these matters.

1.4 Calculating the Screening Length using AdS/CFT

In this section I will introduce what has been learned from the calculation of the potential between a test quark-antiquark pair moving through a strongly coupled hot QGP. This will allow me to pose the questions that shall be addressed in Chapter 2 where the AdS/CFT correspondence is used to study the propagation of mesonic excitations moving through such a medium.

The potential, $E(L)$, between a quark q and an antiquark \bar{q} pair separated by a distance L can be obtained by using a Wilson loop

$$W^F(\mathcal{C}) = \text{Tr} \mathcal{P} \exp \left[i \oint_{\mathcal{C}} ds \dot{x}_\mu A^\mu(x) \right], \quad (1.13)$$

where $\oint_{\mathcal{C}}$ is the line integral along the closed loop \mathcal{C} parametrized by s , $\dot{x}^\mu \equiv \frac{dx^\mu}{ds}$, $A^\mu \equiv A_a^\mu T^a$ is the vector potential and the superscript F indicates that the matrices T^a form a fundamental representation of the gauge group. For this purpose one sets

$\mathcal{C} = \mathcal{C}_{\text{static}}$, where $\mathcal{C}_{\text{static}}$ is a rectangular time-like loop having width L along x_3 and length \mathcal{T} along the time direction t with $\mathcal{T} \gg L$, to obtain

$$\langle W(\mathcal{C}_{\text{static}}) \rangle = \exp[-i\mathcal{T}(E(L) - E_{\text{ren}})], \quad (1.14)$$

where E_{ren} is some renormalization independent of L .

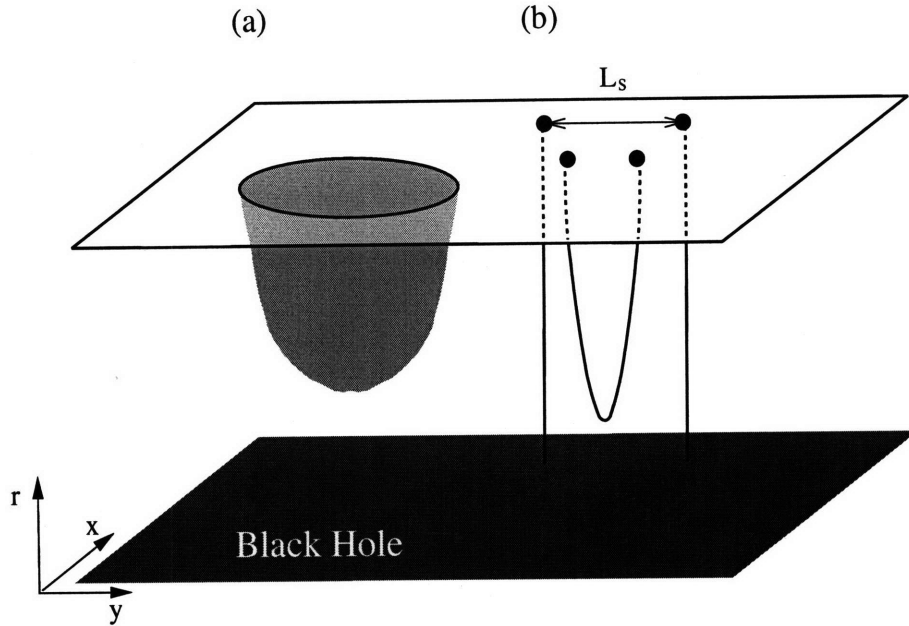


Figure 1-1: The upper plane is the D3-brane at the boundary of AdS_5 ($r = \infty$) and the lower plane is the black hole horizon. (a) The Wilson loop \mathcal{C} with the string world sheet hanging down from the D3-brane at infinity. (b) At $L = L_s$, the string joining the quark-antiquark pair falls into the black hole horizon and the “meson” in the gauge theory dissociates.

In $\mathcal{N} = 4$ SYM, all matter transforms in the adjoint representation. To introduce fundamental matter, a probe D3-brane is placed at the boundary of AdS_5 ($r = \infty$). A string stretching between the probe brane and the stack of N D3-branes at $r = 0$ gives a fundamental “test quark” of mass $m_q \gg \sqrt{\lambda}T$. When $\mathcal{C} = \mathcal{C}_{\text{static}}$ lies on this probe brane, the corresponding Wilson loop is

$$W(\mathcal{C}) = \frac{1}{N} \text{Tr} \mathcal{P} \exp \left[i \oint_{\mathcal{C}} ds \left(A_{\mu} \dot{x}^{\mu} + \vec{n} \cdot \vec{X} \right) \right], \quad (1.15)$$

where \vec{n} is the position of the probe brane in the S^5 and \vec{X} is the vector with compo-

nents equal to the six adjoint scalars in $\mathcal{N} = 4$ SYM. The AdS/CFT correspondence tells us that this Wilson loop is equivalent to

$$\langle W(\mathcal{C}) \rangle = \exp[i(S(\mathcal{C}) - S_0)], \quad (1.16)$$

where $S(\mathcal{C})$ is the action of an extremal string world sheet, bounded at $r \rightarrow \infty$ (r being the fifth dimension of AdS_5) by the world lines of the quark and antiquark (i.e. $\mathcal{C}_{\text{static}}$ with $\mathcal{T} \gg L$) and “hanging down” from these world lines toward smaller r (see Figure 1.4). Hence $q\bar{q}$ potential is obtained by computing a classical action. At zero temperature, this static potential between a heavy external quark and antiquark separated by a distance L is given in the large N and large λ limit by [76, 77]

$$V(L) = -\frac{4\pi^2}{\Gamma(\frac{1}{4})^4} \frac{\sqrt{\lambda}}{L}, \quad (1.17)$$

where the $1/L$ behavior is required by conformal invariance. At nonzero temperature, the potential becomes [78, 79, 80]

$$\begin{aligned} V(L, T) &\approx \sqrt{\lambda} f(L) & L < L_c \\ &\approx \lambda^0 g(L) & L > L_c. \end{aligned} \quad (1.18)$$

In (1.18), at $L_c = 0.24/T$ there is a change of dominance between different saddle points and the slope of the potential changes discontinuously. When $L < L_c$, the potential is determined as at zero temperature by the area of a string world sheet bounded by the worldlines of the quark and antiquark, but now the world sheet hangs down into a different five-dimensional spacetime: introducing nonzero temperature in the gauge theory is dual to introducing a black hole horizon in the five-dimensional spacetime. When $L \ll L_c$, $f(L)$ reduces to its zero temperature behavior (1.17). When $L \gg L_c$, $g(L)$ has the behavior [81]

$$g(L) \propto c_1 - c_2 e^{-m_{\text{gap}} L}, \quad (1.19)$$

with c_1 , c_2 and m_{gap} constants all of which are proportional to T . This large- L potential arises from two disjoint strings, each separately extending downward from the quark or antiquark all the way to the black hole horizon, exchanging supergravity modes the lightest of which has a mass given by $m_{\text{gap}} = 2.34 \pi T$. (There are somewhat lighter modes with nonzero R -charge, but these are not relevant here [82].) It is physically intuitive to interpret L_c as the screening length L_s of the plasma since at L_c the qualitative behavior of the potential changes. Similar criteria are used in the definition of screening length in QCD [32], although in QCD there is no sharply defined length scale at which screening sets in. Lattice calculations of the static potential between a heavy quark and antiquark in QCD indicate a screening length $L_s \sim 0.5/T$ in hot QCD with two flavors of light quarks [30] and $L_s \sim 0.7/T$ in hot QCD with no dynamical quarks [28]. The fact that there *is* a sharply defined L_c in (1.18) is an artifact of the large N , large λ limit.⁴

Given the above geometric interpretation of the $q\bar{q}$ potential in the gravity description, the problem of finding the potential between a moving pair can be mapped to considering a boost in the AdS_5 background. Using this technique, H. Liu, K. Rajagopal and U. A. Wiedemann [66, 67] calculated the potential between a moving $q\bar{q}$ pair and studied the velocity scaling of the screening length L_s in $\mathcal{N} = 4$ super-Yang-Mills theory and found that⁵

$$L_s(v, \theta, T) = \frac{f(v, \theta)}{\pi T} (1 - v^2)^{1/4} , \quad (1.20)$$

⁴The theoretical advantage of using $1/m_{\text{gap}}$ to define a screening length as advocated in [81] is that it can be precisely defined in $\mathcal{N} = 4$ SYM theory at finite λ and N_c , as well as in QCD, as it characterizes the behavior of the static potential in the $L \rightarrow \infty$ limit. The disadvantage of this proposal from a phenomenological point of view is that quarkonia are not sensitive to the potential at distances much larger than their size. For questions relevant to the stability of bound states, therefore, the length scale determined by the static potential that is phenomenologically most important is that at which the potential flattens. Although this length is not defined sharply in QCD, it is apparent in lattice calculations and can be defined operationally for practical purposes [28, 30]. This L_s seems most analogous to L_c in (1.18), and I shall therefore continue to refer to $L_s \equiv L_c$ as the screening length, as in the original literature [78, 79, 80]. Note that L_c is larger than $1/m_{\text{gap}}$ by a purely numerical factor $\simeq 1.8$.

⁵In [66, 67] L_s was defined using a slightly different quantity than L_c in (1.18), such that $L_s = 0.28/T$ for a quark-antiquark at rest. For technical reasons, this other definition was more easily generalizable to nonzero velocity.

where θ is the angle between the orientation of the quark-antiquark dipole and the velocity of the moving thermal medium in the rest frame of the dipole. $f(v, \theta)$ is only weakly dependent on both of its arguments. That is, it is close to constant. So, to a good approximation one can write

$$L_s(v, T) \approx L_s(0, T)(1 - v^2)^{1/4} \propto \frac{1}{T}(1 - v^2)^{1/4} . \quad (1.21)$$

This result, also obtained in [83, 84, 85] and further explored in [86, 87, 88], has proved robust in the sense that it applies in various strongly coupled plasmas other than $\mathcal{N} = 4$ SYM [86, 87, 88]. The velocity dependence of the screening length given in (1.21) suggests that in a theory containing dynamical heavy quarks and meson bound states (which $\mathcal{N} = 4$ SYM does not) the dissociation temperature $T_{\text{diss}}(v)$, defined as the temperature above which mesons with a given velocity do not exist, should scale with velocity as [66]

$$T_{\text{diss}}(v) \sim T_{\text{diss}}(v = 0)(1 - v^2)^{1/4} , \quad (1.22)$$

since $T_{\text{diss}}(v)$ should be the temperature at which the screening length $L_s(v)$ is comparable to the size of the meson bound state. The scaling (1.22) then indicates that slower mesons can exist up to higher temperatures than faster ones. In Chapter 2, the inference that takes me from the calculated result (1.21) to the conclusion (1.22) will be replaced by a calculation of the properties of mesons themselves, specifically their dispersion relations. The result in (1.22) will be reproduced in this more nuanced setting, finding few percent corrections to the basic scaling result inferred previously.

The results (1.21) and (1.22) have a simple physical interpretation which suggests that they could be applicable to a wide class of theories regardless of specific details. First, note that since $L_s(0) \sim \frac{1}{T}$, both (1.21) and (1.22) can be interpreted as if in their rest frame the quark-antiquark dipole experiences a higher effective temperature $T\sqrt{\gamma}$. Although this is not literally the case in a weakly coupled theory, in which the dipole will see a redshifted momentum distribution of quasiparticles coming at it from some directions and a blueshifted distribution from others [65], one can argue

for how this interpretation can nevertheless be sensible. The result (1.21) can then be seen as validating the relevance of this interpretation in a strongly coupled plasma. The argument is based on the idea that quarkonium propagation and dissociation are mainly sensitive to the local energy density of the medium. Now, in the rest frame of the dipole, the energy density (which shall be denoted by ρ) is blue shifted by a factor $\sim \gamma^2$ and since $\rho \propto T^4$ in a conformal theory, the result (1.21) is as if quarks feel a higher effective temperature given by $T\sqrt{\gamma}$.⁶ Lattice calculations indicate that the QGP in QCD is nearly conformal over a range of temperatures $1.5T_c < T \lesssim 5T_c$, with an energy density $\rho \approx bT^4$ where b is a constant about 80% of the free theory value [89, 90]. So it does not seem far-fetched to imagine that (1.21) could apply to QCD. Additionally, the AdS/CFT calculations in other strongly coupled gauge theories with a gravity description are consistent with the interpretation above [87] and that for near conformal theories the deviation from conformal theory behavior appears to be small [87]. If a velocity scaling like (1.21) and (1.22) holds for QCD, it can potentially have important implications for quarkonium suppression in heavy ion collisions. These issues will be discussed from the field theory perspective in Section 1.3 and from the AdS/CFT perspective in Section 2.5.

Further, another curious feature regarding the quark potential is that for any given quark mass m_q there exists a maximal velocity v_c given by

$$v_c^2 = 1 - \frac{\lambda^2 T^4}{16m_q^4}, \quad (1.23)$$

beyond which there is no $\mathcal{O}(\sqrt{\lambda})$ potential between the pair for any value of their separation larger than their Compton wavelength, i.e. for any distance at which a potential can be defined [66, 67]. This result can be interpreted as saying that for any given T and m_q , it is impossible to obtain bound states beyond (1.23), i.e. as indicating that there is a velocity bound (a “speed limit”) for the mesons. One can also turn (1.23) around and infer that for any large m_q and v close to 1, the

⁶Applying a Lorentz boost to ρ yields $\gamma^2(1 + \frac{1}{3}v^2)\rho$. Including the $(1 + \frac{1}{3}v^2)$ factor makes this argument reproduce the result (1.20), including the weak velocity dependence in the function f , more quantitatively than merely tracking the powers of γ .

dissociation temperature is given by

$$T_{\text{diss}} = \frac{2m_q}{\sqrt{\lambda}}(1 - v^2)^{\frac{1}{4}}, \quad (1.24)$$

which is consistent with (1.22). Note that the above argument is at best heuristic since $\mathcal{N} = 4$ SYM itself does not contain dynamical quarks and thus genuine mesons do not exist. In Chapter 2 however, I shall see by deriving them from meson dispersion relations that (1.23) and (1.24) are precisely correct in the limit of large quark mass once fundamentals, and hence mesons, are introduced into the theory. I shall also find that the more dynamical, albeit heuristic, interpretation of (1.23) as a velocity beyond which a quark and antiquark do not feel a potential that can bind them remains of value.

While the argument about the velocity dependence the dissociation temperature for mesons moving in a hot plasma leading from (1.21) to (1.22) is plausible, it is more satisfying to have a set-up within which one can study mesons directly. Direct study of meson bound-states will also yield more insights than the study of the screening length from the potential. It is the purpose of Chapter 2 to examine this issue in a specific model (to be presented in the next section) with dynamical flavors.

1.5 Adding Flavors using the Probe Approximation

To see if AdS/CFT can provide any insights into the dynamics of QCD, one is required to have fundamental matter. All the matter in $\mathcal{N} = 4$ SYM transforms in the adjoint representation. This is required by the large number of supersymmetries that are preserved in it. 't Hooft had pointed out, that in the large N expansion, perturbation theory is just an expansion in $1/N$, with the planar graphs giving the lowest order correction. If the theory has only adjoint matter, using the double line notation, these planar graphs can be interpreted as the genus expansion in closed string perturbation theory. Introducing fundamental matter means that one is introducing boundaries,

which in string perturbation theory arise from open strings. As open strings end on D-branes, this means we can add flavor by adding D-branes that are different from the D3-branes already present in the theory.

Trying to add D-branes is no simple matter, as they are charged under the RR-fields and can source fluxes. An important requirement is that the D-branes introduced in this fashion are stable. If one does not turn on any fluxes, then there is a tachyonic mode that lives on the D-brane, which naively suggests that such a D-brane would be unstable and decay. This issue was examined by A. Karch and E. Katz [91] for several systems including the D3/D7 system with N D3-branes and N_f D7-branes, using a *probe approximation*. A probe approximation means that the gravitational back reaction of the D7-brane, which provides flavor, is ignored. This is reasonable when $N_f \ll N$, with corrections being of order N_f/N . They found that there are indeed tachyonic modes living on the D7-brane which do not lead to an instability because they satisfy the Breitenlohner-Freedman bound [92, 93], which for AdS_{d+1} states that the mode is stable if $m^2 R^2 \geq -\frac{d^2}{4}$, where m^2 is the mass of the mode.

1.5.1 D7-brane Embedding at Zero Temperature

Consider a stack of N coincident D3-branes and N_f coincident D7-branes in 9+1-dimensional Minkowski space, represented by the array

$$\begin{array}{rcccccccccccc}
 \text{D3:} & 0 & 1 & 2 & 3 & \cdot & \cdot & \cdot & \cdot & \cdot & \cdot & \cdot & \cdot & \cdot \\
 \text{D7:} & 0 & 1 & 2 & 3 & 4 & 5 & 6 & 7 & \cdot & \cdot & \cdot & \cdot & \cdot
 \end{array} \tag{1.25}$$

which denotes in which of the 1+9-dimensions the D3- and D7-branes are extended, and in which they occupy only points. The D3-branes sit at the origin of the 89-plane, with L denoting the distance between the D3- and the D7-branes in the 89-plane. Without loss of generality (due to rotational symmetry in 89-plane), take the D7-branes to be at $x_8 = L$, $x_9 = 0$. This is a stable configuration and preserves one quarter of the total number of supersymmetries, meaning that it describes an $\mathcal{N} = 2$ supersymmetric gauge theory as I now sketch [91].

The open string sector of the system contains 3-3 strings, both of whose ends lie on one of the N D3-branes, 7-7 strings ending on N_f D7-branes, and 3-7 and 7-3 strings stretching between D3- and D7-branes. In the low energy limit

$$\alpha' \rightarrow 0, \quad \frac{L}{2\pi\alpha'} = \text{finite}, \quad (1.26)$$

all the stringy modes decouple except for: (i) the lightest modes of the 3-3 strings, which give rise to an $SU(N)$ $\mathcal{N} = 4$ SYM theory in 3+1-dimensional Minkowski space; (ii) the lightest modes of the 3-7 and 7-3 strings, which give rise to N_f hypermultiplets in the $\mathcal{N} = 2$ gauge theory transforming under the fundamental representation of $SU(N)$. The whole theory thus has $\mathcal{N} = 2$ supersymmetry. I will call N_f hypermultiplets quarks below even though they contain both fermions and bosons. The mass of the quarks is given by

$$m_q = \frac{L}{2\pi\alpha'}, \quad (1.27)$$

where $1/(2\pi\alpha')$ is the tension of the strings.

The decoupling limit is taken in the same way as Section 1.2 by taking N large while holding the 't Hooft coupling $\lambda = g_{YM}^2 N$ fixed. The corresponding 't Hooft coupling for the gauge theory living on the D7-branes is $\lambda' = g_s(2\pi l_s)^4 N_f = \lambda 4\pi^3 \alpha'^2 N_f/N$ which vanishes in the low energy limit, $\alpha' \rightarrow 0$. Further, the β -function of the D7-brane gauge coupling also vanishes in this limit, restoring conformal invariance. Hence, in the limit

$$N \rightarrow \infty, \quad N_f = \text{finite}, \quad \lambda = g_{YM}^2 N \gg 1, \quad (1.28)$$

the above gauge theory has a gravity description [91] in terms of D7-branes in the near-horizon geometry of the D3-branes, which is $AdS_5 \times S_5$ with a metric given in (1.5).

In this zero temperature setting, the embedding of the D7-branes in the $AdS_5 \times S_5$ geometry (1.5) can be read directly from (1.25). The D7-brane worldvolumes fill the (t, x_i) coordinates, with $i = 1, \dots, 7$, and are located at the point $x_8 = L$, $x_9 = 0$

in the 89-plane. Since N_f remains finite in the large N limit, the gravitational back-reaction of the D7-branes on the spacetime of the D3-branes (1.5) may be neglected.

The dictionary between the gauge theory and its dual gravity description can thus be summarized as follows. On the gauge theory side we have two sectors: excitations involving adjoint degrees of freedom only and excitations involving the fundamentals. The first type of excitations correspond to closed strings in $AdS_5 \times S^5$ as in the standard AdS/CFT story. The second type is described by open strings ending on the D7-branes⁷. In particular, the low-lying (in a sense that will be defined later) meson spectrum of the gauge theory can be described by fluctuations of $x_{8,9}$ and gauge fields on D7-branes. I shall focus on the fluctuations of $x_{8,9}$ on the D7-brane (equivalently, the fluctuations of the position of the D7-brane in the (x_8, x_9) plane) which describe scalar mesons. There are also gauge fields localized within the D7-brane, and their fluctuations describe vector mesons. The description of the vector mesons is expected to be similar to that of the scalar mesons. I will limit this presentation entirely to the scalar mesons. Further, I will take $N_f = 1$, meaning that the gauge theory is specified by the parameters N , λ and m_q which are related to their counterparts in the dual gravity theory by (1.4), (1.1) and (1.27). We see that the $N \rightarrow \infty$ limit corresponds to $g_s \rightarrow 0$, making the string theory weakly coupled. Considering the theory with the parameter λ taken to ∞ corresponds to taking the string tension to infinity. These limits justify the use of the classical gravity approximation in which the strings are considered as moving in a background spacetime.

For later generalization to finite temperature, it is convenient to describe the D7-brane in a coordinate system which makes the symmetries of its embedding more manifest. I split the \mathbb{R}^6 factor in the last term of (1.5) into $\mathbb{R}^4 \times \mathbb{R}^2$ (i.e. parts longitudinal and transverse to the D7-brane) and express them in terms of polar coordinates respectively. More explicitly,

$$\begin{aligned} r^2 &= \rho^2 + y^2, & \rho^2 &= x_4^2 + x_5^2 + x_6^2 + x_7^2, & y^2 &= x_8^2 + x_9^2, \\ x_8 &= y \cos \phi, & x_9 &= y \sin \phi. \end{aligned} \tag{1.29}$$

⁷I will not consider baryons in this chapter.

The metric (1.5) then becomes

$$ds^2 = \frac{\rho^2 + y^2}{R^2} (-dt^2 + d\vec{x}^2) + \frac{R^2}{\rho^2 + y^2} (d\rho^2 + \rho^2 d\Omega_3^2 + dy^2 + y^2 d\phi^2) . \quad (1.30)$$

The D7-brane now covers $(t, \vec{x}) = (t, x_1, x_2, x_3, \rho, \Omega_3)$ and sits at $y = L$ and $\phi = 0$. Note that in the radial direction the D7-brane extends from $\rho = 0$, at which the size of the three-sphere Ω_3 becomes zero, to $\rho = \infty$. The point $\rho = 0$ corresponds to $r = L$.

The action of the D7-brane is given by the Dirac-Born-Infeld action

$$S_{D7} = -\mu_7 \int d^8\xi \sqrt{-\det \tilde{h}_{ij}} , \quad (1.31)$$

where the ξ^i (with $i = 0, 1, \dots, 7$) denote the worldvolume coordinates of the D7 brane and \tilde{h}_{ij} is the induced metric in the worldvolume

$$\tilde{h}_{ij} = G_{\mu\nu}(X) \frac{\partial X^\mu}{\partial \xi^i} \frac{\partial X^\nu}{\partial \xi^j} . \quad (1.32)$$

The value of the D7-brane tension, $\mu_7 = (2\pi)^{-6} g_s^{-1} \alpha'^{-4}$, will play no role in our considerations. The spacetime metric $G_{\mu\nu}$ is given by (1.30) and $X^\mu(\xi)$ describe the embedding of the D7-brane, where μ runs through all spacetime coordinates. The action (1.31) is invariant under the coordinate transformations $\xi \rightarrow \xi'(\xi)$. I can use this freedom to set $\xi^i = (t, \vec{x}, \rho, \Omega_3)$, and the embedding described below equation (1.30) then corresponds to the following solution to the equations of motion of (1.31):

$$y(\xi) = L, \quad \phi(\xi) = 0 \quad \text{or} \quad x_8(\xi) = L, \quad x_9(\xi) = 0 . \quad (1.33)$$

1.5.2 D7-brane Embedding at Finite Temperature

At nonzero temperature, the embedding of the D7-brane is modified because the D7-brane now feels a gravitational attraction due to the presence of the black hole. To find the embedding, it is convenient to use coordinates which are analogous to those

in (1.30). For this purpose, introduce a new radial coordinate u defined by

$$\frac{dr^2}{f(r)} = \frac{R^2 du^2}{u^2}, \quad \text{i.e.} \quad u^2 = \frac{1}{2} \left(r^2 + \sqrt{r^4 - r_0^4} \right), \quad (1.34)$$

in terms of which (1.6) can then be written as

$$ds^2 = -f dt^2 + \frac{r^2}{R^2} d\vec{x}^2 + \frac{R^2}{u^2} (du^2 + u^2 d\Omega_3^2) \quad (1.35)$$

$$= -f dt^2 + \frac{r^2}{R^2} d\vec{x}^2 + \frac{R^2}{u^2} (d\rho^2 + \rho^2 d\Omega_3^2 + dy^2 + y^2 d\phi^2). \quad (1.36)$$

As in (1.30), I have split the last term of (1.35) in terms of polar coordinates on $\mathbb{R}^4 \times \mathbb{R}^2$, with

$$u^2 = y^2 + \rho^2. \quad (1.37)$$

In (1.35) and (1.36), f and r should now be considered as functions of u ,

$$r^2 = u^2 + \frac{r_0^4}{4u^2}, \quad f(u) = \frac{(u^4 - r_0^4/4)^2}{u^2 R^2 (u^4 + r_0^4/4)}. \quad (1.38)$$

In terms of u , the horizon is now at $u_0 = \frac{r_0}{\sqrt{2}}$.

The D7-brane again covers $\xi^i = (t, \vec{x}, \rho, \Omega_3)$ and its embedding $y(\xi), \phi(\xi)$ in the (y, ϕ) plane will again be determined by extremizing the Dirac-Born-Infeld action (1.31). Because of the rotational symmetry in the ϕ direction, I can choose $\phi(\xi) = 0$. Because of the translational symmetry in the (t, \vec{x}) directions and the rotational symmetry in S^3 , y can depend on ρ only. Thus, the embedding is fully specified by a single function $y(\rho)$. The induced metric on the D7-brane worldvolume can be written in terms of this function as

$$h_{ij} d\xi^i d\xi^j = -f(u) dt^2 + \frac{r^2}{R^2} d\vec{x}^2 + \frac{R^2}{u^2} ((1 + y'(\rho)^2) d\rho^2 + \rho^2 d\Omega_3^2), \quad (1.39)$$

where u in (1.37) and hence $f(u)$ are functions of ρ and $y(\rho)$. Substituting (1.39) into

(1.31), one finds

$$S_{D7} \propto \int d\rho \frac{\rho^3}{u(\rho)^8} \left(16 \left(\frac{u(\rho)}{r_0} \right)^8 - 1 \right) \sqrt{1 + y'(\rho)^2}, \quad (1.40)$$

which leads to the equation of motion

$$\frac{y''}{1 + y'^2} + \frac{3y'}{\rho} + \frac{8r_0^8 (\rho y' - y)}{u^2 (16u^8 - r_0^8)} = 0 \quad (1.41)$$

for $y(\rho)$, where $u^2(\rho) = \rho^2 + y^2(\rho)$.

To solve (1.41) one imposes the boundary condition that $y \rightarrow L$ as $\rho \rightarrow \infty$, and that the induced metric (1.39) is non-singular everywhere. L determines the bare quark mass as in (1.27). It is convenient to introduce a parameter

$$\epsilon_\infty \equiv \frac{u_0^2}{L^2} = \frac{r_0^2}{2L^2} = \frac{\lambda T^2}{8m_q^2} = \frac{\pi^2 T^2}{2M^2}, \quad (1.42)$$

where I have used (1.8) and (2.10). Because $\mathcal{N} = 4$ SYM is scale invariant before introducing the massive fundamentals, meaning that all dimensionful quantities must be proportional to appropriate powers of T , when the fundamentals are introduced, the only way in which the quark mass m_q can enter is through the dimensionless ratio m_q/T . Scale invariance alone does not require that this ratio be accompanied by a $\sqrt{\lambda}$, but it is easy to see that, after rescaling to dimensionless variables as in (2.8), the only combination of parameters that enters (1.41) is ϵ_∞ . The small ϵ_∞ regime can equally well be thought of as a low temperature regime or a heavy quark regime. In the remainder of this section, we shall imagine m_q as fixed and describe the physics as a function of varying T , i.e. varying horizon radius r_0 .

The equation of motion (1.41) that specifies the D7-brane embedding can be solved numerically. Upon so doing, one finds that there are three types of solutions with different topology [94, 95, 96]:

- Minkowski embeddings: The D7-brane extends all the way to $\rho = 0$ with $y(0) > u_0 = \frac{r_0}{\sqrt{2}}$ (see e.g. the upper three curves in Figure 1-2). In order for the solution

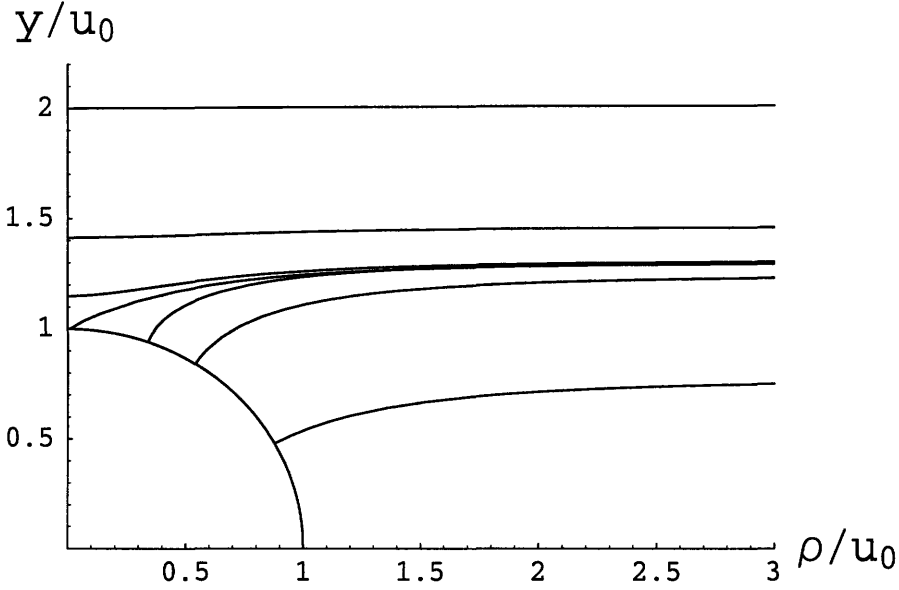


Figure 1-2: Some possible D7-brane embeddings $y(\rho)$. The quark mass to temperature ratio is determined by $y(\infty) = L$. Specifically, $\sqrt{8}m_q/(T\sqrt{\lambda}) = y(\infty)/u_0 \equiv 1/\sqrt{\epsilon_\infty}$. The top three curves are Minkowski embeddings, with $y(\rho)$ extending from $\rho = 0$ to $\rho = \infty$. The bottom three curves are black hole embeddings, in which the D7-brane begins at the black hole horizon at $y^2 + \rho^2 = u_0^2$. The middle curve is the critical embedding. The seven curves, ordered from top to bottom as they occur in the left part of the figure, are drawn for temperatures specified by $\epsilon_\infty = 0.249, 0.471, 0.5865, 0.5948, 0.5863, 0.647$ and 1.656 . Note that the $\epsilon_\infty = 0.5863$ black hole embedding crosses both the $\epsilon_\infty = 0.5948$ critical embedding and the $\epsilon_\infty = 0.5865$ Minkowski embedding.

to be regular one needs $y'(0) = 0$. This gives rise to a one-parameter family of solutions parameterized by $y(0)$. The topology of the brane is $\mathbb{R}^{1,7}$.

- Critical embedding: The D7-brane just touches the horizon, i.e. $y(0) = u_0$ (see e.g. the middle curve in Figure 1-2). The worldvolume metric is singular at the point where the D7-brane touches the horizon.
- Black hole embeddings: The D7-brane ends on the horizon $u_0 = r_0/\sqrt{2}$ at some $\rho > 0$ (see e.g. the lower three curves in Figure 1-2). The topology of the D7-brane is then $\mathbb{R}^{1,4} \times S^3$.

Also see Figure 1.5.2 for a different perspective on the embedding.

It turns out [97, 96] that Minkowski embeddings that begin at $\rho = 0$ with y

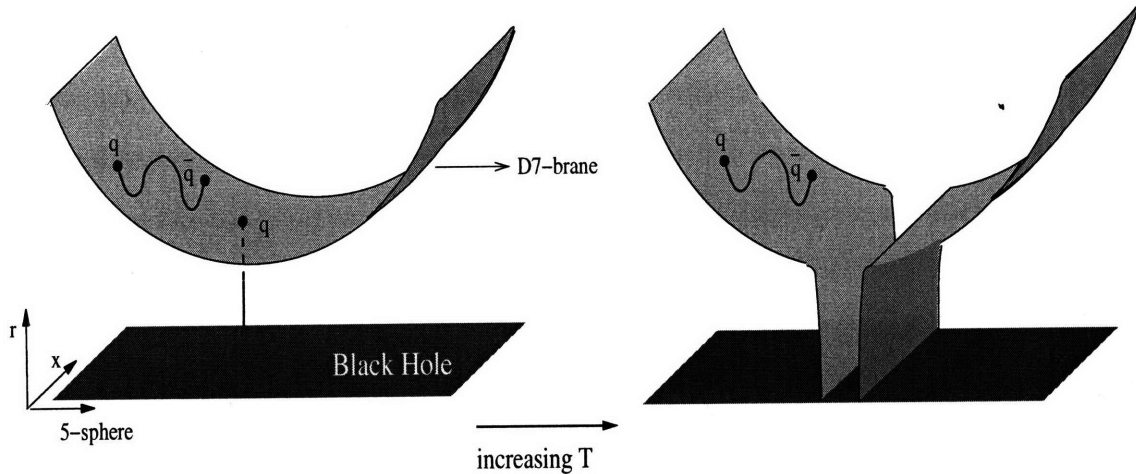


Figure 1-3: This figure shows a different slicing of the D7-brane embedding from the one shown in Figure 1-2. The left-hand panel shows the Minkowski embedding while the right-hand panel shows the black hole embedding. Here T is the temperature, $r = \sqrt{y^2 + \rho^2}$ and x is a direction along the D3-brane. The axis labeled as 5-sphere refers to the angle between y/u_0 and ρ/u_0 in Figure 1-2 where it ranges from 0 to $\frac{\pi}{2}$ in the clock-wise direction. In this figure it ranges from $-\frac{\pi}{2}$ to $\frac{\pi}{2}$. Unlike Figure 1-2, the shape of embeddings in this figure are not the exact solutions to the equations of motion, but have the correct qualitative feature.

close to $r_0/\sqrt{2}$, just above the critical embedding, can cross the critical embedding, ending up at $\rho \rightarrow \infty$ with $y(\infty)$ just below that for the critical embedding. Similarly, embeddings that begin just below the critical embedding can end up just above it. Furthermore, those embeddings that begin even closer to the critical embedding can cross it more than once. This means that there is a range of values around the critical $\epsilon_\infty^c = 0.5948$ for which there are three or more embeddings for each value of ϵ_∞ . At low temperatures (precisely, for $\epsilon_\infty < 0.5834$) this does not occur: there is only a single Minkowski embedding for each value of ϵ_∞ . At high temperatures (precisely, for $\epsilon_\infty > 0.5955$) there is only a single black hole embedding per value of ϵ_∞ . In the intermediate range of temperatures $0.5834 < \epsilon_\infty < 0.5955$, one needs to compare the free energy of each of the three or more different D7-brane embeddings that have the same value of ϵ_∞ to determine which is favored. One finds that there is a first order phase transition at a temperature T_c at which $\epsilon_\infty = 0.5863$, where the favored embedding jumps discontinuously from a Minkowski embedding to a black

hole embedding as a function of increasing temperature [97, 96].⁸

⁸The critical embedding occurs at an $\epsilon_\infty = 0.5948$ which is greater than the ϵ_∞ at which the first order phase transition occurs, meaning that at $\epsilon_\infty = 0.5948$ there is a black hole embedding that has a lower free energy than the critical embedding.

Chapter 2

A Limiting Velocity for Quarkonium Propagation in a Strongly Coupled Plasma via AdS/CFT

2.1 Introduction

An understanding of quarkonium production in heavy ion collisions relies heavily on theoretical modeling as the bridge between experimental observations and the underlying properties of hot QCD matter. This task involves multiple steps. It is of obvious interest to validate or constrain by first principle calculations as many steps as possible, even in a simplified theoretical setting. The work in this chapter is one of a number of recent developments, beginning with G. Policastro et. al. [98] that explore to what extent techniques from string theory, in particular the AdS/CFT correspondence, can contribute to understanding processes in hot QCD by specifying how these processes manifest themselves in a large class of hot strongly coupled non-abelian gauge theories. Although it is not known how to extend the AdS/CFT correspondence to QCD, there are several motivations for turning to this technique.

First, there are a growing number of explicit examples which indicate that a large class of thermal non-abelian field theories with gravity duals share commonalities such that their properties in the thermal sector are either universal at strong coupling, i.e. independent of the microscopic dynamics encoded in the particular quantum field theory under study, or their properties are related to each other by simple scaling laws e.g. depending on the number of elementary degrees of freedom. This supports the working hypothesis that by learning something about a large class of strongly coupled thermal non-abelian quantum field theories, one can gain guidance towards understanding the thermal sector of QCD. Second, the AdS/CFT correspondence allows for a technically rather simple formulation of problems involving real-time dynamics. This is very difficult in finite temperature lattice-regularized calculations, which exploit the imaginary time formalism. In particular, this is the reason why so far lattice QCD calculations treat only static quark-antiquark pairs in the plasma, and why the only nonperturbative calculation of the velocity dependence of quarkonium dissociation exploits the AdS/CFT correspondence. Third, data from experiments at RHIC pertaining to many aspects of the matter produced in heavy ion collisions indicate that this matter is strongly coupled. Since the AdS/CFT correspondence provides a mapping of difficult nonperturbative calculations in a quantum field theory with strong coupling onto relatively simple, semi-classical calculations in a gravity dual, it constitutes a novel — and often the only — technique for addressing dynamical questions about hot strongly coupled non-abelian matter, questions that are being raised directly by experimental results on QCD matter coming from RHIC.

I have focussed here on the larger context of results that are presented in this chapter, which is work I did in collaboration with T. Faulkner, H. Liu, K. Rajagopal and U. A. Wiedemann [8]. In Section 1.4 I reviewed the past results which serve as an immediate motivation for this work, in particular the screening length that characterizes the potential between a static quark and antiquark in a moving plasma wind. Adding fundamental quarks with finite mass m_q , and hence mesons, into $\mathcal{N} = 4$ SYM theory requires adding a D7-brane in the dual gravity theory, as was reviewed in Section 1.5. The fluctuations of the D7-brane are the mesons, which were

review for the case of zero temperature in Section 2.2. In Section 2.3 I set up the analysis of the mesons at nonzero temperature, casting the action for the D7-brane fluctuations in a particularly geometric form, written entirely in terms of curvature invariants. Parts of the derivation are explained in more detail in Appendix A. With all the groundwork in place, in Section 2.4 I derive the meson dispersion relations. In addition to obtaining them numerically without taking any limits as has been done previously [96], I was able to calculate them analytically in three limits: first, upon taking the low temperature limit at fixed k ; second, upon taking the low temperature limit at fixed kT ; and third, using insights from the first two calculations, at large k for any temperature. At large k one obtains

$$\omega = v_0 k + a + \frac{b}{k} + \dots \quad (2.1)$$

where v_0 is independent of meson quantum numbers, depending only on T/m_q . v_0 turns out to be given by the local speed of light at the “tip of the D7-brane,” namely the place in the higher dimensional gravity dual theory where the D7-brane comes closest to the black hole [96]. The solution for a and b in terms of meson quantum numbers and T/m_q is presented in this chapter. The result derived for the limiting velocity v_0 for mesons at a given temperature T can be inverted, obtaining $T_{\text{diss}}(v)$, the temperature above which no mesons with velocity v are found. I find that up to few percent corrections, our result can be summarized by

$$T_{\text{diss}}(v) = (1 - v^2)^{1/4} T_{\text{diss}} , \quad (2.2)$$

where T_{diss} is the temperature at which zero-velocity mesons dissociate, obtained in previous work and introduced in Section 2.2. The results presented here which were obtained by direct calculation of meson dispersion relations confirm inferences reached (in two different ways) from the analysis of the screened potential between a static quark and antiquark in a hot plasma wind, which was presented in Section 1.4. In Section 2.5, I discuss the potential implications of these dispersion relations for quarkonia in QCD as well as a look at open questions. The dispersion relations

that have been calculated in this work describe how mesons propagate and so affect a class of observables, but determining whether quarkonium meson formation from a precursor quark-antiquark pair is suppressed by screening is a more dynamical question that can at present be addressed only by combining the calculation in Section 2.4 and the more heuristic results obtained by H. Liu et. al. [67].

2.2 D3/D7-brane Construction of Mesons

This section contains a review of the gravity dual description of strongly coupled $\mathcal{N} = 4$ SYM theory with gauge group $SU(N)$ coupled to $N_f \ll N$ $\mathcal{N} = 2$ hypermultiplets in the fundamental representation of $SU(N)$, introduced in [91] and studied in [99, 94, 100, 101, 102, 9, 103, 95, 97, 96, 104, 105, 106]. I will first describe the theory at zero temperature and then turn to nonzero temperature. I will work in the limit $N \rightarrow \infty$, $\lambda = g_{YM}^2 N \rightarrow \infty$ and N_f finite (in fact $N_f = 1$). In the deconfined strongly coupled plasma that this theory describes, heavy quark mesons exist below a dissociation temperature that, for mesons at rest, is given by $T_{\text{diss}} = 2.166 m_q / \sqrt{\lambda}$ [94, 95, 97, 96]. In Section 2.4, I will show the calculation of the dispersion relations for these mesons, namely the meson spectrum at nonzero momentum k and in so doing determine $T_{\text{diss}}(v)$ directly, rather than by inference as described in Section 1.4.

2.2.1 Zero Temperature

I now briefly describe how to find the low-lying meson spectrum described by the fluctuations of $x_{8,9}$, given the embedding in (1.33). To find the meson spectrum corresponding to the fluctuations of the brane position, choose

$$x_8 = L + 2\pi\alpha'\psi_1(\xi), \quad x_9 = 0 + 2\pi\alpha'\psi_2(\xi), \quad (2.3)$$

and expand the action (1.31) to quadratic order in $\psi_{1,2}$, obtaining

$$S_{D7} \simeq \mu_7 \int d^8\xi \rho^3 \left(-1 - \frac{1}{2}(2\pi\alpha'R)^2 \frac{h^{ij}}{\rho^2 + L^2} (\partial_i\psi_1\partial_j\psi_1 + \partial_i\psi_2\partial_j\psi_2) \right). \quad (2.4)$$

In (2.4), h_{ij} denotes the induced metric on the D7-brane for the embedding (1.33) in the absence of any fluctuations, i.e.

$$ds^2 = h_{ij}d\xi^i d\xi^j = \frac{\rho^2 + L^2}{R^2} (-dt^2 + d\vec{x}^2) + \frac{R^2}{\rho^2 + L^2} (d\rho^2 + \rho^2 d\Omega_3^2) . \quad (2.5)$$

Note that when $L = 0$, the above metric reduces to $AdS_5 \times S^3$, reflecting the fact that in the massless quark limit the Yang-Mills theory is conformally invariant in the large N/N_f limit.

The equation of motion following from (2.4) is

$$\frac{R^4}{(\rho^2 + L^2)^2} \partial_\alpha \partial^\alpha \psi + \frac{1}{\rho^3} \frac{\partial}{\partial \rho} \left(\rho^3 \frac{\partial}{\partial \rho} \psi \right) + \frac{1}{\rho^2} \nabla_{S^3}^2 \psi = 0 , \quad (2.6)$$

where ψ denotes either ψ_1 or ψ_2 , where $\alpha = 0 \dots 3$, and where $\nabla_{S^3}^2$ denotes the Laplacian operator on the unit S^3 . Eq. (2.6) can be solved exactly and normalizable solutions have a discrete spectrum. It was found in [99] that the four dimensional mass spectrum is given by

$$m_{n\ell} = \frac{4\pi m_q}{\sqrt{\lambda}} \sqrt{(n + \ell + 1)(n + \ell + 2)}, \quad n = 0, 1, \dots, \quad \ell = 0, 1, \dots, \quad (2.7)$$

with degeneracy $(\ell + 1)^2$, where ℓ is the angular momentum on S^3 . The $(\ell + 1)^2$ degeneracy is understood in the field theory as arising because the scalar mesons are in the $(\ell/2, \ell/2)$ representation of a global $SU(2) \times SU(2)$ symmetry corresponding to rotations in the S^3 in the dual gravity theory [99].

The mass scale appearing in (2.7) can also be deduced without calculation via a scaling argument. Letting

$$t \rightarrow \frac{R^2}{L} t, \quad \vec{x} \rightarrow \frac{R^2}{L} \vec{x}, \quad \rho \rightarrow L\rho, \quad (2.8)$$

the metric (2.5) can be solely expressed in terms of dimensionless quantities:

$$\frac{ds^2}{R^2} = (\rho^2 + 1) (-dt^2 + d\vec{x}^2) + \frac{1}{\rho^2 + 1} (d\rho^2 + \rho^2 d\Omega_3^2) . \quad (2.9)$$

Thus, the mass scale for the mesonic fluctuations must be

$$M \equiv \frac{L}{R^2} = \frac{2\pi m_q}{\sqrt{\lambda}}, \quad (2.10)$$

as is indeed apparent in the explicit result (2.7). We see here that the mesons are very tightly bound in the large λ limit with a mass M that is parametrically smaller than the rest mass of a separated quark and antiquark, $2m_q$. This means that the binding energy is $\approx -2m_q$. From this fact and the Coulomb potential (1.17), one can also estimate that the size of the bound states is parametrically of order $\sim \frac{1}{M} \sim \frac{\sqrt{\lambda}}{m_q}$.

Finally, the sense in which this analysis is limited to low-lying mesons can now be explained. I have only analyzed those scalar mesons whose mass is of order M . There are other, stringy, excitations in the theory with meson quantum numbers whose masses are of order $L/(R\sqrt{\alpha'}) \sim M\lambda^{1/4} \sim m_q/\lambda^{1/4}$ and of order $L/\alpha' \sim M\lambda^{1/2} \sim m_q$ [99]. They are parametrically heavier than the mesons analyzed here, and can be neglected in the large λ limit even though those with masses $\sim m_q/\lambda^{1/4}$ are also tightly bound, since their masses are also parametrically small compared to m_q . In Section 2.4, we shall see again in a different way that the analysis of the dispersion relations for the mesons with masses $\sim m_q/\sqrt{\lambda}$ that is focused on here is controlled by the smallness of $1/\lambda^{1/4}$.

2.2.2 Nonzero Temperature

Let us now put the Yang-Mills theory at nonzero temperature, in which case the AdS_5 part of the metric (1.5), as discussed in Section 1.2, is replaced by the metric of an AdS-Schwarzschild black hole given in (1.6) and (1.7). The Hawking temperature at the horizon of this black hole is identified with the temperature of the field theory and the worldvolume of the brane is identified with the field theory volume and is given in (1.8).

The D7-brane embeddings were discussed in Section 1.5.2, where it was discussed there is a critical embedding at $\epsilon_\infty^c = 0.5948$, around which ϵ_∞ is multivalued (i.e. $0.5834 < \epsilon_\infty < 0.5955$). At low temperatures with $\epsilon_\infty < 0.5834$, it is single valued

with only Minkowski embeddings possible. There is a first order phase transition at $\epsilon_\infty = 0.5863$ with temperature T_c .

As I shall study in detail in Section 2.3, fluctuations about a Minkowski embedding describe a discrete meson spectrum with a mass gap of order $O(M)$. In contrast, fluctuations about a black hole embedding yield a continuous spectrum [97, 96]. A natural interpretation of the first order transition is that $T_c = T_{\text{diss}}$, the temperature above which the mesons dissociate [97, 96]. It is interesting, and quite unlike what is expected in QCD, that all the mesons described by the zero temperature spectrum (2.7) dissociate at the same temperature. This is presumably related to the fact that the mesons are so tightly bound, again unlike in QCD. I will therefore focus on the velocity-dependence of the meson spectrum at nonzero temperature — in other words, the meson dispersion relations first studied in [96]. As I have explained in Section 1.3, the velocity-dependence is currently inaccessible to lattice QCD calculations. Hence, even qualitative results are sorely needed. Furthermore, inferences drawn from a previous calculation that I have reviewed in Section 1.4 of the potential between a moving quark-antiquark pair lead to a velocity-scaling (1.22) of T_{diss} that has a simple physical interpretation, which suggests that it could be applicable in varied theories [66]. We shall see this velocity dependence emerge from the meson dispersion relations in Section 2.4.

It is interesting to return to the qualitative estimate of T_{diss} obtained from the static quark-antiquark potential in Section 1.4, and see how it compares to the $T_{\text{diss}} = T_c$ obtained from the analysis of the mesons themselves. Equating the size of a meson with binding energy $2m_q$, determined by the zero-temperature potential (1.17), with the screening length $L_s = L_c = 0.24/T$, determined by the potential (1.18) at nonzero temperature, yields the estimate that T_{diss} should be $\sim 2.1m_q/\sqrt{\lambda}$. This is in surprisingly good agreement with $T_{\text{diss}} = \sqrt{8\epsilon_\infty} m_q/\sqrt{\lambda} = 2.166 m_q/\sqrt{\lambda}$ for $\epsilon_\infty = 0.5863$.

In subsequent sections, I will derive the dispersion relations for mesons at $T < T_{\text{diss}}$. I close this section by introducing some new notation that simplifies the analysis of the Minkowski embedding of the D7-brane, whose fluctuations are of interest here.

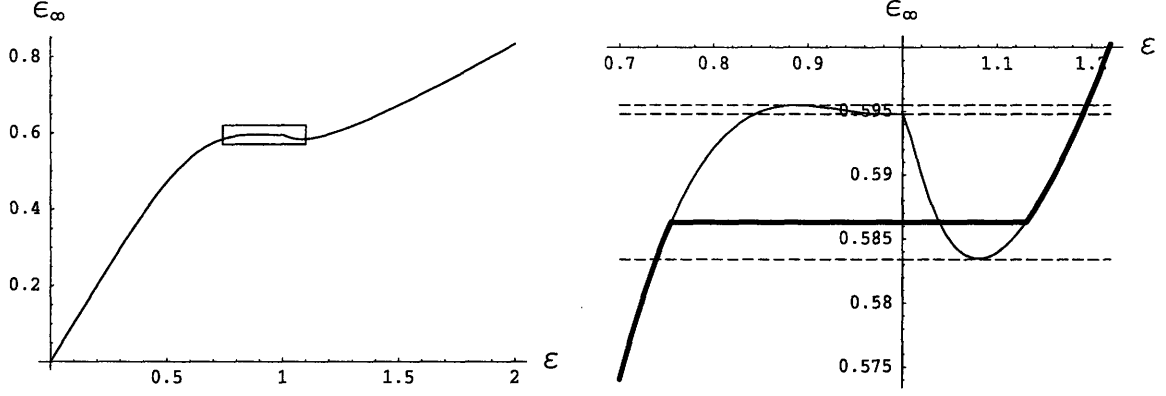


Figure 2-1: ϵ_∞ (determined by the embedding y at infinity) versus ϵ (determined either by $y(0)$, for Minkowski embeddings with $\epsilon < 1$, or by where the embedding intersects the horizon, for $\epsilon > 1$). The right panel zooms in on the vicinity of the critical embedding at $\epsilon = 1$. The stable embeddings and the first order phase transition are indicated by the thick curve; the metastable embeddings are indicated by the thin curves.

I first introduce parameters

$$L_0 \equiv y(0) , \quad \epsilon \equiv \frac{u_0^2}{L_0^2} = \frac{r_0^2}{2L_0^2} . \quad (2.11)$$

For Minkowski embeddings, ϵ takes value in the range $[0, 1]$, with $\epsilon = 0$ corresponding to zero temperature, and $\epsilon = 1$ to the critical embedding. Although ϵ_∞ that was introduced earlier has the advantage of being directly related to the fundamental parameters of the theory according to (1.42), the new parameter has the advantage that there is only one embedding for each value of ϵ . And, ϵ will turn out to be convenient for analyzing the equations of motion (1.41) and the fluctuations on D7-branes. When $\epsilon_\infty \ll 1$, $\epsilon \approx \epsilon_\infty$. A full analytic relation between ϵ and ϵ_∞ is not known, but given an ϵ one can readily find the corresponding ϵ_∞ numerically. For example, at $T = T_c$, $\epsilon = 0.756$ and $\epsilon_\infty = 0.586$ while for the critical embedding, $\epsilon = 1$ and $\epsilon_\infty = \epsilon_\infty^c = 0.5948$. The relation between ϵ_∞ and ϵ is depicted in Figure 2-1. In order to make this figure, for the black hole embeddings I have defined $\epsilon = 1/\sin^2 \theta$ where θ is the angle in the (y, ρ) plane of Figure 1-2 at the point at which the black hole embedding $y(\rho)$ intersects the black hole horizon $y^2 + \rho^2 = u_0^2$. That is, $1 < \epsilon < \infty$ parametrizes black hole embeddings which begin at different points along the black

hole horizon. The seven embeddings in Figure 1-2 have $\varepsilon = 0.25, 0.5, 0.756, 1.00, 1.13, 1.41$ and 4.35 , from top to bottom as they are ordered on the left, i.e. at the tip of the D7-brane at $y = 0$ for the Minkowski embeddings and at the horizon for the black hole embeddings.

Finally, it will also prove convenient to introduce dimensionless coordinates by a rescaling according to

$$t \longrightarrow \frac{R^2}{L_0}t, \quad x_i \longrightarrow \frac{R^2}{L_0}x_i, \quad \rho \longrightarrow L_0\rho, \quad y \longrightarrow L_0y, \quad (2.12)$$

after which the spacetime metric becomes

$$\frac{ds^2}{R^2} = G_{\mu\nu}dx^\mu dx^\nu = -f(u)dt^2 + r(u)^2 d\vec{x}^2 + \frac{1}{u^2} (d\rho^2 + \rho^2 d\Omega_3^2 + dy^2 + y^2 d\phi^2), \quad (2.13)$$

and the induced metric becomes

$$\frac{ds_{D7}^2}{R^2} = h_{ij}d\xi^i d\xi^j = -f(u)dt^2 + r^2 d\vec{x}^2 + \frac{1}{u^2} ((1 + y'(\rho)^2)d\rho^2 + \rho^2 d\Omega_3^2), \quad (2.14)$$

with

$$u^2 = y^2 + \rho^2, \quad f(u) = \frac{(u^4 - \varepsilon^2)^2}{u^2(u^4 + \varepsilon^2)}, \quad r^2(u) = u^2 + \frac{\varepsilon^2}{u^2}, \quad (2.15)$$

where both $G_{\mu\nu}$ and h_{ij} are now dimensionless. The equation of motion for $y(\rho)$ becomes

$$\frac{y''}{1 + y'^2} + 3\frac{y'}{\rho} + \frac{8}{u^2} \left(\frac{\rho y' - y}{\varepsilon^{-4}u^8 - 1} \right) = 0, \quad (2.16)$$

with the boundary conditions

$$y(0) = 1, \quad y'(0) = 0. \quad (2.17)$$

This form of the equations of motion that determine the embedding $y(\rho)$ will be useful in subsequent sections.

2.3 Meson Fluctuations at Nonzero Temperature

In this section I derive linearized equations of motion that describe the small fluctuations of the D7-brane position. A version of these equations have been derived and solved numerically by various authors (see e.g. [94, 100, 97, 96]). Here I will rederive the equations in a different form by choosing the worldvolume fields parameterizing the fluctuations in a more geometric way. The new approach gives a nice geometric interpretation for the embedding and small fluctuations. It also simplifies the equations dramatically, which will enable us to extract analytic information for the meson dispersion relations in the next section. The main ideas and results are presented in this section but the technical details are left to Appendix A. That appendix will also contain a general discussion of the fluctuations of a brane embedded in any curved spacetime.

The action for small perturbations of the D7-brane location can be obtained by inserting

$$X^\mu(\xi) = X_0^\mu(\xi^i) + \delta X^\mu(\xi^i) \quad (2.18)$$

into the D-brane action (1.31) and (1.32), where $X_0^\mu(\xi)$ denotes the background solution that describes the embedding in the absence of fluctuations, and δX^μ describes small fluctuations transverse to the brane. For the D7-brane under consideration, in the coordinates used in (2.13) the general expression (2.18) becomes

$$y(\xi) = y_0(\rho) + \delta y(\xi), \quad \phi(\xi) = \delta\phi(\xi), \quad (2.19)$$

with $y_0(\rho)$ the embedding solution obtained by solving (2.16). The choice of the worldvolume fields $\delta y, \delta\phi$ is clearly far from unique. Any two independent functions of δy and $\delta\phi$ will also do. (This freedom corresponds to the freedom to choose different coordinates for the 10-dimensional space within which the D7-brane is embedded.) In fact, it is awkward to use δy and $\delta\phi$ as worldvolume fields since they are differences in coordinates and thus do not transform nicely under coordinate changes. Using them obscures the geometric interpretation of the equations. Below we will adopt

a coordinate system which makes the geometric interpretation manifest. Since our discussion is rather general, not specific to the particular system under consideration, it will be described initially using general language.

Consider a point $X_0(\xi)$ on the brane. The tangent space at X_0 perpendicular to the D7-brane is a 2-dimensional subspace V_0 spanned by unit vectors n_1^μ, n_2^μ which are orthogonal to the branes, i.e.

$$n_1^\mu \propto \left(\frac{\partial}{\partial y} \right)^\mu - y'_0(\rho) \left(\frac{\partial}{\partial \rho} \right)^\mu, \quad (2.20)$$

$$n_2^\mu \propto \left(\frac{\partial}{\partial \phi} \right)^\mu. \quad (2.21)$$

Any vector η^μ in V_0 can be written as

$$\eta^\mu = \chi_1 n_1^\mu + \chi_2 n_2^\mu. \quad (2.22)$$

One can then establish a map from (χ_1, χ_2) to small perturbations δX^μ in (2.18) by shooting out geodesics of unit affine parameter from X_0 with tangent η^μ . Such a map should be one-to-one for $\chi_{1,2}$ sufficiently small. Clearly χ_1 and χ_2 behave like scalars under coordinate changes and will be used here as the worldvolume fields parameterizing small fluctuations of the position of the brane. By solving the geodesic equation, δX^μ can be expressed in terms of $\chi_{1,2}$ as

$$\delta X^\mu = \eta^\mu - \frac{1}{2} \Gamma_{\sigma\tau}^\mu \eta^\sigma \eta^\tau + \dots, \quad (2.23)$$

where $\Gamma_{\alpha\beta}^\mu$ are the Christoffel symbols of the 10-dimensional metric. Note that the choice of $\chi_{1,2}$ is not unique. There is in fact an $SO(2)$ “gauge” symmetry under which $\chi_{1,2}$ transform as a vector, since one can make different choices of basis vectors n_1 and n_2 that are related by a local $SO(2)$ transformation.

On inserting (2.23) and (2.18) into the Dirac-Born-Infeld action (1.31) and, doing some algebra discussed further in Appendix A, one finds that the equations of motion satisfied by X_0 (i.e. which determine the embedding in the absence of fluctuations)

can be written as

$$K_s = 0, \quad (2.24)$$

and the quadratic action for small fluctuations $\chi_{1,2}$ about X_0 takes the form

$$S_{D7} = \mu_7 R^8 \int d^8 \xi \sqrt{-\det h_{ij}} \left(-\frac{1}{2} D_i \chi_s D^i \chi_s - \frac{1}{2} \chi_s \chi_t (-K_{sij} K_t^{ij} + R_{sijt} h^{ij}) \right), \quad (2.25)$$

where $s, t = 1, 2$ and where the following quantities have been defined:

$$h_{ij} = G_{\mu\nu} \partial_i X_0^\mu \partial_j X_0^\nu, \quad R_{sijt} = n_s^\sigma n_t^\tau \partial_i X_0^\mu \partial_j X_0^\nu R_{\sigma\mu\nu\tau}, \quad (2.26)$$

$$K_{sij} = \partial_i X_0^\mu \partial_j X_0^\nu \nabla_\mu n_{s\nu}, \quad K_s = K_{sij} h^{ij}, \quad (2.27)$$

$$D_i \chi_s = \partial_i \chi_s + U_{ist} \chi_t, \quad U_{ist} = n_{s\nu} \partial_i X_0^\mu \nabla_\mu n_t^\nu. \quad (2.28)$$

Note that h_{ij} is the induced metric on the brane and i, j are raised by h^{ij} . $R_{\sigma\mu\nu\tau}$ is the Riemann tensor for the 10-dimensional spacetime. K_{sij} is the extrinsic curvature of the brane along the direction n_s^μ . U_{ist} (which is antisymmetric in s, t) is an $SO(2)$ connection for the $SO(2)$ gauge symmetry and D_i is the corresponding covariant derivative. We see here that the embedding equations of motion (2.24) have a very simple geometric interpretation as requiring that the trace of the extrinsic curvature in each orthogonal direction has to vanish, which is what one expects since this is equivalent to the statement that the volume of the D7-brane is extremal.

The symmetries of the D7-brane embedding that we are analyzing allow us to further simplify the action (2.25). Because n_2^μ in (2.21) is proportional to a Killing vector and is hypersurface orthogonal, U_{i12} and K_{2ij} vanish identically. (See Appendix A for a proof, and for the definition of hypersurface orthogonal.) With $K_2 = 0$ satisfied as an identity, the remaining equation of motion specifying the embedding, namely $K_1 = 0$, is then equivalent to the equation of motion for y that was derived in Section 2.2, namely (2.16). After some further algebra (see Appendix A) one finds

that the action (2.25) for small fluctuations reduces to

$$S_{D7} = \mu_7 R^8 \int d^8 \xi \sqrt{-\det h_{ij}} \left(-\frac{1}{2} (\partial \chi_1)^2 - \frac{1}{2} (\partial \chi_2)^2 - \frac{1}{2} m_1^2 \chi_1^2 - \frac{1}{2} m_2^2 \chi_2^2 \right) \quad (2.29)$$

with

$$\begin{aligned} m_1^2 &= R_{11} + R_{2112} + 2R_{22} + {}^{(8)}R - R, \\ m_2^2 &= -R_{22} - R_{2112}, \end{aligned} \quad (2.30)$$

where

$$\begin{aligned} R_{2112} &= n_2^\mu n_1^\nu n_1^\sigma n_2^\tau R_{\mu\nu\sigma\tau}, \\ R_{11} &= n_1^\nu n_1^\sigma R_{\nu\sigma}, \\ R_{22} &= n_2^\nu n_2^\sigma R_{\nu\sigma}, \end{aligned} \quad (2.31)$$

and where R is the Ricci scalar for the 10-dimensional spacetime while ${}^{(8)}R$ is the Ricci scalar for the induced metric h_{ij} on the D7 brane. The background metric h_{ij} is given by (2.13). The “masses” m_1^2 and m_2^2 are nontrivial functions of ρ . Since the worldvolume metric is regular for Minkowski embeddings, they are well-defined for $\rho \in [0, \infty)$.

The result in the form (2.25) is very general, applicable to the embedding of any codimension 2 branes in any spacetime geometry. For example, we can apply it to the embedding of D7-branes at zero temperature given by (1.33) and learn that the meson fluctuations at zero temperature are described by (2.29) with

$$m_1^2 = m_2^2 = -\frac{3\rho^2 + 4}{1 + \rho^2}, \quad (2.32)$$

and with h_{ij} in (2.29) given by (2.5). It is also straightforward to check that equations of motion derived from (2.29) with (2.32) and h_{ij} given by (2.5) are equivalent to (2.6). At zero temperature, (2.4) and (2.5) are already simple enough and the formalism described here does not gain us further advantage. However, at nonzero temperature

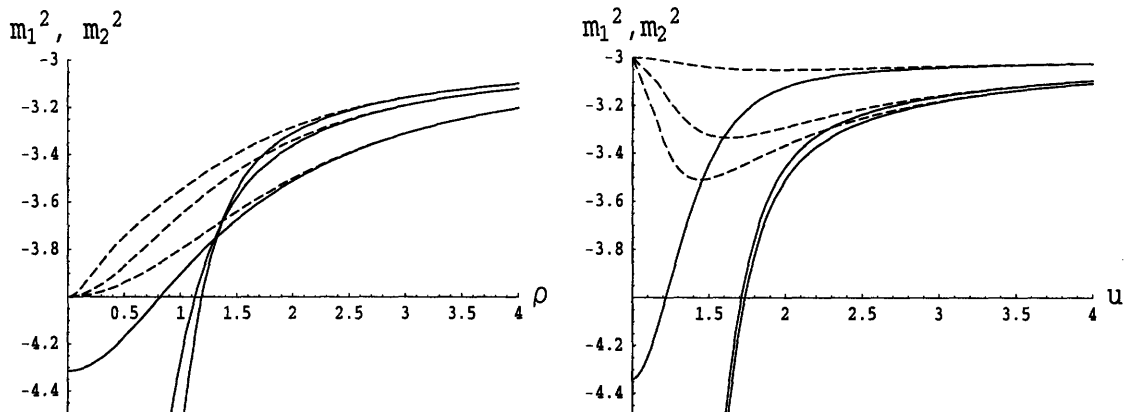


Figure 2-2: The squared “masses” of the two orthonormal geometric modes of the D7-brane fluctuations for Minkowski embeddings (left panel) and black hole embeddings (right panel). In each figure, m_1^2 (m_2^2) is plotted as a solid (dashed) line for three values of ϵ_∞ . The Minkowski embeddings have $\epsilon_\infty = 0.587, 0.471$ and 0.249 (top to bottom) and the black hole embeddings have $\epsilon_\infty = 1.656, 0.647$ and 0.586 (again top to bottom, this time with temperature increasing from top to bottom.) The Minkowski embedding is plotted as a function of ρ and the black hole embedding as a function of u with the horizon on the left at $u = 1$.

the equations of motion obtained from (2.29) yield both technical and conceptual simplification. In Section 2.4, I shall use the formalism that has been developed here to obtain the dispersion relations at large momentum analytically.

Before turning to the dispersion relations, I plot the “masses” m_1^2 and m_2^2 for various D7-brane embeddings at nonzero temperature in Figure 2-2. Using a numerical solution for $y(\rho)$, it is straightforward to evaluate (2.30), obtaining the masses in the figure. For the black hole embeddings, the D7-brane begins at the black hole horizon at $u = 1$ rather than at $\rho = 0$, see Figure 1-2, making it more convenient to plot the masses as a function of u rather than ρ . We can infer several important features from the masses plotted in Figure 2-2. As $\rho \rightarrow \infty$, both m_1^2 and m_2^2 approach -3 for all the embeddings. This implies that χ_1 and χ_2 couple to boundary operators of dimension 3, as shown in [104] by explicit construction of the operators in the boundary theory which map onto χ_1 and χ_2 . As $\epsilon \rightarrow 1$ from below for the Minkowski embeddings (from above for the black hole embeddings), the behavior of m_1^2 at the tip of the D7-brane at $\rho = 0$ (at $u = 1$) becomes singular, diverging to minus infinity. This is

a reflection of the curvature divergence at the tip of the critical embedding at $\rho = 0$ ($u = 1$).

I have referred to m_1^2 and m_2^2 as “masses” in quotes because the equations of motion obtained by straightforward variation of the action (2.29) in which they arise yields

$$\frac{1}{\sqrt{-h}} \partial_i (\sqrt{-h} h^{ij} \partial_j \chi_s) - m_s^2 \chi_s = 0, \quad s = 1, 2, \quad (2.33)$$

with $h \equiv \det h_{ij}$, which is a Klein-Gordon equation in a curved spacetime with spatially varying “masses”. If we could cast the equations of motion in such a way that they take the form of a Schrödinger equation with some potential, this would make it possible to infer qualitative implications for the nature of the meson spectrum immediately via physical intuition, which is not possible to do by inspection of the curves in Figure 2-2. To achieve this, I recast the equations of motion as follows. I introduce a “tortoise coordinate” z defined by

$$dz^2 = \frac{1}{u^2 f(u)} (1 + y_0'(\rho)^2) d\rho^2, \quad (2.34)$$

in terms of which the induced metric on the brane takes the simple form

$$\frac{ds_{D7}^2}{R^2} = f(-dt^2 + dz^2) + r^2(u) d\vec{x}^2 + \frac{\rho^2}{u^2} d\Omega_3^2. \quad (2.35)$$

(The additive constant in the definition of z is chosen so that $z = 0$ at $\rho = 0$.) Then, we need solutions to the equations of motion (2.33) that separate according to the Ansatz

$$\chi_s = \frac{\psi_s(z)}{Z} e^{-i\omega t + i\vec{k} \cdot \vec{x}} Y_{\ell m \tilde{m}}(\Omega_3) \quad (2.36)$$

with

$$Z \equiv \left(\frac{\sqrt{-h}}{f} \right)^{\frac{1}{2}} = \left(\frac{r\rho}{u} \right)^{\frac{3}{2}}. \quad (2.37)$$

Such a solution is the wave function for a scalar meson of type $s = 1$ or $s = 2$ with energy ω and wave vector \vec{k} (note the plane wave form for the dependence on (3+1)-dimensional Minkowski space coordinates) and with quantum numbers ℓ, m

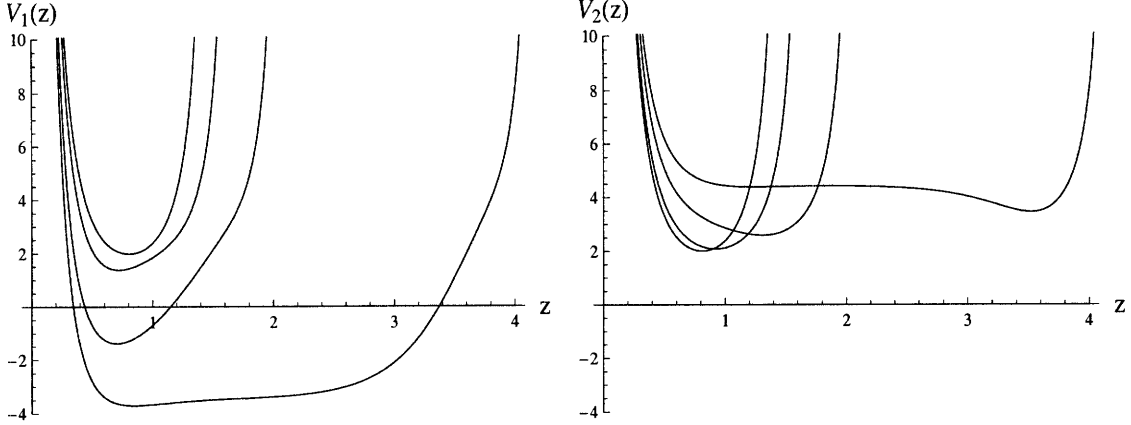


Figure 2-3: Potentials $V_s(z)$ for Minkowski embeddings at various temperatures, all with $k = \ell = 0$. The left (right) panel is for $s = 1$ ($s = 2$). In each panel, the potentials are drawn for $\epsilon_\infty = 0.249, 0.471, 0.586$ and 0.5948 , with the potential widening as the critical embedding is approached, i.e. as ϵ_∞ is increased. The $\epsilon_\infty = 0.586$ potential is that for the Minkowski embedding at the first order transition; the widest potential shown describes the fluctuations of a metastable Minkowski embedding very close to the critical embedding. The potential becomes infinitely wide as the critical embedding is approached, but it does so only logarithmically in $\epsilon_\infty^c - \epsilon_\infty$. Note that the tip of the D7-brane is at $z = 0$, on the left side of the figure, whereas $\rho = \infty$ has been mapped to a finite value of the tortoise coordinate $z = z_{\max}$, corresponding to the “wall” on the right side of each of the potentials in the figure.

and \tilde{m} specifying the angular momentum spherical harmonic on the “internal” 3-sphere. (Rotation symmetry of the 3-sphere guarantees that the quantum numbers m and \tilde{m} will not appear in any equations.) The $\psi_s(z)$ that I must solve for are the wave functions of the meson states in the fifth dimension.

The reasons for the introduction of the tortoise coordinate z and the Ansatz (2.36) for the form of the solution become apparent when we discover that the equations of motion (2.33) now take the Schrödinger form

$$-\frac{\partial^2}{\partial z^2}\psi_s + V_s(k, z)\psi_s = \omega^2\psi_s, \quad (2.38)$$

with potentials for each value of $k = |\vec{k}|$ and for each of the two scalar mesons labelled by $s = 1, 2$ given by

$$V_s(k, z) = \frac{Z''}{Z} + fm_s^2 + \frac{fk^2}{r^2} + \frac{\ell(\ell+2)fu^2}{\rho^2}. \quad (2.39)$$

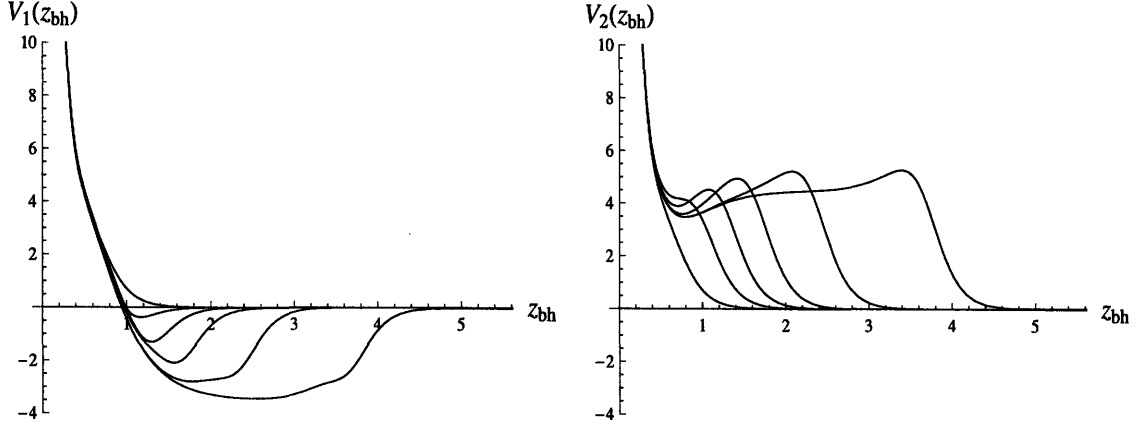


Figure 2-4: Potentials $V_s(z_{bh})$ for black hole embeddings at various temperatures, all with $k = \ell = 0$. The left (right) panel is for $s = 1$ ($s = 2$). In each panel, the potentials are drawn for $\epsilon_\infty = 3584.$, 0.647, 0.586, 0.586, 0.5940 and 0.5948, from narrower to wider, with the potential widening as the critical embedding is approached from the right along the curve in Figure 2-1. Note that z_{bh} is defined such that the horizon is at $z_{bh} = \infty$, and $\rho = \infty$ is at $z_{bh} = 0$. The narrower (wider) of the two potentials with $\epsilon_\infty = 0.586$ is that for the stable (unstable) black hole embedding: at this ϵ_∞ , there is a first order transition (see Figure 2-1) between the stable Minkowski embedding (whose potential is found in Figure 2.3) and the stable black hole embedding. The potentials at $\epsilon_\infty = 0.5940$ and 0.5948 describe fluctuations of metastable black hole embeddings, with the latter being a black hole embedding very close to the critical embedding.

Here, the prime denotes differentiation with respect to z . Recall that $u^2 = \rho^2 + y_0^2(\rho)$ and it should be understood that ρ , u , and y_0 are all functions of the tortoise coordinate z . Figures 2.3 and 2-4 provide plots of $V_s(z)$ with $k = \ell = 0$ for $s = 1, 2$ and for Minkowski (Figure 2.3)) and black hole (Figure 2-4) embeddings at various temperatures. With the tortoise coordinate z defined as described above, in a Minkowski embedding z extends from $z = 0$, which corresponds to the tip of the D7-brane, to

$$z = z_{\max} \equiv \int_0^\infty \frac{d\rho}{u} \sqrt{\frac{1 + y_0'(\rho)^2}{f(u)}}, \quad (2.40)$$

which corresponds to $\rho = \infty$. Here, $u(\rho)$ and $f(u)$ are given in (2.15). This defines the width of the potentials for the Minkowski embeddings shown in Figure 2.3, which get wider and wider as the critical embedding is approached.

If I had used the same tortoise coordinate for the black hole embeddings, the

lower limit of the integral (2.40) is then the ρ at which $y(\rho)$ intersects the horizon and $f(u)$ vanishes, making the integral divergent. This means that $\rho = \infty$ is mapped onto $z = \infty$ for black hole embeddings. It is more convenient to define z_{bh} by first choosing the integration constant such that $\rho = \infty$ corresponds to $z_{bh} = 0$, and then multiplying by -1 . This is the tortoise coordinate that is used in Figure 2-4

The qualitative implications for the meson spectrum can be inferred immediately from Figures 2.3 and 2-4, since we have intuition for solutions of the Schrödinger equation. We can see immediately that the Minkowski embeddings all have a discrete spectrum of meson excitations, while the fluctuations of the black hole embeddings all have continuous spectra. This justifies the identification of the first order phase transition from Minkowski to black hole embeddings that was described in Section 2.2 as the transition at which mesons dissociate.

In addition to the continuum of fluctuations of the black hole embeddings, which are those embeddings where the D7-brane touches the black hole horizon, there are discrete energies at which the fluctuations at the horizon are purely infalling, with no outgoing component. In Figure 2-4, these modes are purely right-moving at $z_{bh} \rightarrow \infty$. Such modes, the real parts of whose energies lie within the continuum, are called quasinormal modes; their energies also have large imaginary parts due to their coupling to the continuum [97, 104].

Other phenomena that are discussed quantitatively in [96, 97, 104] can be inferred qualitatively directly from the potentials in Figures 2.3 and 2-4. For example we can see from the left panel in Figure 2-4 that, in addition to the continuous spectrum characteristic of all black hole embeddings, those embeddings that are close to the critical embedding will have discrete bound states for the ψ_1 fluctuations. These bound states will always have negative mass-squared, representing an instability. This instability arises only in a regime of temperatures at which the black hole embeddings already have a higher free energy than the stable Minkowski embedding, that is, at temperatures below the first order transition [96]. They therefore represent an instability of the branch of the spectrum that was already metastable. Similarly, the left panel of Figure 2.3 shows that Minkowski embeddings close to the critical

embedding also have negative mass-squared bound states; again, this instability only occurs for embeddings that were already only metastable [96]. We can see from the right panel of Figure 2-4 that resonances may also occur in the ψ_2 channel for the black hole embedding. They are interpreted as quasi-normal modes; close to the transition these resonances become more well-defined and may be interpreted as quasi-particle meson excitations [97, 104].

2.4 Dispersion Relations

The groundwork needed to evaluate the dispersion relations for the ψ_1 and ψ_2 scalar mesons, corresponding in the gravity dual to fluctuations of the position of the D7-brane is now complete. These fluctuations are governed by (2.38), which are Schrödinger equations with the potentials $V_1(k, z)$ or $V_2(k, z)$ given by (2.39) and (2.30) and depicted in Figure 2.3. The eigenvalues of these Schrödinger equations are ω^2 for the mesons. So, it is now a straightforward numerical task to find the square root of the eigenvalues of the Schrödinger equation with, say, potential $V_1(k, z)$, at a sequence of values of k . At $k = 0$, this will reproduce the results that were reviewed in Section 2.2.2. As we increase k , the dispersion relation ω of each of the ψ_1 mesons is mapped out. In Figure 2-7 in Section 2.4.3 below, it is shown that the dispersion relations for the ground state ψ_1 meson at several values of the temperature. Such dispersion relations have also been obtained numerically in [96]. In order to more fully understand the dispersion equations, and their implications, let us focus first on analytic results. The potentials are complicated enough that there are no analytic solutions for the general case. I will show, however, that in the low temperature and/or the large- k limit, the equations simplify sufficiently that the dispersion relations can be found analytically. It is the large- k limit that is of interest to us, but it is very helpful to begin first at low temperatures, before then analyzing the dispersion relations in the large- k limit at any temperature below the dissociation temperature.

2.4.1 Low Temperature

At low temperature, $\varepsilon \ll 1$, the D7-branes are far from the horizon of the black hole. In this regime, I can expand various quantities that occur in the potentials (2.39) as power series in ε^2 . I shall then be able to determine the dispersion relations analytically to order ε^2 in two limits: (i) $\varepsilon \rightarrow 0$ at fixed k , meaning in particular that $\varepsilon k \rightarrow 0$; and (ii) $\varepsilon \rightarrow 0$ at fixed, large, εk , meaning that $k \rightarrow \infty$ as $\varepsilon \rightarrow 0$.

Let us begin by seeing how the equation (2.16) that determines the embedding $y(\rho)$ in the absence of fluctuations simplifies at small ε . Expanding $y(\rho)$ as a power series in ε , one immediately finds that $y(\rho)$ is modified only at order ε^4 , i.e.

$$y(\rho) = 1 + \mathcal{O}(\varepsilon^4), \quad (2.41)$$

which in turn implies that

$$\epsilon_\infty = \varepsilon (1 + \mathcal{O}(\varepsilon^4)). \quad (2.42)$$

Thus, if I work only to order ε^2 , I can treat the embedding as being $y(\rho) = 1$, as at zero temperature, and can neglect the difference between ε and ϵ_∞ (which is to say the difference between $y(0)$ and $y(\infty)$). From (2.15), then,

$$u^2 = 1 + \rho^2 + \mathcal{O}(\varepsilon^4), \quad f(u) \approx u^2 \left(1 - \frac{3\varepsilon^2}{u^4} + \mathcal{O}(\varepsilon^4) \right). \quad (2.43)$$

By expanding the curvature invariants in (2.30) to order ε^2 , I find that

$$m_1^2 = m_2^2 = -\frac{4 + 3\rho^2}{1 + \rho^2} + \mathcal{O}(\varepsilon^4), \quad (2.44)$$

meaning that to order ε^2 the mass terms occurring in (2.16) are as in (2.32) at zero temperature. Next, I expand the tortoise coordinate (2.34), finding

$$z = \tan^{-1} \rho + \varepsilon^2 g(\rho) + \mathcal{O}(\varepsilon^4), \quad \text{with } g(\rho) = \frac{3}{16} \left(3 \tan^{-1} \rho + \frac{\rho(5 + 3\rho^2)}{(1 + \rho^2)^2} \right). \quad (2.45)$$

I can then invert (2.45) to obtain ρ in terms of z :

$$\rho = \tan z - \varepsilon^2 \frac{g(\tan z)}{\cos^2 z} + \dots \quad (2.46)$$

Using these equations, I find that the potential (2.39) is given to order $O(\varepsilon^2)$ by

$$V(z) = k^2 + V^0(z) - 4\varepsilon^2 k^2 \cos^4 z + \varepsilon^2 h(z) + \mathcal{O}(\varepsilon^4, \varepsilon^4 k^2), \quad (2.47)$$

where

$$V^0(z) \equiv \frac{4\alpha_\ell}{\sin^2 2z} - 1, \quad \text{with} \quad \alpha_\ell \equiv \frac{3}{4} + \ell(\ell + 2), \quad (2.48)$$

is the potential at zero temperature, and

$$h(z) = \frac{3\alpha_\ell (\sin^2(2z) + 6z \cot(2z) - 3)}{2 \sin^2(2z)} + \frac{9}{4} \sin^2(2z). \quad (2.49)$$

I shall not need the explicit form of $h(z)$ in the following.

Low Temperature at Fixed k

At zero temperature ($\varepsilon = 0$), solving the Schrödinger equation (2.38) with potential $V^0(z)$ yields the eigenvalues (and hence the dispersion relations)

$$\omega^2 - k^2 = m_{n\ell}^2, \quad n = 1, 2, \dots, \quad \ell = 0, 1, \dots, \quad (2.50)$$

with $m_{n\ell}$ given by (2.7) (after restoring its dimensions). If I work in the limit $\varepsilon \rightarrow 0$ with k fixed, then both the $\mathcal{O}(\varepsilon^2)$ and the $\mathcal{O}(\varepsilon^2 k^2)$ terms that describe the effects of nonzero but small temperature in the potential (2.48) can be treated using quantum mechanical perturbation theory. To first order in ε^2 , the dispersion relation becomes

$$\omega^2 = v_{n\ell}^2 k^2 + m_{n\ell}^2 + \varepsilon^2 b_{n\ell} + \mathcal{O}(\varepsilon^4) \quad (2.51)$$

with

$$\begin{aligned}
v_{n\ell}^2 &= 1 - a_{n\ell} \varepsilon^2, \\
a_{n\ell} &= 4 \langle n, \ell | \cos^4 z | n, \ell \rangle, \\
b_{n\ell} &= \langle n, \ell | h(z) | n, \ell \rangle,
\end{aligned} \tag{2.52}$$

where $|n, \ell\rangle$ are the eigenfunctions of the Hamiltonian with the unperturbed potential V^0 of (2.48), with wave functions

$$\psi_{n\ell}^0(z) = \Gamma\left(\ell + \frac{3}{2}\right) 2^{1+\ell} \sqrt{\frac{n(n+\ell+\frac{3}{2})}{\pi\Gamma(n+2\ell+3)}} (\sin z)^{\frac{3}{2}+\ell} C_n^{(\ell+\frac{3}{2})}(\cos z). \tag{2.53}$$

Using the recursion relations for the generalized Gegenbauer polynomials $C_n^{(\alpha)}$ (See Chapter 22 in [107]), $a_{n\ell}$ can be evaluated analytically (using the identities (D.10), (D.11) and (D.12)), yielding

$$a_{n\ell} = 2 - \frac{(n+2\ell+1)(n+2\ell+2)}{4(n+\ell+1/2)(n+\ell+3/2)} - \frac{(n+1)(n+2)}{4(n+\ell+3/2)(n+\ell+5/2)}. \tag{2.54}$$

So, for the ground state with $n = \ell = 0$, $a_{00} = 18/15$. $b_{n\ell}$ can be computed numerically, but I will not do so here. The dispersion relation (2.51) is valid for $\varepsilon^2 \ll 1$ and $\varepsilon^2 k^2 \ll 1$, meaning that at small ε it is valid for $k \ll 1/\varepsilon$. No matter how small ε is, the perturbation theory breaks down for $k \sim \frac{1}{\varepsilon}$ and (2.51) does not apply. In other words, the low temperature $\varepsilon \rightarrow 0$ limit and the high meson momentum $k \rightarrow \infty$ limits do not commute. Even though (2.51) cannot be used to determine the meson velocity at large k , it is suggestive. We shall see below that in the large- k limit, the meson velocity is indeed $1 - \mathcal{O}(\varepsilon^2)$, but the coefficient of ε^2 is not given by (2.54).

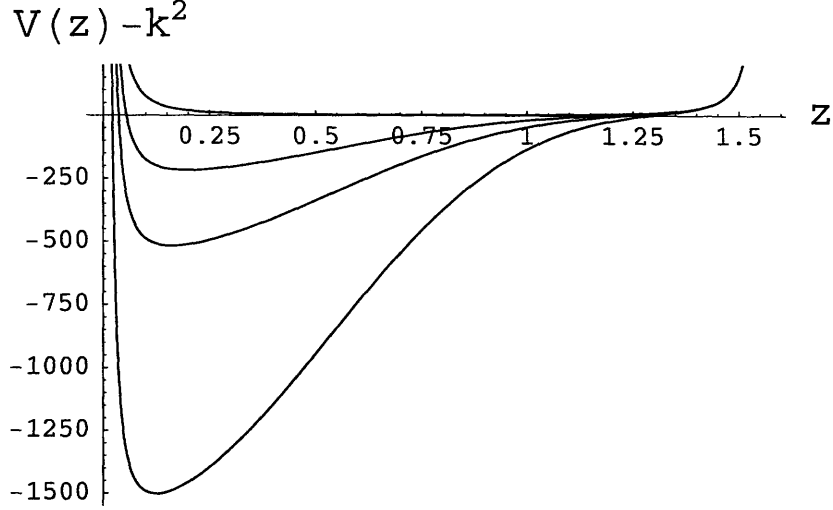


Figure 2-5: The potential (2.56) with $\varepsilon = 0.756$ and $k = 5, 20$ and 100 . We see that as $\Lambda = \varepsilon^2 k^2$ increases, the minimum of the potential moves towards $z = 0$, the potential deepens, and the curvature around the minimum increases.

Low Temperature at Fixed, Large, εk

To explore the behavior of the dispersion relations in the large- k limit, let us now consider the following scaling limit

$$\varepsilon \rightarrow 0, \quad k \rightarrow \infty, \quad \text{with} \quad \Lambda^2 = k^2 \varepsilon^2 = \text{finite}. \quad (2.55)$$

In this limit, the potential (2.39) again greatly simplifies and, consistent with (2.47), becomes

$$V(z) = k^2 + \frac{4\alpha_\ell}{\sin^2 2z} - 1 - 4\Lambda^2 \cos^4 z. \quad (2.56)$$

This potential is valid in the limit (2.55) for any value of Λ , small or large. If Λ is small, the dispersion relation can be determined using perturbation theory as before, yielding (2.51) without the $\varepsilon^2 b_{n\ell}$ term. In order to analyze the large- k regime, consider $\Lambda \gg 1$, and seek to evaluate the dispersion relation as an expansion in $1/\Lambda$. For this purpose, notice that as $\Lambda \rightarrow \infty$ the potential (2.56) develops a minimum at

$$z_0 = \left(\frac{\alpha_\ell}{8\Lambda^2} \right)^{\frac{1}{4}} \rightarrow 0 \quad \text{for} \quad \Lambda \rightarrow \infty, \quad (2.57)$$

as depicted in Figure 2-5. The curvature about the minimum is $V''(z_0) \propto \Lambda^2$. Thus, if we imagine watching how the wave function changes as we take the large- Λ limit, we will see the wave function getting more and more tightly localized around the point $z = z_0$ which gets closer and closer to $z = 0$. That is, the wave function will be localized around the tip of the brane $z = 0$. This motivates us to expand the potential around $z = 0$, getting

$$V(z) - k^2 + 1 = \alpha_l \left(\frac{1}{z^2} + \frac{4}{3} + \frac{16z^2}{15} + \dots \right) - 4\Lambda^2 \left(1 - 2z^2 + \frac{5z^4}{3} + \dots \right). \quad (2.58)$$

If I now introduce a new variable $\xi = \Lambda^{\frac{1}{2}}z$, the Schrödinger equation (2.38) becomes

$$\left(-\partial_\xi^2 + \frac{\alpha_l}{\xi^2} + \frac{1}{4}\Omega^2\xi^2 \right) \psi + \tilde{V}\psi = E\psi, \quad (2.59)$$

where

$$\Omega^2 = 32, \quad E = \frac{1}{\Lambda}(\omega^2 - k^2 + 4\Lambda^2), \quad (2.60)$$

and \tilde{V} contains only terms that are higher order in $1/\Lambda$:

$$\tilde{V} = \frac{1}{\Lambda} \left(\frac{4\alpha_l}{3} - 1 - \frac{20}{3}\xi^4 \right) + \mathcal{O}(1/\Lambda^2). \quad (2.61)$$

Thus to leading order in the large Λ limit, I can drop the \tilde{V} term in (2.59). Upon so doing, and using the expression (2.48) for α_l , the equation (2.59) becomes that of a harmonic oscillator in 4 dimensions with mass $\frac{1}{2}$ and frequency Ω . This quantum mechanics problem can be solved exactly, with wave functions given by

$$\psi_{nl} = \xi^{3/2+\ell} L_\nu^{(\ell+1)} \left(\frac{\Omega}{2}\xi^2 \right) e^{-\frac{\Omega}{4}\xi^2}, \quad (2.62)$$

up to a normalization constant, and with eigenvalues given by

$$E_n = \Omega(n+2), \quad n = 0, 1, \dots \quad (2.63)$$

In (2.62), $L_\nu^{(\alpha)}$ is the generalized Laguerre polynomial of order (See Chapter 22 in [107])

$$\nu = \frac{n - \ell}{2} . \quad (2.64)$$

The allowed values of ℓ are determined by the requirement that ν must be a non-negative integer. The degeneracy of n -th energy level is $\frac{(n+3)!}{3!n!}$. Higher order corrections in $1/\Lambda$ can then be obtained using perturbation theory. For example, with the next order correction included, the degeneracy among states with different ℓ and the same n is lifted and the eigenvalues are given by

$$E_{n\ell} = \Omega(n + 2) + \frac{c_{n\ell}}{\Lambda} + \mathcal{O}(1/\Lambda^2), \quad (2.65)$$

with

$$c_{n\ell} = -\frac{5}{4}(n + 2)^2 + \frac{7}{4}\ell(\ell + 2) . \quad (2.66)$$

Thus, in the small- ε limit with Λ fixed and large, we find using (2.60) that the dispersion relation becomes

$$\omega_{n\ell}^2 = (1 - 4\varepsilon^2)k^2 + 4\sqrt{2}(n + 2)k\varepsilon + c_{n\ell} + \mathcal{O}(1/k) . \quad (2.67)$$

Notice that $c_{n\ell}$ is negative for the ground state, and indeed for any n at sufficiently small ℓ . We learn from this calculation that in the large- k limit, at low temperatures mesons move with a velocity given to order ε^2 by $v = \sqrt{1 - 4\varepsilon^2} = 1 - 2\varepsilon^2$. Recalling that to the order I am working $\epsilon_\infty = \varepsilon$, this result can be expressed in terms of T , m_q and λ using (1.42). In the next subsection, I shall obtain the meson velocity at large k for any ε .

2.4.2 Large- k Dispersion Relation at Generic Temperature

The technique of the previous subsection can be generalized to analyze the dispersion relation in the large- k limit at a generic temperature below the dissociation temperature. For general $\varepsilon < 1$, one again observes that the potential has a sharper and

sharper minimum near the tip of the brane $z = 0$ as k becomes larger and larger. Thus, in the large k limit, I only need to solve the Schrödinger equation near $z = 0$.

To find the potential $V(z)$ as a power series in z near $z = 0$, one needs to know the solution $y(\rho)$ of (2.16) near the tip of the brane at $\rho = 0$:

$$y = 1 + \frac{\rho^2}{\varepsilon^{-4} - 1} + \frac{\varepsilon^4(5 + 5\varepsilon^4 - 3\varepsilon^8)}{3(\varepsilon^4 - 1)^3} \rho^4 + \mathcal{O}(\rho^4). \quad (2.68)$$

At small ρ , using the expansion of y in (2.68), I find the tortoise coordinate z has the expansion

$$z = \frac{\sqrt{1 + \varepsilon^2}}{1 - \varepsilon^2} \rho + \mathcal{O}(\rho^3). \quad (2.69)$$

Using (2.68) and (2.69) in (2.39), after some algebra we find

$$V_s(z) = k^2 \left(v_0^2 + \frac{1}{4} \Omega^2 \varepsilon^2 z^2 + \beta_\ell z^4 + \dots \right) + \frac{\alpha_\ell}{z^2} + \gamma_{s\ell} + \mathcal{O}(z^2), \quad (2.70)$$

where

$$v_0 = \frac{1 - \varepsilon^2}{1 + \varepsilon^2}, \quad (2.71)$$

$$\Omega^2 = \frac{32(1 - \varepsilon^2)^2(1 + \varepsilon^4)}{(1 + \varepsilon^2)^5}, \quad (2.72)$$

$$\beta_\ell = -\Omega^2 \varepsilon^2 \frac{5 - 36\varepsilon^2 + 28\varepsilon^4 - 36\varepsilon^6 + 5\varepsilon^8}{24(1 + \varepsilon^2)^3}, \quad (2.73)$$

$$\gamma_{1\ell} = \frac{\ell(\ell + 2) \left(\frac{4}{3} + 4\varepsilon^2 + \frac{4}{3}\varepsilon^4 + 4\varepsilon^6 + \frac{4}{3}\varepsilon^8 \right) - 56\varepsilon^4}{(1 + \varepsilon^2)^3}, \quad (2.74)$$

$$\gamma_{2\ell} = \gamma_{1\ell} + \frac{80\varepsilon^4}{(1 + \varepsilon^2)^3}, \quad (2.75)$$

and where α_ℓ is given by (2.48). We can understand why the leading difference between the potentials V_1 and V_2 for the mesons ψ_1 and ψ_2 arises in this approximation in the constant terms $\gamma_{1\ell}$ and $\gamma_{2\ell}$ as follows. We can see from (2.39) that the difference between V_1 and V_2 comes only from m_1^2 and m_2^2 , which do not enter multiplied by k^2 and so cannot affect v_0 , Ω^2 or β_ℓ . Furthermore, m_1^2 and m_2^2 are curvature invariants,

see (2.30), and must therefore be smooth as $\rho \rightarrow 0$ because for Minkowski embeddings the D7-brane is smooth at $\rho = 0$. This means that m_1^2 and m_2^2 cannot affect the coefficient of $1/z^2$ in (2.70).

I can now obtain the dispersion relations from the Schrödinger equations with potentials (2.70) as was done in the previous subsection. After making the rescaling $z = k^{-1/2}\xi$, the Schrödinger equation (2.38) takes exactly the form (2.59), with

$$E = \frac{1}{k}(\omega^2 - v_0^2 k^2), \quad (2.76)$$

where Ω and v_0 are given by (2.71) and (2.72) respectively, and where $\tilde{V}_s(z)$ contains only terms that are subleading in the $1/k$ expansion, and is given by

$$\tilde{V}_s(z) = \frac{1}{k} (\gamma_{s\ell} + \beta_\ell \xi^4) + \mathcal{O}(k^{-2}). \quad (2.77)$$

Thus, the large- k dispersion relation is

$$\omega_s^2 = k^2 v_0^2 + k\Omega\varepsilon(n+2) + d_{s n\ell} + \mathcal{O}(1/k), \quad (2.78)$$

with

$$d_{1n\ell} = \frac{1}{(1+\varepsilon^2)^3} \left[\frac{4}{3} \ell(\ell+2) (1 + 3\varepsilon^2 + \varepsilon^4 + 3\varepsilon^6 + \varepsilon^8) - \left(\frac{5}{4} - 9\varepsilon^2 + 7\varepsilon^4 - 9\varepsilon^6 + \frac{5}{4}\varepsilon^8 \right) (n+2)^2 - 56\varepsilon^4 \right], \quad (2.79)$$

and

$$d_{2n\ell} = d_{1n\ell} + \frac{80\varepsilon^4}{(1+\varepsilon^2)^3}. \quad (2.80)$$

Restoring dimensionful quantities in the dispersion relation (2.78), i.e. undoing (2.12), means multiplying the k and constant terms by L_0/R^2 and L_0^2/R^4 , respectively.

I can easily obtain an explicit expression for the wave functions themselves if we neglect the β_ℓ , $\gamma_{s\ell}$ and higher order terms, as the potential (2.70) is then that in the radial wave equation for a four-dimensional harmonic oscillator. To this order, the

wave functions are given up to a normalization constant by

$$\psi = z^{3/2+\ell} L_{\nu}^{(\ell+1)} \left(\frac{1}{2} \Omega \epsilon k z^2 \right) \exp \left(-\frac{1}{4} \Omega \epsilon k z^2 \right), \quad (2.81)$$

where, as before, $\nu = (n - \ell)/2$ is the order of the generalized Laguerre polynomial $L_{\nu}^{(\ell+1)}$.

The dispersion relations (2.78) are the central result of Section 2.4. I shall analyze (2.78) and discuss its consequences at length in Sections 2.4.4 and 2.5. First, however, I close this more technical discussion with a few remarks related to the approximation that has been used here to obtain the large- k dispersion relations:

1. The wave function is localized at the tip of the brane, near $\rho = 0$ which is the fixed point of the $SO(4)$ symmetry at which the S^3 shrinks to zero size and the fluctuations are fluctuations in R^4 . This is the reason why I find a four-dimensional harmonic oscillator.
2. The approximation in this section is valid for wave functions that are tightly localized near $z = 0$. Evidently, this approximation must break down for mesons with high enough n , whose wave functions explore more of the potential. More precisely, if I increase n and ℓ while keeping ν fixed and small, the wave functions are peaked at $z_0 \sim \left(\frac{n}{k\Omega\epsilon} \right)^{\frac{1}{2}}$ with a width $\frac{1}{(k\Omega\epsilon)^{\frac{1}{2}}}$. Or, if I increase n and ν while keeping ℓ fixed and small, the wave functions become wider, with ν oscillations over a range of z from near zero to near $z_0 \sim \left(\frac{n}{k\Omega\epsilon} \right)^{\frac{1}{2}}$ and hence a wavelength $\sim \frac{1}{(nk\Omega\epsilon)^{\frac{1}{2}}}$. In either case, this approximation must break down for $n \sim k$, since for n this large z_0 is no longer small and the wave function is no longer localized near $z = 0$.
3. It is important to ask at what k (or, at what ω) stringy effects that I have neglected throughout may become important in the dispersion relations for the mesons that I have analyzed. We can answer this question by comparing the length scale over which the meson wave functions that we have computed varies to the string length scale $\alpha'^{\frac{1}{2}}$. Considering first the case where ν is small, I

can see from (2.35) that the proper distance between the maximum of the wave function at $z = z_0$ and the tip of the brane at $z = 0$ is

$$l_0 \sim \sqrt{f(0)} R z_0 \sim \frac{1 - \varepsilon^2}{\sqrt{1 + \varepsilon^2}} R \left(\frac{4n}{k\Omega\varepsilon} \right)^{\frac{1}{2}}, \quad (2.82)$$

and the width of the wave function is

$$\delta l \sim \frac{1 - \varepsilon^2}{\sqrt{1 + \varepsilon^2}} R \left(\frac{1}{k\Omega\varepsilon} \right)^{\frac{1}{2}}. \quad (2.83)$$

Stringy effects can be neglected as long as $\delta l \gg \alpha'^{\frac{1}{2}}$, meaning

$$k < \mathcal{O}(\lambda^{\frac{1}{4}} M), \quad (2.84)$$

where in the last expression I have restored the dimensions of k using (2.10) and (2.12). (Since $\omega = v_0 k$ at large k , this parametric criterion is the same for ω as for k .) If ν is large, the wavelength of the wave function should be compared to $\alpha'^{\frac{1}{2}}$ meaning that δl is reduced by a factor $\sim 1/\sqrt{\nu}$ and stringy effects can be neglected only as long as

$$k < \mathcal{O}(\lambda^{\frac{1}{4}} M/\nu). \quad (2.85)$$

I can conclude from either (2.84) or (2.85) that it is justified to use the dispersion relation that have been derived here in the $k \rightarrow \infty$ limit, as long as one takes the $\lambda \rightarrow \infty$ limit first.¹

4. Notice that as $\varepsilon \rightarrow 1$ (i.e. approaching the critical embedding), both v_0 and Ω vanish. The approximation done here will therefore break down at the critical embedding. (One way to see this is to note that in the leading terms in (2.70)

¹Recall that although the mesons that we have focussed on have masses of order $M \sim m_q/\sqrt{\lambda}$, there are also higher-lying stringy mesonic excitations with masses of order $M\lambda^{\frac{1}{4}} \sim m_q/\lambda^{\frac{1}{4}}$. Requiring $\lambda^{1/4}$ to be large is what justifies neglecting these stringy mesonic excitations, just as it justifies neglecting stringy corrections to the dispersion relations of the low-lying mesons. Note also that the latter becomes important at an ω of order the mass of the former.

we will then have zero times infinity, meaning that it is no longer obvious that these *are* the leading terms.) However, the first order phase transition occurs at $\varepsilon = 0.756$, long before this happens.

2.4.3 Numerical Results

I can also obtain the meson wave functions and dispersion relations numerically, without making either a small ε or a large- k approximation. In this subsection I plot a few examples of such results, and compare them to the analytic expressions that I have derived above upon making the large- k approximation.

In Figure 2-6, I plot the potentials (2.39) and ground state wave functions for those potentials that have been obtained numerically for three values of k . Note the changing vertical scale in the plots of V ; as k increases, V deepens. We can see that as k increases and the potential deepens, the wave function gets more and more localized near $z = 0$ and, correspondingly, the expression (2.81) for the wave function that was derived in the large- k limit using the fact that the wave function becomes localized becomes a better and better approximation to the exact wave function.

Figure 2-7 shows the dispersion relations obtained numerically for the ground state ψ_1 meson at several values of the temperature. At each k , the Schrödinger equation has been solved to find the ground state (using the shooting method) and ω^2 is obtained from the eigenvalue and hence a point on the dispersion relation. Doing this at many k 's gives the curves plotted and the linear approximation to the large- k dispersion relations is over-layed, that I shall discuss in Section 2.4.4. Figure 2-8 shows the corresponding group velocities.

2.4.4 Summary, Limiting Velocity and Dissociation Temperature

In this section I restate the central result for the dispersion relation and then discuss its implications vis à vis a limiting velocity for mesons at a given temperature as well as a limiting temperature below which mesons with a given velocity are found, and

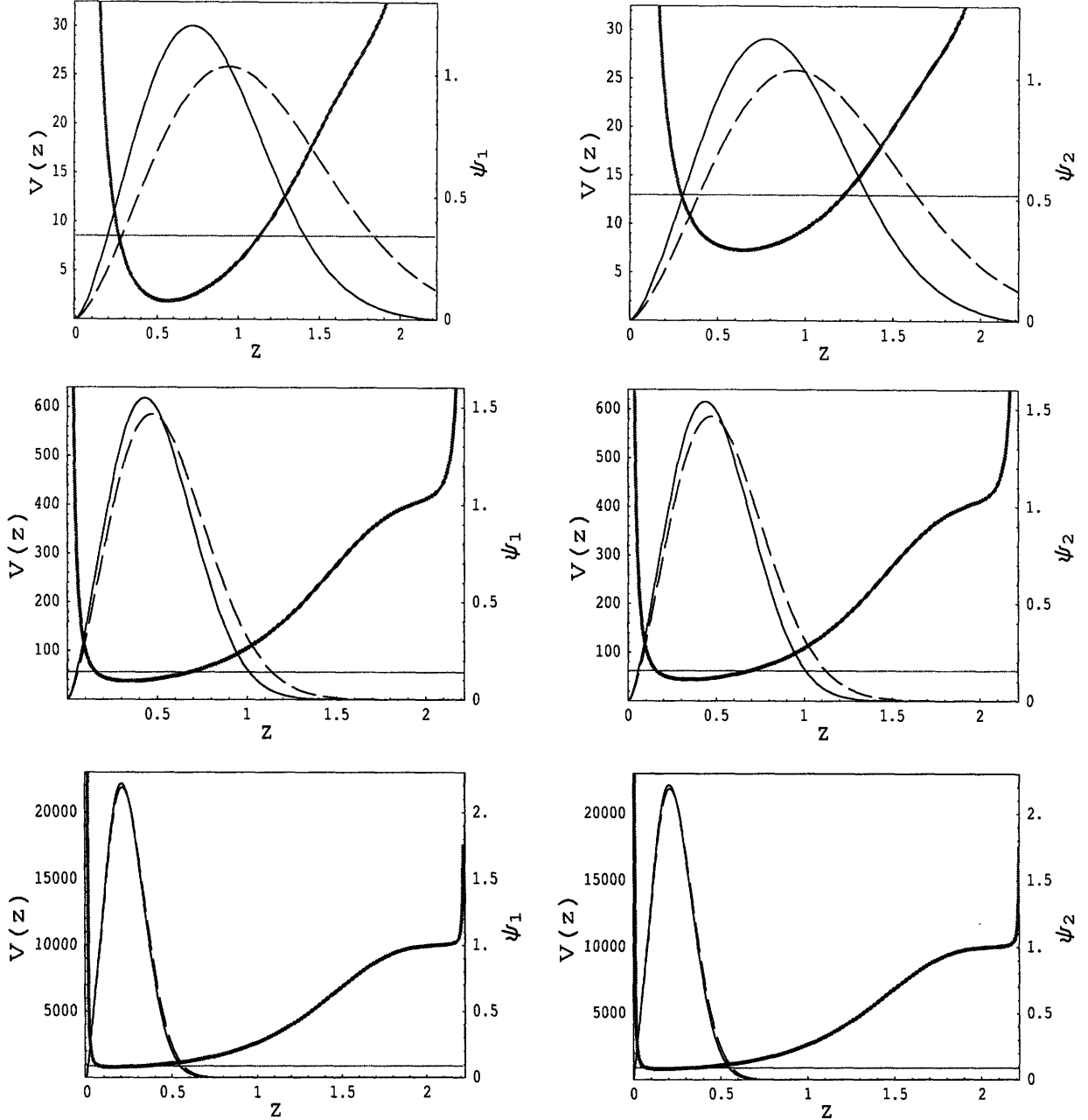


Figure 2-6: Potential and ground state wave function for ψ_1 (left three panels) and ψ_2 (right three panels) for k given by 5, 20 and 100 (top to bottom). All plots have $\varepsilon = 0.756$, corresponding to the Minkowski embedding at the dissociation transition. $V(z)$ and the ground state ($n = \ell = 0$) solutions to the Schrödinger equation in the potentials V are both shown as solid lines, and the ground state energies are indicated by the horizontal (red) lines. The dashed lines show the approximation (2.81) to the wave functions.

above which they are not.

In Section 2.4.2, I have derived the large- k approximation to the meson dispersion

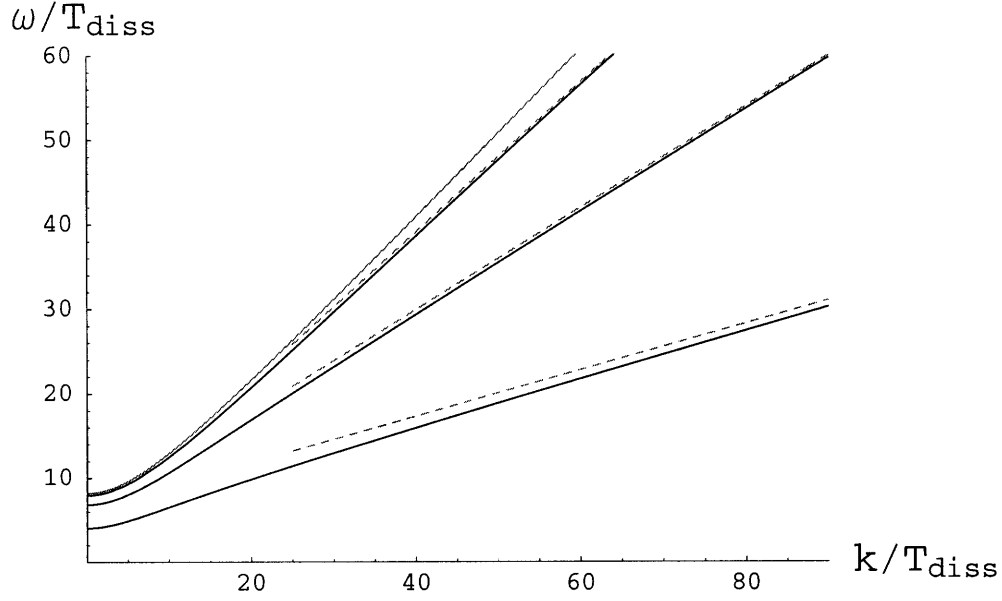


Figure 2-7: Dispersion relations for the ground state ψ_1 meson with $n = \ell = 0$ at various values of ε (i.e. at various temperatures). The top (red) curve is the zero temperature dispersion relation $\omega = \sqrt{k^2 + m^2}$ with m given by (2.7) and with a group velocity that approaches 1 at large k , as required in vacuum by Lorentz invariance. The next three solid (black) curves are the dispersion relations for $\varepsilon = 0.25, 0.5$ and 0.756 , top to bottom, the latter corresponding to the Minkowski embedding at the temperature T_{diss} at which the first order phase transition occurs. The dashed (red) lines are the large- k approximation discussed in Section 2.4.4, given by $\omega(k) = v_0 k + \Omega \varepsilon L_0 / (v_0 R^2)$ with Ω specified by (2.93). We see that the dispersion relations approach their large- k linear behavior from below. The limiting velocity v_0 decreases with increasing temperature. Had I plotted dispersion relations for $0.756 < \varepsilon < 1$ corresponding to metastable Minkowski embeddings with $T > T_{\text{diss}}$, I would have seen $v_0 \rightarrow 0$ as $\varepsilon \rightarrow 1$, approaching the critical embedding.

relations at any temperature below the dissociation transition. I have checked this result against numerical solutions valid at any k in Section 2.4.3. Let us begin by restating the analytic result (2.78):

$$\omega^2 = v_0^2 k^2 + \Omega \varepsilon (n + 2) \frac{L_0}{R^2} k + d_{sn\ell} \frac{L_0^2}{R^4}, + \mathcal{O}(1/k), \quad (2.86)$$

where

$$v_0 = \frac{1 - \varepsilon^2}{1 + \varepsilon^2}, \quad \Omega^2 = \frac{32(1 - \varepsilon^2)^2(1 + \varepsilon^4)}{(1 + \varepsilon^2)^5}. \quad (2.87)$$

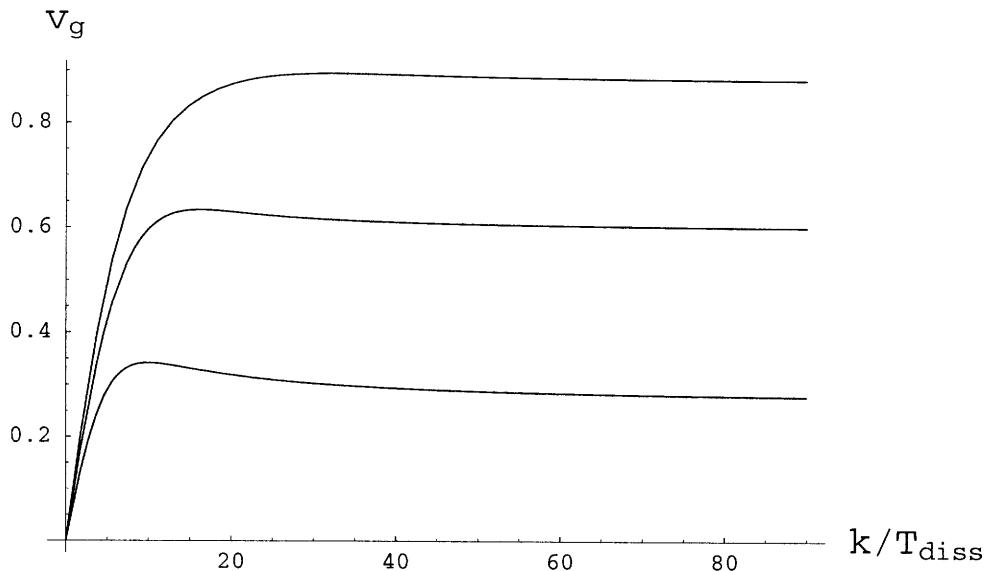


Figure 2-8: Group velocities $v_g = d\omega/dk$ for the dispersion relations from Fig. 2-7, with $\varepsilon = 0.25, 0.5$ and 0.756 (top to bottom). We see that the group velocity approaches its large- k value v_0 from above. And, we see v_0 decreasing with increasing temperature. (Again, v_0 would approach zero if we included the metastable Minkowski embeddings with $T > T_{\text{diss}}$.)

The constant term $d_{sn\ell}$ (which depends on whether the ψ_1 or ψ_2 mesons are being discussed — $s = 1$ or $s = 2$ — and on the quantum numbers n and ℓ) was given in (2.79) and (2.80). In writing the dispersion relation (2.86) I have restored dimensions by undoing the rescaling (2.12). The dimensionful quantity that I had scaled out and have now restored can be written as

$$\frac{L_0}{R^2} = \left(\frac{2\pi m_q}{\sqrt{\lambda}} \right) \sqrt{\frac{\epsilon_\infty}{\varepsilon}}, \quad (2.88)$$

where I have used (1.8), (1.42) and (2.11). The first factor in (2.88) is a (dimensionful) constant. The quantity $\epsilon_\infty/\varepsilon$ appearing in the second, dimensionless, factor is weakly temperature dependent: it can be read from Figure 2-1, and is not constant to the degree that the curve in this plot is not a straight line (in the relevant regime $0 < \varepsilon < 0.756$, as $\varepsilon = 0.756$ corresponds to $T = T_{\text{diss}}$.) Although using dimensionless variables obtained via scaling by the temperature-dependent L_0/R^2 was very convenient in deriving all the results, in plotting the dispersion relation and

group velocity in Figures 2-7 and 2-8, ω and k have instead been plotted in units of $T_{\text{diss}} = 2.166 m_q / \sqrt{\lambda}$, which is a relevant, constant, physical, quantity comparable in magnitude to L_0/R^2 . In the remainder of this section, I shall analyze (2.86).

In the large- k limit, the asymptotic value of the group velocity $d\omega/dk$ is given by v_0 . This velocity decreases with increasing temperature, and vanishes as $\varepsilon \rightarrow 1$ on the critical embedding that separates Minkowski and black hole embeddings in Figures 1-2 and 2-1. At the temperature at which the first order dissociation transition occurs, $\varepsilon = 0.756$ and $v_0 = 0.273$.

There is a natural explanation within the dual gravity theory for how the asymptotic velocity v_0 can arise. Using (2.15), it is easy to show that v_0 in (2.87) can also be written as

$$v_0^2 = \frac{f(\rho = 0)}{r^2(\rho = 0)}, \quad (2.89)$$

which we can see from (2.13) is precisely the local speed of light at the tip of the D7-brane. (The local speed of light is 1 at $u = \infty$, and decreases with decreasing u , decreasing to v_0 at the tip of the D7-brane where $\rho = 0$ and $u = y = 1$.) Since we have seen that in the large- k limit the wave function of the meson fluctuations becomes more and more localized closer and closer to the tip of the D7-brane, this makes it natural that v_0 emerges as the asymptotic velocity for mesons with large k .

In the low temperature (equivalently, heavy quark) limit, I find (either directly from (2.87) or, initially, in (2.67) in Section 2.4.1) that

$$v_0^2 \approx 1 - 4\varepsilon^2. \quad (2.90)$$

Since $\varepsilon_\infty \approx \varepsilon$ at small ε , using (1.42) I have

$$v_0^2 \approx 1 - \frac{\lambda^2 T^4}{16m_q^4}, \quad (2.91)$$

which is precisely the critical velocity (1.23) obtained in [67] from the screening calculation as the velocity above which the potential between two moving quarks of mass m_q cannot be defined. This is the first of two quantitative comparisons that I will be

able to make between the present results for meson propagation and results obtained previously via the screening calculation. We can see from Figure 2-9 that (2.90) works very well where $T \ll m_q/\sqrt{\lambda}$, which is where it was derived (both here and in [66]).

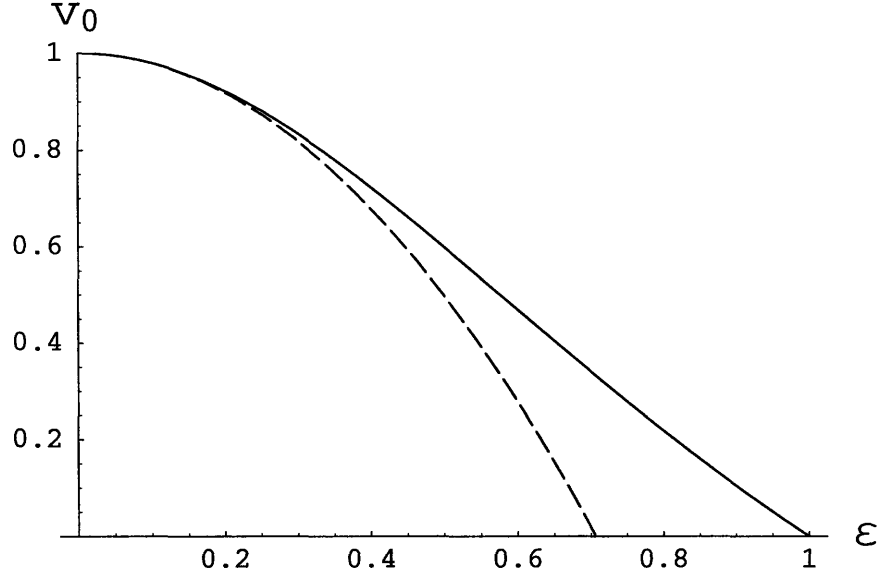


Figure 2-9: The asymptotic velocity v_0 from (2.87) as a function of ϵ . The low temperature approximation (2.90) is plotted as a dashed line. Recall that the dissociation transition occurs at $\epsilon = 0.756$.

In order to analyze (2.86) beyond the k^2 term, it is instructive to rewrite it as a large- k approximation to the dispersion relation ω itself rather than to ω^2 , yielding

$$\omega(k) = v_0 k + \frac{\Omega \epsilon (n+2) L_0}{2v_0 R^2} + \frac{4d_{sn\ell} v_0^2 - \Omega^2 \epsilon^2 (n+2)^2}{8v_0^3} \frac{L_0^2}{R^4} \frac{1}{k} + \mathcal{O}(1/k^2), \quad (2.92)$$

in the form I discussed in Section 1.3. The term linear in k in (2.86) yields a constant shift in the meson energies in (2.92). Whereas v_0 is independent of s , n and ℓ , the constant term in (2.92) results in evenly spaced dispersion relations for mesons with differing n quantum number, separated by

$$\frac{\Omega \epsilon L_0}{2v_0 R^2} = \left(\frac{2\pi m_q}{\sqrt{\lambda}} \right) \sqrt{\frac{8\epsilon_\infty \epsilon (1 + \epsilon^4)}{(1 + \epsilon^2)^3}}, \quad (2.93)$$

which are plotted in Figure 2-10.

If I neglect the $\mathcal{O}(1/k)$ and higher order terms in (2.92), the dispersion relations

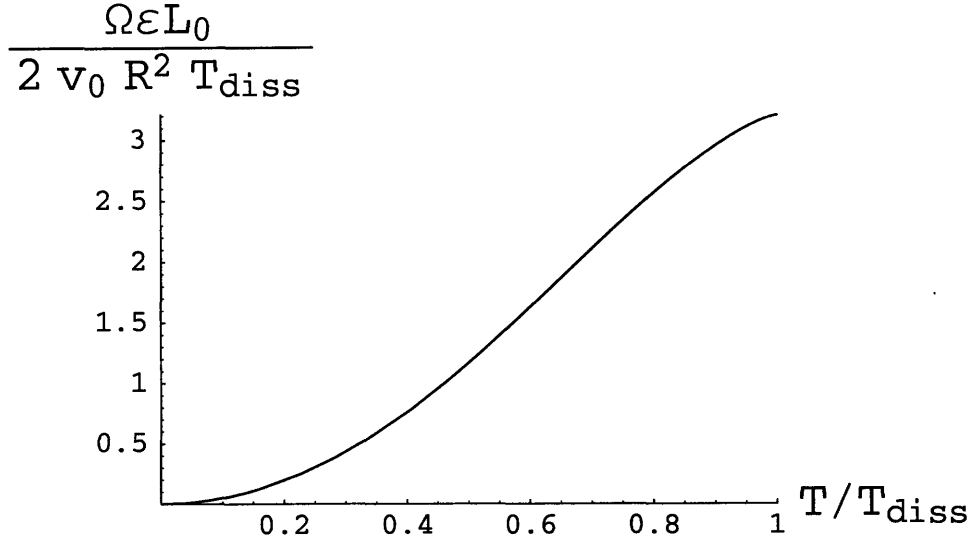


Figure 2-10: The k -independent spacing $\Omega\varepsilon L_0/2v_0R^2$ between the dispersion relations for any two mesons whose n quantum numbers differ by 1, in units of T_{diss} . See (2.93).

are the same for mesons ψ_1 and ψ_2 and are independent of ℓ . These degeneracies are broken at order $\mathcal{O}(1/k)$, where $d_{sn\ell}$ first appears. I find that the coefficient of $1/k$ in $\omega(k)$ of (2.92) is typically negative: it is negative at all $\varepsilon < 1$ if $\ell = 0$ for any n ; it can become positive only if ε , n and ℓ are all large enough. When this coefficient is negative, it means that $\omega(k)$ approaches its large- k asymptotic behavior (which is a straight line with slope v_0 offset by the constant term in (2.92)) from below. This means that $d^2\omega/dk^2 < 0$ at large k and means that the group velocity $v = d\omega/dk$ approaches v_0 from above at large k , as shown in Figure 2-8. However, at $k = 0$ the group velocity vanishes and $d^2\omega/dk^2 > 0$. (This has been shown analytically at small ε in Section 2.4.1, see (2.51), and the numerical results as in Section 2.4.3 indicate that this is so at all ε .) So, as a function of increasing k , the group velocity begins at zero, increases to some maximum value that is greater than v_0 , and then decreases to v_0 as $k \rightarrow \infty$ as depicted in Figure 2-8². Although v_0 is not the maximum possible group velocity, it appears that the maximal velocity exceeds v_0 only by a small margin.

²This behavior is not inconsistent with our identification of v_0 with the local speed of light at the tip of the brane: it is only for $k \rightarrow \infty$ that the meson wave function is squeezed down to the tip of the brane; at finite k , the wave function is peaked where the local speed of light exceeds v_0 .

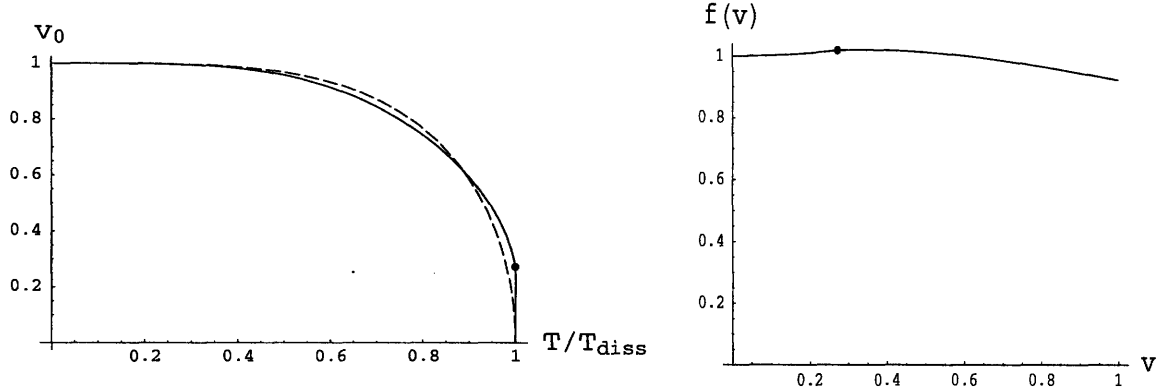


Figure 2-11: Left panel: The solid curve is the limiting velocity v_0 as a function of T/T_{diss} , where T_{diss} is the temperature of the dissociation transition at zero velocity. The dissociation transition occurs at the dot, where $v_0 \approx 0.273$. The dashed curve is the approximation obtained by setting $f(v) = 1$ in (2.94). Right panel: $f(v)$, the ratio of the solid and dashed curves in the left panel at a given v . We see that $f(v)$ is within a few percent of 1 at all velocities.

For example, for the ground state ψ_1 meson whose dispersion relations are given in Figures 2-7 and 2-8, I find that $v_0 = 0.882, 0.6$, and 0.273 for $\varepsilon = 0.25, 0.5$, and 0.756 whereas the maximal velocities are $0.896, 0.634$ and 0.342 , respectively. I shall therefore simplify the following discussion by taking the maximal possible meson velocity at a given temperature to be the limiting velocity v_0 , neglecting the slight imprecision that this introduces.

To compare the results for the limiting meson velocity v_0 at a given temperature to the result (1.22) inferred (qualitatively) from the analysis of screening in a hot wind in [67], first convert $v_0(\varepsilon)$ into $v_0(T)$, meaning that we must convert from ε to ε_∞ as discussed in and around Figure 2-1. The result is the solid curve in the left panel of Figure 2-11, where v_0 has been plotted versus T/T_{diss} . This curve has been derived as a limiting meson velocity at a given temperature. However, it can just as well be read (by asking where it cuts horizontal lines rather than vertical ones) as giving $T_{\text{diss}}(v)$, the temperature below which mesons with a given velocity v are found and above which no mesons with that velocity exist. Here $T_{\text{diss}}(v) \rightarrow 0$ for $v \rightarrow 1$, the regime where v_0 is given by (2.91) and $T_{\text{diss}}(v)$ is therefore given by (1.24). In order

to compare our result for $T_{\text{diss}}(v)$ at all velocities to (1.22), I parametrize the result as

$$T_{\text{diss}}(v) = f(v)(1 - v^2)^{1/4}T_{\text{diss}}(0) . \quad (2.94)$$

In the left panel of Figure 2-11 this full result (the solid curve) is compared to (2.94) with $f(v)$ set to 1, which is of course (1.22). In the right panel $f(v)$ is plotted. We can see that this function is close to 1 at all velocities, varying between 1.021 at its maximum and 0.924 at $v = 1$. The weakness of the dependence of $f(v)$ on v is a measure of the robustness with which the simple scaling (1.22) describes the result for the meson dissociation temperature at all velocities.

2.5 Discussion and Open Questions

In this chapter, the AdS/CFT correspondence has been used to compute the dispersion relation $\omega(k)$ for the heavy “quarkonium” mesons that exist as stable bound states in the strongly coupled plasma of $\mathcal{N} = 4$ SYM to which heavy fundamental quarks with mass m_q have been added. In Section 2.3 a new, and more geometrical, method of analyzing these mesons was introduced that has allowed, in Section 2.4, to obtain the dispersion relations at large- k analytically in the form (2.92), which can be summarized as in Section 1.3 by writing

$$\omega(k) = v_0 k + a + \frac{b}{k} + \dots . \quad (2.95)$$

a and b have been explicitly and analytically computed in Section 2.4, but at present there is no argument that the behavior of these coefficients, which depend on the meson quantum numbers, could teach us lessons that generalize beyond the particular theory in which they have been computed them. On the other hand, the limiting large- k meson velocity v_0 seems to encode much physics that may generalize to meson bound states in other strongly coupled gauge theory plasmas.

- The explicit result obtained in this chapter is

$$v_0 = \frac{1 - \varepsilon^2}{1 + \varepsilon^2}, \quad (2.96)$$

where ε is related to $\varepsilon_\infty = \lambda T^2 / (8m_q^2)$ as in Figure 2-1. I find that v_0 depends on the temperature (in the combination $\sqrt{\lambda T / m_q}$) but not on the meson quantum numbers. I see in Figures 2-7 and 2-8 that v_0 decreases with increasing temperature, becoming much less than 1 as the temperature approaches T_{diss} , the temperature at which mesons at rest dissociate. I see in these figures that the coefficient b in (2.95) can be negative, meaning that the group velocity approaches its large- k value v_0 from above. Thus, v_0 is the limiting meson velocity at large k , but the maximal velocity occurs at finite k and is slightly larger than v_0 . This is described quantitatively in Section 2.4, but it is a small effect and in this discussion I shall ignore the distinction between v_0 and the maximal velocity.

- I find that v_0 , which in the gauge theory is the limiting velocity of the mesons that they attain at large k , also has a nice interpretation in the dual gravity theory. It is precisely the local velocity of light at the “tip” of the D7-brane, namely where the D7-brane reaches closest to the black hole. This is physically sensible because we have shown that the D7-brane fluctuations — i.e. the mesons in the dual gravity theory — are localized at the D7-brane tip in the large- k limit.
- At low temperatures or, equivalently, for heavy quarks I find

$$v_0 \approx 1 - \frac{\lambda^2 T^4}{32m_q^4}. \quad (2.97)$$

This is precisely, i.e. even including the numerical factor, the criterion for meson dissociation inferred from a completely different starting point in [67]. The logic there was that the screening length that characterizes the potential between a quark and antiquark moving with $v > v_0$ is shorter than the quark Compton

wavelength, meaning that if a quark and antiquark moving with $v > v_0$ are separated by more than a Compton wavelength, to leading order in $\sqrt{\lambda}$ they feel no attractive force. By inference, no mesons should exist with $v > v_0$. This result can now be seen as emerging by direct calculation of meson dispersion relations, rather than by inference.

- I have a result for $v_0(T)$, the limiting velocity beyond which there are no meson bound states, at all $T < T_{\text{diss}}$ not just at low temperatures, see Figure 2-11. I can just as well read this as determining a temperature $T_{\text{diss}}(v)$ above which no meson bound states with velocity v exist. I find that up to few percent corrections, see Figure 2-11, this is given by

$$T_{\text{diss}}(v) = (1 - v^2)^{1/4} T_{\text{diss}} . \quad (2.98)$$

Once again, this is a result that, as described in Section 1.4, was previously inferred from analysis of the velocity dependence of the screening length characterizing the potential between a quark and antiquark moving through the plasma [66]. This result has now been derived and the (few percent) corrections to it for the mesons whose dispersion relations were explicitly constructed in this chapter. I should also note that it is a slight abuse of terminology to call $T_{\text{diss}}(v)$ at $v > 0$ a “dissociation” temperature: although it *is* a temperature above which no mesons with velocity v exist, if I imagine heating the plasma through $T_{\text{diss}}(v)$ I have not shown that any mesons present therein dissociate — they may simply slow down. The question of what happens in this hypothetical context is a dynamical one that cannot be answered just from the dispersion relations analyzed here.

- As was discussed in Section 1.4, the result (2.98) can be read as saying that no mesons with velocity v exist when the energy density of the strongly coupled plasma exceeds $\rho_{\text{diss}}(v)$ where, up to small corrections,

$$\rho_{\text{diss}}(v) = (1 - v^2) \rho_{\text{diss}} , \quad (2.99)$$

with ρ_{diss} the energy density at which mesons at rest dissociate. Correspondingly, the low temperature result (2.97) can be written as

$$1 - v_0 = \text{constant} \frac{\rho}{\rho_{\text{diss}}} , \quad (2.100)$$

valid when $\rho \ll \rho_{\text{diss}}$ and v_0 is close to 1. Thinking as in [87], one can ask whether the same result holds in other theories. It will be interesting to address this question in 1 + 3-dimensional gauge theories that are in various senses more QCD-like than $\mathcal{N} = 4$ SYM. At present, however, I have only investigated the 1 + p -dimensional gauge theories described by N D p -branes [108] into which fundamental quarks, and hence mesons, have been introduced by embedding a D q -brane [109, 103, 95, 96]. The D p -branes fill coordinates $0, 1, \dots, p$. The D q -brane fills the first $d + 1$ of these coordinates $0, 1, \dots, d$, where d may be less than or equal to p , as well as $q - d$ of the remaining $9 - p$ coordinates. Appendix B contains the sketch of an investigation of those theories for which $p - d + q - d = 4$. (The case that has been analyzed throughout the rest of this chapter is $p = d = 3, q = 7$.) These theories are not conformal for $p \neq 3$, as their coupling constant λ has dimension $p - 3$. It is convenient to introduce a dimensionless $\lambda_{\text{eff}} \equiv \lambda T^{p-3}$. I have not repeated our entire construction for the D p /D q -brane theories. However, I expect that the wave functions for large- k mesons will again be localized at the tip of the D q -brane, and therefore expect that in these theories v_0 will again be given by the local velocity of light at this location. The computations of this velocity is presented in Appendix B. Assuming that this is indeed the limiting meson velocity, one finds that

$$v_0 = \left(\frac{1 - \varepsilon^{(7-p)/2}}{1 + \varepsilon^{(7-p)/2}} \right) , \quad (2.101)$$

where ε is given at small T/m_q by

$$\varepsilon \approx \varepsilon_\infty \propto \left(\frac{T}{m_q} \right)^2 \lambda_{\text{eff}}^{2/(5-p)} = \frac{\lambda^{2/(5-p)} T^{4/(5-p)}}{m_q^2} . \quad (2.102)$$

(Relating ε to ε_∞ beyond the small T/m_q limit requires solving the embedding equation given in Appendix B.) In these theories, the energy density of the plasma depends on parameters according to [108]

$$\rho \propto N^2 T^{p+1} \lambda_{\text{eff}}^{(p-3)/(5-p)} = N^2 \lambda^{(p-3)/(5-p)} T^{(14-2p)/(5-p)}, \quad (2.103)$$

and zero-velocity mesons dissociate at some energy density ρ_{diss} corresponding to $\varepsilon = \varepsilon_{\text{diss}}$ where $\varepsilon_{\text{diss}} = \mathcal{O}(1)$. From these results we notice that at small ε

$$\varepsilon^{(7-p)/2} \propto \frac{\lambda^{(7-p)/(5-p)} T^{(14-2p)/(5-p)}}{m_q^{7-p}} \propto \frac{\rho}{\rho_{\text{diss}}}, \quad (2.104)$$

meaning that the velocity v_0 of (2.101) can be written in the form (2.100) for all values of p . Appendix B contains a description of the verification that (2.98) also holds, but only when phrased as in (2.99) in terms of energy density rather than temperature.

Emboldened by these successes, I advocate investigating the consequences that follow from hypothesizing that Υ and J/Ψ mesons in the strongly coupled QGP of QCD propagate with a dispersion relation (2.95) with v_0 dropping dramatically as the temperature approaches T_{diss} from below, and with no bound states with velocity v possible if $T > T_{\text{diss}}(v)$ given by (2.98). In applying (2.98) to QCD, it is important to scale $T_{\text{diss}}(v)$ relative to the T_{diss} for Υ and J/Ψ mesons in QCD itself. The result $T_{\text{diss}} = 2.166 m_q / \sqrt{\lambda}$ for the mesons that have been analyzed is surely affected by the fact that they are deeply bound and so should not be used as a guide to quarkonia in QCD. For example, it seems to overestimate T_{diss} for J/Ψ mesons by a factor of 2 or 3. However, as argued in [66, 67] and as has been discussed above, the velocity scaling (2.98) may transcend the detailed meson physics in any one theory and apply to mesonic bound states in any strongly coupled plasma. The successful comparison of the above detailed results to this simple scaling form supports this conjecture.

As was explained at length in Section 1.3, meson propagation is only one piece of the physics that must be treated in order to understand quarkonium suppression in

heavy ion collisions. Introducing the dispersion relation and limiting velocity that has been found into such a treatment is something I leave to the future, instead making only a few qualitative remarks.

First, from the dispersion relations alone I *cannot* conclude that if a quark-antiquark pair is produced (from an initial hard scattering) with a velocity $v > v_0(T)$, with $v_0(T)$ the limiting meson velocity in the plasma of temperature T in which the quark-antiquark pair finds itself, then the quark-antiquark pair do not bind into a meson. The reason that I cannot make this inference is that the dispersion relations describe stable mesons with arbitrarily large momentum k , making it a logical possibility that a high velocity quark-antiquark pair with arbitrarily high momentum interacts with the medium in some way such as to slow down and lose energy while conserving its momentum, and thus in some way dresses itself into a meson with arbitrarily high momentum k , and velocity v_0 . That is, since the dispersion relations describe the propagation of mesons with arbitrarily large momentum, by themselves they do not require that quarkonium production is suppressed when the precursor quark-antiquark pair has velocity $v > v_0(T)$. Excluding this possibility, allowed by the kinematics, requires some consideration of the dynamics. The heuristic argument of [67] provides guidance: the precursor quark-antiquark pair with $v > v_0(T)$ do not attract each other and so even though it is kinematically allowed by the meson dispersion relations for them to slow down and form a meson, instead they will propagate independently through the medium. Thus, the p_T -dependent quarkonium suppression pattern proposed in [66], with the production of quarkonium states with T_{diss} higher than the temperature reached in a given heavy ion collision experiment nevertheless becoming suppressed above a threshold transverse momentum at which a quark-antiquark pair with that transverse momentum has velocity $v_0(T)$, rests upon the dynamical argument of [67]. It is natural that analyzing quarkonium suppression requires consideration of both the precursor quark-antiquark pair and the putative meson, and only the latter is described by the meson dispersion relation. It is then nice to discover that the limiting meson velocity $v_0(T)$ agrees precisely with the velocity at which quark-antiquark pairs can no longer feel a force at order $\sqrt{\lambda}$.

I have just argued that the very large- k region of the meson dispersion relation is unlikely to be populated in heavy ion collisions. But, whether or not such large- k modes are excited, it is clear from Figure 2-7 that at temperatures near to T_{diss} mesons at any k move much more slowly than they would if they propagated with their vacuum dispersion relation. There are several in-principle-observable signatures of the slow velocity of quarkonium mesons. First, it increases the separation in space long after the collision between those mesons that are produced at the surface of the fireball moving outwards, and hence escape into vacuum promptly, and those which are produced in the center of the plasma and hence move more slowly than if they had their vacuum dispersion relation. An increase in the typical separation of identical mesons because of this slow velocity effect will shift the onset of Bose-Einstein enhancement in the two particle momentum correlation to a lower relative momentum. This simple idea underlies a technique widely used in heavy ion physics and often referred to as Hanbury-Brown Twiss (HBT) two-particle interferometry, in which identical two-particle momentum correlations are used to determine spatio-temporal characteristics of the collision region. For a review, see Ref. [110]. Quarkonium HBT interferometry would thus in principle be able to find signatures of a depressed meson velocity. Second, non-identical two-particle correlation functions are sensitive to whether one particle species A is emitted from the medium on average before or after another particle species B . Such a difference in average emission times could result, for instance, if the maximal velocities in the dispersion relations for A and B differ because of their different mass. The analysis of the effect of a difference in average emission times on non-identical two-particle correlation functions can be found in [111]. In principle, this provides a second way of finding signatures of a depressed velocity for those mesons for which the plasma reaches temperatures close to their dissociation temperature.

Quarkonium mesons in the QGP of QCD have nonzero width. In contrast, the mesons that have been analyzed in this chapter at $T < T_{\text{diss}}$ are stable, with zero width. The dispersion relations that have been found in this chapter have no imaginary part. This is certainly an artifact of the large number of colors N and large

coupling λ limits that have been taken throughout. Processes in which one meson decays into two mesons are suppressed by $1/N$. And, thermal fluctuations which unbind a meson whose binding energy is $2m_q$ are suppressed by the Boltzmann factor

$$\exp(-2m_q/T) = \exp(-0.92\sqrt{\lambda}T_{\text{diss}}/T) , \quad (2.105)$$

which at some fixed T/T_{diss} is nonperturbative in an expansion about infinite λ . A calculation of the imaginary part of the meson dispersion relations at finite λ remains for the future, but this simple consideration is enough to be sure that it is nonzero, as is the case in QCD at weak coupling [44, 45, 46, 47]. As soon as the mesons have nonzero width, their slow velocity has a further consequence in the context of heavy ion collisions: because they move more slowly, they spend a longer time in the medium giving the absorptive imaginary part more time to effect the dissociation of the meson than would otherwise be the case.

The discussion in this section has highlighted three different avenues of further investigation opened up by the analysis of meson dispersion relations in a strongly coupled gauge theory plasma. The first is the investigation of the phenomenological consequences for J/Ψ and Υ suppression in heavy ion collisions of a dispersion relation of the form (2.95) with (2.98). Second, it appears that the most interesting open question about the mesons whose dispersion relations have been analyzed here is extending the calculation to finite λ and analyzing the width of the mesons. And, third, we could gain significant confidence in the application of the lessons we have learned to QCD by repeating our analysis for heavy quark mesons in the plasma of other strongly coupled gauge theories, in particular those with a controlled degree of nonconformality.

Chapter 3

Finite Temperature Solution for Fully Localized D2/D6-brane System

3.1 Introduction

The gauge/gravity correspondence can be extended to gauge theories with fundamental matter at finite temperatures. The temperature of a gauge theory has the geometric interpretation of the temperature at the horizon of certain non-extremal D-branes (as discussed in Section 1.2), while fundamental matter is introduced by adding different types of D-branes to a given string background (see Section 1.5). Many solutions involving different types of D-branes are known where some of them are smeared over certain directions [15, 112, 17] or the additional branes are treated as probes, ignoring their full gravitational back-reaction [91]. However, the construction of localized solutions involving different types of D-branes, taking into account their full back-reaction, is a very difficult problem. S. A. Cherkis and A. Hashimoto [10] constructed the supergravity solution involving a stack of N_2 D2-branes that is completely localized on N_6 coincident D6-branes at zero temperature. This solution has several nice features. It is completely specified by one function of two variables given

in closed form. Moreover, in an appropriate decoupling limit, this solution is the gravity dual description of a 1+2-dimensional, super-renormalizable, $\mathcal{N} = 2$ SYM with fundamental hypermultiplets. This is just the gauge theory living on the D2-branes with the fundamental matter being provided by the D6-branes. Additionally, N_2 and N_6 are free parameters in this solution. In this chapter, I will present a supergravity solution that describes the gravity description dual to this gauge theory at finite temperature, in its linear limit. This solution goes beyond the probe approximation [91] which would assume in this case that $N_6/N_2 \ll 1$. A similar assumption was made in Section 1.5.2 where $\mathcal{N} = 2$ hypermultiplets were introduced in the hot plasma of $\mathcal{N} = 4$ SYM by adding a probe D7-brane in the asymptotically $AdS_5 \times S^5$ black hole background arising from the non-extremal D3-branes.

The non-extremal solution to the localized D2/D6-brane system would give us the opportunity to study the strongly coupled plasma of the dual SYM, in particular the effect of flavor on transport coefficients of the hot plasma, like the entropy density, s , the shear viscosity, η , the bulk viscosity, ζ , and the speed of sound, c_s . However, finding such a solution is very difficult, as it involves solving non-linear, coupled, partial differential equations in two variables involving at least five functions. To make some progress, I assume that the energy density added to the extremal system is small, allowing me to linearize the system of equations. In this limit, the solutions can only be determined up to some integration constants, which I try to fix by considering the $N_6 \rightarrow \infty$ and $N_6 \rightarrow 0$ limits. As will be explained in Section 3.5, these limits do not successfully determine the ambiguity in the constants, severely limiting any applications of this solution. There have been some attempts to construct such a solution, e.g. by examining the system close to core of the D6-branes ($N_6 \gg 1$) and obtaining the lowest order correction in which the problem reduces to determining two functions depending only on one variable [113]. However, in this approximation, the solution diverges close to the horizon.

I shall discuss the extremal localized solution of the D2/D6-brane configuration [10] in Section 3.2, with emphasis on the method used in obtaining the solution and its limits as $N_6 \gg 1$ and $N_6 \ll 1$. In Section 3.3, I shall present the method

used by me in determining the non-extremal, linear solution. I shall explain here how the problem of finding the non-extremal solution, which should involve two RR-fluxes coupling to the D2- and D6-branes in type IIA supergravity, can be reduced to a problem of finding the black hole in $\mathbb{R}^{1,4} \times \text{Taub-NUT}$ with no matter sources. I shall then linearize the Einstein equations in this background and solve them up to some integration constants, which non-trivially depend on N_6 . In Section 3.4, I will show how to generate the D2/D6-brane solution at finite temperature from the 9-dimensional black hole presented in Section 3.3. I will end this chapter with a discussion of the results and their limitations in Section 3.5.

3.2 The Localized D2/D6-brane Solution

In this section I will review the extremal supergravity solution found by S. A. Cherkis and A. Hashimoto [10]. This is a solution in which the D2-branes are parallel to the D6-branes and the branes are completely localized. This requires that the full gravitational back-reaction of all the branes be taken into account.

Intersecting brane solutions with branes sufficiently smeared over some directions are very easy to construct [15, 112, 17], but finding a localized, fully back-reacted solution involving two or more types of branes is extremely difficult. In constructing the extremal supergravity solution involving a stack of N_2 D2-branes completely localized on coincident N_6 D6-branes, a key role is played by the fact that the M-theory lift of the D6-brane is just a background involving the Taub-NUT space. Upon finding the M2-brane solution in this background, the D2-brane solution can be obtained from M-theory by a trivial dimensional reduction along a certain transverse direction. The M-theory lift of the D6-brane solution is given by [114]

$$ds^2 = -dt^2 + dx \cdot dx + ds_{TN}^2, \quad (3.1)$$

where $dx \cdot dx$ is the metric on \mathbb{R}^6 , ds_{TN}^2 is the Taub-NUT space, whose metric is given below in (3.2). The RR-potential, C_7 , to which the D6-brane couples is determined by

$dA_1 = *_{10}dC_7$ where $\vec{\nabla} \times \vec{A} = \vec{\nabla} \left(1 + \frac{\mu_0}{r}\right)$ (the components of \vec{A} are the components of the 1-form A_1 and $\vec{\nabla}$ is the gradient operator in \mathbb{R}^3 determined by the coordinates r, θ, ϕ in (3.2)). The metric ds_{TN}^2 for the Taub-NUT space is

$$ds_{TN}^2 = \left(1 + \frac{\mu_0}{r}\right) [dr^2 + r^2(d\theta^2 + \sin^2\theta d\phi^2)] + \frac{(4m)^2}{1 + \frac{\mu_0}{r}} \left[d\psi' + \frac{N_6}{2} \cos\theta d\phi\right]^2, \quad (3.2)$$

$$= \left(1 + \frac{\mu_0}{r}\right) [dr^2 + r^2(d\theta^2 + \sin^2\theta d\phi^2)] + \frac{1}{1 + \frac{\mu_0}{r}} [d\psi + \mu_0 \cos\theta d\phi]^2. \quad (3.3)$$

where $4m$ is the radius of the Taub-NUT space, $r \geq 0$, $0 < \phi, \psi' \leq 2\pi$ and $0 < \theta \leq \pi$. In the second equality, I have re-scaled ψ' to define $\psi \equiv 4m\psi'$ and called $\mu_0 = 2mN_6$. ψ then has a period of $8\pi/m = 4\pi\mu_0/N_6$. Near the core of the Taub-NUT $r = 0$, it is useful to introduce

$$r = \frac{z^2}{4\mu_0}, \quad z^2 = 4\mu_0 r. \quad (3.4)$$

Then the Taub-NUT metric becomes

$$ds_{TN}^2 \longrightarrow dz^2 + \frac{z^2}{4} \left(d\Omega_2^2 + [d\tilde{\psi} + \cos\theta d\phi]^2\right) \quad (3.5)$$

where $\tilde{\psi} = \frac{\psi}{\mu_0}$, which has a period of $\frac{4\pi}{N_6}$. Thus near the center the metric becomes that of $\mathbb{R}^4/\mathbb{Z}_{N_6}$. Note that (3.5) applies when

$$z \ll 4mN_6 = 2\mu_0. \quad (3.6)$$

These facts suggest that the M-theory lift of the completely localized D2/D6-brane solution will be the solution of M2-branes in the background $\mathbb{R}^{1,6} \times \text{Taub-NUT}$, with the Taub-NUT transverse to the M2-brane. This reduces the original complicated problem to finding the harmonic function in $\mathbb{R}^4 \times \text{Taub-NUT}$. This solution has been found in closed form, and interpolates nicely between the solution one expects to get for just D2-branes or just D6-branes in the appropriate limits discussed later in this section. The M2-brane metric in 11-dimensional supergravity in the background

$\mathbb{R}^{1,6} \times \text{Taub-NUT}$ is

$$ds^2 = H(y, r)^{-2/3} (-dt^2 + dx_1^2 + dx_2^2) + H(y, r)^{1/3} (dy^2 + y^2 d\Omega_3^2 + ds_{TN}^2), \quad (3.7)$$

where $y \geq 0$ and $d\Omega_3^2 = d\chi_1^2 + \sin^2 \chi_1 d\chi_2^2 + \sin^2 \chi_1 \sin^2 \chi_2 d\chi_3^2$ is the metric on S^3 with $0 < \chi_1, \chi_2 \leq \pi, 0 < \chi_3 \leq 2\pi$. In the presence of the M2-brane, the 4-form flux is

$$F_4 = -dH^{-1} \wedge dt \wedge dx_1 \wedge dx_2. \quad (3.8)$$

All of the supergravity equations are either satisfied identically or require that the warp factor, $H(y, r)$, is a harmonic function on $\mathbb{R}^4 \times \text{Taub-NUT}$, i.e.

$$\nabla^2 H(y, r) \equiv \frac{1}{r + \mu_0} \frac{1}{r^2} \frac{\partial}{\partial r} \left(r^2 \frac{\partial H}{\partial r} \right) + \frac{1}{y^3} \frac{\partial}{\partial y} \left(y^3 \frac{\partial H}{\partial y} \right) = 0. \quad (3.9)$$

Here the second term in (3.9) involving the y -derivatives is just the laplacian in \mathbb{R}^4 , hence one can do a fourier transform in \mathbb{R}^4 using for $H(y, r)$ the Ansatz

$$H(y, r) = 1 + Q_{M2} N_6 \int \frac{d^4 p}{(2\pi)^2} e^{ip \cdot y} h(p, r) \quad (3.10)$$

$$= 1 + Q_{M2} N_6 \int dp p^2 \frac{J_1(py)}{y} h(p, r), \quad (3.11)$$

where in the second equality the integral over the angular directions has been carried out using (D.20) and (D.21), and Q_{M2} is the M2-brane charge which is expressed in terms of the Plank length l_{pl} and the number of M2-branes N_2 as

$$Q_{M2} = 32\pi^2 N_2 l_{pl}^6. \quad (3.12)$$

Using (3.11) in (3.9) leads to the fact that $h(p, r)$ satisfies the ordinary differential equation

$$\mathbb{D}h \equiv \frac{1}{r + \mu_0} \left(\frac{d^2}{dr^2} + \frac{2}{r} \frac{d}{dr} \right) h - p^2 h = 0. \quad (3.13)$$

This is a generalized confluent hypergeometric equation with solution (see Section D.1)

$$h(p, r) = p^2 c_p e^{-pr} \mathcal{U}\left(1 + \frac{p\mu_0}{2}, 2, 2pr\right), \quad (3.14)$$

where the factor of p^2 is determined by dimensional analysis, c_p is a dimensionless constant of integration and $\mathcal{U}(a, b, z)$ is the confluent hypergeometric function which satisfies (D.1).

Now let's consider various limits of this solution:

1. In the limit $r \rightarrow 0$ or $N_6 \rightarrow \infty$ one expects to recover the harmonic function in \mathbb{R}^8 as the Taub-NUT space is $\mathbb{R}^4/\mathbb{Z}_{N_6}$. Using the coordinate (3.4) and keeping pz fixed while taking $p\mu_0 \rightarrow \infty$, (3.13) reduces to a modified Bessel equation (9.6.1 in [107])

$$\frac{d^2 h}{dz^2} + \frac{3}{z} \frac{dh}{dz} - p^2 h = 0, \quad (3.15)$$

which has the solution

$$h \propto \frac{K_1(pz)}{pz}, \quad (3.16)$$

where $K_1(pz)$ is the modified Bessel function that tends to zero as $z \rightarrow \infty$. It can be checked using (D.16) that the solution in (3.14) reduces to (3.16) above if the constant of integration is

$$c_p = \tilde{c}_p \Gamma\left(\frac{p\mu_0}{2}\right), \quad (3.17)$$

where \tilde{c}_p is another dimensionless constant which depends on $p\mu_0$, i.e.

$$\lim_{p\mu_0 \rightarrow \infty} \Gamma\left(\frac{p\mu_0}{2}\right) e^{-pr} \mathcal{U}\left(1 + \frac{p\mu_0}{2}, 2, 2pr\right) = \frac{4}{pz} K_1(pz). \quad (3.18)$$

Further, with $\lim_{p\mu_0 \rightarrow \infty} \tilde{c}_p = 1/32$

$$H(y, r) = 1 + \frac{Q_{M2} N_6}{8} \int dp p^3 \frac{J_1(py)}{y} \frac{K_1(pz)}{z} = 1 + \frac{Q_{M2} N_6}{(y^2 + z^2)^3}, \quad (3.19)$$

as expected. The above expression applies when $y \sim z \ll \mu_0$. The factor of N_6 in equations above can be understood as the images arising from \mathbb{Z}_{N_6} orbifold.

2. As the Taub-NUT space reduces to $\mathbb{R}^3 \times S^1$ in the limit $r \rightarrow \infty$ or $N_6 \rightarrow 0$, one expects the supergravity solution to reduce to that of an M2-brane smeared over the circle S^1 . This means that $H(y, r)$ must reduce to the harmonic function in \mathbb{R}^7 . Keeping pr fixed while taking $p\mu_0 \rightarrow 0$, one finds that (3.13) reduces to

$$r^2 \frac{d^2 h}{dr^2} + 2r \frac{dh}{dr} - p^2 r^2 h = 0, \quad (3.20)$$

which has the solution

$$h \propto \frac{e^{-pr}}{pr}. \quad (3.21)$$

This is precisely the solution obtained from (3.14) using (D.14). Combining this with (3.11), (3.17), (D.28) and $\lim_{p\mu_0 \rightarrow 0} \tilde{c}_p = 1/32$ leads to the result

$$H(y, r) = 1 + \frac{3Q_{M2}}{64m} \frac{1}{(y^2 + r^2)^{\frac{5}{2}}} = 1 + \frac{Q_{D2}}{(y^2 + r^2)^{\frac{5}{2}}}, \quad (3.22)$$

where using (3.12) and $l_{pl} = g_s^{1/3} l_s$, I find

$$Q_{D2} = \frac{3}{64m} Q_{M2} = 6\pi^2 g_s N_2 l_s^5, \quad (3.23)$$

which agrees with the supergravity solution of a stack of N_2 D2-branes including the numerical factors. The above expression applies when $y \sim r \gg \mu_0$. Thus in this limit the metric asymptotes to that of a smeared membrane over a circle.

As $\lim_{p\mu_0 \rightarrow \infty} \tilde{c}_p = \lim_{p\mu_0 \rightarrow 0} \tilde{c}_p = 1/32$, it is consistent to set $\tilde{c}_p \equiv 1/32$ for all values of $p\mu_0$.

To summarize

$$h(p, r) = \frac{1}{32} p^2 \Gamma\left(\frac{p\mu_0}{2}\right) e^{-pr} \mathcal{U}\left(1 + \frac{p\mu_0}{2}, 2, 2pr\right). \quad (3.24)$$

Dimensional reduction of the above solution along the ψ coordinate of the Taub-NUT geometry gives rise to the type IIA supergravity solution describing D2-branes localized along the world volume of D6-branes. The metric part of the solution is given by

$$ds^2 = H(y, r)^{-1/2} \left(1 + \frac{\mu_0}{r}\right)^{-1/2} (-dt^2 + dx_1^2 + dx_2^2) + H(y, r)^{1/2} \left[\left(1 + \frac{\mu_0}{r}\right)^{-1/2} (dy^2 + y^2 d\Omega_3^2) + \left(1 + \frac{\mu_0}{r}\right)^{1/2} (dr^2 + r^2 d\Omega_2^2) \right], \quad (3.25)$$

It is clear that when I set $Q_{M2} = 0$ the solution reduces to the supergravity solution containing only the D6-branes. Similarly, in the $N_6 \rightarrow 0$ limit,

$$H(y, r) = 1 + \frac{Q_{D2}}{(y^2 + r^2)^{5/2}}. \quad (3.26)$$

The Decoupling Limit: The gauge theory coupling and the corresponding 't Hooft coupling for the D2-branes is

$$g_{YM2}^2 = \frac{g_s}{l_s}, \quad \lambda_2 = g_{YM2}^2 N_2 = \frac{g_s}{l_s} N_2, \quad (3.27)$$

and for the D6-branes is

$$g_{YM6}^2 = (2\pi)^4 g_s l_s^3, \quad \lambda_6 = g_{YM6}^2 N_6 = (2\pi)^4 g_s l_s^3 N_6, \quad (3.28)$$

respectively. The decoupling limit is taken by $l_s \rightarrow 0$ and $g_s \rightarrow 0$ with g_s/l_s fixed. The near horizon geometry in the metric (3.25) can be identified using the re-scaling

$$Y = \frac{y}{l_s^2}, \quad U = \frac{r}{l_s}, \quad (3.29)$$

with Y and U fixed in the decoupling limit. In this limit

$$1 + \frac{\mu_0}{r} = 1 + \frac{g_s l_s N_6}{2r} = 1 + \frac{g_{YM2}^2 N_6}{2U}, \quad (3.30)$$

$$H(Y, U) = 1 + \frac{1}{l_s^4} \tilde{H}(Y, U) \longrightarrow \frac{1}{l_s^4} \tilde{H}(Y, U), \quad (3.31)$$

where

$$\tilde{H}(Y, U) = g_{YM2}^4 \pi^2 N_2 N_6 \int dP P^4 \frac{J_1(PY)}{Y} \Gamma\left(\frac{g_{YM2}^2 N_6 P}{4}\right) e^{-PU} \mathcal{U}\left(1 + \frac{g_{YM2}^2 N_6 P}{4}, 2, 2PU\right). \quad (3.32)$$

Hence one sees that in this decoupling limit, the 1 in the warp factor H , which is sourced by the D2-branes, is dropped while the 1 in the harmonic function sourced by the D6-branes is retained. In the limit (3.28), both g_{YM6}^2 and λ_6 vanish. Hence the dynamics on the D6-branes decouples and one is left with a 1+2-dimensional maximally symmetric $SU(N_2)$ SYM with fundamental matter in $N_6 \mathcal{N} = 2$ hypermultiplets.

3.3 The Non-extremal Solution

As an opportunity to understand the effect of flavors on finite temperature properties of hot gauge theory plasmas, an important matter at hand would be to find the non-extremal D2/D6-brane solution or the black M2-brane in the $\mathbb{R}^{1,6} \times \text{Taub-NUT}$ background. The problem can be simplified further by noting that it is possible to generate the M2 brane solution by starting with the 9-dimensional Schwarzschild solution which is demonstrated in Appendix C. Using this method, I reduce the problem to finding a black hole solution in $\mathbb{R}^{1,4} \times \text{Taub-NUT}$. Given the symmetries of the problem, the most general Ansatz allowed is

$$ds_9^2 = -p_1 dt^2 + \left(1 + \frac{p_2}{p_1}\right) dy^2 + y^2 d\Omega_3^2 + 2\frac{p_4}{p_1} dy dr + \left(1 + \frac{\mu_0}{r} + \frac{p_3}{p_1}\right) dr^2 + \left(1 + \frac{\hat{\mu}}{r}\right) r^2 [d\theta^2 + \sin^2 \theta d\phi^2] + \left(1 + \frac{\hat{\mu}}{r}\right)^{-1} [d\psi + \mu_0 \cos \theta d\phi]^2, \quad (3.33)$$

where p_1, p_2, p_3, p_4 and $\hat{\mu}$ are all function of both y and r . I will assume here that p_1 has a single zero at the horizon and $p_{2,3,4}$ and $\hat{\mu}$ do not have any zero or poles at and outside the horizon. The problem of finding the non-extremal localized solution of the D2/D6-brane system has now been reduced to finding the vacuum solution of the above Ansatz. Even then, the equations to be solved are coupled, non-linear, partial differential equations in two variables involving at least 5 function, which is quite intractable. I will only present the solution to the linearized system. But before doing this, let's check if the determinant of this metric,

$$\det g_{\mu\nu} = \left[(r + \mu_0)(p_1 + p_2) + p_3 + r \frac{p_2 p_3 - p_4^2}{p_1} \right] (r + \hat{\mu}) r^2 y^6 \sin^2 \theta \sin^4 \chi_1 \sin^2 \chi_2, \quad (3.34)$$

is non-degenerate. This is the case provided

$$p_2 p_3 - p_4^2 = p_1 f, \quad (3.35)$$

with f some arbitrary function.

To linearize the system, I introduce

$$p_1 = 1 - \epsilon q_1, \quad p_{2,3,4} = \epsilon q_{2,3,4} \quad \hat{\mu} = \mu_0 + \epsilon r \mu_1. \quad (3.36)$$

where ϵ is a small dimensionless parameter which can be thought of as dialing the energy density and q_1, q_2, q_3, q_4 and μ_1 are all function of y and r . The linearized metric is

$$ds^2 = -(1 - \epsilon q_1) dt^2 + (1 + \epsilon q_2) dy^2 + y^2 d\Omega_3^2 + 2\epsilon q_4 dy dr + \left(1 + \frac{\mu_0}{r} + \epsilon q_3\right) dr^2 + \left(1 + \frac{\mu_0}{r} + \epsilon \mu_1\right) r^2 (d\theta^2 + \sin^2 \theta d\phi^2) + \left(1 - \frac{\epsilon \mu_1}{1 + \frac{\mu_0}{r}}\right) \frac{[d\psi + \mu_0 \cos \theta d\phi]^2}{1 + \frac{\mu_0}{r}}. \quad (3.37)$$

The equations of motion are just the Einstein equations in vacuum, i.e. $R_{\mu\nu} = 0$. The non-vanishing components of the Ricci tensor are the nine diagonal components and two off-diagonal components R_{yr} and $R_{\phi\psi}$, not all of which are independent:

1. By the symmetries of S^3 , $R_{\chi_3\chi_3} = \sin^2 \chi_2 R_{\chi_2\chi_2} = \sin^2 \chi_1 \sin^2 \chi_2 R_{\chi_1\chi_1}$.
2. $R_{\phi\phi}$ can be expressed as $R_{\phi\phi} = R_{\phi\phi}^{(1)} + R_{\phi\phi}^{(2)} \cos 2\theta$, with $2R_{\phi\phi}^{(1)} = \mu_0^2 R_{\psi\psi} + R_{\theta\theta}$ and $2R_{\phi\phi}^{(2)} = \mu_0^2 R_{\psi\psi} - R_{\theta\theta}$.
3. Note that $\mu_0 \cos \theta R_{\theta\theta} = R_{\theta\psi}$.

This reduces the total number of non-vanishing components by 4. In the following, I will only use R_{tt} , R_{yy} , R_{rr} , R_{yr} , $R_{\chi_1\chi_1}$, $R_{\theta\theta}$, and $R_{\psi\psi}$, which only depend on y and r .

In the rest of this section, I will show how the solutions to the Einstein equations are obtained, in particular the solutions for q_1 , q_2 , q_3 , q_4 and μ_1 . As these are linear, homogeneous equations, all solutions will be determined only up to constants of integration.

3.3.1 Solutions for q_1 and q_2

$R_{tt} = 0 \Leftrightarrow \nabla^2 q_1 = 0$, which has already been solved in Section 3.2 and the solution is

$$q_1(y, r) = Q_{M2} N_6 \int dp p^2 \frac{J_1(py)}{y} Q_1(p, r), \quad (3.38)$$

$$Q_1 = b_1(p\mu_0) \Gamma\left(\frac{p\mu_0}{2}\right) p^2 e^{-pr} \mathcal{U}\left(1 + \frac{p\mu_0}{2}, 2, 2pr\right), \quad (3.39)$$

where $b_1(p\mu_0)$ is a dimensionless integration constant and the $\Gamma\left(\frac{p\mu_0}{2}\right)$ is motivated in the discussion below (3.16).

The combination $y(\partial_y R_{\chi_1\chi_1} - R_{yy}) - R_{\chi_1\chi_1} = 0$ leads to a second order differential equation for q_2

$$-4(r + \mu_0)q_2 + y^2(2\partial_r + r\partial_r^2)q_2 + y(r + \mu_0)(\partial_y + y\partial_y^2)q_2 = 0, \quad (3.40)$$

which can be re-written as

$$\nabla_{TN,6}^2 \left(\frac{q_2}{y^2}\right) \equiv \frac{1}{1 + \frac{\mu_0}{r}} \frac{1}{r^2} \partial_r \left(r^2 \partial_r \left(\frac{q_2}{y^2}\right) \right) + \frac{1}{y^5} \partial_y \left(y^5 \partial_y \left(\frac{q_2}{y^2}\right) \right) = 0, \quad (3.41)$$

where ∇_6^2 is the laplacian on the background $\mathbb{R}^6 \times \text{Taub-NUT}$. Remember that q_1 is a harmonic function in $\mathbb{R}^4 \times \text{Taub-NUT}$. Employing the same methods as were used for solving (3.9), I separate the equations by doing a fourier transform in \mathbb{R}^6 . This gives

$$\frac{q_2}{y^2} = Q_{M2} N_6 \int \frac{d^6 p}{(2\pi)^3} e^{i p \cdot y} Q_2(p, r) = Q_{M2} N_6 \int dp \frac{J_2(py)}{y^2} Q_2(p, r), \quad (3.42)$$

where the dot product, $p \cdot y$, is now in \mathbb{R}^6 . Inserting (3.42) into (3.41) gives

$$\mathbb{D}Q_2 = 0, \quad \implies Q_2(p, r) = p^2 b_2(p\mu_0) \Gamma\left(\frac{p\mu_0}{2}\right) e^{-pr} \mathcal{U}\left(1 + \frac{p\mu_0}{2}, 2, 2pr\right), \quad (3.43)$$

where $b_2(p\mu_0)$ is again a dimensionless constant of integration and p^2 is determined by dimensional analysis. Doing the integral over the angles in (3.42), with the help of (D.20) and (D.21), and inserting the solution for Q_2 gives the solution

$$q_2(y, r) = Q_{M2} N_6 \int dp p^5 J_2(py) b_2(p\mu_0) \Gamma\left(\frac{p\mu_0}{2}\right) e^{-pr} \mathcal{U}\left(1 + \frac{p\mu_0}{2}, 2, 2pr\right). \quad (3.44)$$

3.3.2 Solutions for q_3 and q_4

The combination $(\mu_0 + 2r)R_{\psi\psi} - \frac{\mu_0}{(\mu_0+r)^2}R_{\theta\theta} = 0$ leads to an equation for q_3 in terms of derivatives of μ_1 only

$$q_3(y, r) = \mu_1 + \frac{(\mu_0 + r)^3}{\mu_0} k + 2(\mu_0 + r) \partial_r \mu_1, \quad (3.45)$$

where the function k is defined by the equation

$$\nabla^2 \mu_1 \equiv k. \quad (3.46)$$

The homogeneous solution to this equation would be the same as the solution for q_1 .

The combination $(R_{\psi\psi} + R_{\theta\theta})/(2y(r + \mu_0)^3)$ gives a first order equation in q_4 ,

$$\begin{aligned} \frac{2}{y^3} \partial_y (y^3 q_4) &= \frac{(2r + 3\mu_0)}{(r + \mu_0)^2} (q_3 - \mu_1) + \frac{r}{(r + \mu_0)} \partial_r (\mu_1 - q_3) + \partial_r (q_2 - q_1) \\ &= -2 (r \partial_r^2 \mu_1 + 3 \partial_r \mu_1) - \frac{(r + \mu_0)(5r + 3\mu_0)}{\mu_0} k - \frac{r(r + \mu_0)^2}{\mu_0} \partial_r^2 k \\ &\quad + \partial_r (q_2 - q_1), \end{aligned} \quad (3.47)$$

where (3.45) has been used to eliminate q_3 in the last equality. This expressions can be easily integrated to obtain

$$\begin{aligned} 2q_4 &= -2 (r \partial_r^2 \tilde{\mu}_1 + 3 \partial_r \tilde{\mu}_1) - \frac{(r + \mu_0)(5r + 3\mu_0)}{\mu_0} \tilde{k} - \frac{r(r + \mu_0)^2}{\mu_0} \partial_r^2 \tilde{k} \\ &\quad + \partial_r (\tilde{q}_2 - \tilde{q}_1) + \frac{2g(r)}{y^3}, \end{aligned} \quad (3.48)$$

where the $\tilde{}$ defines the integral

$$\tilde{f} = \frac{1}{y^3} \int dy y^3 f. \quad (3.49)$$

In the next section, I will demonstrate that the solution for μ_1 and k has the same y -dependence as q_1 given in (3.38). So let's assume

$$\mu_1(y, r) = Q_{M2} N_6 \int \frac{d^4 p}{(2\pi)^2} e^{ip \cdot y} M(p, r) = Q_{M2} N_6 \int dp p^2 \frac{J_1(py)}{y} M(p, r), \quad (3.50)$$

$$k(y, r) = Q_{M2} N_6 \int \frac{d^4 p}{(2\pi)^2} e^{ip \cdot y} K(p, r) = Q_{M2} N_6 \int dp p^2 \frac{J_1(py)}{y} K(p, r). \quad (3.51)$$

Then using the integrals of Bessel functions given in (D.22) and (D.23), the solution for q_4 becomes

$$\begin{aligned} 2q_4 &= Q_{M2} N_6 \int dp \left\{ p^2 J_3(py) \partial_r Q_2 - p \frac{J_2(py)}{y} \right. \\ &\quad \times \left[\frac{2}{r^2} \partial_r (r^3 \partial_r M) + \frac{(r + \mu_0)(5r + 3\mu_0)}{\mu_0} K \right. \\ &\quad \left. \left. + \frac{r(r + \mu_0)^2}{\mu_0} \partial_r^2 K + \partial_r Q_1 \right] \right\} + 2 \frac{g(r)}{y^3}, \end{aligned} \quad (3.52)$$

where I can set $g(r) \equiv 0$. Similarly by inserting (3.50) and (3.51) into (3.45), I obtain

$$q_3(y, r) = Q_{M_2} N_6 \int dp p^2 \frac{J_1(py)}{y} \left\{ M + \frac{(\mu_0 + r)^3}{\mu_0} K + 2(\mu_0 + r) \partial_r M \right\}. \quad (3.53)$$

The functions Q_1 and Q_2 are given in (3.39) and (3.43) respectively while K and M will be given later in (3.70) and (3.73).

3.3.3 Solution for μ_1

The Einstein equation $R_{yr} = 0$ leads to

$$6(r + \mu_0)^2 \partial_r q_2 + (4r + 3\mu_0)y(\partial_y q_3 - \partial_y \mu_1) + 2y(r + \mu_0)^2 \partial_r \partial_y q_1 - 2r(r + \mu_0)y \partial_r \partial_y \mu_1 = 0 \quad (3.54)$$

Using (3.45) and (3.46) the above equation can be further simplified to

$$\partial_r q_2 + \frac{(\mu_0 + r)(4r + 3\mu_0)}{6\mu_0} y \partial_y k + \frac{y}{3} \partial_r \partial_y q_1 + y \partial_r \partial_y \mu_1 = 0 \quad (3.55)$$

Integrating (3.55) w.r.t. r leads to

$$q_2 = -y \partial_y \left(\frac{1}{3} q_1 + \mu_1 + k_1 \right) + f(y), \quad (3.56)$$

where

$$k_1 \equiv \frac{1}{6\mu_0} \int dr (\mu_0 + r)(4r + 3\mu_0) k \quad (3.57)$$

Given the fact that

$$\nabla_{TN,6}^2 (y^{-1} \partial_y) = y^{-1} \partial_y \nabla^2, \quad (3.58)$$

the application of $\nabla_{TN,6}^2$ on (3.56) gives

$$\nabla^2 (\mu_1 + k_1) = 0, \quad (3.59)$$

along with the requirement $f(y) = f_0 y^{-2}$, with f_0 some constant which is set to zero. (3.59) is again the same equation which is satisfied by H and q_1 . So the solution is

$$\mu_1 + k_1 = Q_{M_2} N_6 \int dp p^2 \frac{J_1(py)}{y} \left(p^2 b_{\mu_1}(p\mu_0) \Gamma\left(\frac{p\mu_0}{2}\right) \mathcal{U}\left(1 + \frac{p\mu_0}{2}, 2, 2pr\right) \right). \quad (3.60)$$

One can check that indeed $\nabla^2 k_1 = -k$. This means that k_1 is the particular integral for μ_1 .

To determine k , I use the combination $(R_{rr} - \mu_0 y (r + \mu_0)^2 (3.47) - 2ry(r + \mu_0)^3 \partial_r (3.47))$, which leads to an equation involving only μ_1 and q_3

$$y(2r + 5\mu_0)(q_3 - \mu_1) + y(2r - \mu_0)\partial_r(q_3 - \mu_1) - y(r + \mu_0)^3 \nabla^2 q_3 = 0. \quad (3.61)$$

On eliminating q_3 using (3.45), I obtain second order partial differential equation for k ,

$$(5\mu_0 + 4r)k + (\mu_0 + r)^3 \left(\frac{3}{y} \partial_y k + \partial_y^2 k \right) + (\mu_0 + r)(5\mu_0 + 6r)\partial_r k + r(\mu_0 + r)^2 \partial_r^2 k = 0. \quad (3.62)$$

By doing the fourier transform given in (3.51), (3.62) reduces to an ordinary differential given by

$$(5\mu_0 + 4r)K - p^2(\mu_0 + r)^3 K + (\mu_0 + r)(5\mu_0 + 6r)\partial_r K + r(\mu_0 + r)^2 \partial_r^2 K = 0. \quad (3.63)$$

In the limit $p\mu_0 \rightarrow 0$ with pr fixed, this differential equation reduces to

$$r^2 \frac{d^2 K}{dr^2} + 6r \frac{dK}{dr} + (4 - p^2 r^2)K = 0, \quad (3.64)$$

which has a solution

$$K \propto \frac{e^{-pr}}{(pr)^4} (1 + pr). \quad (3.65)$$

In the limit $p\mu_0 \rightarrow \infty$ with pz fixed where $z^2 = 4\mu_0 r$, the differential equation (3.63)

reduces to

$$\frac{d^2 K}{dz^2} + \frac{9}{z} \frac{dK}{dz} - p^2 K = 0, \quad (3.66)$$

which has the solution

$$K \propto \frac{K_4(pz)}{z^4}, \quad (3.67)$$

where $K_4(pz)$ is a modified Bessel function.

To solve (3.63), set

$$K = \frac{K_p(r)}{r^{5/2}(r + \mu_0)^{1/2}}, \quad r = -\mu_0 \xi, \quad (3.68)$$

which gives the second order differential equation

$$\frac{d^2}{d\xi^2} K_p(\xi) + \left(-p^2 \mu_0^2 + \frac{p^2 \mu_0^2 - 5/2}{\xi} + \frac{5/2}{\xi - 1} - \frac{15/4}{\xi^2} - \frac{3/4}{(\xi - 1)^2} \right) K_p(\xi) = 0. \quad (3.69)$$

This is the same type of confluent Heun equation which is discussed in [115], and given in Appendix D.2, with the choice of parameters $\sigma = 1/2$, $\tau = -2/(p\mu_0)$ and $\lambda = p\mu_0$. The solution can be deduced from (D.9) with these parameters which gives

$$K(p, r) = p^3 k_p \Gamma \left(1 + \frac{p\mu_0}{2} \right) \frac{e^{-pr}}{r + \mu_0} \times \left\{ \mathcal{U} \left(2 + \frac{p\mu_0}{2}, 5, 2pr \right) + \left(\frac{p\mu_0}{2} - 2 \right) \mathcal{U} \left(3 + \frac{p\mu_0}{2}, 5, 2pr \right) \right\}, \quad (3.70)$$

where k_p is an arbitrary dimensionless function that depends on $p\mu_0$. By using (3.4) and (D.16), I obtain

$$\lim_{p\mu_0 \rightarrow \infty} \Gamma \left(\frac{p\mu_0}{2} - 2 \right) \left(\mathcal{U} \left(2 + \frac{p\mu_0}{2}, 5, 2pr \right) + \left(\frac{p\mu_0}{2} - 2 \right) \mathcal{U} \left(3 + \frac{p\mu_0}{2}, 5, 2pr \right) \right) \propto \frac{K_4(pz)}{(pz)^4}, \quad (3.71)$$

which agrees with (3.67). On the other hand

$$\lim_{p\mu_0 \rightarrow 0} \left(\mathcal{U} \left(2 + \frac{p\mu_0}{2}, 5, 2pr \right) + \left(\frac{p\mu_0}{2} - 2 \right) \mathcal{U} \left(3 + \frac{p\mu_0}{2}, 5, 2pr \right) \right) \propto \frac{(1+pr)}{(pr)^3}, \quad (3.72)$$

as expected in (3.65).

As a further check of the self-consistency of this solution, the derivative of (3.59) with respect to r gives (3.62). Hence the solution for M is

$$\begin{aligned} M = & p^2 b_{\mu_1}(p\mu_0) e^{-pr} \mathcal{U} \left(1 + \frac{p\mu_0}{2}, 2, 2pr \right) \\ & - \frac{1}{6\mu_0} \int dr (4r + 3\mu_0) p^3 k_p(p\mu_0) e^{-pr} \\ & \times \left(\mathcal{U} \left(2 + \frac{p\mu_0}{2}, 5, 2pr \right) + (p\mu_0/2 - 2) \mathcal{U} \left(3 + \frac{p\mu_0}{2}, 5, 2pr \right) \right) \end{aligned} \quad (3.73)$$

The solutions given in (3.38), (3.39), (3.44), (3.60) for $q_1, q_2, \mu_1 + k_1$ each contain integration constants. These constants are related by

$$b_2(p\mu_0) = \frac{b_1(p\mu_0)}{3} + b_{\mu_1}(p\mu_0). \quad (3.74)$$

This relationship is obtained by inserting the solutions derived in this and the previous sections into (3.56) and using (D.17).

3.3.4 $N_6 \gg 1$ Limit

Very close to core of the Taub-NUT, $y, r \ll \mu_0$ or $N_6 \gg 1$, the non-extremal solution presented in this chapter must reduce to the Schwarzschild black hole in 9-dimensions whose metric, when linearized, is

$$ds_{9,SS}^2 \longrightarrow - (1 - \epsilon f_9(\rho)) dt^2 + \left\{ 1 + \epsilon \frac{y^2}{y^2 + z^2} f_9(\rho) \right\} dy^2 + y^2 d\Omega_{3(1)}^2 \quad (3.75)$$

$$+ 2\epsilon \frac{yz}{y^2 + z^2} f_9(\rho) dy dz + \left\{ 1 + \epsilon \frac{z^2}{y^2 + z^2} f_9(\rho) \right\} dz^2 + z^2 d\Omega_{3(2)}^2, \quad (3.76)$$

where $f_9(\rho) = \rho_H^6/\rho^6$ with horizon at $\rho^6 = \rho_H^6$. In this limit, the appropriate coordinates have $z^2 = 4\mu_0 r$ fixed and the Ansatz in (3.37) take the form

$$\begin{aligned}
ds_{9,\text{lin}}^2 = & -(1 - \epsilon q_1) dt^2 + (1 + \epsilon q_2) dy^2 + y^2 d\Omega_3^2 + 2\epsilon \frac{q_4}{\mu_0} z dz dy \\
& + \left(1 + \frac{4\mu_0^2}{z^2} + \epsilon q_3\right) \frac{z^2 dz^2}{4\mu_0^2} + \left(1 + \frac{4\mu_0^2}{z^2} + \epsilon \mu_1\right) \frac{z^4}{16\mu_0^2} (d\theta^2 + \sin^2 \theta d\phi^2) \\
& + \left(1 + \frac{4\mu_0^2}{z^2}\right)^{-1} \left\{1 - \frac{\epsilon \mu_1}{1 + \frac{4\mu_0^2}{z^2}}\right\} [d\psi + \mu_0 \cos \theta d\phi]^2. \tag{3.77}
\end{aligned}$$

Comparing (3.77) to (3.75) tells us that in this limit I must obtain

$$\begin{aligned}
q_1 & \longrightarrow \frac{\rho_H^6}{(y^2 + z^2)^3}, & \frac{q_3}{\mu_0^2} & \longrightarrow \frac{4\rho_H^6}{(y^2 + z^2)^4} \\
q_2 & \longrightarrow \frac{y^2 \rho_H^6}{(y^2 + z^2)^4}, & \frac{q_4}{\mu_0} & \longrightarrow \frac{2y\rho_H^6}{(y^2 + z^2)^4}. \tag{3.78}
\end{aligned}$$

Choosing $\lim_{p\mu_0 \rightarrow \infty} k_p(p\mu_0) = 0$ gives $K = 0$. Next choose Then in the limit $y, r \ll \mu_0$ (with $r = \frac{z^2}{4\mu_0}$ and using (D.24))

$$\mu_1 = \frac{32b_{\mu_1}}{(y^2 + z^2)^3} \tag{3.79}$$

With this and using the integrals (D.24)-(D.27) in the solutions for q_i , $i = 1, \dots, 4$, reduce to

$$q_1 \longrightarrow Q_{M2} \frac{32b_1}{(y^2 + z^2)^3} \tag{3.80}$$

$$q_2 \longrightarrow Q_{M2} \left(b_{\mu_1} + \frac{b_1}{3}\right) \frac{192y^2}{(y^2 + z^2)^4} = Q_{M2} \frac{32b_1 y^2}{(y^2 + z^2)^4} \tag{3.81}$$

$$q_3 \longrightarrow Q_{M2} \left[\mu_1 + 2 \left(\mu_0 + \frac{z^2}{4\mu_0}\right) \frac{2\mu_0}{z} \partial_z \mu_1\right] = 32b_{\mu_1} Q_{M2} \frac{-24\mu_0^2 + y^2 - 5z^2}{(y^2 + z^2)^4} \tag{3.82}$$

$$= 4\mu_0^2 Q_{M2} \frac{32b_1}{(y^2 + z^2)^4} \tag{3.83}$$

$$q_4 \longrightarrow Q_{M2} \mu_0 \frac{64b_1 y}{(y^2 + z^2)^4} \quad (\text{for } b_{\mu_1} = -\frac{1}{6}b_1) \tag{3.84}$$

Matching of the above solution to the Schwarzschild solution requires $b_{\mu_1} = -\frac{1}{6}b_1$, which has been used in the last equality in every equation. If I set $32b_1Q_{M2} = \rho_H^6$, I get the desired limit in (3.78).

3.3.5 $N_6 \ll 1$ Limit

Far from the core of the Taub-NUT, $y, r \gg \mu_0$ or $N_6 \ll 1$, I want the non-extremal solution presented here to reduce to the linearized Schwarzschild solution in $\mathbb{R}^{1,7}$ which is

$$ds_{8,SS}^2 \longrightarrow - (1 - \epsilon f_8(x))dt^2 + (1 + \epsilon f_8(x))dx^2 + x^2 d\Omega_6^2, \quad (3.85)$$

$$\begin{aligned} &= - (1 - \epsilon f_8(x))dt^2 + \left\{ 1 + \epsilon \frac{y^2}{y^2 + r^2} f_8(x) \right\} dy^2 + y^2 d\Omega_3^2 \\ &\quad + 2\epsilon \frac{yr}{y^2 + r^2} f_8(x) dydr + \left\{ 1 + \epsilon \frac{r^2}{y^2 + r^2} f_8(x) \right\} dr^2 + r^2 d\Omega_2^2, \end{aligned} \quad (3.86)$$

with $x^2 = y^2 + r^2$, $f_8(x) = x_H^5/x^5$ and $x = x_H$ is the horizon of the black hole. Comparing this with my solution after a dimensional reduction along ψ , I must obtain

$$\begin{aligned} q_1 &\longrightarrow \frac{x_H^5}{(y^2 + r^2)^{5/2}}, & q_3 &\longrightarrow \frac{r^2 x_H^5}{(y^2 + r^2)^{7/2}} \\ q_2 &\longrightarrow \frac{y^2 x_H^5}{(y^2 + r^2)^{7/2}}, & q_4 &\longrightarrow \frac{2yr x_H^5}{(y^2 + r^2)^{7/2}}, \end{aligned} \quad (3.87)$$

when $N_6 \ll 1$.

To obtain a membrane smeared over an S^1 , along which the system is dimensionally reduced in this limit, it must be true that $\lim_{N_6 \rightarrow 0} \mu_1 \rightarrow 0$. This is true if

$$\lim_{p\mu_0 \rightarrow 0} k_p = -6 \lim_{p\mu_0 \rightarrow 0} b_{\mu_1}. \quad (3.88)$$

Thus from equation (3.60), I find

$$\begin{aligned} k_1 &\approx \frac{1}{y} \int dp p^2 b_{\mu_1} J_1(py) e^{-pr} \mathcal{U} \left(1 + \frac{p\mu_0}{2}, 2, 2pr \right) \\ &\approx \frac{1}{y} \int dp p^2 b_{\mu_1} J_1(py) \frac{e^{-pr}}{2pr}, \end{aligned} \quad (3.89)$$

where in the last expression, I have used (D.14), which is true when $y, r \gg \mu_0$. Thus

$$\frac{k}{\mu_0} \approx \frac{6}{4r^2} \partial_r k_1 \approx -\frac{3}{4r^4 y} \int dp p b_{\mu_1} J_1(py) e^{-pr} (1 + pr) \quad (3.90)$$

and

$$q_3 \approx \frac{r^3 k}{\mu_0}, \quad (3.91)$$

$$q_4 \approx -\frac{1}{2} \partial_r (\tilde{q}_1 - \tilde{q}_2) - \frac{5r^2}{2\mu_0} \tilde{k} - \frac{r^3}{2\mu_0} \partial_r \tilde{k} \quad (3.92)$$

with

$$\frac{\tilde{k}(y, r)}{\mu_0} = \frac{1}{y^3} \int dy y^3 \frac{k}{\mu_0} = -\frac{6}{8r^4 y} \int dp b_{\mu_1} J_2(py) e^{-pr} (1 + pr), \quad (3.93)$$

$$\tilde{q}_1(y, r) = \frac{1}{2ry} \int dp b_1 J_2(py) e^{-pr}, \quad (3.94)$$

$$\tilde{q}_2(y, r) = \frac{1}{2r} \int dp p b_2 J_3(py) e^{-pr}. \quad (3.95)$$

In the limit $y, r \gg \mu_0$ (using the integrals in (D.28)-(D.31))

$$q_1 = Q_{M2} \frac{3b_1}{\mu_0} \frac{1}{(y^2 + r^2)^{\frac{5}{2}}} \quad (3.96)$$

$$q_2 = Q_{M2} \frac{15}{\mu_0} \left(b_{\mu_1} + \frac{b_1}{3} \right) \frac{y^2}{(y^2 + r^2)^{\frac{7}{2}}} = Q_{M2} \frac{3b_1}{\mu_0} \frac{y^2}{(y^2 + r^2)^{\frac{7}{2}}} \quad (3.97)$$

$$\frac{k}{\mu_0} \approx -Q_{M2} \frac{6b_{\mu_1}}{4\mu_0 r} \frac{15}{(r^2 + y^2)^{7/2}} \quad (3.98)$$

$$q_3 = -Q_{M2} \frac{6b_{\mu_1}}{4\mu_0} \frac{15r^2}{(r^2 + y^2)^{7/2}} = Q_{M2} \frac{3b_1}{\mu_0} \frac{r^2}{(r^2 + y^2)^{7/2}} \quad (3.99)$$

$$q_4 = Q_{M2} \frac{3b_1}{\mu_0} \frac{yr}{(r^2 + y^2)^{7/2}} \quad (b_1 = -\frac{2}{15} b_{\mu_1}) \quad (3.100)$$

where in the last equality of all equations I have fixed $b_{\mu_1} = -\frac{2}{15}b_1$. Again setting $x_H^5 \equiv 3b_1 Q_{M2}/\mu_0$ gives us the desired result in (3.87) in the limit $N_6 \rightarrow 0$. However, the relationship between b_1 and b_{μ_1} is different here from the case where $N_6 \gg 1$. Hence I discover that these constants of integration depend non-trivially on N_6 .

3.4 The 11-dimensional Solution

As mentioned in the previous section, the black hole in $\mathbb{R}^{1,4} \times \text{Taub-NUT}$ can be used to generate the non-extremal M2-brane solution in 11-dimensional supergravity in $\mathbb{R}^{1,6} \times \text{Taub-NUT}$ with the M2-brane transverse to the Taub-NUT space. And as discussed in Section 3.2, a dimensional reduction along ψ would lead to the non-extremal, localized D2/D6-brane solution. In this section, I will use the solution given in Section 3.3 to generate M2-brane solution in the desired background, following closely the discussion in Appendix C which is based on Section 2.5 in [116].

I first add a trivial direction x_1 to the 9-dimensional Ansatz (3.37).

$$\begin{aligned}
ds_{10}^2 = & (-dt^2 + dx_1^2) + \epsilon q_1(y, r) dt^2 + (1 + \epsilon q_2(y, r)) dy^2 + y^2 d\Omega_3^2 + 2\epsilon q_4(y, r) dy dr + \\
& + \left(1 + \frac{\mu_0}{r} + \epsilon q_3(y, r)\right) dr^2 + \left(1 + \frac{\mu_0}{r} + \epsilon \mu_1(y, r)\right) r^2 (d\theta^2 + \sin^2 \theta d\phi^2) \\
& + \left(1 + \frac{\mu_0}{r}\right)^{-1} \left\{1 - \frac{\epsilon \mu_1(y, r)}{1 + \frac{\mu_0}{r}}\right\} [d\psi + \mu_0 \cos \theta d\phi]^2.
\end{aligned} \tag{3.101}$$

This is automatically a solution in 10-dimensional supergravity with all other fields set to zero. Performing a Lorentz boost in the $t - x_1$ plane with boost parameter γ

$$\begin{pmatrix} dt \\ dx_1 \end{pmatrix} \longrightarrow \begin{pmatrix} \cosh \gamma & \sinh \gamma \\ \sinh \gamma & \cosh \gamma \end{pmatrix} \begin{pmatrix} dt \\ dx_1 \end{pmatrix} \tag{3.102}$$

gives the metric

$$\begin{aligned}
ds_{10}^2 = & -dt^2(1 - \epsilon q_1(y, r) \cosh^2 \gamma) + dx_1^2(1 + \epsilon q_1(y, r) \sinh^2 \gamma) + 2dt dx_1 \cosh \gamma \sinh \gamma \\
& (1 + \epsilon q_2(y, r)) dy^2 + y^2 d\Omega_3^2 + 2\epsilon q_4(y, r) dy dr + \\
& + \left(1 + \frac{\mu_0}{r} + \epsilon q_3(y, r)\right) dr^2 + \left(1 + \frac{\mu_0}{r} + \epsilon \mu_1(y, r)\right) r^2 (d\theta^2 + \sin^2 \theta d\phi^2) \\
& + \left(1 + \frac{\mu_0}{r}\right)^{-1} \left\{1 - \frac{\epsilon \mu_1(y, r)}{1 + \frac{\mu_0}{r}}\right\} [d\psi + \mu_0 \cos \theta d\phi]^2
\end{aligned} \tag{3.103}$$

This is a background with no matter, in particular the dilaton $\Phi = 0$ and Neveu-Shwarz (NS) 2-form $B_{\mu\nu} = 0$. On T-dualizing along the x_1 direction, I get both a dilaton $\tilde{\Phi}$ and a 2-form potential $\tilde{B}_{\mu\nu}$ using the Buscher rules (see [117] and references therein), where the \sim denotes the T-dual quantities and μ and ν indicate all the directions transverse to x_1 . The results of this transformation for the dilaton the NS 2-form are

$$e^{\tilde{\Phi}} = \frac{e^{\Phi}}{G_{x_1 x_1}} = \frac{1}{1 + \epsilon q_1(y, r) \sinh^2 \gamma}, \tag{3.104}$$

$$\tilde{B}_{\mu\nu} = B_{\mu\nu} - \frac{B_{\mu x_1} G_{\nu x_1} - B_{\nu x_1} G_{\mu x_1}}{G_{x_1 x_1}} = 0, \tag{3.105}$$

$$\begin{aligned}
\tilde{B}_{\mu x_1} &= \frac{G_{\mu x_1}}{G_{x_1 x_1}} = \delta_{\mu t} \frac{\epsilon q_1(y, r) \cosh \gamma \sinh \gamma}{1 + \epsilon q_1(y, r) \sinh^2 \gamma} \\
&= -\delta_{\mu t} \coth \gamma [(1 + \epsilon q_1(y, r) \sinh^2 \gamma)^{-1} - 1],
\end{aligned} \tag{3.106}$$

while for the metric are

$$\tilde{G}_{x_1 x_1} = \frac{1}{G_{x_1 x_1}} = \frac{1}{1 + \epsilon q_1(y, r) \sinh^2 \gamma}, \quad (3.107)$$

$$\tilde{G}_{\mu x_1} = \frac{B_{\mu x_1}}{G_{x_1 x_1}} = 0, \quad (3.108)$$

$$\begin{aligned} \tilde{G}_{\mu\nu} &= G_{\mu\nu} - \frac{G_{\mu x_1} G_{\nu x_1} - B_{\mu x_1} B_{\nu x_1}}{G_{x_1 x_1}} \\ &= G_{\mu\nu} - \delta_{\mu t} \delta_{\nu t} \frac{(\epsilon q_1)^2 \cosh^2 \gamma \sinh^2 \gamma}{1 + \epsilon q_1(y, r) \sinh^2 \gamma} \\ &= \begin{cases} G_{\mu\nu} & \text{for } \mu \text{ or } \nu \neq t \\ -\frac{1 - \epsilon q_1(y, r)}{1 + \epsilon q_1(y, r) \sinh^2 \gamma} & \text{for } \mu = \nu = t \end{cases} \end{aligned} \quad (3.109)$$

Lifting to one higher dimension and using the Weyl transformation

$$ds^2 \longrightarrow (1 + \epsilon q_1(y, r) \sinh^2 \gamma)^{1/3} ds^2,$$

leads to the non-extremal solution

$$\begin{aligned} ds_{11}^2 &= (1 + \epsilon q_1(y, r) \sinh^2 \gamma)^{-2/3} [-(1 - \epsilon q_1(y, r)) dt^2 + dx_1^2 + dx_2^2] \\ &\quad + (1 + \epsilon q_1(y, r) \sinh^2 \gamma)^{1/3} [(1 + \epsilon q_2(y, r)) dy^2 + y^2 d\Omega_3^2 + 2\epsilon q_4(y, r) dy dr + \\ &\quad + \left(1 + \frac{\mu_0}{r} + \epsilon q_3(y, r)\right) dr^2 + \left(1 + \frac{\mu_0}{r} + \epsilon \mu_1(y, r)\right) r^2 (d\theta^2 + \sin^2 \theta d\phi^2) \\ &\quad + \left(1 + \frac{\mu_0}{r}\right)^{-1} \left\{1 - \frac{\epsilon \mu_1(y, r)}{1 + \frac{\mu_0}{r}}\right\} [d\psi + \mu_0 \cos \theta d\phi]^2] \end{aligned} \quad (3.110)$$

$$\tilde{B}_{tx_1 x_2} = -\coth \gamma (1 + \epsilon q_1(y, r) \sinh^2 \gamma)^{-1}, \quad (3.111)$$

where I identify $\tilde{B}_{tx_1 x_2}$ with the 3-form potential that couples to the M2-brane. Note here that in the limit $\epsilon \rightarrow 0$, $\gamma \rightarrow \infty$ with $\epsilon \sinh^2 \gamma = \alpha$ (α is some constant), I recover here the extremal M2-brane solution given in (3.7). As q_1 determines the extremal solution, I can fix $b_1 = 1/(32\alpha)$.

3.5 Conclusions

As discussed in Section 3.1, the non-extremal solution to the localized D2/D6 system would provide us with useful information about the hot plasma of the dual gauge theory including its thermodynamic quantities (e.g. temperature, entropy, free energy) and hydrodynamic transport coefficients (e.g. shear viscosity, bulk viscosity, speed of sound). However, as was discussed in Section 3.3, this is a highly non-trivial problem requiring the solution of a system of at least seven second order, coupled, non-linear partial differential equations with at least five dependent and two independent variables. Given this complexity of the problem, I linearized the system by introducing a dimensionless parameter ϵ which dials the amount of non-extremality of the system and treating everything as a power series expansion in it which is valid for $\epsilon \ll 1$. The solutions obtained involve un-determined constants of integration, b_1 , b_2 , b_{μ_1} and k_p (the first three are related by (3.74)), which depend non-trivially on $p\mu_0$. b_1 is fixed by the limit in which the extremal solution is recovered ($\epsilon \rightarrow 0$, $\gamma \rightarrow \infty$ with $\epsilon \sinh^2 \gamma = \text{constant}$) and has the same value in the two limits $N_6 \rightarrow 0, \infty$. However, the others are required by the known solutions to take different values in the limits $N_6 \rightarrow 0, \infty$, making them necessarily non-constant functions of the physical parameters in the problem. In particular, I find that when $N_6 \gg 1$, $b_{\mu_1} = -\frac{1}{6}b_1$ and $k_p = 0$, and when $N_6 \ll 1$, $b_{\mu_1} = -\frac{2}{15}b_1$ and $k_p = -6b_{\mu_1}$.

The finite temperature supergravity solution presented in this chapter hints that the horizon of the non-extremal D2-branes must be non-spherical for general values of N_2 and N_6 . However, in the appropriate limits of $N_6 \rightarrow \infty$ and $N_6 \rightarrow 0$, it gives the expected spherically symmetric horizons for black holes in $\mathbb{R}^{1,8}$ and $\mathbb{R}^{1,7}$ respectively. Whether or not more physical information can be extracted from this solution needs further investigation.

Chapter 4

Cascading Renormalization Group Flows from Sasaki-Einstein Manifolds

4.1 Introduction

An important extension of the basic AdS/CFT correspondence [2, 4, 3] (discussed in Chapter 1) is studying solutions of supergravity obtained by placing a stack of N D3 branes at the singular tip of a 6-dimensional Ricci flat, Kaehler cone (a Calabi-Yau manifold) [118, 119, 120, 121, 122, 123]. With the choice of an appropriate 5-form field strength, these give rise to solutions of type IIB supergravity of the form $AdS_5 \times X_5$.

In this chapter, I present work done in collaboration with C. P. Herzog and I. Klebanov [13], to address a number of issues concerning the gauge/gravity duality when X_5 is a Sasaki-Einstein space denoted by $Y^{p,q}$. This includes matching the spectra of dibaryon operators in the gauge theory with that of wrapped D3-branes in string theory and considering gauge theories that arise upon the addition of M fractional D3-branes at the apex of the cone, which break conformal invariance. I show that these gauge theories can undergo duality cascades, and construct the dual warped supergravity solutions with $(2, 1)$ flux.¹

¹The duality cascade was first developed for the conifold in [11, 124] and later generalized in

In Section 4.2, this interesting generalization of the basic AdS/CFT correspondence (which results from studying branes at conical singularities) will be presented. In this section, a stack of N D3-branes is placed at the apex of a Ricci-flat 6-dimensional cone C_6 whose base was a 5-d Einstein manifold X_5 . Comparing the metric with the D-brane description leads one to conjecture that type IIB string theory on $AdS_5 \times X_5$, with N units of 5-form flux, is dual to the low-energy limit of the world volume theory on the D3-branes at the singularity. Previously well-known examples of X_5 include the orbifolds S^5/Γ where Γ is a discrete subgroup of $SO(6)$ [118, 119]. In these cases, X_5 has the local geometry of a 5-sphere. Constructions of the dual gauge theories for Einstein manifolds X_5 , which are not locally equivalent to S^5 , are also possible. The simplest example is $X_5 = T^{1,1} = (SU(2) \times SU(2))/U(1)$ [121] and is discussed in this section. As mentioned earlier, the dual gauge theory is the conformal limit of the world volume theory on a stack of N D3-branes placed at the apex of the conifold [121, 122], which is a cone over $T^{1,1}$. This $\mathcal{N} = 1$ superconformal field theory (SCFT) has gauge group $SU(N) \times SU(N)$ with bifundamental fields A_α, B_β , $\alpha, \beta = 1, 2$, and a quartic superpotential.

A new infinite class of Sasaki-Einstein manifolds $Y^{p,q}$ of topology $S^2 \times S^3$ was discovered [132, 133]. Following progress in [134], the $\mathcal{N} = 1$ superconformal gauge theories dual to $AdS_5 \times Y^{p,q}$ were ingeniously constructed in [135]. These quiver theories have gauge groups $SU(N)^{2p}$, bifundamental matter, and marginal superpotentials involving both cubic and quartic terms. These constructions generalize the SCFT on D3-branes placed at the apex of the complex cone over dP_1 [136], corresponding to $Y^{2,1}$ [134]. Impressive comparisons of the conformal anomaly coefficients between the AdS and the CFT sides were carried out for dP_1 in [137], and in full generality in [135]. The discussion in this chapter generalizes the one for the $Y^{2,1}$ case [129, 130, 131].

In Section 4.3, I discuss relevant aspects of the geometry of the $Y^{p,q}$ spaces, while in Section 4.4, I review the relevant properties of the gauge theory dual to the type IIB solution involving the $Y^{p,q}$ spaces, including its conformal surface in the absence

[125, 126, 127, 128, 129, 130, 131].

of fractional branes. In Section 4.5, I present the identification of new supersymmetric 3-cycles, whose volumes are found to agree to the values of the R -charges of the dual dibaryon operators, as predicted by the correspondence. In Section 4.6, I construct the supergravity solution in the presence of fractional D5-branes, which break conformal invariance and lead to non-zero β -functions in the gauge theory. This solution is used in Section 4.7 to verify the prediction for the β -function for the coupling of the gauge theory living on the D5-branes. In Section 4.8 the duality cascades for $Y^{p,1}$ and $Y^{p,p-1}$ are presented. The last section gives a summary of the results in this chapter.

4.2 Conifold Theories

In this section, I will discuss some properties of supergravity solutions with the Freund-Rubin Ansatz and focus on the specific example of $X_5 = T^{1,1}$. While the $AdS_5 \times S^5$ is the simplest example in the study of the correspondence, other examples of the correspondence are given by solutions of type IIB supergravity of the general form $AdS_5 \times X_5$, where X_5 is a five dimensional manifold. Here the curvature of the AdS_5 space is supported by the 5-form flux which, because it is self-dual and AdS_5 is an Einstein manifold with negative curvature, requires that X_5 be a 5-dimensional positive curvature Einstein manifold with $R_{ab} = 4g_{ab}$, where a and b label the X_5 directions.

The manifolds X_5 can be used to construct Calabi Yau 3-folds (which have 6 real dimensions) with metric

$$ds^2(C_6) = dr^2 + r^2 ds^2(X_5), \quad (4.1)$$

where $ds(X_5)^2$ is the metric on X_5 . The metric $ds^2(C_6)$ is Ricci flat because X_5 is Einstein. These cones always have singularity at the origin unless X_5 is the S^5 . Examples of X_5 include the orbifolds S^5/Γ where Γ is a discrete subgroup of $SO(6)$ [118, 119]. These orbifolds have less supersymmetry than S^5 , but still have the local geometry of a 5-sphere. Another well-known example of X_5 , which is not topologically

S^5 is $T^{1,1}$. This section will focus on the study of the correspondence for this example. This example also shows how the correspondence can be extended to the case when the gauge theory is no longer conformal.

One way to obtain solutions that satisfy the Freund-Rubin Ansatz is to place N D3-branes at a singular point of a Calabi-Yau 3-fold C_6 in the 10-dimensional product space $\mathbb{R}^{1,3} \times C_6$ and take the near horizon limit. The solution to the supergravity equations of motion is given by the metric

$$ds^2 = \left(1 + \frac{R^4}{r^4}\right)^{-1/2} [-dt^2 + dx_1^2 + dx_2^2 + dx_3^2] + \left(1 + \frac{R^4}{r^4}\right)^{1/2} ds^2(C_6), \quad (4.2)$$

provided there is N units of 5-form flux through X_5 . This N is related to the radius of the AdS_5 by equating the ADM tension of the N D3-branes to N times the tension of a single brane:

$$\frac{2}{\kappa^2} R^4 \text{vol}(X_5) = N \frac{\sqrt{\pi}}{\kappa} \quad \implies \quad R^4 = \frac{\sqrt{\pi}}{2} \frac{\kappa N}{\text{vol}(X_5)}. \quad (4.3)$$

In particular, $\text{vol}(S^5) = \pi^3$, which gives the relationship in (1.4).

The dual description is in terms of some superconformal Yang-Mills theory. The number of supersymmetries preserved by the SYM are related to the number of globally defined killing spinors defined on the dual geometry. For $AdS_5 \times X_5$, the dual theory must have $\mathcal{N} = 1$ supersymmetry unless X_5 is just the round sphere or an orbifold of it [123]. This is equivalent to the requirement that the dual geometry have a globally defined constant norm killing vector, called the Reeb vector. This Reeb vector arises from the $U(1)$ fibration. In such a case, the metric on the X_5 can be written as

$$ds_5^2 = ds_4^2 + \left(\frac{1}{3}d\psi' + \sigma\right)^2, \quad (4.4)$$

where the base space with metric ds_4^2 is a Kaehler manifold with Kaehler form $d\sigma =$

$2J_4$. Then the Kaehler form on C_6 is given by

$$J = r^2 J_4 + r dr \wedge \left(\frac{1}{3} d\psi' + \sigma \right). \quad (4.5)$$

A manifold with such a structure is called a Sasaki-Einstein (SE) manifold. Depending on the properties of orbits of this $U(1)$ Reeb vector, the manifold is classified as either being regular, quasi-regular or irregular. If the orbits of this vector are compact, the $U(1)$ action is well-defined, and it produces a quotient space that is locally Kaehler-Einstein with positive curvature. More generally, the $U(1)$ Killing vector generates finite isotropy sub-groups, because it has constant norm. The action is free when the isotropy group of every point is trivial. SE manifolds with a free $U(1)$ action are called regular and they are global Kaehler-Einstein spaces. But in general, the base of this $U(1)$ fibration will have orbifold singularities. In such a case, it is called quasi-regular. $T^{1,1}$ is an example of a quasi-regular SE manifold. When the orbits of $U(1)$ are non-compact, the SE metrics are called irregular. The $Y^{p,q}$ manifolds considered in this chapter are quasi-regular or irregular.

I will now discuss the example where X_5 is the SE manifold $T^{1,1}$ with topology $S^2 \times S^3$. $T^{1,1}$ is the coset space $(SU(2) \times SU(2))/U(1)$, where the $U(1)$ is chosen to be the sum $\frac{1}{2}\sigma_3 + \frac{1}{2}\tau_3$ of generators of the two $SU(2)$'s, and its metric is given by

$$ds^2 = \frac{1}{6} (d\theta^2 + \sin^2 \theta d\phi^2 + d\omega^2 + \sin^2 \omega d\nu^2) + \frac{1}{9} [d\psi - \cos \theta d\phi - \cos \omega d\nu]^2. \quad (4.6)$$

The terms in the first pair of brackets is just the product manifold $S^2 \times S^2$ with $0 \leq \theta, \omega < \pi$ and $0 \leq \phi, \nu < 2\pi$. In the second pair of brackets, ψ is an angular co-ordinate which can range from 0 to 4π (or 2π which gives the orbifold $T^{1,1}/\mathbb{Z}_2$) and represents the non-trivial $U(1)$ fibre over S^2 , making the geometry $S^2 \times S^3$. This metric has been normalized to $R_{ab} = 4g_{ab}$ and its volume is $16\pi^3/27$. It is straight forward to see that the isometries of $T^{1,1}$ are $SU(2) \times SU(2) \times U(1)$.

The metric in (4.6) has the form (4.4), with $3\sigma = -\cos \theta d\phi - \cos \omega d\nu$. The Kaehler form for the 4-dimensional base is $2J_4 = d\sigma$, which can be used to construct

the Kaehler form for the 6-dimensional cone from (4.5)

$$J = \frac{r^2}{6} (\sin \theta d\theta \wedge d\phi + \sin \omega d\omega \wedge d\nu) + \frac{1}{3} r dr \wedge (d\psi - \cos \theta d\phi - \cos \omega d\nu) . \quad (4.7)$$

The Ricci flat cone over $T^{1,1}$, $C(T^{1,1})$, is a three complex dimensional manifold and can be embedded in \mathbb{C}^4 by the equation

$$\sum_{i=1}^4 z_i^2 = 0, \quad (4.8)$$

where $z_i \in \mathbb{C}$ and its base is determined by its intersection with $\sum_{i=1}^4 |z_i|^2 = 1$. This intersection has $SO(4) \sim SU(2) \times SU(2)$ symmetry and a $U(1)$ R -symmetry under which $z_i \rightarrow e^{i\theta} z_i$, hence the isometries of the base of this conifold match with those of $T^{1,1}$. This space is a Kaehler manifold with Kaehler potential $K = (\sum_{i=1}^4 |z_i|^2)^{2/3}$. This potential gives rise to a metric on this manifold, which can be recast into that of $C(T^{1,1})$ given by (4.1) with $T^{1,1}$ as its base. This cone is a Calabi-Yau as it has $SU(3)$ holonomy, in addition to being Ricci flat and Kaehler.

Given the holonomy of C_6 , the dual field theory is the $\mathcal{N} = 1$ SYM in $d = 4$ with gauge group $SU(N) \times SU(N)$ coupled to two chiral superfields fields A_α, B_α ($\alpha=1, 2$), with the A_α transforming in the $(\mathbf{N}, \overline{\mathbf{N}})$ and the B_α in $(\overline{\mathbf{N}}, \mathbf{N})$. They also transform as $(\mathbf{2}, \mathbf{0})$ and $(\mathbf{0}, \mathbf{2})$ under the global $SU(2) \times SU(2)$. The superpotential for this theory is $\mathcal{W} = \epsilon^{\alpha\beta} \epsilon^{\gamma\delta} \text{Tr} A_\alpha B_\gamma A_\beta B_\delta$. This field theory also contains dibaryon operators of the form A^N and B^N . More precisely

$$\mathcal{B}_{1l} = \epsilon_{a_1 \dots a_N} \epsilon^{r_1 \dots r_N} D_l^{\alpha_1 \dots \alpha_N} \prod_{k=1}^N A_{\alpha_k r_k}^{a_k}, \quad \mathcal{B}_{2l} = \epsilon^{a_1 \dots a_N} \epsilon_{r_1 \dots r_N} D_l^{\alpha_1 \dots \alpha_N} \prod_{k=1}^N B_{\alpha_k a_k}^{r_k}, \quad (4.9)$$

where a is an index in the first $SU(N)$ and r in the second one, and $D_l^{\alpha_1 \dots \alpha_N}$ is the completely symmetric Clebsch-Gordan coefficient coming from the direct product of N doublets of $SU(2)$. The fields A and B have conformal dimension $3/4$, which makes the dimensions of these dibaryon operators $3N/4$. Note that these dibaryon operators are defined in a conformal theory.

The dibaryons in (4.9) are described in the dual description by D3-branes wrapped on the S^3 given by $\theta = \phi = \text{constant}$ or $\omega = \nu = \text{constant}$. The two types of dibaryons arise from the fact that the base of the $U(1)$ bundle is $S^2 \times S^2$. This was proposed by S. S. Gubser and I. R. Klebanov [12] because $\pi_3(T^{1,1}) = \mathbb{Z}$. For $\theta = \phi = \text{constant}$, (4.7) can be used to show that

$$\frac{1}{2} J \wedge J \Big|_{\theta=\phi=\text{constant}} = \frac{1}{18} r^3 dr \wedge \sin \theta d\theta \wedge d\phi \wedge \psi. \quad (4.10)$$

This is precisely the volume of the S^3 whose metric is obtained from (4.6) by setting by $\theta = \phi = \text{constant}$. This explicitly shows that this 3-cycle is supersymmetric, as it is calibrated by J . The mass of this D3-brane is given by $m = \text{vol}(S^3) \sqrt{\pi}/\kappa = 8\pi^5/2R^3/9\kappa$, which for large mR , gives the conformal dimension $3N/4$

$T^{1,1}$ also has $\pi_2(T^{1,1}) = \mathbb{Z}$. This fact can be used to wrap D5-branes on these two cycles, with the other directions parallel to the D3-branes and give rise to fractional D3 branes². This wrapping corresponds to turning on the RR and NSNS 3-fluxes, F_3 and H_3 , respectively, where

$$\frac{1}{4\pi^2\alpha'} \int_{S^3} F_3 = M, \quad \frac{1}{(4\pi^2\alpha')^2} \int_{T^{1,1}} F_5 = N. \quad (4.11)$$

These forms are not $SL(2, \mathbb{Z})$ invariant and break conformal symmetry, inducing a β -function flow in the couplings. The evidence for this can be seen in the warp factor which gets modified by a logarithmic term. In the near-horizon limit, it is given by

$$h = \frac{27\pi(\alpha')^2}{4r^4} \left[g_s N + \frac{3}{2\pi} (g_s M)^2 \left(\ln \frac{r}{R_0} + \frac{1}{4} \right) \right], \quad (4.12)$$

where R_0 is a UV scale. This modifies the gauge group of the dual theory from $SU(N) \times SU(N)$ to $SU(N + M) \times SU(N)$.

The simplest example of a Seiberg duality cascade occurs in the $SU(N + (k -$

²Fractional D3 branes are D5 branes with two directions wrapped on a shrinking 2-cycle. The tension of these branes is proportional to r , which is minimized at $r = 0$, which localizes them at this point. In this case, the D5 brane is wrapped on one of the two S^2 s, which shrink to zero size at $r = 0$, the location of the D3 branes.

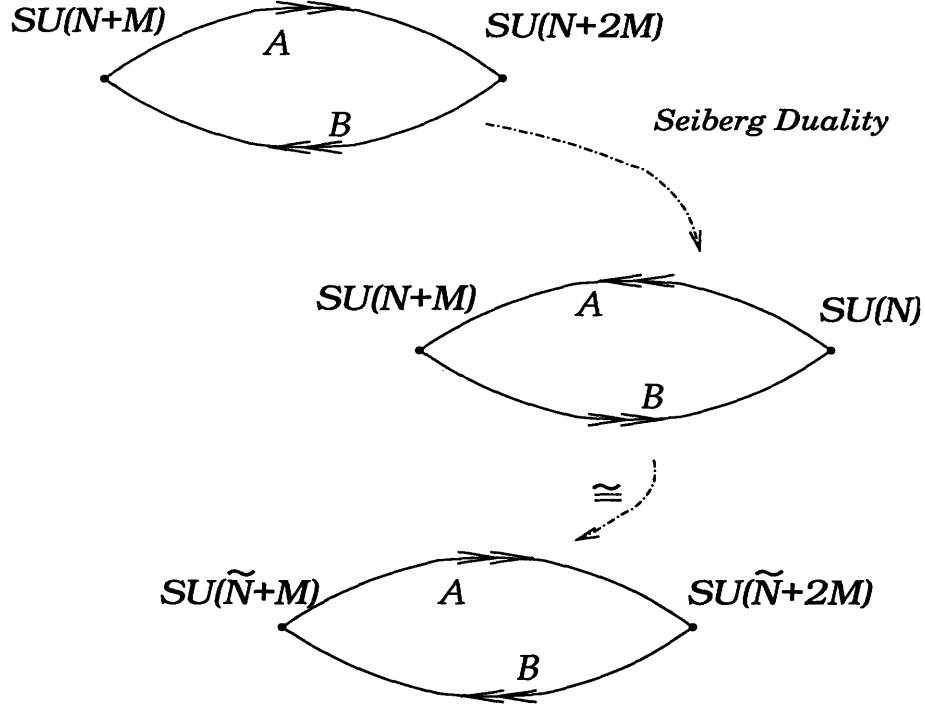


Figure 4-1: This figure shows Seiberg duality in Klebanov-Strassler theory with gauge group $SU(N + M) \times SU(N + 2M)$ (i.e. $k = 2$) using quiver diagrams. The vertices of the quiver denote gauge groups while the lines indicate bifundamental fields, their number being given by the number of arrows. Under Seiberg duality, the fundamental fields become anti-fundamental and vice versa, indicated by the reversal in the direction of arrows. The \cong symbol indicates that the second and third quiver are identical, as can be seen by interchanging the two vertices ($\tilde{N} = N - M$). The duality has a self-similar structure under $N \rightarrow \tilde{N} \equiv N - M$, which allows a cascade to occur.

$1)M) \times SU(N + kM)$ gauge theory (k is a positive integer) with bifundamental fields A_i, B_j , $i, j = 1, 2$, and a quartic superpotential [11, 124]. (The theory with $M = 0$ is conformal – the addition of the M D5-branes breaks the conformal symmetry.) In this case the gauge coupling of $SU(N + kM)$ blows up after a finite amount of RG flow. To continue the flow beyond this point, one applies the duality transformation to this gauge group [124]. After this transformation, and an interchange of the two gauge groups, the new gauge theory is $SU(\tilde{N} + (k - 1)M) \times SU(\tilde{N} + kM)$ with the same matter and superpotential, with $\tilde{N} = N - M$. The case when $k = 2$ is shown in Figure 4-1. This self-similar structure of the gauge theory under Seiberg duality is the crucial fact that allows the cascade to happen. If $N = kM$, where k is an integer, then the cascade stops after k steps, and one finds $SU(M) \times SU(2M)$ gauge theory at the

bottom of this cascade. (The interested reader can find a brief discussion of Seiberg duality in the conformal window in Appendix E.) This IR gauge theory exhibits a multitude of interesting effects visible in the dual supergravity background, such as confinement, and chiral symmetry breaking [124]. Particularly interesting is the appearance of an entire “baryonic branch” of the moduli space in the gauge theory [124, 138], whose existence in the dual supergravity was confirmed in [139, 140, 141]. The presence of the baryonic operators in the IR gauge theory is related to the fact that for the $SU(2M)$ gauge group, the number of flavors equals the number of colors.

4.3 The Geometry of $Y^{p,q}$ Spaces.

This section contains a discussion about some of the important features of the geometry of $Y^{p,q}$ manifolds. This infinite family of five dimensional manifolds falls under the class of Sasaki-Einstein manifolds with topology $S^2 \times S^3$ and is labeled by two non-negative integers $p > q \geq 0$, $p > 1$. Their geometry can be described by saying that they are principle $U(1)$ bundles over an axially squashed S^2 bundle over a round S^2 . I will first present the metrics and then in the discussion that follows, explain the terminology just used.

The metric on $Y^{p,q}$ takes the form [132, 133]

$$d\Omega_{Y^{p,q}}^2 = \frac{1-cy}{6}(d\theta^2 + \sin^2\theta d\phi^2) + \frac{1}{w(y)v(y)}dy^2 + \frac{v(y)}{9}(d\psi - \cos\theta d\phi)^2 + w(y)[d\alpha + u(y)(d\psi - \cos\theta d\phi)]^2 \quad (4.13)$$

$$\equiv ds^2(B) + w(y)[d\alpha + A]^2 \quad (4.14)$$

where

$$w(y) = \frac{2(b-y^2)}{1-cy}, \quad v(y) = \frac{b-3y^2+2cy^3}{b-y^2}, \quad u(y) = \frac{bc-2y+cy^2}{6(b-y^2)}. \quad (4.15)$$

When $c = 0$, the metric reduces to the homogeneous metric on $T^{1,1}$. When $c \neq 0$, a diffeomorphism can be used to set $c = 1$. I will assume that $c = 1$ throughout the

rest of this chapter, unless stated otherwise. The coordinates over the round S^2 are θ, ϕ with $0 \leq \theta < \pi, 0 \leq \phi < 2\pi$. The coordinates of the axially squashed S^2 are ψ and y with $0 \leq \psi < 2\pi$ and $y_1 \leq y \leq y_2$. Here

$$y_1 = \frac{1}{4p} \left(2p - 3q - \sqrt{4p^2 - 3q^2} \right), \quad (4.16)$$

$$y_2 = \frac{1}{4p} \left(2p + 3q - \sqrt{4p^2 - 3q^2} \right), \quad (4.17)$$

are the south and north poles respectively of the axially squashed S^2 , with $y_1 < 0$ and $y_2 > 0$ being the smaller of the three roots of the cubic

$$b - 3y^2 + 2y^3 = 0. \quad (4.18)$$

The three roots of the cubic satisfy $y_1 + y_2 + y_3 = 3/2$, so the biggest root, which will be used later in this chapter, is

$$y_3 = \frac{1}{4p} \left(2p + 2\sqrt{4p^2 - 3q^2} \right). \quad (4.19)$$

The period of the coordinate over the $U(1)$ fibration, α is $2\pi\ell$ where

$$\ell = -\frac{q}{4p^2 y_1 y_2} = \frac{q}{3q^2 - 2p^2 + p\sqrt{4p^2 - 3q^2}}. \quad (4.20)$$

The metric is complete provided,

$$b = \frac{1}{2} - \frac{p^2 - 3q^2}{4p^3} \sqrt{4p^2 - 3q^2}. \quad (4.21)$$

The volume of $Y^{p,q}$ is

$$\text{Vol}(Y^{p,q}) = \frac{q(2p + \sqrt{4p^2 - 3q^2})\ell\pi^3}{3p^2} = \frac{q^2 \left(2p + \sqrt{4p^2 - 3q^2} \right)}{3p^2 \left(3q^2 - 2p^2 + p\sqrt{4p^2 - 3q^2} \right)}, \quad (4.22)$$

and satisfies the bounds

$$\text{Vol}(T^{1,1}/\mathbb{Z}_p) > \text{Vol}(Y^{p,q}) > \text{Vol}(S^5/\mathbb{Z}_p \times \mathbb{Z}_2). \quad (4.23)$$

The metric in (4.13) is an Einstein manifold because $R_{ab} = 4g_{ab}$, where a, b label the X_5 directions. It has a Sasaki structure because the 6-dimensional metric cone $C(Y^{p,q})$ defined over it

$$ds^2(C(Y^{p,q})) = dr^2 + r^2 ds^2(X_5), \quad (4.24)$$

is a Calabi-Yau 3-fold, ie it is Ricci flat and Kaehler with $SU(3)$ holonomy. To show explicitly the Sasaki structure of $Y^{p,q}$, the metric in (4.13) can be re-written, using the coordinate transformations $\alpha = -\beta/6 - \psi'/6$, $\psi = \psi'$ as

$$\begin{aligned} d\Omega_{Y^{p,q}} = & \frac{1-y}{6} (d\theta^2 + \sin^2 \theta d\phi^2) + \frac{dy^2}{w(y)v(y)} + \frac{1}{36} w(y)v(y) (d\beta + \cos \theta d\phi)^2 \\ & + \frac{1}{9} [d\psi' - \cos \theta d\phi + y(d\beta + \cos \theta d\phi)]^2, \end{aligned} \quad (4.25)$$

which is of the form given in (4.4). The Kaehler form J_4 is given by (equation (2.24) of [134])

$$J_4 = \frac{1-y}{6} \sin \theta d\theta \wedge d\phi + \frac{1}{6} dy \wedge (d\beta + \cos \theta d\phi) \quad (4.26)$$

This gives the Kaehler form for $C(Y^{p,q})$ by

$$\begin{aligned} J &= r^2 J_4 + r dr \wedge \left(\frac{1}{3} d\psi' + \sigma \right) \\ &= r^2 \frac{1-y}{6} \sin \theta d\theta \wedge d\phi \\ &+ \frac{1}{3} r dr \wedge (d\psi - \cos \theta d\phi) - d(yr^2) \wedge \left(d\alpha + \frac{1}{6} (d\psi - \cos \theta d\phi) \right). \end{aligned} \quad (4.27)$$

The Reeb vector, which is a constant norm killing vector giving the non-anomalous

$U(1)_R$ symmetry in the dual description, is obtained by taking the dual to the 1-form constructed by contracting the Euler vector $r \frac{\partial}{\partial r}$ with the Kaehler form (4.27) [134]. It is given by

$$K = \frac{\partial}{\partial \psi'} = 3 \frac{\partial}{\partial \psi} - \frac{1}{2} \frac{\partial}{\partial \alpha}. \quad (4.28)$$

For the $Y^{p,q}$, the metrics are quasi-regular when p and q are solutions to the Diophantine equation $4p^2 - 3q^2 = n^2$. In this case, all the roots and volumes are rational. Otherwise these metrics are irregular.

The isometry group (which is dual to the R -symmetry of the gauge theory) of this space is $SU(2) \times U(1) \times U(1)$ which contains $U(1)^3$. This means that $C(Y^{p,q})$ is a toric Calabi-Yau.

Some of the previously known metrics in this class are those of dP_1 ($p = 2, q = 1$), $S^5/\mathbb{Z}_p \times \mathbb{Z}_2$ ($p = q$) and $T^{1,1}$. The local metric on $T^{1,1}$ (4.6) is obtained from (4.13) by setting $c = 0$, $b = 3$ and introducing new co-ordinates $\cos \omega = y$, $\nu = 6\alpha$. The first brackets contain canonical metric for $S^2 \times S^2$ if the period for ν is 2π . The second set of brackets here shows a trivial fibration of the base over $U(1)$. This metric is $T^{1,1}$ or $T^{1,1}/\mathbb{Z}_2$ if the period of ψ is 4π or 2π respectively. A discussion of the gauge/gravity correspondence for this case was given in section 4.2.

4.4 The Conformal Surface of $Y^{p,q}$ Gauge Theories

This section contains a review of the construction of the $Y^{p,q}$ gauge theories and a discussion that they flow to an IR conformal “fixed surface” of dimension two. That this surface has dimension two will be more or less clear from the gravity side where the two free complex parameters are $C - ie^{-\phi}$ and $\int_{S^2}(C_2 - ie^{-\phi} B_2)$.

As derived in [135], the quivers for these $Y^{p,q}$ gauge theories can be constructed from two basic units, σ and τ . These units are shown in Figure 4-2. To construct a general quiver for $Y^{p,q}$, we define some basic operations with σ and τ . First, there are the inverted unit cells, $\tilde{\sigma}$ and $\tilde{\tau}$, which are mirror images of σ and τ through

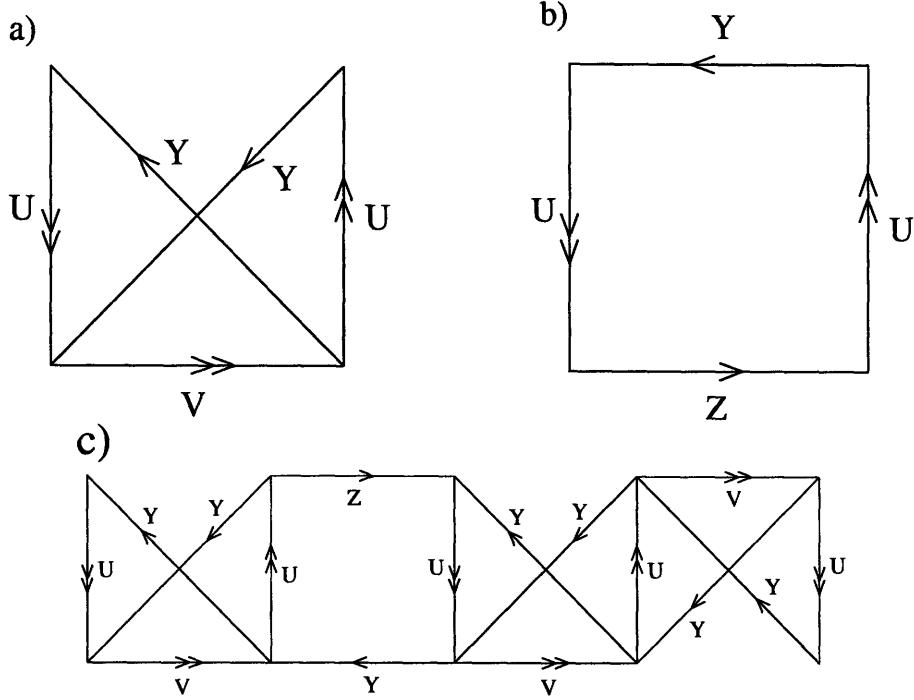


Figure 4-2: Shown are a) the unit cell σ ; b) the unit cell τ ; and c) the quiver for $Y^{4,3}$, $\sigma\tilde{\sigma}\tilde{\sigma}$.

a horizontal plane. To glue the cells together, we identify the double arrows corresponding to the U^α fields on two unit cells. The arrows have to be pointing in the same direction for the identification to work. So for instance, the quiver $\sigma\tilde{\tau} = \tilde{\tau}\sigma$ is allowed, but $\sigma\tau$ is not. In this notation, the first unit cell is to be glued not only to the cell on the right but also to the last cell in the chain. A general quiver might look like

$$\sigma\tilde{\sigma}\sigma\tilde{\tau}\tilde{\sigma} . \quad (4.29)$$

In general, a $Y^{p,q}$ quiver consists of p unit cells of which q are of type σ . The $Y^{p,p-1}$ gauge theories will have only one τ type unit cell, while the $Y^{p,1}$ theories will have only one σ type unit cell.

Each node of the quiver corresponds to a gauge group while each arrow is a chiral field transforming in a bifundamental representation. For the $Y^{p,q}$ spaces, there are four types of bifundamentals labeled U^α , V^α , Y , and Z where $\alpha = 1$ or 2 . To get a conformal theory, we take all the gauge groups to be $SU(N)$. Later in this paper, the

addition of D5-branes will change the ranks of some of the gauge groups and break the conformal symmetry.

The superpotential for this quiver theory is constructed by summing over gauge invariant operators cubic and quartic in the fields U^α , V^α , Y , and Z . For each σ unit cell in the gauge theory, one adds two cubic terms to the superpotential of the form

$$\epsilon_{\alpha\beta} U_L^\alpha V^\beta Y \quad \text{and} \quad \epsilon_{\alpha\beta} U_R^\alpha V^\beta Y . \quad (4.30)$$

Here, the indices R and L specify which group of U^α enter in the superpotential, the U^α on the right side or the left side of σ . The trace over the color indices has been suppressed. For each τ unit cell, one adds the quartic term

$$\epsilon_{\alpha\beta} Z U_R^\alpha Y U_L^\beta . \quad (4.31)$$

An analysis of the locus of conformal field theories *in this space of couplings* begins with counting the fundamental degrees of freedom which are in this case the $2p$ gauge couplings and the $p + q$ superpotential couplings (assuming an unbroken $SU(2)$ symmetry for the U^α and V^α). Here all the gauge groups are assumed to have equal ranks. There are in total $3p + q$ fields and thus $3p + q$ anomalous dimensions which we can tune to get a conformal theory. The $3p + q$ β -functions can be thought of as functions of the $3p + q$ anomalous dimensions which are in turn functions of the $3p + q$ coupling strengths, $\beta_j(\gamma_i(g_k))$.

Let us first check that one set of solutions of $\beta_j = 0$ involves setting the anomalous dimensions of all the Z fields equal, the anomalous dimensions of all the Y fields equal, and similarly for the U^α and V^α . Instead of working with the anomalous dimensions γ , of the fields, it is convenient to work with the R charges, R_Y , R_Z , R_U , and R_V . (For superconformal gauge theories, recall that $2(1 + \gamma) = 3R$.)

There are $p + q$ β -functions for the superpotential couplings. $p - q$ of the β -functions vanish when $R_Z + R_Y + 2R_U = 2$ and are associated with loops in the τ unit cells, while the remaining $2q$ vanish when $R_U + R_Y + R_V = 2$ and are associated to loops in the σ unit cells.

The $2p$ gauge coupling β -functions contain exactly the same information as the superpotential β -functions. This happens because $2q$ of these couplings are associated with the σ unit cells, and the β -functions for these couplings vanish when $2 = R_U + R_V + R_Y$ while the remaining $2p - 2q$ belong to the τ unit cells and vanish when $R_Z + R_Y + 2R_U = 2$.

It could be that there are more solutions to setting the $\beta_j = 0$ which involve more generic values of the anomalous dimensions. However, such solutions would require even more degeneracy among the $3p + q$ β -functions, which is unlikely. Assuming that this is the most general solution of $\beta_j = 0$, one finds that only $3p + q - 4 + 2$ of the $\beta_j = 0$ are linearly independent. Thus there is seemingly a two dimensional plane in the space of allowed anomalous dimensions which produce conformal field theories. Of course a -maximization [142] will pick out the right anomalous dimensions.

However, there is a different way of looking at these $3p + q - 2$ linearly independent β -functions. They place $3p + q - 2$ constraints on the $3p + q$ couplings, leaving a space of conformal theories with two complex dimensions. By construction, this space preserves the $SU(2) \times U(1) \times U(1)$ global flavor symmetry of the $Y^{p,q}$. If I allow a breaking of this symmetry, then there may exist additional exactly marginal superpotential deformations (see [143]).

4.5 Dibaryons and New 3-Cycles

This section contains a discussion of the identification of some new supersymmetric 3-cycles in the $Y^{p,q}$ geometry. D. Martelli and J. Sparks [134] identified two supersymmetric 3-cycles, denoted Σ_1 and Σ_2 in their paper. These 3-cycles are obtained by setting $y = y_1$ or $y = y_2$ respectively. At these values for y , the circle parametrized by ψ shrinks to zero size, and the three cycles can be thought of as a $U(1)$ bundle parametrized by α over the round S^2 parametrized by θ and ϕ . For completeness,

note that the volume of these cycles is calibrated by the Kaehler form J , ie

$$\frac{1}{2} J \wedge J \Big|_{y=y_{1,2}} = \frac{r^3 y_{1,2} (1 - y_{1,2})}{3} \sin \theta d\theta \wedge d\phi \wedge d\alpha \wedge dr. \quad (4.32)$$

$$= \text{Vol}(\Sigma_{1,2}), \quad (4.33)$$

because $w(y_i) = 4y_i^2$.

Martelli and Sparks [134] computed the R -charges of the dibaryons corresponding to D3-branes wrapped on Σ_1 and Σ_2 . In general, these R -charges are given by the formula [12, 144]

$$R(\Sigma_i) = \frac{\pi N}{3} \frac{\text{Vol}(\Sigma_i)}{\text{Vol}(Y^{p,q})}. \quad (4.34)$$

From this general formula, it follows that

$$R(\Sigma_1) = \frac{N}{3q^2} \left(-4p^2 + 2pq + 3q^2 + (2p - q)\sqrt{4p^2 - 3q^2} \right), \quad (4.35)$$

$$R(\Sigma_2) = \frac{N}{3q^2} \left(-4p^2 - 2pq + 3q^2 + (2p + q)\sqrt{4p^2 - 3q^2} \right). \quad (4.36)$$

These R -charges should correspond to operators $\det(Y)$ and $\det(Z)$ made out of the bifundamental fields that are singlet under the global $SU(2)$ symmetry. Dividing these dibaryon R -charges by N , I observe a perfect match with the R -charges of the Y and Z singlet fields determined from gauge theory by S. Benvenuti, S. Franco, A. Hanany, D. Martelli, and J. Sparks [135], $R_Y = R(\Sigma_1)/N$ and $R_Z = R(\Sigma_2)/N$.³

I now find the 3-cycles which correspond to the dibaryons made out of the $SU(2)$ doublet fields U^α and V^α . Such dibaryons carry spin $N/2$ under the global $SU(2)$. On the string side, the wrapped D3-brane should therefore have an $SU(2)$ collective coordinate (see [12, 144] for an analogous discussion in the case of $T^{1,1}$). The only possibility is that this $SU(2)$ is precisely the $SU(2)$ of the round S^2 in the metric. Therefore, the 3-cycles corresponding to these dibaryons should be localized at a point on the S^2 .

³The gauge theory computation for $Y^{2,1}$ was performed earlier by [137].

Now recall from the gauge theory analysis of [135] that

$$R_U = (2p(2p - \sqrt{4p^2 - 3q^2}))/3q^2, \quad (4.37)$$

$$R_V = (3q - 2p + \sqrt{4p^2 - 3q^2})/3q. \quad (4.38)$$

Before proceeding, note that $R_V = R_U + R_Z$. So if a cycle, called Σ_3 , corresponds to U^α , we can deduce that V^α is just a sum of Σ_3 and Σ_2 .

As discussed above, the 3-cycle Σ_3 should correspond to fixing a point on the S^2 and integrating over the fiber. Setting $\phi = \theta = \text{const}$, the induced metric on this three cycle becomes

$$ds^2 = \frac{1}{wv} dy^2 + \frac{v}{9} d\psi^2 + w(d\alpha + u d\psi)^2. \quad (4.39)$$

This 3-cycle can be characterized more precisely. The metric on Σ_3 can be thought of as a principal $U(1)$ bundle over an S^2 where the S^2 is parametrized by y and ψ . A principal $U(1)$ bundle over S^2 is a Lens space S^3/\mathbb{Z}_k where k is given by the first Chern class c_1 of the fibration. The $A = u d\psi$ is a connection one-form on the $U(1)$ bundle. Because α ranges from 0 to $2\pi\ell$, $dA = 2\pi c_1/\ell$. Integrating c_1 over the S^2 yields

$$\int_{S^2} c_1 = \frac{u(y_2) - u(y_1)}{\ell} = -p. \quad (4.40)$$

In other words, the new cycle Σ_3 identified here is the Lens space S^3/\mathbb{Z}_p . In [134], Σ_1 and Σ_2 were identified as the Lens spaces S^3/\mathbb{Z}_{p+q} and S^3/\mathbb{Z}_{p-q} respectively.

Further

$$\text{Vol}(\Sigma_3) = \int \sqrt{g} dy d\alpha d\psi = \frac{4\pi^2\ell}{3}(y_2 - y_1), \quad (4.41)$$

where $\sqrt{g} = 1/3$ for the metric in (4.39) has been used in the second equality. Plugging into the formula for the R -charge, indeed $R(\Sigma_3) = NR_U$.

Σ_3 is a supersymmetric cycle because the form $\frac{1}{2}J \wedge J$, where J is the Kaehler form on the cone over $Y^{p,q}$, restricts to the induced volume form on the cone over Σ_3 . More formally, this is the statement that Σ_3 is calibrated by $\frac{1}{2}J \wedge J$. J given in

(4.27), when restricted to Σ_3 is

$$J|_{\Sigma_3} = \frac{1}{3}rdr \wedge d\psi + d(yr^2) \wedge \left(d\alpha + \frac{1}{6}d\psi \right) . \quad (4.42)$$

Thus

$$\frac{1}{2}J \wedge J \Big|_{\Sigma_3} = \frac{r^3}{3}dr \wedge d\psi \wedge dy \wedge d\alpha = \text{Vol}(\Sigma_3). \quad (4.43)$$

I now imagine that V^α corresponds to adding the cycles Σ_3 and Σ_2 together. Indeed, these two cycles intersect along a circle at $y = y_2$. This completes the identification of dibaryon operators of the field theory in the gravity description.

4.6 Warped Solutions with (2,1) Flux

The first step in constructing supersymmetric warped solutions for these $Y^{p,q}$ spaces is constructing a harmonic (2,1) form $\Omega_{2,1}$. The metric can be re-written so that there is locally a $U(1)$ fiber over a Kaehler-Einstein manifold. From (2.17) of [134], the metric is

$$d\Omega_{Y^{p,q}}^2 = (e^\theta)^2 + (e^\phi)^2 + (e^y)^2 + (e^\beta)^2 + (e^\psi)^2 \quad (4.44)$$

with the one forms defined by

$$e^\theta = \sqrt{\frac{1-y}{6}}d\theta, \quad e^\phi = \sqrt{\frac{1-y}{6}}\sin\theta d\phi, \quad (4.45)$$

$$e^y = \frac{1}{\sqrt{wv}}dy \quad e^\beta = \frac{\sqrt{wv}}{6}(d\beta + \cos\theta d\phi), \quad (4.46)$$

$$e^\psi = \frac{1}{3}(d\psi - \cos\theta d\phi + y(d\beta + \cos\theta d\phi)). \quad (4.47)$$

In terms of the original coordinates $\beta = -6\alpha - \psi$. Here, the ψ is a coordinate on the local $U(1)$ fiber.

The local Kaehler form, J_4 , on the Kaehler-Einstein base:

$$J_4 = e^\theta \wedge e^\phi + e^y \wedge e^\beta. \quad (4.48)$$

Based on [129, 130], I construct $\Omega_{2,1}$ from a $(1, 1)$ form ω using this local Kaehler-Einstein metric such that $*_4\omega = -\omega$ ($*_4$ is the Hodge dual along the base ds_4^2), $d\omega = 0$, and $\omega \wedge J_4 = 0$. The choice

$$\omega = F(y)(e^\theta \wedge e^\phi - e^\psi \wedge e^\beta), \quad (4.49)$$

is clearly anti-self-dual and orthogonal to J_4 . Using a complex basis of one-forms constructed in (2.27) of [134], it is not hard to check that ω is indeed a $(1, 1)$ form. The condition $d\omega = 0$ then implies that

$$F(y) = \frac{1}{(1-y)^2}. \quad (4.50)$$

This can be used to construct a $(2, 1)$ form from the wedge product of a $(1, 0)$ form and ω :

$$\Omega_{2,1} = K \left(\frac{dr}{r} + ie^\psi \right) \wedge \omega, \quad (4.51)$$

where K is a normalization constant for later convenience. This $(2, 1)$ form also satisfies $d\Omega_{2,1} = 0$ and $*_6\Omega_{2,1} = i\Omega_{2,1}$.

The integral of $\Omega_{2,1}$ over the three 3-cycles Σ_i ($i = 1, 2, 3$),

$$\int_{\Sigma_i} \Omega_{2,1}, \quad (4.52)$$

gives

$$\int_{\Sigma_1} \Omega_{2,1} = -K \frac{8i\pi^2 \ell}{3} \frac{y_1}{1-y_1}, \quad (4.53)$$

$$\int_{\Sigma_2} \Omega_{2,1} = -K \frac{8i\pi^2 \ell}{3} \frac{y_2}{1-y_2}, \quad (4.54)$$

$$\int_{\Sigma_3} \Omega_{2,1} = -K \frac{4i\pi^2 \ell}{3} \left(\frac{1}{1-y_2} - \frac{1}{1-y_1} \right). \quad (4.55)$$

The ratios between these integrals superficially appear to be irrational. However, the

ratios must be rational, and the choice

$$K = \frac{9}{8\pi^2}(p^2 - q^2) \quad (4.56)$$

gives integer results for these integrals:

$$\int_{\Sigma_1} \Omega_{2,1} = -i(-p + q) , \quad (4.57)$$

$$\int_{\Sigma_2} \Omega_{2,1} = -i(p + q) , \quad (4.58)$$

$$\int_{\Sigma_3} \Omega_{2,1} = -ip . \quad (4.59)$$

Now, to construct a supergravity solution, take the real RR F_3 and NSNS H_3 forms to be

$$iK'\Omega_{2,1} = F_3 + \frac{i}{g_s}H_3 , \quad (4.60)$$

$$F_3 = -KK'e^\psi \wedge \omega ; \quad H_3 = g_sKK'\frac{dr}{r} \wedge \omega , \quad (4.61)$$

where K' another normalization constant. In particular, F_3 should be quantized such that

$$\int_{\Sigma_1} F_3 = 4\pi^2\alpha'M(p - q) \quad (4.62)$$

where M is the number of D5-branes. Thus $K' = 4\pi^2\alpha'M$. (See [145, 146] for the normalization conventions used here.) This choice for the RR and NSNS 3-forms satisfies $F_3^2 = g_sH_3^2$. This sets the source of the dilaton to zero. Hence the solution presented here will be a constant dilaton solution.

4.6.1 Derivation of 5-form Flux

For the metric and F_5 consider the usual Ansatz with the warp factor h ,

$$ds^2 = h^{-1/2}dx_4^2 + h^{1/2}(dr^2 + r^2d\Omega_{Y^{p,q}}^2) , \quad (4.63)$$

$$g_sF_5 = d(h^{-1}) \wedge d^4x + *_{10}[d(h^{-1}) \wedge d^4x] . \quad (4.64)$$

Due to the appearance of the y -dependent factor $F(y)$ in the $(2, 1)$ flux, it is inconsistent to assume that h is a function of r only. Instead, similar to the gravity duals of fractional branes on the \mathbb{Z}_2 orbifold [147], h is a function of two variables, r and y . For $q \ll p$ the y -dependence can be ignored, and the warp factor approaches that found for the warped conifold in [11]. On the other hand, for $p - q \ll p$ we find that h gets sharply peaked near $y = 1$, and the solutions approach the gravity duals of fractional branes in orbifold theories [148, 149, 147]. Thus, the warped solutions we find with the $Y^{p,q}$ serve as interesting interpolations between the conifold and the orbifold cases.

More explicitly, the first term in (4.64) is

$$-h^{-2} \left(\frac{\partial h}{\partial r} dr + \sqrt{wv} \frac{\partial h}{\partial y} e^y \right) \wedge d^4 x . \quad (4.65)$$

Working out its Hodge dual, and substituting into the equation

$$dF_5 = H_3 \wedge F_3 , \quad (4.66)$$

gives a second order PDE

$$-(1-y) \frac{\partial}{\partial r} \left(r^5 \frac{\partial h}{\partial r} \right) - r^3 \frac{\partial}{\partial y} \left((1-y) wv \frac{\partial h}{\partial y} \right) = \frac{C}{r(1-y)^3} , \quad (4.67)$$

where $C \equiv 2(g_s K K')^2$. Note that dividing the PDE by $r^5(1-y)$ gives the standard equation

$$-\nabla_{pq}^2 h = \frac{1}{6} |H_3|^2 \quad (4.68)$$

where ∇_{pq}^2 is the Laplacian on the cone over $Y^{p,q}$.

A supergravity solution, based on $\Omega_{2,1}$ is expected to be supersymmetric if it has no curvature singularities [150, 151, 152]. The supergravity lore predicts that supersymmetric solutions should obey a first order system of differential equations. Naively, this first order system could be easier to solve than the second order PDE

(4.67). Such a first order system for F_5 can be generated starting from the Ansatz

$$F_5 = B_2 \wedge F_3 + dC_4 \quad (4.69)$$

where

$$g_s C_4 = h(r, y)^{-1} d^4 x + \frac{f(r, y)}{(1-y)\sqrt{wv}} e^\psi \wedge e^\theta \wedge e^\phi \wedge e^\beta, \quad (4.70)$$

and B_2 is given in (4.89). Enforcing the self-dual constraint $F_5 = *F_5$, one finds

$$\begin{aligned} \frac{\partial h}{\partial r} r^5 &= \frac{\partial f}{\partial y} \frac{1}{1-y} + \frac{C}{(1-y)^4} \ln r, \\ \frac{\partial h}{\partial y} r^3 (1-y) wv &= -\frac{\partial f}{\partial r}, \end{aligned}$$

which is indeed a first order system (a similar type of system appears in a somewhat different context in [153]). Unfortunately, as it involves one more function than the PDE in (4.67), it seems no easier to solve; in fact this system is equivalent to (4.67) as a constraint on $h(r, y)$.

4.6.2 Solving for the Warp Factor

Before solving (4.67), let us understand the boundary conditions at $y = y_1$ and $y = y_2$. At these points the radius of the circular coordinate ψ smoothly shrinks to zero. Defining the coordinate $\rho \sim \sqrt{y - y_1}$ near the boundary, I find that the metric in these two dimensions (with other coordinates fixed) is locally

$$ds_2^2 = d\rho^2 + \rho^2 d\psi^2. \quad (4.71)$$

The behavior of ψ -independent modes in these radial coordinates is well-known. The boundary condition is $\frac{dh}{d\rho} = 0$, so that

$$h = h_0 + h_2 \rho^2 + \dots = h_0 + \tilde{h}_2 (y - y_1) + \dots \quad (4.72)$$

In terms of the y -coordinate, this gives the boundary conditions that $\frac{\partial h}{\partial y}$ is finite at the boundaries, while h is positive there.

Substitute into (4.67)

$$h = r^{-4} f(t, y) , \quad t = \ln(r/R_0) . \quad (4.73)$$

The PDE for $f(t, y)$ assumes the simpler form

$$(1 - y) \left(-\frac{\partial^2 f}{\partial t^2} + 4\frac{\partial f}{\partial t} \right) - \frac{\partial}{\partial y} \left(2(b - 3y^2 + 2y^3) \frac{\partial f}{\partial y} \right) = \frac{C}{(1 - y)^3} . \quad (4.74)$$

Now, it is clear that there are solutions of the form

$$f(t, y) = At + s(y) , \quad (4.75)$$

where A is a constant, and the ODE for $s(y)$ is

$$-\frac{d}{dy} \left(2(b - 3y^2 + 2y^3) \frac{ds}{dy} \right) = \frac{C}{(1 - y)^3} - 4A(1 - y) . \quad (4.76)$$

The boundary conditions for h translate into the condition that s' is finite at both end-points. Therefore, integrating the LHS from y_1 to y_2 I must find zero. This imposes a constraint on A that

$$\int_{y_1}^{y_2} dy \left[\frac{C}{(1 - y)^3} - 4A(1 - y) \right] = 0 , \quad (4.77)$$

whose solution is

$$A = \frac{C}{4(1 - y_1)^2(1 - y_2)^2} . \quad (4.78)$$

Equation (4.76) can be integrated twice to give

$$s(y) = -\frac{C}{4(b - 1)} \left[\frac{1}{1 - y} + \frac{(1 + 2y_1)(1 + 2y_2) \ln(y_3 - y)}{2(b - 1)} \right] + \text{const} . \quad (4.79)$$

This function has singularities at $y = y_3$ and $y = 1$, but they are safely outside the

region $y_1 < y < y_2$ for all admissible p and q . To summarize, the warp factor I find is

$$h(r, y) = \frac{A \ln(r/R_0) + s(y)}{r^4}, \quad (4.80)$$

with A given by (4.78) and $s(y)$ given by (4.79). Just like the solution found in [11], this solution has a naked singularity for small enough r . It should be interpreted as the asymptotic form of the solution. In the conifold case, the complete solution [124] involves the deformation of the conifold that is important in the IR, but in the UV the solution indeed approaches the asymptotic form found earlier in [11]. Finding the complete solutions for cones over $Y^{p,q}$, non-singular in the IR, remains an important problem.

There are two interesting special limits of the solutions in (4.80). For $q \ll p$,

$$y_1 = -\frac{3q}{4p} + O(q^2/p^2), \quad y_2 = \frac{3q}{4p} + O(q^2/p^2). \quad (4.81)$$

In this limit the range of y becomes narrow, and both end-points approach zero. Since $\frac{\partial h}{\partial y}$ is finite, the variation of h in the y -direction can be ignored, and $h \sim \ln(r/R_0)/r^4$, as in [11]. This is not surprising, since for $q \ll p$ the spaces $Y^{p,q}$ may be approximated by a \mathbb{Z}_p orbifold of $T^{1,1}$.

The other special case is $q = p - l$, with $l \ll p$. Now

$$b = 1 - \frac{27l^2}{4p^2} + O(l^3/p^3), \quad (4.82)$$

and

$$y_1 = -\frac{1}{2} + \frac{3l^2}{2p^2} + O(l^3/p^3), \quad y_2 = 1 - \frac{3l}{2p} + O(l^2/p^2), \quad y_3 = 1 + \frac{3l}{2p} + O(l^2/p^2). \quad (4.83)$$

Note that y_2 approaches 1 from below, while y_3 from above, as $\frac{l}{p} \rightarrow 0$. In this limit, I find that h depends on y strongly and gets sharply peaked near $y = 1$. While $\frac{\partial h}{\partial y}$ is finite at y_2 for any finite l and p , it diverges in the limit $l/p \rightarrow 0$. The limiting form

of the warp factor is

$$h(r, y) \rightarrow 6 \frac{(\alpha' g_s M)^2 p^4}{r^4} \left[\frac{4}{3} \ln(R_0) + \frac{1}{1-y} - \frac{2}{3} \ln(1-y) \right]. \quad (4.84)$$

To facilitate comparison with the solution found for the S^5/\mathbb{Z}_2 orbifold case in [147], it is convenient to introduce a new coordinate ρ

$$\frac{2}{3}(1-y) = 1 - \frac{\rho^2}{r^2}, \quad (4.85)$$

and an auxiliary radial variable $r' = \sqrt{r^2 - \rho^2}$. For $q = p$ the variable ρ ranges from 0 to r while r' ranges from r to 0.

The geometry of $Y^{p,p}$ is that of the \mathbb{Z}_p orbifold of S^5/\mathbb{Z}_2 . In [133], the space $Y^{1,1}$ was identified with the $\mathcal{N} = 2$ preserving S^5/\mathbb{Z}_2 orbifold. In the limit $q \rightarrow p$, the metric (4.13) is independent of both p and q . Only the period of the $U(1)$ fiber coordinate α , which becomes π/p in this limit, depends on p . In the limit $p = q$, I can rewrite the metric on the cone over (4.13), $dr^2 + r^2 d\Omega_{Y^{p,p}}^2$, in the form

$$ds^2 = dr'^2 + \frac{1}{4} r'^2 [d\theta^2 + \sin^2 \theta d\phi^2 + (-d\psi - 2d\alpha + \cos \theta d\phi)^2] + d\rho^2 + 4\rho^2 (d\alpha)^2. \quad (4.86)$$

From this form of the metric, one can see that the cone over $Y^{p,p}$ factors into a cone over an orbifolded S^3 and a cone over an orbifolded S^1 . The cone over S^3 is locally \mathbb{C}^2 parametrized by $\theta, \phi, \psi + 2\alpha$, and the auxiliary radial coordinate r' . In this Euler angle parametrization, $-\psi - 2\alpha$ gives the overall phase of $(z_1, z_2) \in \mathbb{C}^2$. The cone over S^1 is parametrized by the angle α and the radial coordinate ρ .

The orbifold action sends $\alpha \rightarrow \alpha - \pi/p$, acting as \mathbb{Z}_p on this cone over S^1 . If the range of α ran from zero to π instead of from zero to π/p , then the cone over S^1 would be smooth. This same action shifts the phase $\psi + 2\alpha \rightarrow \psi + 2\alpha - 2\pi/p$. For the S^3 to be un-orbifolded, the Euler angle $-\psi - 2\alpha$ should run from zero to 4π . We conclude the orbifold acts on this cone over S^3 as \mathbb{Z}_{2p} .

Putting the two cones together I find the \mathbb{Z}_{2p} orbifold of \mathbb{C}^3 described in [135]. More precisely, the cone over $Y^{p,p}$ is the orbifold generated by $\zeta : (z_1, z_2, z_3) \rightarrow$

$(\omega^{a_1} z_1, \omega^{a_2} z_2, \omega^{a_3} z_3)$, where ω is a $2p$ 'th root of unity and, keeping track of the signs of the angles, $\vec{a} = (1, 1, -2)$. We see that ζ^p generates a \mathbb{Z}_2 subgroup of \mathbb{Z}_{2p} . Moreover, ζ^p acts as the identity on z_3 , fixing a circle in $Y^{p,p}$.

From this discussion, $y = 1$ (or equivalently $\rho = r$) is the location of the circle fixed by ζ^p . In terms of the coordinate ρ , the warp factor in (4.84) becomes

$$h(r, \rho) \rightarrow 4 \frac{(\alpha' g_s M)^2 p^4}{r^4} \left[\ln \left(\frac{r^4}{r^2 - \rho^2} \right) + \frac{r^2}{r^2 - \rho^2} + \text{const} \right]. \quad (4.87)$$

This matches the warp factor (44) of [147] exactly.

4.7 Matching the β -Function

The gauge/gravity correspondence predicts that the β -functions from the supergravity and gauge theory calculations should match. It is shown in this section that this prediction is true. On the supergravity side, I can calculate the running of the gauge coupling constant g on the stack of D5-branes from the integral of B_2 (recall $dB_2 = H_3$) over a 2-cycle. In particular

$$\frac{8\pi^2}{g^2} = \frac{1}{2\pi\alpha'g_s} \int_{\mathcal{C}} B_2. \quad (4.88)$$

Now

$$B_2 = (\ln r)(4\pi^2\alpha'g_s M)K\omega. \quad (4.89)$$

It is unclear how to describe the two-cycle \mathcal{C} in terms of the metric coordinates. However, based on [129, 130], one can expect that the harmonic form Poincare dual to \mathcal{C} is $K e^\psi \wedge \omega$. Thus,

$$K \int_{\mathcal{C}} \omega = K^2 \int_{Y^{p,q}} e^\psi \wedge \omega \wedge \omega. \quad (4.90)$$

One quickly finds

$$K \int_{\mathcal{C}} \omega = \frac{p^2}{2\pi} \left(p + \sqrt{4p^2 - 3q^2} \right) \quad (4.91)$$

and hence that

$$\frac{8\pi^2}{g^2} = (\ln r)Mp^2 \left(p + \sqrt{4p^2 - 3q^2} \right) . \quad (4.92)$$

On the gauge theory side, the β -function is given by

$$\beta_{D5} = \sum s^i \beta_i \quad (4.93)$$

where the vector s^i describes how adding a D5-brane changes the ranks of the gauge groups. In [129, 130], it was demonstrated that a cubic anomaly involving the R and $U(1)_B$ charges is related in a precise way to this particular weighted sum of β -functions:

$$\text{tr}RU(1)_B^2 = -\frac{2}{3M} \sum s^i \beta^i . \quad (4.94)$$

In the derivation of this formula, it was assumed that the anomalous dimensions of the chiral fields are determined by the R -charges of the conformal theory. In principle, there could be coupling constant corrections to these anomalous dimensions if I start at a point away from the conformal surface described in Section 4.4 and then add D5-branes. Even if I start on the conformal surface, the addition of D5-branes could conceivably introduce M/N corrections to these anomalous dimensions. The fact that the geometric and gauge theory calculations will agree indicates that these corrections should begin at order $(M/N)^2$, as discussed in [129, 130].

Using R -charges for the chiral fields (4.35), (4.36), (4.37), and (4.38), which were first derived for $Y^{2,1}$ in [137] and later for all $Y^{p,q}$ in [135] using a -maximization, I can compute

$$\begin{aligned} \text{tr}RU(1)_B^2 &= (p-1)(R_Z - 1)(p+q)^2 + 2p(R_U - 1)(-p)^2 \\ &\quad + 2q(R_V - 1)q^2 + (p+q)(R_Y - 1)(p-q)^2 \\ &= -\frac{2}{3}p^2 \left(p + \sqrt{4p^2 - 3q^2} \right) , \end{aligned}$$

which combined with (4.94) agrees with the intersection calculation above in (4.92).

This calculation seems like a bit of magic. As part of a more general discussion of

Seiberg duality [154] cascades, I will repeat this calculation using brute force for two classes $Y^{p,p-1}$ and $Y^{p,1}$ of spaces.

4.8 Cascades in the Dual Gauge Theories

The self-similar structure of the gauge theory under the duality, discussed briefly in Section 4.2, which allows the cascade to occur, can be found in more complicated quiver diagrams as well. In [129, 130, 131] the cascade in the gauge theory dual to $AdS_5 \times Y^{2,1}$ was analyzed. The relevant gauge theory is $SU(N+M) \times SU(N+3M) \times SU(N+2M) \times SU(N+4M)$. If the initial conditions are such that the biggest gauge group flows to infinite coupling first, then after applying a duality transformation to this group and permuting factor groups, one finds exactly the same theory, with $N \rightarrow N - M$. For a generic choice of initial conditions, the biggest gauge group will flow to infinite coupling again, and the cascade repeats until N reaches zero far in the infrared.

In fact, this structure of the cascade is possible for all gauge theories dual to $AdS_5 \times Y^{p,p-1}$ and $AdS_5 \times Y^{p,1}$.

4.8.1 Cascades for $Y^{p,p-1}$

As shown in [135], the systematics of the quiver diagram emerges most clearly for $p > 2$ where, placing the gauge groups at the vertices of a regular polygon, I find that the outer edge of the diagram consists of $2p$ vertices connected by double arrows pointing in the same direction, except for one “impurity” where the double arrow is replaced by a single one. The effect of the impurity is also to merge two inner single arrows into one (see Figure 4-3, which is reproduced from Figure 4 of [135]). In the language of section 2, the $Y^{p,p-1}$ gauge theories consist of $(p-1)$ σ unit cells and one τ unit cell.

Upon addition of M fractional branes, the single arrow “impurity” connects the smallest gauge group $SU(N+M)$ with the biggest gauge group $SU(N+2pM)$. In the case of $p = 4$ corresponding to Figure 4-3, the action of the Seiberg duality

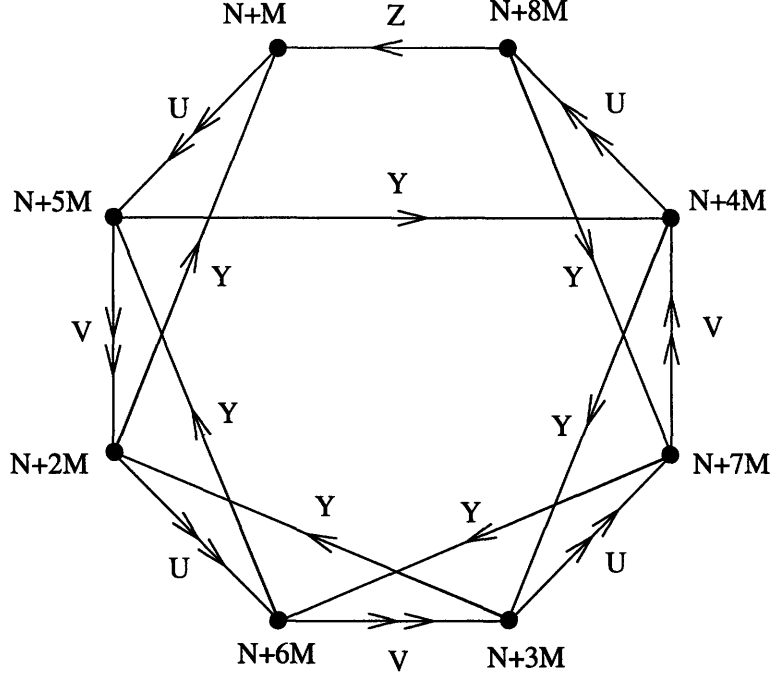


Figure 4-3: The quiver for $Y^{4,3}$, which is identical to Figure 4-2c.

on $SU(N + 8M)$ gives $SU(N)$ because the group effectively has $2N + 8M$ flavors. Permuting the adjacent vertices corresponding to $SU(N)$ and $SU(N + 4M)$ gives a quiver identical to the one I started with, except with $N \rightarrow N - M$. Compared to the original diagram, the impurity moved two steps clockwise around the outer edge.

For the general p , there are $2p$ gauge groups. On the conformal surface, the gauge groups are all $SU(N)$. However, I can add M D5-branes which shift the gauge groups to

$$\prod_{i=1}^{2p} SU(N_i) \tag{4.95}$$

where

$$N_{2n-1} = N + nM ; \quad N_{2n} = N + (p + n)M . \tag{4.96}$$

To be painfully explicit, the gauge group becomes

$$\begin{aligned}
& SU(N + M) \times SU(N + (p + 1)M) \\
& \quad \times SU(N + 2M) \times SU(N + (p + 2)M) \times \dots \\
& \quad \dots \times SU(N + pM) \times SU(N + 2pM) . \quad (4.97)
\end{aligned}$$

Clearly, this action of Seiberg duality generalizes to higher p . The action on the biggest gauge group $SU(N + 2pM)$ reduces it to $SU(N)$. Subsequent permutation of adjacent vertices $SU(N)$ and $SU(N + pM)$ turns the quiver into the one we started with, but with $N \rightarrow N - M$.

The gauge group with the most colors $SU(N + 2pM)$ is also the gauge group with the largest β -function, which can be seen below (M has been set to one as all β -functions are proportional to M .)

$$\beta_1 = 3 + \frac{3}{2} [2(p + 1)(R_U - 1) + 2(R_Y - 1) + 2p(R_Z - 1)] , \quad (4.98)$$

$$\begin{aligned}
\beta_{2n} = & 3(n + p) + \frac{3}{2} [2(n + 1)(R_V - 1) + (n + p + 1)(R_Y - 1) + \\
& (n + p - 1)(R_Y - 1) + 2n(R_U - 1)] , \quad (4.99)
\end{aligned}$$

$$\begin{aligned}
\beta_{2n-1} = & 3n + \frac{3}{2} [2(p + n)(R_U - 1) + (n + 1)(R_Y - 1) + \\
& (n - 1)(R_Y - 1) + 2(p + n - 1)(R_V - 1)] , \quad (4.100)
\end{aligned}$$

$$\beta_{2p} = 6p + \frac{3}{2} [(R_Z - 1) + (2p - 1)(R_Y - 1) + 2p(R_U - 1)] , \quad (4.101)$$

where for the β_{2n} , $1 \leq n \leq p - 1$ and for the β_{2n-1} , $2 \leq n \leq p$.

The fact that the superpotential has R -charge two gives $R_U + R_V + R_Y = 2$ and $2R_U + R_Y + R_Z = 2$, from which it follows that

$$\begin{aligned}
\beta_1 = -\beta_{2p} &= \frac{3}{2} (R_Y - R_Z - 2p(R_U + R_Y)) , \\
\beta_{2n-1} = -\beta_{2n} &= 3(1 - R_V - pR_Y) .
\end{aligned}$$

From (4.35), (4.36), (4.37), and (4.38), one can check that

$$\beta_1 < \beta_{2n-1} < 0 < \beta_{2n} < \beta_{2p} . \quad (4.102)$$

In particular,

$$\beta_1 = -5p + \sqrt{p^2 - (p-1)^2} < 0 , \quad (4.103)$$

for $p \geq 1$. Moreover, consider the difference

$$\beta_{2n-1} - \beta_1 = \frac{2p^2 \left(2p - \sqrt{p^2 + 6p - 3} \right)}{(1-p)^2} . \quad (4.104)$$

This difference is strictly greater than zero for $p \geq 1$. This demonstrates that β_1 and β_{2p} have the largest magnitude of the $2p$ β -functions. Therefore, as the theory flows to the IR, the coupling will generically blow up first for the biggest gauge group $SU(N + 2pM)$, necessitating an application of Seiberg duality.

To make sure that there are no errors in the above computation, I shall now explicitly check that (4.93) is true i.e.

$$\beta_{D5} = \sum s^i \beta_i = \sum_{n=1}^p n \beta_{2n-1} + \sum_{n=1}^p (p+n) \beta_{2n} , \quad (4.105)$$

where the s^i is the D5-brane vector. Lo and behold,

$$\sum s^i \beta_i = p^2 \left(p + \sqrt{4p^2 - 3(p-1)^2} \right) M , \quad (4.106)$$

in agreement with (4.92).

4.8.2 Cascades for $Y^{p,1}$

The $Y^{2,1}$ theory is not only the simplest example of $Y^{p,p-1}$ but also of $Y^{p,1}$. The $Y^{p,1}$ quivers, in the language of Section 4.4, contain $(p-1)$ τ unit cells and one σ unit cell. The quiver for $Y^{4,1}$ is shown as Figure 4-4.

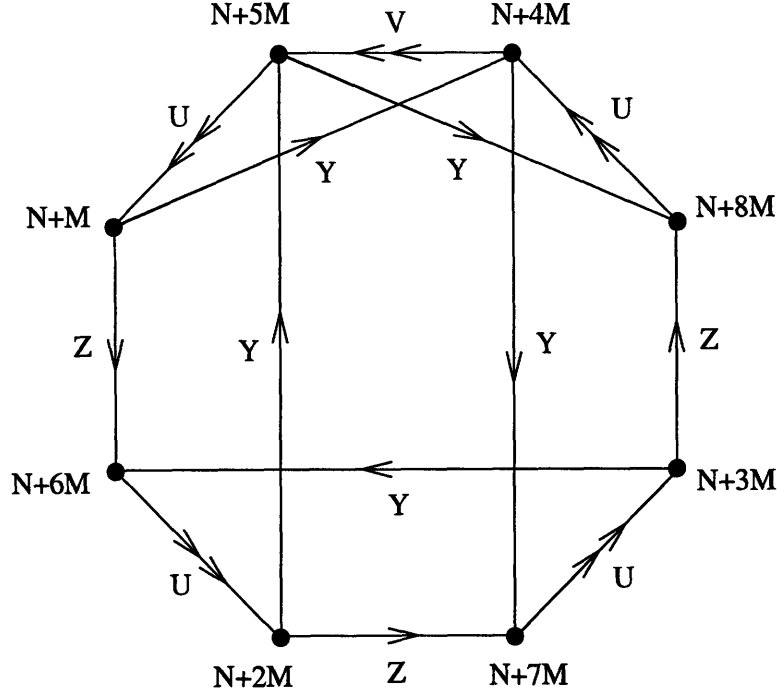


Figure 4-4: The quiver theory for $Y^{4,1}$, involving three τ unit cells and one σ unit cell.

The gauge groups for the $Y^{p,1}$ spaces are

$$\prod_{i=1}^{2p} SU(N_i), \quad (4.107)$$

with

$$N_{2n-1} = N + (p + n)M ; \quad N_{2n} = N + nM , \quad (4.108)$$

where the σ unit cell contains both the first and second and also the last and second to last gauge groups.

The gauge groups with the largest and smallest numbers of colors are associated with the impurity, i.e. the σ unit cell. The gauge group with the largest number of colors $SU(N + 2pM)$ has $2N + 2pM$ flavors. Thus, after a Seiberg duality, the gauge group will change to $SU(N)$. Switching this $SU(N)$ gauge group with its neighbor $SU(N + pM)$ I find the same quiver but with the σ impurity shifted one cell to the left and $N \rightarrow N - M$ (see Figure 4-5).

Again, Seiberg duality will generically happen at the gauge group with the largest

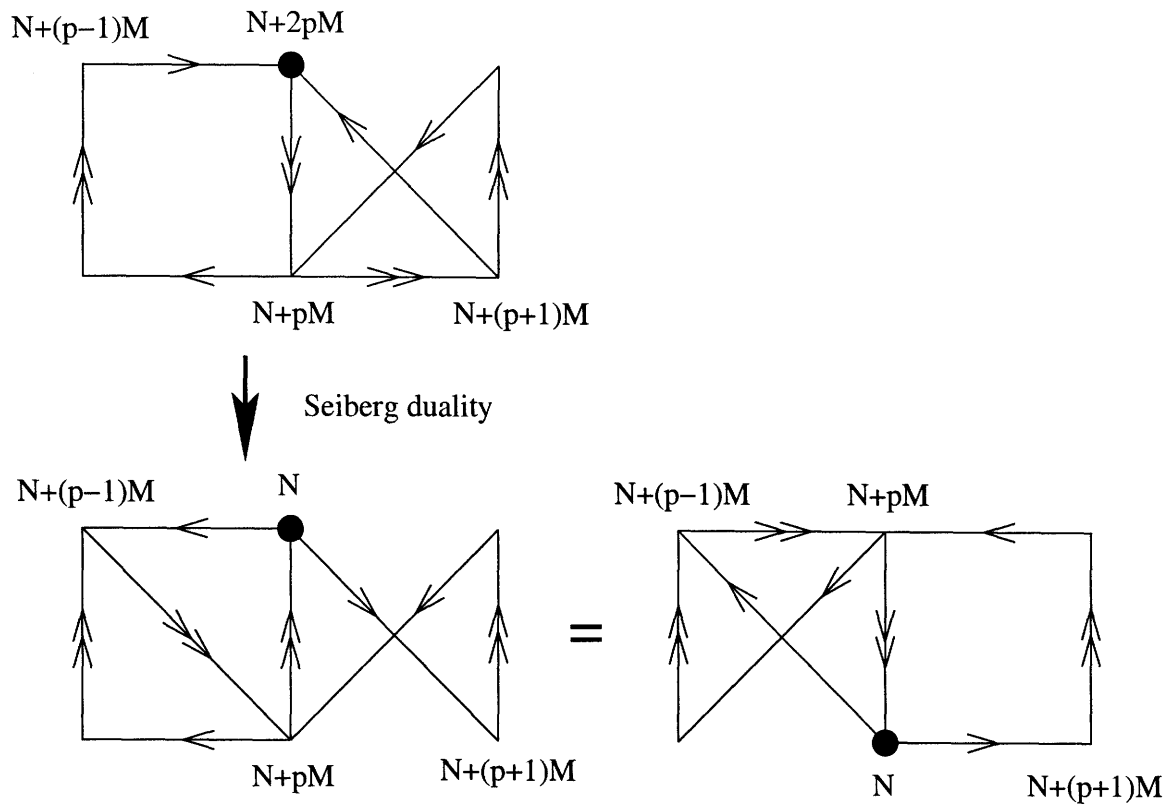


Figure 4-5: Seiberg duality for the $Y^{p,1}$ quiver: $(\cdots \tau \tilde{\tau} \sigma \tilde{\tau} \cdots) \rightarrow (\cdots \tau \tilde{\sigma} \tau \tilde{\tau} \cdots)$.

number of colors. The β -functions for the $2p$ gauge groups are

$$\begin{aligned}\beta_1 &= -\beta_{2p} = 3(p-1 + (1-p)R_U + R_Y)M, \\ \beta_{2n+1} &= -\beta_{2n} = 3\left(p + \frac{1}{2}R_Y - \frac{1}{2}R_Z\right)M,\end{aligned}$$

where $1 \leq n < p$. From (4.35), (4.36), (4.37), and (4.38), one can check that

$$\beta_{2n} < \beta_{2p} < 0 < \beta_1 < \beta_{2n+1}. \quad (4.109)$$

Indeed, the gauge group with the largest number of colors has the largest β -function. However, an important difference between the $Y^{p,p-1}$ and the $Y^{p,1}$ gauge theories is that in the present case, there are $p-2$ other gauge groups which share the same large β -function. It may happen that Seiberg duality occurs first at the node with the largest number of colors, but the situation is less generic than before.

Finally, the sum

$$\sum_{i=1}^{2p} s^i \beta_i = \sum_{n=1}^p (p+n)\beta_{2n-1} + \sum_{n=1}^p n\beta_{2n} = p^2 \left(p + \sqrt{4p^2 - 3}\right) M, \quad (4.110)$$

agrees with the result in (4.92).

4.9 Discussions and Conclusions

The work presented here is part of the work done in verifying the gauge/gravity correspondence in the case of $Y^{p,q}$ spaces.

The two new supersymmetric 3-cycles in Section 4.5 complete the identification of D3-branes wrapped on these 3-cycles with dibaryon operators in the gauge theory.

The explicit metric for the supergravity solutions in the presence of fractional D3-branes is presented in Section 4.6. It is shown that these solutions are consistent with known solutions of S^5/\mathbb{Z}_{2p} and $T^{1,1}/\mathbb{Z}_p$ in the limits when $p-q \ll p$ and $p \gg q$ respectively. The logarithmic dependence in the warp factor indicates that the gauge

theory is no longer conformal. This is confirmed by calculating the β -function of the gauge coupling on the D5-brane in the next section.

A special case of the $Y^{p,q}$ spaces is $T^{1,1}$, which in the presence of fractional D3-branes undergoes a series of duality cascades. A study of these duality cascades, based on the values of the β -functions, is carried out for $Y^{p,q}$ for the special cases of $q = p - 1$ and $q = 1$ in Section 4.8. It is shown that the quivers do indeed have a self similar structure under $N \rightarrow \tilde{N} = N - M$ and that the β -function for the gauge group with the highest rank diverges first.

Further, both for $Y^{p,1}$ and $Y^{p,p-1}$, if N is initially a multiple of M then far in the IR N is reduced to zero, so that I find the gauge group $SU(M) \times SU(2M) \times \dots \times SU(2pM)$. Note that for the $SU(2pM)$ factor there are effectively $2pM$ flavors. Hence it can contain baryon operators. In this sense the cascade obtained is rather analogous to the cascade found with $T^{1,1}$. (The latter case formally corresponds to $p = 1$ and $q = 0$.) It is therefore possible that all these theories have a baryonic branch where the $U(1)_B$ and the $U(1)_F$ continuous symmetries are spontaneously broken. This idea needs further investigation because the dynamics of the $SU(M) \times SU(2M) \times \dots \times SU(2pM)$ gauge theory is necessarily more complex than for the $SU(M) \times SU(2M)$ case found for the deformed conifold.

Appendix A

Discussion of Brane Embedding and Fluctuations

In this appendix I present a general discussion of brane embedding in a curved spacetime (in the absence of fluxes) and its small fluctuations and then specialize to the case of D7-branes embedded in the $AdS_5 \times S^5$ black hole geometry. The results of this appendix are used in Chapter 2, in particular Section 2.3

A.1 General Discussion

Consider a $p + 1$ -dimensional brane in a D -dimensional target space whose action is

$$S_{Dp} = -\mu_p \int d^{p+1}\xi \sqrt{-\det \tilde{h}_{ij}} , \quad (\text{A.1})$$

where $\xi^i, i = 0, 1, \dots, p$ denote the worldvolume coordinates and \tilde{h}_{ij} is the induced metric in the worldvolume

$$\tilde{h}_{ij} = G_{\mu\nu}(X) \frac{\partial X^\mu}{\partial \xi^i} \frac{\partial X^\nu}{\partial \xi^j}, \quad \mu = 0, 1, \dots, D - 1 . \quad (\text{A.2})$$

Suppose that $X_0^\mu(\xi^i)$ solves the equations of motion following from (A.1), thus describing an embedding of the brane in the target spacetime. The goal is to understand

the behavior of small fluctuations around X_0 . For this purpose, let

$$X^\mu(\xi) = X_0^\mu(\xi^i) + \delta X^\mu(\xi^i). \quad (\text{A.3})$$

The action for δX^μ can then be obtained straightforwardly from (A.1). The resulting action and equations of motion for δX^μ are, however, not geometrically transparent. This is due to the fact that $\delta X^\mu(\xi^i)$ is the difference between coordinates and thus does not have good properties under coordinate transformations. A more convenient way to parameterize $\delta X^\mu(\xi)$ is to use the exponential map to express it in terms of a vector in the tangent space at X_0^μ , as I now describe. (Such techniques have also been used in the calculation of string worldsheet β -functions [155].) Given a vector η^μ , shoot out geodesics of unit affine parameter from X_0 with tangent η^μ . The end point of such a geodesic is identified with $X_0^\mu + \delta X^\mu$. Such a map should be one-to-one within a small neighborhood of X_0 . To second order in η one may solve the geodesic differential equation, finding

$$\delta X^\mu = \eta^\mu - \frac{1}{2} \Gamma_{\sigma\tau}^\mu(X_0) \eta^\sigma \eta^\tau + \dots \quad (\text{A.4})$$

Note that the appearance of Γ is consistent with the coordinate dependence of δX ; they can both be shown to have the same variation under a coordinate transformation.

Using the parametrization (A.4) gives

$$\begin{aligned} \tilde{h}_{ij} &= G_{\mu\nu}(X_0 + \delta X) \partial_i (X_0^\nu + \delta X^\nu) \partial_j (X_0^\mu + \delta X^\mu) \\ &= h_{ij} + 2G_{\mu\nu} \lambda_{(i}^\mu \nabla_{j)} \eta^\mu + G_{\mu\nu} \nabla_i \eta^\mu \nabla_j \eta^\nu + \eta^\sigma \eta^\tau \lambda_{(i}^\mu \lambda_{j)}^\nu R_{\nu\tau\sigma\mu} \end{aligned} \quad (\text{A.5})$$

with

$$h_{ij} = G_{\mu\nu}(X_0) \partial_i X_0^\mu \partial_j X_0^\nu = \lambda_i^\mu \lambda_{j\mu}, \quad \nabla_i = \lambda_i^\mu \nabla_\mu, \quad \lambda_i^\mu = \partial_i X_0^\mu. \quad (\text{A.6})$$

where λ_i^μ are vector fields along the brane directions. The simplest way to find (A.5) is to use the Riemann Normal coordinates at X_0 in which the Christoffel symbols

vanish. h_{ij} is the induced metric in the worldvolume theory and below indices i, j will be raised and lowered by h . To quadratic order in η , the lagrangian is

$$\sqrt{-\det\tilde{h}_{ij}} = \sqrt{-\det h_{ij}} \left(1 + \lambda_\nu^i \nabla_j \eta^\nu + \frac{1}{2} \nabla^i \eta^\mu \nabla_i \eta_\mu - (\lambda_{i\mu} \nabla_j \eta^\mu) (\lambda_\nu^{(i} \nabla^{j)}) \eta^\nu \right. \\ \left. + \frac{1}{2} (\lambda_\nu^i \nabla_i \eta^\nu)^2 + \frac{1}{2} \eta^\sigma \eta^\tau h^{ij} \lambda_i^\mu \lambda_j^\nu R_{\sigma\mu\nu\tau} \right). \quad (\text{A.7})$$

Now take η^μ to be orthogonal to the brane worldvolume (which corresponds to choosing the static gauge), i.e.

$$\eta^\mu = \chi_s n_s^\mu(X_0), \quad s = 1, \dots, D - p - 1, \quad (\text{A.8})$$

where $n_s(X_0)$ are unit vectors orthogonal to the worldvolume direction. Note that λ_i^μ and n_s^μ together span the full tangent space at X_0 . i.e.

$$\lambda_i^\mu n_{s\mu} = 0, \quad n_{s\mu} n_t^\mu = \delta_{st}, \quad \lambda_i^\mu \lambda_\mu^j = \delta_i^j, \quad (\text{A.9})$$

and

$$\delta_\nu^\mu = \lambda_i^\mu \lambda_\nu^i + n_s^\mu n_{s\nu}. \quad (\text{A.10})$$

Now introduce

$$K_{sij} = \lambda_i^\mu \lambda_j^\nu \nabla_\mu n_{s\nu}, \quad K_s = K_{sij} h^{ij}, \quad U_{st}^i = n_s^\nu \nabla_i n_{t\nu} = n_s^\nu \lambda_i^\mu \nabla_\mu n_{t\nu}. \quad (\text{A.11})$$

K_{sij} is the extrinsic curvature of the brane in the s -direction, and is symmetric in i, j . (This follows from the fact that a surface orthogonal to n_s^μ satisfies $\nabla_{[\mu} n_{\nu]}^t = \sum_s v_{[\mu}^s n_{\nu]}^s$ for some one-form v_μ^s . Note also that K_{sij} can be written as $K_{sij} = \frac{1}{2} L_{n_s} h_{ij}$, where L_n is the Lie derivative along n -direction.) U_{st}^i , which is antisymmetric in s, t , is an $SO(D - 1 - p)$ connection for the transverse directions. Note that the choice of n_s^μ (and thus χ_s) is not unique. One can choose a different set of basis vectors by making an arbitrary local $SO(D - 1 - p)$ transformation. Thus χ_s transforms as a vector under the $SO(D - 1 - p)$ “gauge” symmetry and U_{st}^i transform as a connection. Note

that this gauge symmetry is not dynamical. With these definitions

$$\nabla_i \eta_\mu = (D_i \chi_s) n_{s\mu} + K_{sij} \chi_s \lambda_\mu^j, \quad (\text{A.12})$$

where

$$D_i \chi_s = \partial_i \chi_s + U_{ist} \chi_t \quad (\text{A.13})$$

is an $SO(D - p - 1)$ covariant derivative. Using (A.12) in (A.7), leads to

$$S_{Dp} = -\mu_p \int d^{p+1} \xi \sqrt{-\text{deth}_{ij}} \left(1 + \chi_s K_s + \frac{1}{2} D_i \chi_s D^i \chi^s + \frac{1}{2} \chi_s \chi_t (-K_{sij} K_t^{ij} + R_{sijt} h^{ij} + K_s K_t) \right) \quad (\text{A.14})$$

with $R_{sijt} = n_s^\alpha n_t^\beta \lambda_i^\mu \lambda_j^\nu R_{\alpha\mu\nu\beta}$. For X_0 to satisfy the equations of motion, the terms in (A.14) that are linear in the χ 's have to vanish. This implies that

$$K_s = K_{sij} h^{ij} = 0, \quad s = 1, \dots, D - p - 1. \quad (\text{A.15})$$

These are the embedding equations for the background. Thus, the action (A.14) for the small fluctuations to quadratic order becomes

$$S_{Dp} = \mu_p \int d^{p+1} \xi \sqrt{-\text{deth}_{ij}} \left(-\frac{1}{2} D_i \chi_s D^i \chi^s - \frac{1}{2} \chi_s \chi_t (-K_{sij} K_t^{ij} + R_{sijt} h^{ij}) \right). \quad (\text{A.16})$$

Here both the embedding equations (A.15) and the action for the small fluctuations (A.16) in Section 2.3 have been used.

The action (A.16) can be further simplified if n_s^μ satisfies additional constraints. For example, if n_s^μ is proportional to a Killing vector, then

$$K_{sij} = 0. \quad (\text{A.17})$$

This follows from the fact that n_s^μ satisfies $\nabla_{(\mu} n_{\nu)}^s = v_{(\mu} n_{\nu)}^s$ for some v_μ . If in addition

n_s^μ is a hypersurface orthogonal, i.e. if it satisfies $\nabla_{[\mu} n_{\nu]}^s = w_{[\mu} n_{\nu]}^s$ for some one form w_μ , then

$$U_{ist} = 0, \quad \text{for all } t. \quad (\text{A.18})$$

This simplification has been used in Section 2.3.

Finally, note that equation (A.16) was written using the coordinate split (A.9). One can write it and other equations in a more covariant way by introducing

$$h_{\mu\nu} = h^{ij} \lambda_{i\mu} \lambda_{j\nu}, \quad h_\mu{}^\nu = h^{ij} \lambda_{i\mu} \lambda_j^\nu, \quad h^{\mu\nu} = h^{ij} \lambda_i^\mu \lambda_j^\nu, \quad (\text{A.19})$$

and using these objects in place of h_{ij} and λ_i^μ in various places. $h_{\mu\nu} = g_{\mu\nu} - n_{s\mu} n_{s\nu}$ is the covariant induced metric on the brane and $h_\mu{}^\nu$ is the projector onto the world-volume directions.

A.2 D7-branes in $AdS_5 \times S^5$ Black Hole

Specialize now to the case of D7-branes considered in the main text, where there are two transverse directions with

$$n_1^\nu = \frac{1}{N_1} \left(\left(\frac{\partial}{\partial y} \right)^\nu - y'_0(\rho) \left(\frac{\partial}{\partial \rho} \right)^\nu \right), \quad n_2^\nu = \frac{1}{N_2} \left(\frac{\partial}{\partial \phi} \right)^\nu, \quad (\text{A.20})$$

where $N_{1,2}$ are normalization factors. In this case U_{st}^i is proportional to the two-dimensional antisymmetric tensor ϵ_{st} . It is easy to see that n_2^ν is both hypersurface orthogonal and proportional to a Killing vector (since nothing depends on ϕ). This leads to $K_{2ij} = 0$ and $U_{12}^i = 0$. The action (A.16) now reduces to the form used in Section 2.3, namely

$$S_{D7} = \mu_7 \int d^8 \xi \sqrt{-h} \left(1 + \frac{1}{2} (\partial \phi_1)^2 + \frac{1}{2} (\partial \phi_2)^2 + \frac{1}{2} m_1^2 \phi_1^2 + \frac{1}{2} m_2^2 \phi_2^2 \right), \quad (\text{A.21})$$

where the “masses” are given by

$$m_1^2 = -R_{11} - R_{2112} - K_{1ij}K_1^{ij} , \quad (\text{A.22})$$

$$m_2^2 = -R_{22} - R_{2112} , \quad (\text{A.23})$$

with R_{2112} , R_{11} and R_{22} as defined in (2.31). In writing (A.21)–(A.23) the following identities have been used

$$R_{sijt}h^{ij} = n_s^\sigma n_i^\tau h^{ij} \lambda_i^\mu \lambda_j^\nu R_{\sigma\mu\nu\tau} = -R_{st} - R_{s11t} - R_{s22t}, \quad s, t = 1, 2 \quad (\text{A.24})$$

along with the fact that $R_{12} = 0$ for the $AdS_5 \times S^5$ black hole spacetime. One can also use the generalization of the Gauss-Codazzi relation for a codimension two surface, whose derivation is contained in Section A.3 (see (A.28)), to write

$$K_{1ij}K_1^{ij} = -{}^{(8)}R + R - 2R_{11} - 2R_{22} - 2R_{2112} . \quad (\text{A.25})$$

Therefore, m_1^2 in (A.22) can equivalently be written as

$$m_1^2 = R_{11} + R_{2112} + 2R_{22} + {}^{(8)}R - R , \quad (\text{A.26})$$

which is the form that was used in Section 2.3.

A.3 Gauss-Codazzi Relations for Co-dimension 2

Define the covariant derivative on the D7 brane as

$$D_\sigma s^\tau \equiv h_\sigma^\mu h_\nu^\tau \nabla_\mu s^\nu . \quad (\text{A.27})$$

This is equivalent to the covariant derivative defined with respect to h_{ij} . We can now use D_σ to define the curvature of the D7-brane and then relate it to the curvature of

the full space. Calculations similar to those in [156] reveal that

$${}^{(8)}R_{ijk}{}^l = P(R)_{ijk}{}^l + (K^s)_{ik}(K^s)_j{}^l - (K^s)_{jk}(K^s)_i{}^l, \quad (\text{A.28})$$

where s labels the two directions perpendicular to the brane and is summed over. $P(R)$ is the projection of the full Riemann tensor onto the D7-brane,

$$P(R)_{ijk}{}^l = \lambda_i^\mu \lambda_j^\nu \lambda_k^\sigma \lambda_\tau{}^l R_{\mu\nu\sigma\tau}. \quad (\text{A.29})$$

Taking further contractions of (A.28) with δ_j^l and h^{ik} and using (A.10) gives

$${}^{(8)}R = R - 2R_{ss} - R_{tsst} + K_s K_s - (K_{sij} K_s^{ij}), \quad (\text{A.30})$$

where s, t are both summed. In the case of interest, where $K_{2ij} = 0$ because n_2^μ is proportional to a Killing vector and where $K_s = 0$ is the embedding equation, this gives (A.25).

Appendix B

Dp/Dq -brane Theories

It will be of interest in future to study the degree to which the meson dispersion relations that were derived in Chapter 2, together with their consequences like (2.97) and (2.98), change as one modifies the gauge theory to make it more QCD-like. In this appendix, I report on a check that was mentioned in Section 2.5 in which the gauge theory is modified, albeit not in the direction of QCD. I consider the $(p + 1)$ -dimensional gauge theories described by N Dp -branes [108] into which fundamental quarks, and hence mesons, have been introduced by embedding N_f Dq -branes [109, 103, 95, 96]. The Dp -branes fill coordinates $0, 1, \dots, p$. The Dq -branes fill coordinates $0, 1, \dots, d$, where $d \leq p$, as well as $q - d$ of the remaining $9 - p$ coordinates. In the large- N limit, the near horizon geometry of the Dp -branes is dual to a $(p + 1)$ -dimensional supersymmetric Yang-Mills theory with 16 supercharges that is non-conformal for $p \neq 3$. I will restrict to $p < 5$. In the $N_f/N \rightarrow 0$ approximation, the Dq -branes live in the background Dp -brane geometry, and their back-reaction on the geometry can be neglected. Strings which stretch between the Dq - and the Dp -branes are dual to N_f fundamental quarks in the gauge theory. We shall set $N_f = 1$. And, scalar mesons in the gauge theory are represented by fluctuations of the position of the Dq -brane. The specific case that we have analyzed throughout most of Chapter 2 is $p = d = 3$, $q = 7$. In this more general setting, as in the specific case, there is a dissociation transition at some T_{diss} at which the spectrum of meson fluctuations changes from discrete to continuous.

The background Dp -brane geometry is described by the metric [108]

$$ds^2 = R^2 \left(\frac{R}{L_0} \right)^{(3-p)/2} \times \left(-f dt^2 + r^{(7-p)/2} dx_p^2 + \frac{r^{(p-3)/2}}{u^2} (d\rho^2 + dy^2 + \rho^2 d\Omega_{q-d-1}^2 + y^2 d\Omega_{8-p-q+d}^2) \right) \quad (\text{B.1})$$

and the dilaton

$$e^\phi = \left(\frac{L_0}{R} \right)^{(p-3)(7-p)/4} g_s r^{(p-3)(7-p)/4} , \quad (\text{B.2})$$

where

$$f = u^{-(7-p)/2} \frac{(u^{7-p} - \varepsilon^{(7-p)/2})^2}{u^{7-p} + \varepsilon^{(7-p)/2}} , \quad (\text{B.3})$$

$$r^{(7-p)/2} = u^{-(7-p)/2} (u^{7-p} + \varepsilon^{(7-p)/2}) , \quad (\text{B.4})$$

$$u^2 = y^2 + \rho^2 , \quad (\text{B.5})$$

and where coordinates are dimensionless as in (2.13). The black hole horizon is located at $u = u_0 \equiv \sqrt{\varepsilon}$. L_0 specifies the position where the Dq -brane that is introduced will sit, as follows. The Dq -brane embedding is described, in the absence of fluctuations, by a curve $y(\rho)$ with the Dq -brane placed such that its tip is located at $\rho = 0$ and $y = L_0$, and then use L_0 to re-scale metric coordinates such that the tip of the Dq -brane is at $y(0) = 1$. After this re-scaling, the metric and dilaton are given by (B.1) and (B.2). The holographic dictionary determines the coupling, number of colors, and temperature in the gauge theory via

$$\lambda = \frac{(16\pi^3)^{(p-3)/2}}{\Gamma\left(\frac{7-p}{2}\right)} R^{7-p} \alpha'^{p-5} , \quad (\text{B.6})$$

$$\frac{\lambda}{N} = 2^{p-1} \pi^{p-2} g_s \alpha'^{(p-3)/2} , \quad (\text{B.7})$$

$$T = \frac{(7-p)2^{(5-p)/(7-p)}}{4\pi} u_0^{(5-p)/2} R^{-1} \left(\frac{L_0}{R} \right)^{(5-p)/2} . \quad (\text{B.8})$$

Note that λ has dimension $p-3$, making it useful to define the dimensionless coupling

$$\lambda_{\text{eff}} \equiv \lambda T^{p-3} . \quad (\text{B.9})$$

The differential equation that specifies the shape of the embedding curve $y(\rho)$ can be derived as was done in obtaining (1.41). For the special case in which $p-d+q-d=4$, the embedding equation simplifies, becoming

$$\frac{y''}{1+y'^2} + \frac{(q-d-1)y'}{\rho} = \frac{2\varepsilon^{(7-p)/2}(y-y'\rho)}{u^2} \left(\frac{(3-d)u^{7-p} + (q-d)\varepsilon^{(7-p)/2}}{u^{2(7-p)} - \varepsilon^{7-p}} \right) . \quad (\text{B.10})$$

The variables have been scaled so that the tip of the D q -brane is at $y(0) = 1$; the smoothness of the embedding requires that $y'(0) = 0$; using these boundary conditions, one can then solve the embedding equation and obtain $y(\infty)$, which defines ϵ_∞ via $y(\infty) = \sqrt{\varepsilon/\epsilon_\infty}$. Finally, the mass m_q of the quarks that are of interest is given via

$$m_q^2 = \frac{\varepsilon L_0^2}{4\pi^2 \epsilon_\infty \alpha'^2} . \quad (\text{B.11})$$

(B.6), (B.8) and (B.11) lead to

$$\epsilon_\infty = a_p \left(\frac{T}{m_q} \right)^2 \lambda_{\text{eff}}^{2/(5-p)} = a_p \frac{\lambda^{2/(5-p)} T^{4/(5-p)}}{m_q^2} , \quad (\text{B.12})$$

where the constant a_p is given by

$$a_p = \frac{2^{(10-2p)/(7-p)} \pi^{(3-p)/(5-p)}}{(7-p)^{4/(5-p)}} \left(\Gamma \left(\frac{7-p}{2} \right) \right)^{2/(5-p)} . \quad (\text{B.13})$$

Also note that the energy density of the plasma is given by [108]

$$\rho = b_p N^2 T^{p+1} \lambda_{\text{eff}}^{(p-3)/(5-p)} = b_p N^2 \lambda^{(p-3)/(5-p)} T^{(14-2p)/(5-p)} , \quad (\text{B.14})$$

where the constant b_p is given by

$$b_p = \frac{(9-p) 2^6 \pi^{(13-3p)/(5-p)}}{(7-p)^{(19-3p)/(5-p)}} \left(\Gamma \left(\frac{7-p}{2} \right) \right)^{2/(5-p)} . \quad (\text{B.15})$$

This means that

$$\left(\frac{\epsilon_\infty}{\epsilon_\infty^{\text{diss}}}\right)^{(7-p)/2} = \frac{\rho(T)}{\rho_{\text{diss}}}, \quad (\text{B.16})$$

where the zero-velocity mesons dissociate at a temperature T_{diss} corresponding to $\rho = \rho_{\text{diss}}$ and $\epsilon_\infty = \epsilon_\infty^{\text{diss}}$, with $\epsilon_\infty^{\text{diss}}$ a constant of order unity.

I shall not repeat the construction of the meson wave functions and dispersion relations for the Dp/Dq system here. Instead, I shall assume that in the large- k limit the meson wave functions become localized at the tip of the Dq brane at $\rho = 0$ and $y = 1$, as was found for the $D3/D7$ system. As a consequence, the limiting meson velocity will be given by the local speed of light at the tip of the Dq -brane. This velocity can be read from the metric (B.1), and is given by

$$v_0 = \left(\frac{1 - \epsilon^{(7-p)/2}}{1 + \epsilon^{(7-p)/2}}\right). \quad (\text{B.17})$$

Section 2.5 contained the analysis of this result in the small ϵ limit, showing that in this limit it takes on the form (2.100) for any p . This illustrates the generality of the result (2.97) when it is phrased in terms of the energy density. Here, let us analyze (B.17) at arbitrary $\epsilon < 1$, seeking to compare it to (2.98). From (B.17) and (B.16) we can see that the critical velocity satisfies

$$\frac{1 - v_0}{1 + v_0} = \frac{1 - v_0^2}{(1 + v_0)^2} = \epsilon^{(7-p)/2} = \frac{\rho}{\rho_{\text{diss}}} \left(\frac{\epsilon_\infty^{\text{diss}}}{\epsilon_\infty}\right)^{(7-p)/2}. \quad (\text{B.18})$$

Recall that $\epsilon_\infty^{\text{diss}}$ is a constant of order unity and that ϵ/ϵ_∞ is a weak function of temperature and hence of ρ , obtained by solving the embedding equation and making a plot of ϵ_∞ vs. ϵ as in Fig. 2-1, and reading off the ratio.

As much as we did in Section 2.5, we can see (B.18) either as giving the limiting velocity v_0 as a function of ρ , or as giving $\rho_{\text{diss}}(v)$, the energy density above which no mesons with velocity v exist, via

$$\rho_{\text{diss}}(v) = (1 - v^2)\rho_{\text{diss}} \left[\frac{1}{(1 + v)^2} \left(\frac{\epsilon_\infty^{\text{diss}}}{\epsilon_\infty}\right)^{(p-7)/2} \right]. \quad (\text{B.19})$$

This is the generalization of (2.98) to the Dp/Dq system. It is written somewhat implicitly, since $\varepsilon/\varepsilon_\infty$ which occurs within the square brackets is a weak function of $\rho_{\text{diss}}(v)$. It is nevertheless manifest that the entire expression in the square brackets is a weak function of v , varying from one constant of order one at $v = 0$ to some different constant of order one at $v = 1$. As in (2.94), one can then define a function $f(v)$ by rewriting (B.19) as

$$\rho_{\text{diss}}(v) = [f(v)]^{(14-2p)/(5-p)} \frac{\rho_{\text{diss}}(0)}{\gamma^2}, \quad (\text{B.20})$$

where $\gamma = 1/\sqrt{1-v^2}$ is the Lorentz boost factor. Equivalently, using (B.14) one can write

$$T_{\text{diss}}(v) = f(v) \frac{T_{\text{diss}}(0)}{\gamma^{(5-p)/(7-p)}}. \quad (\text{B.21})$$

We have seen in Figure 2-11 that for the D3/D7 brane system, $f(v)$ is everywhere close to 1, with $f(1) = 0.924$ being the farthest it gets from 1. Also for $p = 4$ the embedding equations the D4/D6 brane system with $d = 3$ one finds that the farthest that $f(v)$ gets from $f(v) = 1$ is $f(1) = 1.048$.

Given its derivation via (B.18), it would have been reasonable to try writing

$$\rho_{\text{diss}}(v) = [\tilde{f}(v)]^{(14-2p)/(5-p)} \rho_{\text{diss}}(0) \frac{1-v}{1+v} \quad (\text{B.22})$$

instead of (B.20). This does not work as well, yielding a $\tilde{f}(v)$ that reaches 1.306 for the D3/D7 system and 1.261 for the D4/D6 system. So although there is no important parametric difference between (B.22) and (B.20), I have focussed on the form (B.20), and hence (B.21), throughout Chapter 2.

The most important conclusion from this Dp/Dq investigation in this appendix comes by comparing (B.20) and (B.21). In all the Dp/Dq systems that were analyzed here, the leading velocity dependence of $\rho_{\text{diss}}(v)$ is proportional to $1/\gamma^2$, as if the mesons see a boosted energy density. This was also discussed in Section 1.4. In contrast, $T_{\text{diss}}(v)$ scales with a power of γ that depends on p .

Appendix C

Generating the M2-brane Solution

It is possible to find the various D p - and M-brane solutions by starting with a Schwarzschild solution in the appropriate dimensions and applying lifts, Lorentz boosts and various dualities (see, for example, Section 2.5 in [116]). I shall illustrate this here by generating the non-extremal M2-brane solution in 11-dimensional supergravity starting from the Schwarzschild black hole in 9 dimensions. This technique will be employed in Chapter 3 in setting up the problem of finding the non-extremal D2/D6-brane solution.

The 9-dimensional Schwarzschild solution is

$$ds_{9,SS}^2 = -(1 - f_9(\rho))dt^2 + (1 - f_9(\rho))^{-1}d\rho^2 + \rho^2 d\Omega_7^2, \quad f_9(\rho) = \left(\frac{\rho_H}{\rho}\right)^6, \quad (\text{C.1})$$

where $\rho \geq 0$, $f_9(\rho)$ is the harmonic function in $\mathbb{R}^{1,8}$ and $d\Omega_7^2$ is the metric on S^7 . By adding in a trivial direction, x_1 , I get

$$ds_{10}^2 = (-dt^2 + dx_1^2) + f_9(\rho)dt^2 + (1 - f_9(\rho))^{-1}d\rho^2 + \rho^2 d\Omega_7^2$$

This will automatically be a solution in 10-dimensional and supergravity. Performing

a Lorentz boost in the t - x_1 plane with boost parameter γ

$$\begin{pmatrix} dt \\ dx_1 \end{pmatrix} \rightarrow \begin{pmatrix} \cosh \gamma & \sinh \gamma \\ \sinh \gamma & \cosh \gamma \end{pmatrix} \begin{pmatrix} dt \\ dx_1 \end{pmatrix}$$

leads to the metric

$$ds_{10}^2 = -dt^2(1 - f_9(\rho) \cosh^2 \gamma) + dx_1^2(1 + f_9(\rho) \sinh^2 \gamma) + 2dt dx_1 \cosh \gamma \sinh \gamma + (1 - f_9(\rho))^{-1} d\rho^2 + \rho^2 d\Omega_7^2. \quad (\text{C.2})$$

This is a background with no matter, in particular the dilaton $\Phi = 0$ and Neveu-Schwarz (NS) 2-form $B_{\mu\nu} = 0$. On T-dualizing along the x_1 direction, I get both a dilaton $\tilde{\Phi}$ and a 2-form potential $\tilde{B}_{\mu\nu}$ using the Buscher rules (see [117] and references therein), where the $\tilde{}$ denotes the T-dual quantities and μ and ν indicate all the directions transverse to x_1 . The results of this transformation are

$$e^{\tilde{\Phi}} = \frac{e^\Phi}{G_{x_1 x_1}} = \frac{1}{1 + f_9(\rho) \sinh^2 \gamma}, \quad (\text{C.3})$$

$$\tilde{B}_{\mu\nu} = B_{\mu\nu} - \frac{B_{\mu x_1} G_{\nu x_1} - B_{\nu x_1} G_{\mu x_1}}{G_{x_1 x_1}} = 0 \quad (\text{C.4})$$

$$\begin{aligned} \tilde{B}_{\mu x_1} &= \frac{G_{\mu x_1}}{G_{x_1 x_1}} = \delta_{\mu t} \frac{f_9(\rho) \cosh \gamma \sinh \gamma}{1 + f_9(\rho) \sinh^2 \gamma} \\ &= -\delta_{\mu t} \coth \gamma [(1 + f_9(\rho) \sinh^2 \gamma)^{-1} - 1] \end{aligned} \quad (\text{C.5})$$

$$\tilde{G}_{x_1 x_1} = \frac{1}{G_{x_1 x_1}} = \frac{1}{1 + f_9(\rho) \sinh^2 \gamma} \quad (\text{C.6})$$

$$\tilde{G}_{\mu x_1} = \frac{B_{\mu x_1}}{G_{x_1 x_1}} = 0 \quad (\text{C.7})$$

$$\begin{aligned} \tilde{G}_{\mu\nu} &= G_{\mu\nu} - \frac{G_{\mu x_1} G_{\nu x_1} - B_{\mu x_1} B_{\nu x_1}}{G_{x_1 x_1}} \\ &= G_{\mu\nu} - \delta_{\mu t} \delta_{\nu t} \frac{f_9^2(\rho) \cosh^2 \gamma \sinh^2 \gamma}{1 + f_9(\rho) \sinh^2 \gamma} \\ &= \begin{cases} G_{\mu\nu} & \text{for } \mu \text{ or } \nu \neq t \\ -\frac{1 - f_9(\rho)}{1 + f_9(\rho) \sinh^2 \gamma} & \text{for } \mu = \nu = t \end{cases} \end{aligned} \quad (\text{C.8})$$

Adding another dimension x_2 and using a Weyl transformation

$ds^2 \longrightarrow (1 + f_9(\rho) \sinh^2 \gamma)^{1/3} ds^2$, I obtain the non-extremal M2 brane solution (see, for example, [116])

$$ds_{11}^2 = (1 + f_9(\rho) \sinh^2 \gamma)^{-2/3} [-(1 - f_9(\rho)) dt^2 + dx_1^2 + dx_2^2] \\ + (1 + f_9(\rho) \sinh^2 \gamma)^{1/3} [(1 - f_9(\rho))^{-1} d\rho^2 + \rho^2 d\Omega_7^2] \quad (\text{C.9})$$

$$\tilde{B}_{tx_1x_2} = -\coth \gamma (1 + f_9(\rho) \sinh^2 \gamma)^{-1}, \quad (\text{C.10})$$

where $\tilde{B}_{tx_1x_2}$ is the 3-form potential that couples to the M2-brane. Notice that it has the form $\tilde{B} \propto -H^{-1} dt \wedge dx_1 \wedge dx_2$, where $H = (1 + f_9(\rho) \sinh^2 \gamma)$ is the warp factor that appears in the supergravity solution of the non-extremal M2-brane. The extremal solution can be obtained by taking the limit $\rho_H \rightarrow 0$ and $\gamma \rightarrow \infty$, with $\rho_H^6 \sinh^2 \gamma$ held fixed.

Appendix D

Related Special Functions

This appendix contains a list of some properties of Bessel functions, confluent hypergeometric functions and Gegenbauer polynomials used in this dissertation and integrals involving them. (D.10)-(D.12) are used in Section 2.4.1 while the rest are used in Chapter 3. These properties are mostly taken from [107] and the corresponding equation numbers are displayed in bold on the right side, e.g. **13.1.1** is the equation number for (D.1) in [107]. Section D.2 gives a special Heun equation, the solution for which is known in terms of confluent hypergeometric functions.

D.1 Generalized Confluent Hypergeometric Equation

The confluent hypergeometric function $\mathcal{U}(a, b, z)$ satisfies the differential equation is

$$\mathbf{13.1.1} \quad z \frac{d^2}{dz^2} \mathcal{U}(a, b, z) + (b - z) \frac{d}{dz} \mathcal{U}(a, b, z) - a \mathcal{U}(a, b, z) = 0. \quad (\text{D.1})$$

The generalized confluent hypergeometric equation is

$$\mathbf{13.1.35} \quad 0 = y'' + \left[\frac{2A}{x} + 2f' + \frac{bg'}{g} - g' - \frac{g''}{g} \right] y' + \left\{ \left[\frac{bg'}{g} - g' - \frac{g''}{g} \right] \left[\frac{A}{x} + f' \right] + \frac{A(A-1)}{x^2} + \frac{2Af'}{x} + f'' + (f')^2 - \alpha \frac{(g')^2}{g} \right\} y, \quad (\text{D.2})$$

where α , A and b are constants, y , f and h are functions of x and (\prime) denotes derivative with respect to x . The two linearly independent solutions are

$$13.1.36 \quad y_1 = x^{-A} e^{-f(x)} F_1(\alpha; b; g(x)), \quad (D.3)$$

$$13.1.37 \quad y_2 = x^{-A} e^{-f(x)} \mathcal{U}(\alpha, b, g(x)). \quad (D.4)$$

For the following values

$$x = r; \quad y(x) = h(p, r); \quad A = 0; \quad b = 2; \quad f = pr; \quad g = 2pr; \quad \alpha = 1 + \frac{p\mu_0}{2}, \quad (D.5)$$

one recovers (3.13). Hence, the solution in closed form for $h(p, r)$, which decays at large r is

$$h(p, r) \propto e^{-pr} \mathcal{U}\left(1 + \frac{p\mu_0}{2}, 2, 2pr\right), \quad (D.6)$$

where $\mathcal{U}(a, b, z)$ is the confluent hypergeometric function.

D.2 A Special Confluent Heun Equation

A Heun equation has 4 regular poles, where as the hypergeometric equations have 3. An analytic solution to the Heun equation is generally difficult to construct. However, there are a few special cases in which the solution involves the known special functions. (3.63) can be converted to the a confluent Heun equation whose solution in terms of confluent hypergeometric functions is known [115]. This Heun equation is

$$y'' = \left(\lambda^2 + \frac{2(\sigma - 1)\lambda^2 - \tau\lambda + 1/2}{x} + \frac{\tau\lambda - 1/2}{x - 1} + \frac{(\tau^2 - 2\sigma + 1)\lambda^2 - 1/4}{x^2} + \frac{3/4}{(x - 1)^2} \right) y, \quad (D.7)$$

The solution to this equation is given by

$$\begin{aligned}
y &= \frac{1}{\sqrt{x-1}} [c_1 \{ \lambda(\tau + \sigma)M_{\alpha,\beta}(2\lambda x) + ((1-\sigma)\lambda - \beta)M_{\alpha-1,\beta}(2\lambda x) \} \\
&\quad + c_2 \{ W_{\alpha,\beta}(2\lambda x) + \lambda(\tau - \sigma)W_{\alpha-1,\beta}(2\lambda x) \}], \\
&= \frac{e^{-\lambda x}(2\lambda x)^{\frac{1}{2}+\beta}}{\sqrt{x-1}} \left[c_1 \left\{ \lambda(\tau + \sigma)M \left(\frac{1}{2} + \beta - \alpha, 1 + 2\beta, 2\lambda x \right) \right. \right. \\
&\quad \left. \left. + ((1-\sigma)\lambda - \beta)M \left(\frac{3}{2} + \beta - \alpha, 1 + 2\beta, 2\lambda x \right) \right\} \right. \\
&\quad \left. + c_2 \left\{ \mathcal{U} \left(\frac{1}{2} + \beta - \alpha, 1 + 2\beta, 2\lambda x \right) \right. \right. \\
&\quad \left. \left. + \lambda(\tau - \sigma)\mathcal{U} \left(\frac{3}{2} + \beta - \alpha, 1 + 2\beta, 2\lambda x \right) \right\} \right], \tag{D.8}
\end{aligned}$$

where in the second equality I have used (D.19) and

$$\alpha = \frac{1}{2} + (1 - \sigma)\lambda, \quad \beta = \sqrt{1 - 2\sigma + \tau^2}\lambda. \tag{D.9}$$

D.3 Some Properties of Special Functions

$$\mathbf{22.7.21} \quad 2\alpha(1-x^2)C_{n-1}^{\alpha+1}(x) = (2\alpha+n-1)C_{n-1}^{\alpha}(x) - nx C_n^{\alpha}(x) \tag{D.10}$$

$$\mathbf{22.7.22} \quad = (n+2\alpha)x C_n^{\alpha}(x) - (n+1)C_{n+1}^{\alpha}(x) \tag{D.11}$$

$$\mathbf{22.2.3} \quad \int_{-1}^1 dx (1-x^2)^{\alpha-\frac{1}{2}} [C_n^{\alpha}(x)]^2 = \frac{\pi 2^{1-2\alpha} \Gamma(n+2\alpha)}{n!(n+\alpha) [\Gamma(\alpha)]^2}. \tag{D.12}$$

$$\mathbf{13.6.29} \quad \mathcal{U}(\nu + \frac{1}{2}, 2\nu + 1; 2z) = \frac{e^z}{\sqrt{\pi}(2z)^{\nu}} K_{\nu}(z) \tag{D.13}$$

$$\mathcal{U}(1, 2; 2z) = \frac{e^z}{\sqrt{\pi}(2z)^{\frac{1}{2}}} K_{\frac{1}{2}}(z) = \frac{1}{2z} \tag{D.14}$$

$$\mathbf{13.1.8} \quad \mathcal{U}(a, b; z) = z^{-a} (1 + O(1/|z|)), \quad \text{Re } z \rightarrow \infty \tag{D.15}$$

$$\mathbf{13.3.3} \quad \lim_{a \rightarrow \infty} \Gamma(1+a-b)\mathcal{U}(a, b; z/a) = 2z^{\frac{1-b}{2}} K_{b-1}(2\sqrt{z}) \tag{D.16}$$

$$\partial_y \left(\frac{J_1(py)}{y} \right) = -\frac{p}{y} J_2(py) \quad (\text{D.17})$$

$$9.1.27 \quad J_{n-1}(x) + J_{n+1}(x) = \frac{2n}{x} J_n(x). \quad (\text{D.18})$$

The Whittaker function $W_{\kappa,\mu}(z)$ is related to the confluent hypergeometric function by

$$13.1.33 \quad W_{\kappa,\mu}(z) = e^{-z/2} z^{1/2+\mu} \mathcal{U}(1/2 + \mu - \kappa, 1 + 2\mu, z) \quad (\text{D.19})$$

D.4 Useful Integrals

The Bessel function can be defined as

$$9.1.21 \quad J_n(z) = \frac{i^{-n}}{\pi} \int_0^\pi e^{iz \cos(\theta)} \cos(n\theta) d\theta. \quad (\text{D.20})$$

The area of a d -dimensional unit sphere is

$$\text{Vol}(S^d) = \int d\Omega_d = \frac{2\pi^{\frac{1}{2}(d+1)}}{\Gamma(\frac{1}{2}(d+1))}. \quad (\text{D.21})$$

Chapter 3 uses the integrals listed below, which have been computed using Mathematica 5. Section 3.3.2 uses

$$\int dx J_1(x)x^2 = x^2 J_2(x), \quad (\text{D.22})$$

$$\int dx J_2(x)x^3 = x^3 J_3(x). \quad (\text{D.23})$$

Section 3.3.4 uses

$$\int_0^\infty dp p^3 J_1(py) K_1(pz) = \frac{8yz}{(y^2 + z^2)^3}, \quad (\text{D.24})$$

$$\int_0^\infty dp p^2 J_2(py) K_1(pz) = \frac{2y^2}{z(y^2 + z^2)^2}, \quad (\text{D.25})$$

$$\int_0^\infty dp p^4 J_2(py) K_1(pz) = \frac{48y^2 z}{(y^2 + z^2)^4}, \quad (\text{D.26})$$

$$\int_0^\infty dp p^3 J_3(py) K_1(pz) = \frac{8y^3}{z(y^2 + z^2)^3}. \quad (\text{D.27})$$

Section 3.3.5 uses

$$\int_0^\infty dp p^2 J_1(py) e^{-pr} = \frac{3yr}{(y^2 + r^2)^{\frac{5}{2}}}, \quad (\text{D.28})$$

$$\int_0^\infty dp p^3 J_2(py) e^{-pr} = \frac{15y^2 r}{(y^2 + r^2)^{\frac{7}{2}}}, \quad (\text{D.29})$$

$$\int_0^\infty dp p J_2(py) e^{-pr} = -\frac{2r^3 + 3ry^2}{y^2(y^2 + r^2)^{3/2}} + \frac{2}{y^2}, \quad (\text{D.30})$$

$$\int_0^\infty dp p^2 J_3(py) e^{-pr} = -\frac{r(8r^4 + 20r^2 y^2 + 15y^4)}{y^3(y^2 + r^2)^{5/2}} + \frac{8}{y^3}. \quad (\text{D.31})$$

Appendix E

Aspects of Seiberg Duality

This appendix contains a discussion of Seiberg duality with the view towards understanding duality cascades for the gauge theory dual to the supergravity solutions involving $Y^{p,q}$ spaces in the presence of fractional branes, which is discussed in Chapter 4. Seiberg duality involves two supersymmetric gauge theories theories, with the same global symmetries but different gauge groups. The discussion will only involve what is called the conformal window.

This appendix is organized as follows: I first discuss the interacting conformal fixed point for supersymmetric quantum chromodynamics (SQCD) with N_f flavors, establishing the conformal window. I then describe the Seiberg dual to SQCD, which will be called SQCD+M. This is followed by a discussion of when Seiberg duality may be considered as an exact duality. After this I add quartic operators and discuss how they modify the discussion of the duality. In the end, I specialize/generalize some aspects of the discussion to obtain the gauge theory dual of $AdS_5 \times T^{1,1}$ and devote some space to discussing the duality cascade in this theory. This discussion relies heavily on the discussions in the lecture notes by M. Strassler [157] and P. Argyres [158].

E.1 SQCD and Seiberg Duality

Supersymmetric quantum chromodynamics or SQCD is a supersymmetric $SU(N)$ Yang-Mills theory with chiral matter Q^r and \tilde{Q}_u (gauge indices are suppressed, r and

u are flavor indices and the flavor group is described below). The lagrangian can be written, using superspace notation [158] as

$$\mathcal{L} = \int d^4\theta \left(\bar{Q}_r e^V Q^r + \bar{\tilde{Q}}^u e^{-V} \tilde{Q}_u \right) + \int d^2\theta \left(\frac{\tau}{32\pi i} \text{tr} W^2 + \mathcal{W}(Q, \tilde{Q}) \right) + h.c., \quad (\text{E.1})$$

where the first integral gives the non-holomorphic Kaehler terms and $h.c.$ denotes the hermitian conjugate of the second integral, which is holomorphic. Here V is a real vector superfield and $e^{\pm V}$ gives the gauge covariant derivatives in the kinetic terms of the chiral matter; $\int d^2\theta \text{tr} W^2$ gives rise to the gauge kinetic terms, where W_α is a chiral superfield which is related to the real vector superfield V by $4W_\alpha = -\bar{D}^2 D_\alpha V$ (D_α is the supersymmetric covariant derivative), $\tau \equiv \frac{1}{2\pi} \left[\vartheta + i \frac{8\pi^2}{g^2} \right]$ is the holomorphic gauge coupling and \mathcal{W} is the superpotential term. Initially I will set the superpotential $\mathcal{W} = 0$. The global symmetries are $SU(N_f)_L \times SU(N_f)_R \times U(1)_B \times U(1)_R$, where N_f is the number of flavors and the subscripts B and R on the $U(1)$ factors refer to the baryon number symmetry and the R symmetry respectively. The theory has composite meson fields, $M_u^r = Q_a^r \tilde{Q}_u^a$, where a is a gauge index. For $N_f > N$, the theory also contains two types of baryons, formed by anti-symmetrizing the gauge indices of Q^r and \tilde{Q}_u , which we will denote by B and \tilde{B} . Table E.1 summarizes the information about the various representations.

Table E.1: Assignment of Representations and Charges in SQCD

	$SU(N)$	$SU(N_f)_L$	$SU(N_f)_R$	$U(1)_B$	$U(1)_R$
Q	\mathbf{N}	\mathbf{N}_f	$\mathbf{1}$	1	$1 - \frac{N}{N_f}$
\tilde{Q}	$\bar{\mathbf{N}}$	$\mathbf{1}$	$\bar{\mathbf{N}}_f$	-1	$1 - \frac{N}{N_f}$

The β -function for the gauge coupling g can be written down using the Norikov-Shifman-Vainshtein-Zakharov (NSVZ) β -function [159, 160, 161]

$$\beta_{\frac{8\pi^2}{g^2}} = \frac{b_0 + \frac{1}{2} \sum_i T(R_i) \gamma_i}{1 - g^2 N / 8\pi^2} = -\frac{16\pi^2}{g^3} \beta_g, \quad (\text{E.2})$$

where the index i runs over all the chiral superfields appearing in the theory, $b_0 =$

$\frac{3}{2}T(adj) - \frac{1}{2}\sum_i T(R_i)$ is the contribution at one loop and γ 's are the anomalous dimensions that come in via wave function renormalization from the Kaehler terms. For $SU(N)$ SQCD, $b_0 = 3N - N_f$ and there is enough symmetry that all the chiral fields have the same anomalous dimension, which will be called γ_0 . Thus

$$\beta_g = -\frac{g^3}{16\pi^2} \frac{3N - N_f(1 - \gamma_0)}{1 - g^2 N/8\pi^2}, \quad (\text{E.3})$$

The non-renormalization theorems guarantee that the β -function receives no contributions from the superpotential terms. Hence even with a non-zero \mathcal{W} , the β -function given above remains valid.

When $N_f \geq 3N$, the β -function in (E.3) is positive and the theory flows to a free gauge theory in the infra-red (IR). This can be seen by noting that when $g = 0$ then $\gamma_0 = 0$, so for $g \ll 1$, it must be true that γ_0 is small and is given by

$$\gamma_0 = -\frac{g^2}{8\pi^2} \frac{N^2 - 1}{N} + O(g^4) \quad (\text{E.4})$$

which is actually negative when $g \ll 1$. SQCD also has a fixed point when $N, N_f \gg 1$ and $3N - N_f \ll N$. In this case, (E.4) gives $\gamma_0 = -cg^2 N + O(g^2 N)^2$, where c is a positive number of order 1. Then the β -function vanishes when

$$g = g_* = \sqrt{\frac{b_0}{3c}} \frac{1}{N}. \quad (\text{E.5})$$

This two loop fixed point, shown in Figure E-1, is called the Banks-Zaks fixed point. In the large N limit, the appropriate coupling to consider is the 't Hooft coupling $\lambda = g^2 N$ which at this fixed point goes like $\lambda_* \sim N^{-1}$ and is small for large N . Thus this fixed point persists to all orders in perturbation theory for large N . Although I have shown here the existence of the fixed point for N_f very close to $3N$, there is an unproven suggestion of Seiberg that such a fixed point persists in the range $\frac{3}{2}N < N_f < 3N$. To make some sense of this, let's look at the mesons $M_u^r = (Q^r \tilde{Q}_u)$ (the gauge indices are contracted), which contains some important information. It is a gauge-invariant, spin zero, chiral operator. Hence by properties of the superconformal

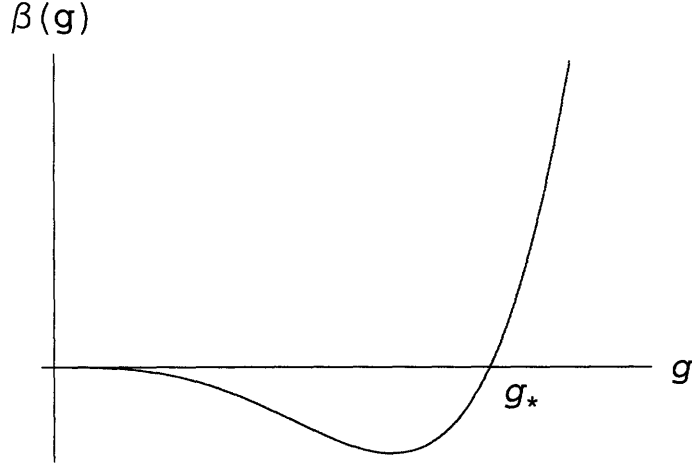


Figure E-1: The beta function and the IR conformal fixed point $g = g_*$ of SQCD when N_f is very close to but less than $3N$, with $N, N_f \gg 1$.

algebra, the dimension $D(M)$ and the R -charge $R(M)$ are related by

$$D(M) = \frac{3}{2}R(M). \quad (\text{E.6})$$

The definition of the R -charge in this discussion for M is completely unambiguous because M has charge zero under baryon-number current (refer to Table E.1), which could otherwise be combined with the R -current to give a different value for the R -charge for fields with non-zero baryon number. For $N_f \geq 3N$, we have a free gauge theory, which means $D(M) = 2$. If there is a fixed point, $D(M) = 3(1 - N/N_f)$, which gives $D(M) = 1$ when $N_f = \frac{3}{2}N$ and $D(M) \leq 1$ when $N_f \leq \frac{3}{2}N$. Now $D(M) = 1$ means that it is a free field. Further, from superconformal representation theory, $D(M) < 1$ is not allowed as it violates unitarity. (The highest weight representation will have a negative norm state.) Hence, $D(M) = 1$ and there cannot be a superconformal fixed point when $N_f < \frac{3}{2}N$. These values of $D(M)$ are summarized in Figure E-2. As $D(M) = 1$, this means that in the Seiberg dual description the mesons and consequently the theory must be free. Because the global symmetries remain the same the dual theory must have $3\tilde{N} < N_f$ when $N_f \leq \frac{3}{2}N$. This constraint is satisfied by the choice $\tilde{N} = N_f - N$.

The other theory has gauge group $SU(\tilde{N})$ ($\tilde{N} \equiv N_f - N$) and the same global

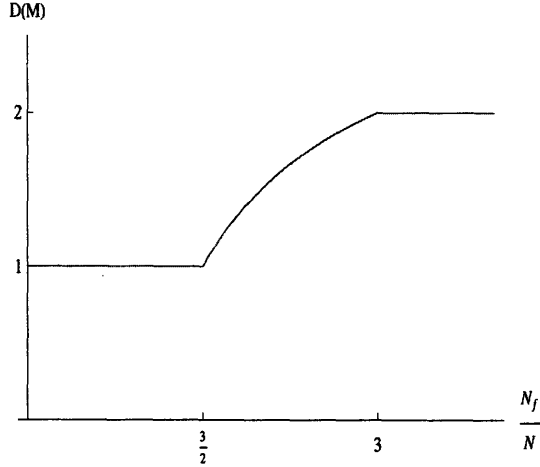


Figure E-2: The dimension of M , $D(M)$, is 2 in an IR free gauge theory ($N_f > 3N$), is bounded from below by unitarity and in the conformal window is proportional to the sum of the R -charges of q and \tilde{q} .

symmetries as SQCD. This theory has chiral fields q_r and \tilde{q}^u and M_u^r , which transform as $(\overline{\mathbf{N}}_f, 1)$, $(1, \mathbf{N}_f)$ and $(\mathbf{N}_f, \overline{\mathbf{N}}_f)$ under $SU(N_f)_L \times SU(N_f)_R$. The field M_u^r is uncharged under the baryon number symmetry of the theory. This theory also has a non-zero cubic superpotential, which preserves all the global symmetries and is given by

$$\mathcal{W} = y M_u^r q_r \tilde{q}^u. \quad (\text{E.7})$$

I will call this theory SQCD+M¹. Note that when SQCD is in the conformal window, so is SQCD+M, ie $\frac{3}{2}\tilde{N} < N_f < 3\tilde{N}$. Table E.1 gives a summary of charges of the microscopic fields of SQCD+M.

Table E.2: Assignment of Representations and Charges in SQCD+M

	$SU(\tilde{N})$	$SU(N_f)_L$	$SU(N_f)_R$	$U(1)_B$	$U(1)_R$
q	$\tilde{\mathbf{N}}$	$\overline{\mathbf{N}}_f$	$\mathbf{1}$	N/\tilde{N}	$1 - \frac{\tilde{N}}{N_f}$
\tilde{q}	$\overline{\tilde{\mathbf{N}}}$	$\mathbf{1}$	\mathbf{N}_f	$-N/\tilde{N}$	$1 - \frac{\tilde{N}}{N_f}$
M_u^r	$\mathbf{1}$	\mathbf{N}_f	$\overline{\mathbf{N}}_f$	0	$2\frac{\tilde{N}}{N_f}$

¹This nomenclature is not standard, but is used in the lecture notes by M. Strassler [157]

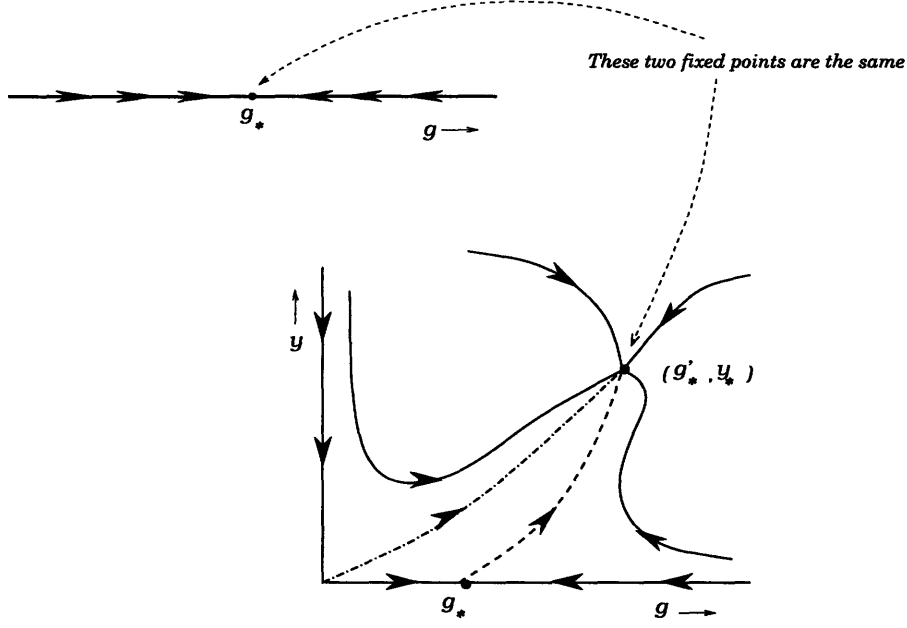


Figure E-3: According to Seiberg duality, the fixed point g_* of SQCD (top panel) is identical to the fixed point (g'_*, y_*) of SQCD+M (bottom panel) in the IR. Although the symbol g is used for the gauge coupling in both SQCD and SQCD+M, they are couplings of different gauge groups with generically different values.

If the superpotential vanishes, then I again have just SQCD, with some free gauge singlets M_u^r . There will then be a Banks-Zaks fixed point and $D(M) = 1$ which at the fixed point gives $R(M) = 2/3$. On turning on \mathcal{W} with $y \ll 1$, $D(M) = 1 + O(y^2)$, which is inconsistent with $R(M) = 2\frac{\tilde{N}}{N_f}$. So the coupling must flow away from the fixed point at $y = 0$. As a check of this claim, let's look at the β -function of y around $y = 0$, $g = g_*$. Using $D(M) = 1 + \frac{1}{2}\gamma_M$ and $D(q) = 1 + \frac{1}{2}\gamma_0$ the β -function, up to order y^2 corrections, is

$$\begin{aligned} \beta_y &= \frac{1}{2}y(\gamma_M + 2\gamma_0) = -y(3 - D(M) - D(q\tilde{q})) \\ &= -y \left(3 - 1 - 3 \left[1 - \frac{\tilde{N}}{N_f} \right] \right) = y \left(1 - \frac{\tilde{N}}{N_f} \right), \end{aligned} \quad (\text{E.8})$$

where in the third equality, I have used $D(M) = 1$ and $R(q\tilde{q}) = 2R(q) = \frac{2}{3}D(q\tilde{q})$. Hence, the coupling does indeed flow away to another fixed point (g'_*, y_*) . As a further check of consistency, the R -symmetries assigned in Table E.1 give $\beta_g = \beta_y = 0$.

SQCD+M contains baryons, which are identified under the duality with the baryons in SQCD. The gauge invariant operator M_u^r is identified with the composite meson $Q^r \tilde{Q}_u$. However, because of the superpotential, the composite meson $q_r \tilde{q}^u$ is not part of the vacuum of the theory (the F-term constraints set its expectation value to zero). The Seiberg dual fixed points g_* of SQCD and (g', y_*) of SQCD+M in the IR are shown in Figure E-3.

E.2 Quartic Operators and Seiberg Duality

This section contains a discussion of quartic terms in the superpotential. These terms not only illustrate important concepts involved in discussing whether a coupling is relevant or irrelevant, but are also present in the gauge theory dual to type IIB supergravity solution on $AdS_5 \times T^{1,1}$ discussed in Section 4.2.

Consider a theory called theory A, which is obtained by adding to SQCD the superpotential

$$\mathcal{W} = h(Q^r \tilde{Q}_u)(Q_r \tilde{Q}^u) \equiv \frac{\eta}{\mu}(Q^r \tilde{Q}_u)(Q_r \tilde{Q}^u), \quad (\text{E.9})$$

where the brackets indicate gauge contractions (indices are raised and lowered with the Kronecker delta functions $\delta_{r'}^r, \delta_s^s$) and in the second equality the dimensionless coupling $\eta \equiv h\mu$ is defined, where μ is the scale of the theory. This superpotential breaks the global $SU(N_f)_L \times SU(N_f)_R$ down to a diagonal $SU(N_f)$. The coupling h has mass dimension -1 , which makes it classically irrelevant. So quantum mechanically is the coupling relevant or irrelevant? To examine this consider the following properties of the anomalous dimension γ_0 that we know of: (a) If $g = 0$, $\eta \neq 0$, then $\gamma_0 > 0$ (I will not use this in the following discussion), (b) if $\eta \neq 0$ and the gauge coupling is small but non-zero, then $\gamma_0 < 0$ and (c) in the conformal window, there exists a non-trivial conformal fixed point at $(g, \eta) = (g_*, 0)$ where $\gamma_0 = 2(D(Q) - 1) = 3R(Q) - 2 = 1 - 3\frac{N}{N_f}$. The β -functions of the quartic and gauge

couplings are

$$\beta_\eta = \eta \left[1 + \frac{1}{2}(4\gamma_0) \right] = \eta(1 + 2\gamma_0) = 3\eta \left(1 - 2\frac{N}{N_f} \right) \quad (\text{E.10})$$

$$\beta_g \propto -[3N - N_f + N_f\gamma_0] = 0, \quad (\text{E.11})$$

where the last equality for β_η and β_g is true only in the conformal window. This shows that η is irrelevant when $N_f > 2N$, relevant when $N_f < 2N$, and is marginal when $N_f = 2N$ with $\gamma_0 = -\frac{1}{2}$. This last case will be discussed in Section E.4.

In the dual description (theory B), (E.9) corresponds to adding a mass term for M_u^r . The superpotential is now given by

$$\mathcal{W} = yM_u^r q_r \tilde{q}^u + \hat{h}M_u^r M_r^u = yM_u^r q_r \tilde{q}^u + \hat{\eta}\mu M_u^r M_r^u, \quad (\text{E.12})$$

where, in the second equality, $\hat{\eta} \equiv \hat{h}/\mu$ is the dimensionless coupling corresponding to the mass \hat{h} . The equation of motion for M_u^r can be used to integrate it out, which in the IR is just $yq_r \tilde{q}^u + \hat{h}M_r^u = 0$ in the IR (where I can ignore the acceleration term). This gives

$$\mathcal{W} \longrightarrow \mathcal{W}_L = -\frac{y^2}{4\hat{h}}(q^r \tilde{q}_u)(q_r \tilde{q}^u) = \tilde{h}(q^r \tilde{q}_u)(q_r \tilde{q}^u) = \frac{\tilde{\eta}}{\mu}(q^r \tilde{q}_u)(q_r \tilde{q}^u). \quad (\text{E.13})$$

This has the same form as the superpotential in theory A with $\tilde{h} \equiv -y^2/4\hat{h}$ and $\tilde{\eta} \equiv \mu\tilde{h}$ giving the corresponding dimensionless coupling.

Now let's see if this makes sense. Classically, both η and $\tilde{\eta}$ are irrelevant, which in the latter case follows from the fact that $\hat{\eta}$ is relevant. This means that in the IR both theory A and theory B are SQCD with gauge groups $SU(N)$ in one description and $SU(\tilde{N})$ in the other description. This clearly does not make sense when $N_f \neq 2N$. However, quantum corrections resolve this contradiction as I will now discuss. To see this, first consider the case when $3N > N_f > 2N$. Then in theory B, $\frac{3}{2}\tilde{N} < N_f < 2\tilde{N}$. The β -function in (E.10) shows that η is irrelevant, but $\tilde{\eta}$ is relevant (which has the same β -function with N replaced by \tilde{N}). $\tilde{\eta}$ is a dangerously irrelevant coupling. This

means that $\hat{\eta}$ is irrelevant (whereas it was classically relevant), so in the IR, theory A flows to SQCD and theory B flows to SQCD+M. Hence both theories flow to the same IR fixed point.

It is useful to work out the other case also, which is when $2N > N_f > \frac{3}{2}N$ and $2\tilde{N} < N_f < 3\tilde{N}$. In this case, the quartic coupling η in theory A is relevant, as well as the mass term in theory B (as $\tilde{\eta}$ is irrelevant). As the mass term in theory B grows the mesons can be integrated out, which leaves us with $SU(\tilde{N})$ SQCD at the IR fixed point. In theory A, on the other hand, where there are no mesons to begin with, one can understand how the duality operates by introducing auxiliary fields \mathcal{M}_r^u [143] and re-writing the superpotential as

$$\mathcal{W} = \hat{y}\mathcal{M}_r^u Q^r \tilde{Q}_u + m\mathcal{M}_r^u \mathcal{M}_u^r. \quad (\text{E.14})$$

On integrating out \mathcal{M}_r^u , one obtains the quartic potential (E.9) in theory A, with the relationship $h = -\hat{y}^2/2m$. In the range $2N > N_f > \frac{3}{2}N$, h is relevant, which makes m an irrelevant coupling. Hence in the IR, we get mesons \mathcal{M} . This means that theory A flows to SQCD+M with gauge group $SU(N)$.

E.3 When is Seiberg Duality Exact?

This section will argue that Seiberg duality extends beyond just a duality between two theories at an IR fixed point.

To understand this better, first let's ignore the quartic term in the superpotentials and instead add a superpotential

$$\mathcal{W} = mQ^1 \tilde{Q}_1 \quad (\text{E.15})$$

to theory A, which without the quartic coupling is just SQCD. This superpotential breaks the flavor group, $SU(N_f) \rightarrow SU(N_f - 1)$ by removing a quark flavor at scales below m .

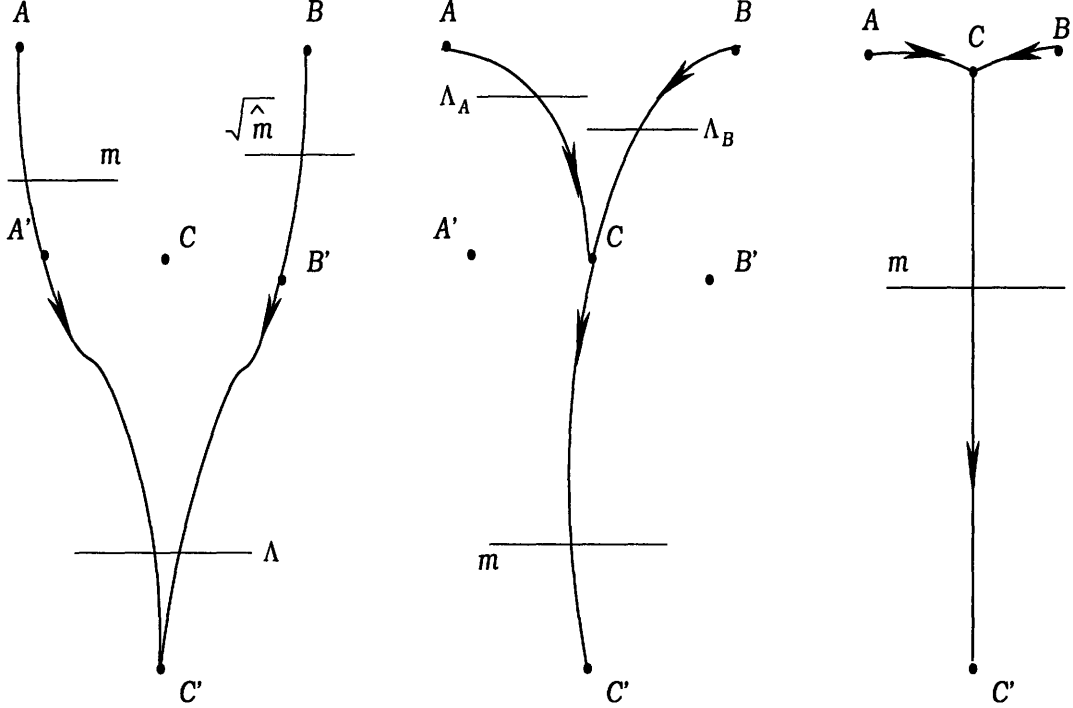


Figure E-4: Seiberg duality can be extended beyond just a duality at a single conformal fixed point in IR by taking the scales $\Lambda_A, \Lambda_B \gg m \sim \sqrt{\hat{m}}$.

In the dual description, this corresponds to modifying the superpotential to

$$\mathcal{W} = yqM\tilde{q} + \hat{m}M_1^1. \quad (\text{E.16})$$

The F-term conditions give $\langle q_1\tilde{q}^1 \rangle \neq 0$, which reduces both the flavor and gauge symmetries by one i.e. $\tilde{N} \rightarrow \tilde{N} - 1$ and $N_f \rightarrow N_f - 1$. Call this theory B'. Note that it is Seiberg dual to A' in the IR as they will both flow to a Banks-Zaks fixed point C'.

If $m > \Lambda_A$, the strong coupling scale of theory A, then the theory flows as $A \rightarrow A' \rightarrow C'$, where C' is the conformal fixed point of A' and B'. But if $m < \Lambda_A$, then $A \rightarrow C \rightarrow C'$. Similarly, if $\sqrt{\hat{m}} > \Lambda_B$, the strong coupling scale of theory B, then $B \rightarrow B' \rightarrow C'$, while on the other hand if $\sqrt{\hat{m}} < \Lambda_B$, then $B \rightarrow C \rightarrow C'$. Now keeping $m \sim \sqrt{\hat{m}} \ll \Lambda_A, \Lambda_B$ and sending Λ_A, Λ_B to infinity, gives the non-trivial result that the theories A and B have a dual description all along the flow from theory C to C'. These various possibilities are discussed in Figure E-4.

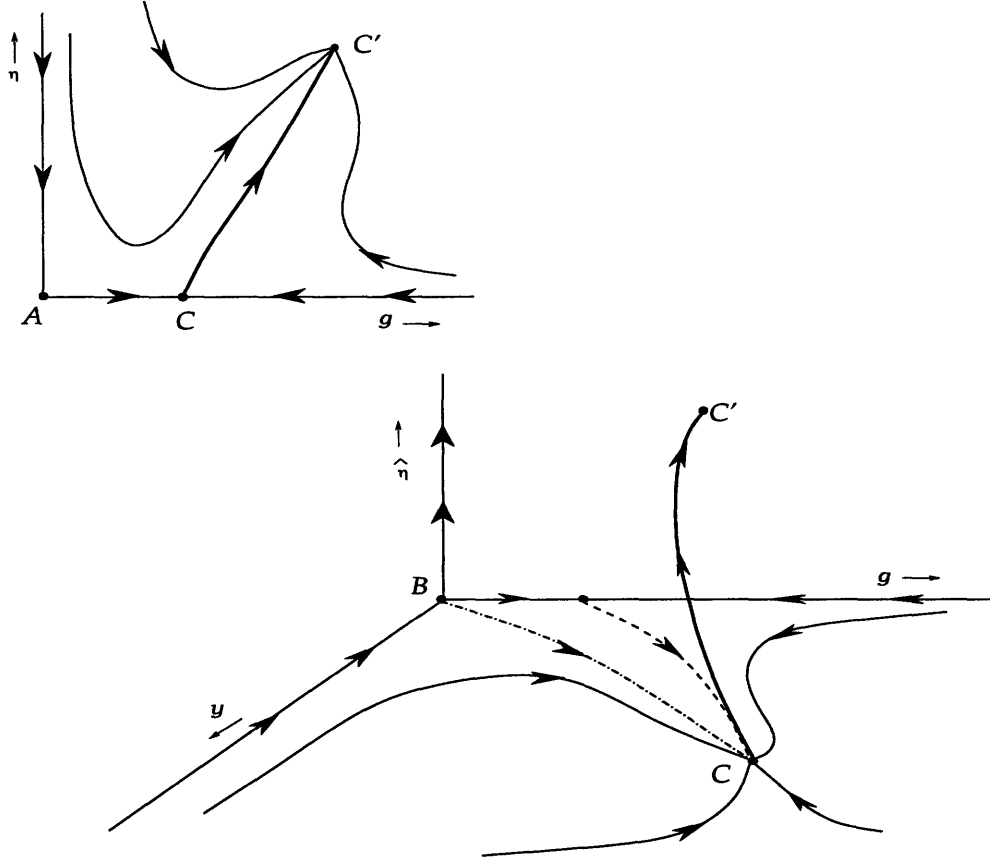


Figure E-5: This figure shows the flows of couplings in the presence of a quartic superpotential in SQCD in the range $\frac{3}{2}N < N_f < 2N$. The point C in the top panel is SQCD with N colors and N_f flavors. This theory is Seiberg dual to the point C in the bottom panel which is SQCD+M with \tilde{N} colors and N_f flavors. The duality holds everywhere along the flow from C to C' . Notice that the horizontal axis/plane is just Figure E-3.

This whole discussion generalizes in the presence of quartic couplings. The discussion for $2N < N_f < 3N$ is straightforward with the coupling η irrelevant classically and quantum mechanically. When $\frac{3}{2}N < N_f < 2N$, the situation is more complicated and the flow of couplings is shown in Figure E-5. In the top panel the Seiberg fixed point C has a quartic superpotential whose coupling η is relevant in the IR. If η is initially small, SQCD flows from a free theory A to a Seiberg fixed point C (where η is small) to C' , where $\eta = \infty$. As discussed in Section E.2, one integrates in mesons \mathcal{M} , giving us at the IR fixed point C' SQCD+M with N colors and N_f flavors. At point B , which corresponds to SQCD+M with massless mesons, even a small meson

mass term is relevant and then B flows to C. In the IR, as the mass gets large the mesons can be integrated out, giving us a quartic superpotential in the IR with an irrelevant coupling, $\tilde{\eta}$. Hence SQCD+M will start with a small mass term flowing from a free theory at B to the same fixed point C where $\tilde{\eta}$ is large (small mass term), to C' where $\tilde{\eta} \rightarrow 0$ and $\hat{\eta} \rightarrow \infty$. In these dual variables, C' is SQCD with \tilde{N} colors and N_f flavors.

E.4 $N_f = 2N$ and Exactly Marginal Operators

When $N_f = 2N$, the two β -functions are proportional to each other,

$$\beta_\eta = \eta(1 + 2\gamma_0); \quad \beta_g \propto -[3N - 2N(1 - \gamma_0)] = N(1 + 2\gamma_0), \quad (\text{E.17})$$

and there is a conformal fixed point when $\gamma_0 = -\frac{1}{2}$. As γ_0 is a function of two couplings, such a solution will generically be a one complex dimensional space of solutions. As there is a fixed point g_* when $h = 0$, then we expect that $\gamma_0(g_*, h = 0) = -\frac{1}{2}$. Further, the existence of such a IR fixed point means there is a continuous space of fixed points starting at $(g_*, 0)$. Call the coupling that parameterizes this space ρ . Here, a classically irrelevant, $(Q\tilde{Q}Q\tilde{Q})$, operator has been converted to an exactly marginal operator.

This appearance of a marginal operator in supersymmetric theories is by no means unique. Such operators also appear in $\mathcal{N} = 1$, $SU(N)$ with three adjoint chiral superfields, $\Phi_{1,2,3}$, with a superpotential $\mathcal{W} = \sqrt{2}y\text{tr}(\Phi_1[\Phi_2, \Phi_3])$. When $g = y$, this becomes $\mathcal{N} = 4$ SYM, which has an exactly marginal operator.

Now let's see what happens in the dual description which has a fixed point at $(\tilde{g}, y, \hat{\eta}) = (\tilde{g}_*, y_*, 0)$. The beta functions are

$$\beta_{\hat{\eta}} = \hat{\eta}(-1 + \gamma_M); \quad \beta_y = \frac{1}{2}y(\gamma_M + 2\gamma_0); \quad \beta_{\tilde{g}} \propto -N(1 + 2\gamma_0). \quad (\text{E.18})$$

The fixed point is given by $\gamma_M = -1$ and $\gamma_0 = -\frac{1}{2}$. There are now two constraints on three couplings, which again gives a one complex dimensional space of fixed points

starting of at the conformal fixed point. This is exactly what one would expect from Seiberg duality.

E.5 Klebanov-Witten Theory and Seiberg Duality

In this section, I will discuss how the gauge theory dual to $AdS_5 \times T^{1,1}$, which is mentioned in Section 4.2, can be obtained from SQCD with $N_f = 2N$. In this case $\tilde{N} = N$. In the presence of the quartic superpotential, the global symmetries are $SU(2N) \times U(1)_B \times U(1)_R$. The fundamental representation of $SU(2N)$ can be written as $2N = N \otimes 2$. Upon gauging the N , we are left with a global $SU(2)$ and the dual quarks decompose as $q_r \equiv q_{r',\alpha}$, where $r' = 1, \dots, N$ and α is an $SU(2)$ index. The superpotential, after integrating out the mesons becomes $\mathcal{W} = \tilde{h}(q^{r',\alpha} \tilde{q}_{u',\beta})(q_{r',\alpha} \tilde{q}^{u',\beta})$. From here on, drop the primes on the indices and call $q_{r,\alpha}^a \equiv (A_\alpha)_r^a$ and $\tilde{q}_a^{r,\alpha} \equiv (B_\alpha)_a^r$. Note that it doesn't matter whether the $SU(2)$ index is a superscript or subscript as $\bar{2} = 2$.

The theory now is a $\mathcal{N} = 1$ SYM in $d = 4$ with gauge group $SU(N) \times SU(N)$ with two bi-fundamental chiral superfields A_α, B_α ($\alpha=1, 2$), with the A_α transforming in the (N, \bar{N}) and the B_α in (\bar{N}, N) . The superpotential is modified to

$$\mathcal{W} = h \text{Tr} \det_{\alpha,\beta} (A_\alpha B_\beta) = h \epsilon^{\alpha\beta} \epsilon^{\gamma\delta} \text{Tr} A_\alpha B_\gamma A_\beta B_\delta \quad (\text{E.19})$$

$$= h [(A_1)_r^a (B_1)_b^r (A_2)_s^b (B_2)_a^s - (A_1)_r^a (B_2)_b^r (A_2)_s^b (B_1)_a^s]. \quad (\text{E.20})$$

where a, b are indices in the first gauge group and r, s in the second one. This superpotential enhances the global symmetries to $SU(2) \times SU(2) \times U(1)$. The fields A_α transform as $(\mathbf{2}, \mathbf{0})$ and the fields B_α transform as $(\mathbf{0}, \mathbf{2})$ under this enhanced global $SU(2) \times SU(2)$.

The β -functions for the gauge and quartic couplings are

$$\beta_{g_i} = -\frac{g_i^3}{16\pi^2} \frac{N + 2N\gamma_0}{1 - g_i^2 N/8\pi^2}; \quad i = 1, 2 \quad (\text{E.21})$$

$$\beta_\eta = \eta(1 + 2\gamma_0). \quad (\text{E.22})$$

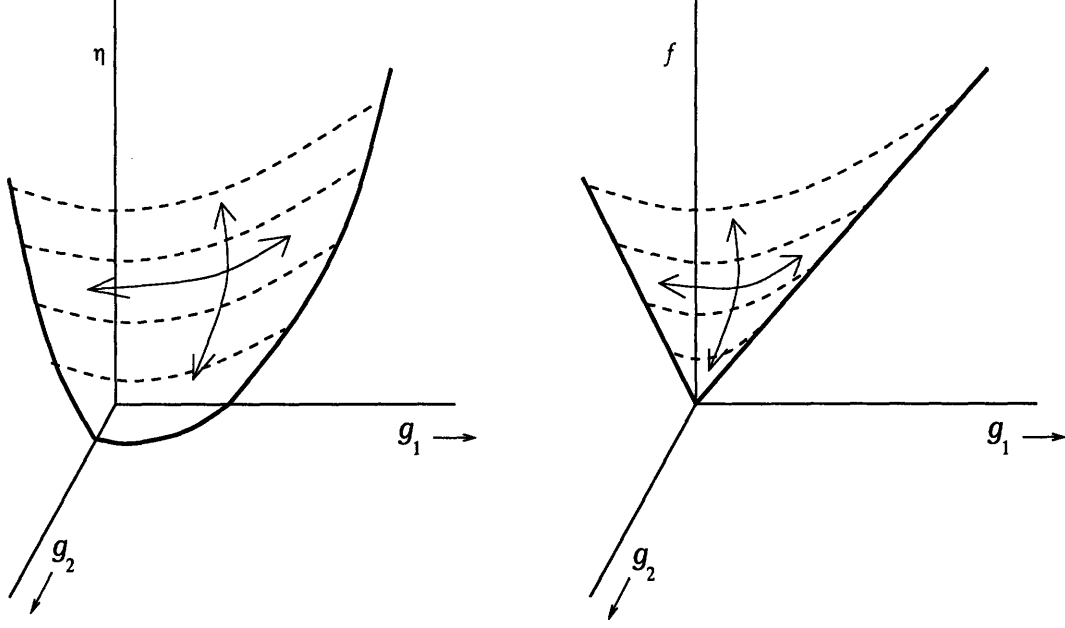


Figure E-6: The left hand panel shows the conformal surface in Klebanov-Witten and the right-hand panel shows the conformal surface in $\mathcal{N} = 2$ theory which can be thought of as the UV completion of Klebanov-Witten. The left right arrows are the action of Seiberg duality or $\tau_- \rightarrow \tau_- + 2\tau_+$ while the top bottom arrows indicate the action of $SL(2, \mathbb{Z})$ transformation.

As there are three couplings and only one constraint $\gamma_0(g_1, g_2, h) = -\frac{1}{2}$, this theory has a surface of conformal fixed points which is depicted in Figure E-6.

This surface of conformal fixed points must be symmetric under the exchange of the two gauge couplings. The manifold describing the conformal fixed points in the space of couplings can be described using two holomorphic co-ordinates ρ_+ and ρ_- which are symmetric and anti-symmetric under $g_1 \longleftrightarrow g_2$ respectively.

Much insight can be gained by understanding how this gauge theory can arise from an $\mathcal{N} = 2$ gauge theory with a mass deformation. This also settles the question of non-renormalizability of our gauge theory, which will have this $\mathcal{N} = 2$ gauge theory as its UV completion. On adding an adjoint chiral superfield in each of the gauge groups, Φ_1 and Φ_2 along with the superpotential

$$\mathcal{W} = f \text{tr} [A_\alpha \Phi_1 B^\alpha - A^\beta \Phi_2 B_\beta]. \quad (\text{E.23})$$

This term breaks the $SU(2) \times SU(2)$ to a single $SU(2)$. This theory is UV finite and has two holomorphic marginal couplings τ_+ and τ_- , created from the marginal couplings of the gauge groups $\tau_{1,2}$ by $\tau_{\pm} \equiv \tau_1 \pm \tau_2$. The manifold of conformal fixed points (which is determined by $\gamma_0 = 0$ and hence passes through the origin) is acted on by dualities $\tau_+ \rightarrow -1/\tau_+$ and $\tau_- \rightarrow \tau_- + 2\tau_+$. The first of these duality transformations corresponds to $SL(2, \mathbb{Z})$ and the second to exchanging g_1 and g_2 . These transformations are inherited by the conformal surface of the $\mathcal{N} = 1$ theory and are depicted in Figure E-6.

Note that in the dual description, we have the same theory, except the quartic coupling is inversely related to the original coupling.

E.6 Klebanov-Strassler Theory and the Duality Cascade

If the gauge group is modified from $SU(N) \times SU(N)$ of KW theory to $SU(N+M) \times SU(N)$, the theory is no longer conformal and is known as Klebanov-Strassler (KS) theory. But our above discussion still gives us a lot of insight when $N \gg M$, because then the theory is very close to being conformal. In particular, choose $N = (k-1)M$, then the gauge theory is $SU(kM) \times SU([k-1]M)$.

Let us denote the β -function for the gauge coupling g_p corresponding to the gauge group $SU(pM)$ by β_p and define

$$F(p) \equiv \frac{g_p^3}{16\pi^2} \frac{1}{1 - g_p^2(pM)} \quad \gamma_0 \equiv -\frac{1}{2} + \delta_0. \quad (\text{E.24})$$

The β -functions for $SU(kM) \times SU([k-1]M)$ are given by

$$\beta_k = -F(k)M(3 + 2(k-1)\delta_0), \quad \beta_{k-1} = -F(k-1)M(-3 + 2k\delta_0), \quad \beta_\eta = 2\eta\delta_0. \quad (\text{E.25})$$

When $k \gg 1$ the β -functions give the conformal surface of Klebanov-Witten (i.e.

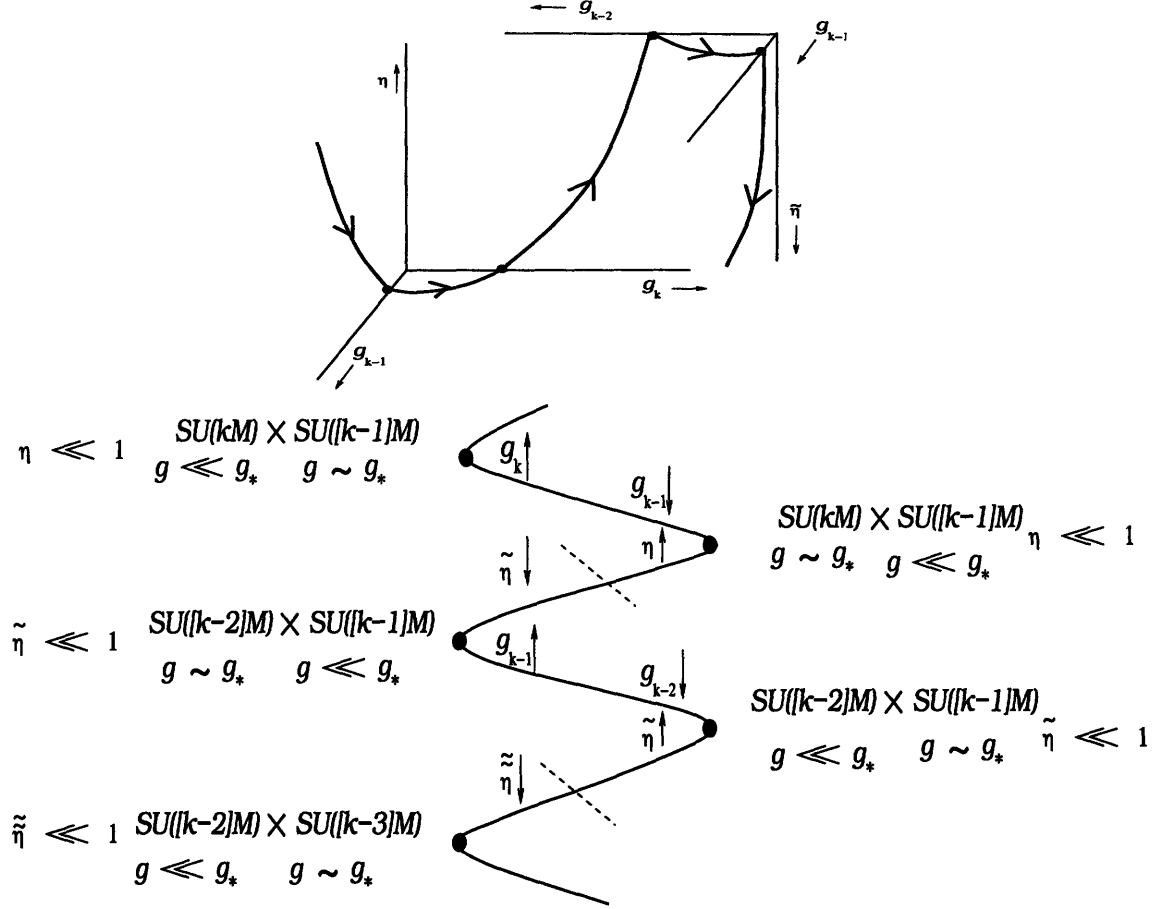


Figure E-7: The top panel shows the flow along the boundary of the conformal surface, with the Seiberg fixed points shown when one of the gauge couplings and the quartic coupling is zero. The flow connecting g_k to g_{k-2} indicates switching to the Seiberg dual description. The bottom panel shows the same flow with the vertical axes for the quartic couplings suppressed.

$\delta_0 = 0$), up to $\mathcal{O}(1/k)$ corrections. Hence there is a narrow region in the space of couplings where $\gamma_0 \approx -\frac{1}{2}$ and $|\delta_0| \ll 1$, which is infrared stable in the same sense as the Klebanov-Witten theory- i.e. all RG flows reach this region in the IR.

Although the theory no longer has a continuous surface of conformal fixed points, there are isolated fixed points, e.g. if $g_k = \eta = 0$, then the theory is $SU([k-1]M)$ SQCD with $2kM$ flavors, which lies in the conformal window when $k > 3$. Using the fact that $1 + \frac{1}{2}\gamma_0 = D(A) = \frac{3}{2}R(A) = \frac{3}{4}(1 + \frac{1}{k})$ gives $\delta_0 = \frac{3}{2k}$. Hence at this fixed

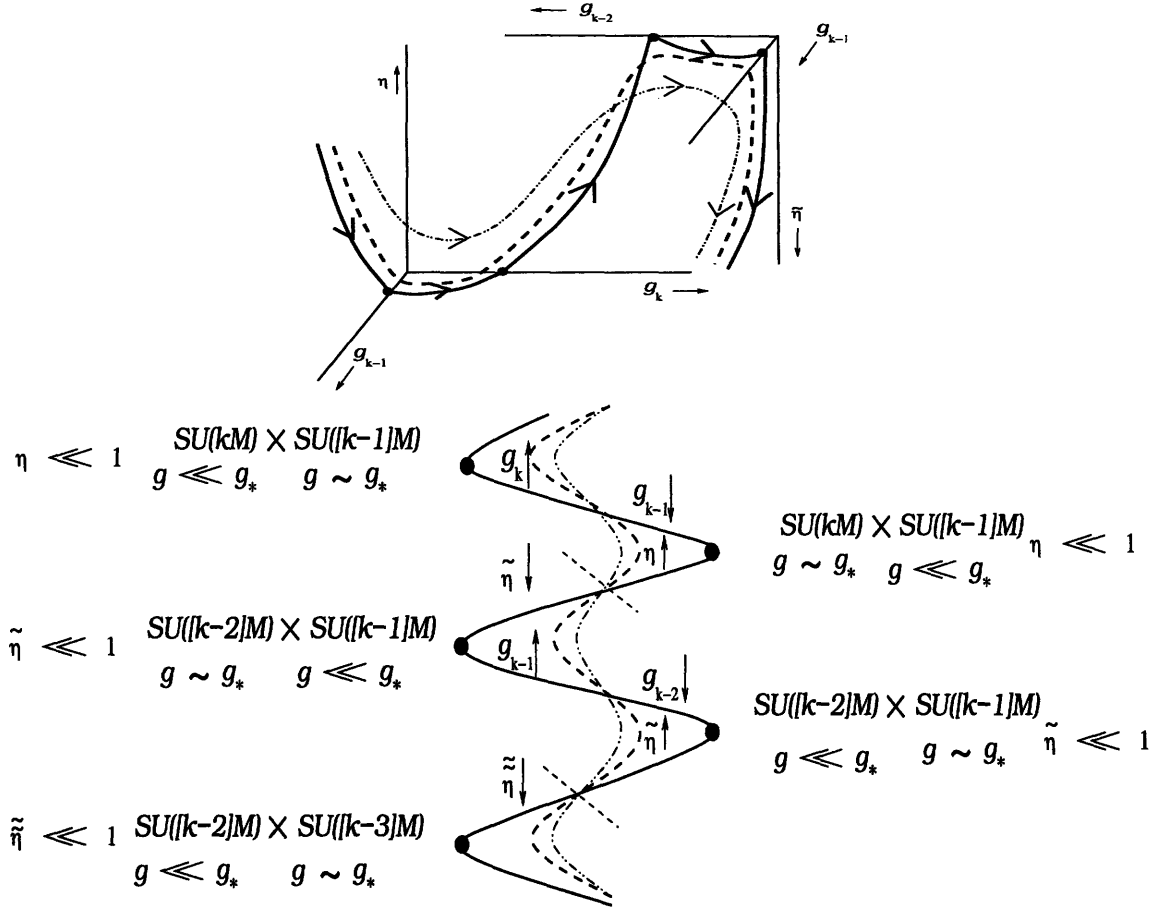


Figure E-8: This figure is a generalization of E-7 and shows the flow for more generic values of the couplings which do not lie on the conformal surface, i.e. $\delta_0 \sim \frac{1}{2}$.

point,

$$\beta_k = -F(k)6M < 0, \quad \beta_{k-1} = 0, \quad \beta_\eta = \frac{3\eta}{k} > 0. \quad (\text{E.26})$$

On the other hand if $g_{k-1} = \eta = 0$, then the theory is $SU(kM)$ SQCD with $2[k-1]M$ flavors, which lies in the conformal window when $k > 4$. Again using the fact that $1 + \frac{1}{2}\gamma_0 = D(A) = \frac{3}{2}R(A) = \frac{3}{4}\left(1 + \frac{1}{k}\right)$ gives $\delta_0 = -\frac{3}{2(k-1)} \approx -\frac{3}{2k}$. Hence at this fixed point the signs are reversed:

$$\beta_k = 0, \quad \beta_{k-1} = -F(k-1)(-6M) > 0, \quad \beta_\eta = -\frac{3\eta}{k} < 0. \quad (\text{E.27})$$

Now suppose we start at the Seiberg fixed point of $SU([k-1]M)$ where $g_k = 0$. If

$\eta \neq 0$, then according to (E.26), $\beta_\eta > 0$ and the theory will flow back to the conformal fixed point, but if $\eta = 0$, flows along the edge to the $SU(kM)$ SQCD fixed point. Note that the number of flavors in the $SU(kM)$ theory are $N_f = 2(k-1)M < 2kM = 2N$, the number of colors, hence the discussion in Section E.2 applies. Here, according to (E.10), η is relevant. As η grows, this theory can be replaced by its Seiberg dual description where the gauge group is $SU([k-2]M)$ and the quartic coupling is $\tilde{\eta} \sim 1/\eta$. This is shown in Figure E-7.

The flow discussed above is along the boundary of the KW conformal surface. For starting values different from the boundary, the flow still follows the same pattern, but never quite reaches the conformal fixed points, as shown in Figure E-8.

The interested reader can refer to Section 4 in M. Strassler's lecture notes [157] for a comprehensive treatment of this subject.

A crude summary of this discussion is that both of these gauge groups are asymptotically free but the first one runs faster than the second one because $b_0^{kM} = 3kM - 2[k-1]M = (k+2)M$ and $b_0^{[k-1]M} = 3[k-1]M - 2kM = (k-3)M$, with the superscript denoting the gauge group for which b_0 is computed. So at some strong coupling scale, $SU(kM)$ is replaced by its Seiberg dual with $\tilde{N} = 2[k-1]M - kM = [k-2]M$ and the gauge group is $SU([k-1]M) \times SU([k-2]M)$. This has precisely the same form as the gauge group we started with but with $k \rightarrow k-1$. This self-similar structure of the duality is what allows the cascade to occur.

The discussion here was only for the case when the theory was nearly conformal. However as the cascade continues, k gets smaller and smaller. When $k = 2$, the analysis of the gauge theory shows that the $SU(2M)$ factor has the same number of colors and flavors. This theory is known to have confinement and chiral symmetry breaking, the discussion of which is beyond the scope of this appendix.

Bibliography

- [1] J. Polchinski, *Dirichlet-Branes and Ramond-Ramond Charges*, *Phys. Rev. Lett.* **75** (1995) 4724–4727 [hep-th/9510017].
- [2] J. M. Maldacena, *The large N limit of superconformal field theories and supergravity*, *Adv. Theor. Math. Phys.* **2** (1998) 231–252 [hep-th/9711200].
- [3] E. Witten, *Anti-de Sitter space and holography*, *Adv. Theor. Math. Phys.* **2** (1998) 253–291 [hep-th/9802150].
- [4] S. S. Gubser, I. R. Klebanov and A. M. Polyakov, *Gauge theory correlators from non-critical string theory*, *Phys. Lett.* **B428** (1998) 105–114 [hep-th/9802109].
- [5] O. Aharony, S. S. Gubser, J. M. Maldacena, H. Ooguri and Y. Oz, *Large N field theories, string theory and gravity*, *Phys. Rept.* **323** (2000) 183–386 [hep-th/9905111].
- [6] E. Witten, *Anti-de Sitter space, thermal phase transition, and confinement in gauge theories*, *Adv. Theor. Math. Phys.* **2** (1998) 505–532 [hep-th/9803131].
- [7] **PHENIX** Collaboration, A. Adare *et. al.*, *J/ψ production vs centrality, transverse momentum, and rapidity in Au + Au collisions at $s(NN)^{1/2} = 200$ - GeV*, *Phys. Rev. Lett.* **98** (2007) 232301 [nucl-ex/0611020].
- [8] Q. J. Ejaz, T. Faulkner, H. Liu, K. Rajagopal and U. A. Wiedemann, *A limiting velocity for quarkonium propagation in a strongly coupled plasma via AdS/CFT*, 0712.0590.

- [9] I. Kirsch and D. Vaman, *The D3/D7 background and flavor dependence of Regge trajectories*, *Phys. Rev.* **D72** (2005) 026007 [hep-th/0505164].
- [10] S. A. Cherkis and A. Hashimoto, *Supergravity solution of intersecting branes and AdS/CFT with flavor*, *JHEP* **11** (2002) 036 [hep-th/0210105].
- [11] I. R. Klebanov and A. A. Tseytlin, *Gravity duals of supersymmetric $SU(N) \times SU(N+M)$ gauge theories*, *Nucl. Phys.* **B578** (2000) 123–138 [hep-th/0002159].
- [12] S. S. Gubser and I. R. Klebanov, *Baryons and domain walls in an $N = 1$ superconformal gauge theory*, *Phys. Rev.* **D58** (1998) 125025 [hep-th/9808075].
- [13] C. P. Herzog, Q. J. Ejaz and I. R. Klebanov, *Cascading RG flows from new Sasaki-Einstein manifolds*, *JHEP* **02** (2005) 009 [hep-th/0412193].
- [14] L. Susskind and E. Witten, *The holographic bound in anti-de Sitter space*, hep-th/9805114.
- [15] S. S. Gubser, I. R. Klebanov and A. W. Peet, *Entropy and Temperature of Black 3-Branes*, *Phys. Rev.* **D54** (1996) 3915–3919 [hep-th/9602135].
- [16] A. Fotopoulos and T. R. Taylor, *Comment on two-loop free energy in $N = 4$ supersymmetric Yang-Mills theory at finite temperature*, *Phys. Rev.* **D59** (1999) 061701 [hep-th/9811224].
- [17] S. S. Gubser, I. R. Klebanov and A. A. Tseytlin, *Coupling constant dependence in the thermodynamics of $N = 4$ supersymmetric Yang-Mills theory*, *Nucl. Phys.* **B534** (1998) 202–222 [hep-th/9805156].
- [18] A. Buchel, J. T. Liu and A. O. Starinets, *Coupling constant dependence of the shear viscosity in $N=4$ supersymmetric Yang-Mills theory*, *Nucl. Phys.* **B707** (2005) 56–68 [hep-th/0406264].

- [19] P. Arnold, G. D. Moore and L. G. Yaffe, *Transport coefficients in high temperature gauge theories. I: Leading-log results*, *JHEP* **11** (2000) 001 [hep-ph/0010177].
- [20] P. Kovtun, D. T. Son and A. O. Starinets, *Holography and hydrodynamics: Diffusion on stretched horizons*, *JHEP* **10** (2003) 064 [hep-th/0309213].
- [21] D. Teaney, *Effect of shear viscosity on spectra, elliptic flow, and Hanbury Brown-Twiss radii*, *Phys. Rev.* **C68** (2003) 034913 [nucl-th/0301099].
- [22] T. Matsui and H. Satz, *J/psi Suppression by Quark-Gluon Plasma Formation*, *Phys. Lett.* **B178** (1986) 416.
- [23] H. Satz, *Colour deconfinement and quarkonium binding*, *J. Phys.* **G32** (2006) R25 [hep-ph/0512217].
- [24] J. Kuti, J. Polonyi and K. Szlachanyi, *Monte Carlo Study of SU(2) Gauge Theory at Finite Temperature*, *Phys. Lett.* **B98** (1981) 199.
- [25] L. D. McLerran and B. Svetitsky, *A Monte Carlo Study of SU(2) Yang-Mills Theory at Finite Temperature*, *Phys. Lett.* **B98** (1981) 195.
- [26] L. D. McLerran and B. Svetitsky, *Quark Liberation at High Temperature: A Monte Carlo Study of SU(2) Gauge Theory*, *Phys. Rev.* **D24** (1981) 450.
- [27] O. Kaczmarek, F. Karsch, P. Petreczky and F. Zantow, *Heavy quark anti-quark free energy and the renormalized Polyakov loop*, *Phys. Lett.* **B543** (2002) 41–47 [hep-lat/0207002].
- [28] O. Kaczmarek, F. Karsch, F. Zantow and P. Petreczky, *Static quark anti-quark free energy and the running coupling at finite temperature*, *Phys. Rev.* **D70** (2004) 074505 [hep-lat/0406036].
- [29] P. Petreczky and K. Petrov, *Free energy of a static quark anti-quark pair and the renormalized Polyakov loop in three flavor QCD*, *Phys. Rev.* **D70** (2004) 054503 [hep-lat/0405009].

- [30] O. Kaczmarek and F. Zantow, *Static quark anti-quark interactions in zero and finite temperature QCD. I: Heavy quark free energies, running coupling and quarkonium binding*, *Phys. Rev.* **D71** (2005) 114510 [[hep-lat/0503017](#)].
- [31] Y. Maezawa *et. al.*, *Static quark free energies at finite temperature with two flavors of improved Wilson quarks*, *PoS LAT2006* (2006) 141 [[hep-lat/0610013](#)].
- [32] F. Karsch, *Properties of the quark gluon plasma: A lattice perspective*, *Nucl. Phys.* **A783** (2007) 13–22 [[hep-ph/0610024](#)].
- [33] M. Asakawa, T. Hatsuda and Y. Nakahara, *Maximum entropy analysis of the spectral functions in lattice QCD*, *Prog. Part. Nucl. Phys.* **46** (2001) 459–508 [[hep-lat/0011040](#)].
- [34] T. Umeda, R. Katayama, O. Miyamura and H. Matsufuru, *Study of charmonia near the deconfining transition on an anisotropic lattice with $O(a)$ improved quark action*, *Int. J. Mod. Phys.* **A16** (2001) 2215 [[hep-lat/0011085](#)].
- [35] T. Umeda, K. Nomura and H. Matsufuru, *Charmonium at finite temperature in quenched lattice QCD*, *Eur. Phys. J.* **C39S1** (2005) 9–26 [[hep-lat/0211003](#)].
- [36] M. Asakawa and T. Hatsuda, *J/ψ and η/c in the deconfined plasma from lattice QCD*, *Phys. Rev. Lett.* **92** (2004) 012001 [[hep-lat/0308034](#)].
- [37] S. Datta, F. Karsch, P. Petreczky and I. Wetzorke, *Behavior of charmonium systems after deconfinement*, *Phys. Rev.* **D69** (2004) 094507 [[hep-lat/0312037](#)].
- [38] H. Iida, T. Doi, N. Ishii and H. Suganuma, *J/ψ at high temperatures in anisotropic lattice QCD*, *PoS LAT2005* (2006) 184 [[hep-lat/0509129](#)].
- [39] A. Jakovac, P. Petreczky, K. Petrov and A. Velytsky, *Quarkonium correlators and spectral functions at zero and finite temperature*, *Phys. Rev.* **D75** (2007) 014506 [[hep-lat/0611017](#)].

- [40] R. Morrin *et. al.*, *Charmonium spectral functions in $N_f = 2$ QCD*, *PoS LAT2005* (2006) 176 [hep-lat/0509115].
- [41] G. Aarts *et. al.*, *Charmonium spectral functions in $N_f = 2$ QCD at high temperature*, *PoS LAT2006* (2006) 126 [hep-lat/0610065].
- [42] G. Aarts, C. Allton, M. B. Oktay, M. Peardon and J.-I. Skullerud, *Charmonium at high temperature in two-flavor QCD*, *Phys. Rev. D* **76** (2007) 094513 [0705.2198].
- [43] M. B. Oktay, M. J. Peardon, J. I. Skullerud, G. Aarts and C. R. Allton, *Charmonium properties in the quark-gluon plasma*, *PoS LAT2007* (2007) 227 [0710.2795].
- [44] M. Laine, O. Philipsen, P. Romatschke and M. Tassler, *Real-time static potential in hot QCD*, *JHEP* **03** (2007) 054 [hep-ph/0611300].
- [45] M. Laine, *A resummed perturbative estimate for the quarkonium spectral function in hot QCD*, *JHEP* **05** (2007) 028 [0704.1720].
- [46] M. Laine, O. Philipsen and M. Tassler, *Thermal imaginary part of a real-time static potential from classical lattice gauge theory simulations*, *JHEP* **09** (2007) 066 [0707.2458].
- [47] Y. Burnier, M. Laine and M. Vepsalainen, *Heavy quarkonium in any channel in resummed hot QCD*, *JHEP* **01** (2008) 043 [0711.1743].
- [48] F. Karsch, D. Kharzeev and H. Satz, *Sequential charmonium dissociation*, *Phys. Lett.* **B637** (2006) 75–80 [hep-ph/0512239].
- [49] **NA50** Collaboration, B. Alessandro *et. al.*, *A new measurement of J/ψ suppression in Pb - Pb collisions at 158-GeV per nucleon*, *Eur. Phys. J.* **C39** (2005) 335–345 [hep-ex/0412036].
- [50] **NA60** Collaboration, R. Arnaldi *et. al.*, *J/ψ suppression in In In collisions at 158- GeV/nucleon*, *Nucl. Phys.* **A783** (2007) 261–268 [nucl-ex/0701033].

- [51] ALICE Collaboration, e. . Carminati, F. *et. al.*, *ALICE: Physics performance report, volume I*, *J. Phys.* **G30** (2004) 1517–1763.
- [52] ALICE Collaboration, e. . Alessandro, B. *et. al.*, *ALICE: Physics performance report, volume II*, *J. Phys.* **G32** (2006) 1295–2040.
- [53] E. . d’Enterria, David G. *et. al.*, *CMS physics technical design report: Addendum on high density QCD with heavy ions*, *J. Phys.* **G34** (2007) 2307–2455.
- [54] PHENIX Collaboration, K. Adcox *et. al.*, *Formation of dense partonic matter in relativistic nucleus nucleus collisions at RHIC: Experimental evaluation by the PHENIX collaboration*, *Nucl. Phys.* **A757** (2005) 184–283 [nucl-ex/0410003].
- [55] B. B. Back *et. al.*, *The PHOBOS perspective on discoveries at RHIC*, *Nucl. Phys.* **A757** (2005) 28–101 [nucl-ex/0410022].
- [56] BRAHMS Collaboration, I. Arsene *et. al.*, *Quark gluon plasma and color glass condensate at RHIC? The perspective from the BRAHMS experiment*, *Nucl. Phys.* **A757** (2005) 1–27 [nucl-ex/0410020].
- [57] STAR Collaboration, J. Adams *et. al.*, *Experimental and theoretical challenges in the search for the quark gluon plasma: The STAR collaboration’s critical assessment of the evidence from RHIC collisions*, *Nucl. Phys.* **A757** (2005) 102–183 [nucl-ex/0501009].
- [58] J.-W. Qiu, *Factorization for hadronic heavy quarkonium production*, *Nucl. Phys.* **A783** (2007) 309–316 [nucl-th/0610128].
- [59] J.-w. Qiu, J. P. Vary and X.-f. Zhang, *J/psi suppression in nucleus nucleus collisions*, *Phys. Rev. Lett.* **88** (2002) 232301 [hep-ph/9809442].
- [60] D. Kharzeev and K. Tuchin, *Signatures of the color glass condensate in J/psi production off nuclear targets*, *Nucl. Phys.* **A770** (2006) 40–56 [hep-ph/0510358].

- [61] R. L. Thews, M. Schroedter and J. Rafelski, *Enhanced J/ψ production in deconfined quark matter*, *Phys. Rev.* **C63** (2001) 054905 [hep-ph/0007323].
- [62] L. Grandchamp and R. Rapp, *Thermal versus direct J/ψ production in ultrarelativistic heavy-ion collisions*, *Phys. Lett.* **B523** (2001) 60–66 [hep-ph/0103124].
- [63] A. Andronic, P. Braun-Munzinger, K. Redlich and J. Stachel, *Statistical hadronization of charm in heavy-ion collisions at SPS, RHIC and LHC*, *Phys. Lett.* **B571** (2003) 36–44 [nucl-th/0303036].
- [64] F. Karsch and R. Petronzio, *χ and J/ψ suppression in heavy ion collisions and a model for its momentum dependence*, *Z. Phys.* **C37** (1988) 627.
- [65] M. C. Chu and T. Matsui, *Dynamic debye screening for a heavy anti-quark pair traversing a quark-gluon plasma*, *Phys. Rev.* **D39** (1989) 1892.
- [66] H. Liu, K. Rajagopal and U. A. Wiedemann, *An AdS/CFT calculation of screening in a hot wind*, *Phys. Rev. Lett.* **98** (2007) 182301 [hep-ph/0607062].
- [67] H. Liu, K. Rajagopal and U. A. Wiedemann, *Wilson loops in heavy ion collisions and their calculation in AdS/CFT*, *JHEP* **03** (2007) 066 [hep-ph/0612168].
- [68] S. J. Brodsky and A. H. Mueller, *Using Nuclei to Probe Hadronization in QCD*, *Phys. Lett.* **B206** (1988) 685.
- [69] S. Gavin, M. Gyulassy and A. Jackson, *Hadronic J/ψ Suppression in Ultrarelativistic Nuclear Collisions*, *Phys. Lett.* **B207** (1988) 257–262.
- [70] N. Armesto and A. Capella, *A quantitative reanalysis of J/ψ suppression in nuclear collisions*, *Phys. Lett.* **B430** (1998) 23–31 [hep-ph/9705275].
- [71] D. Kharzeev and H. Satz, *Quarkonium interactions in hadronic matter*, *Phys. Lett.* **B334** (1994) 155–162 [hep-ph/9405414].

- [72] S. G. Matinyan and B. Muller, *A model of charmonium absorption by light mesons*, *Phys. Rev.* **C58** (1998) 2994–2997 [nucl-th/9806027].
- [73] L. Maiani, F. Piccinini, A. D. Polosa and V. Riquer, *J/psi absorption in heavy-ion collisions*, *Nucl. Phys.* **A741** (2004) 273–286 [hep-ph/0402275].
- [74] D. Kharzeev and H. Satz, *Charmonium interaction in nuclear matter*, *Phys. Lett.* **B356** (1995) 365–372 [hep-ph/9504397].
- [75] PHENIX Collaboration, S. S. Adler *et. al.*, *J/psi production and nuclear effects for d + Au and p + p collisions at $s(NN)^{1/2} = 200$ -GeV*, *Phys. Rev. Lett.* **96** (2006) 012304 [nucl-ex/0507032].
- [76] S.-J. Rey and J.-T. Yee, *Macroscopic strings as heavy quarks in large N gauge theory and anti-de Sitter supergravity*, *Eur. Phys. J.* **C22** (2001) 379–394 [hep-th/9803001].
- [77] J. M. Maldacena, *Wilson loops in large N field theories*, *Phys. Rev. Lett.* **80** (1998) 4859–4862 [hep-th/9803002].
- [78] S.-J. Rey, S. Theisen and J.-T. Yee, *Wilson-Polyakov loop at finite temperature in large N gauge theory and anti-de Sitter supergravity*, *Nucl. Phys.* **B527** (1998) 171–186 [hep-th/9803135].
- [79] A. Brandhuber, N. Itzhaki, J. Sonnenschein and S. Yankielowicz, *Wilson loops in the large N limit at finite temperature*, *Phys. Lett.* **B434** (1998) 36–40 [hep-th/9803137].
- [80] J. Sonnenschein, *What does the string / gauge correspondence teach us about Wilson loops?*, hep-th/0003032.
- [81] D. Bak, A. Karch and L. G. Yaffe, *Debye screening in strongly coupled N=4 supersymmetric Yang-Mills plasma*, *JHEP* **08** (2007) 049 [0705.0994].
- [82] I. Amado, C. Hoyos-Badajoz, K. Landsteiner and S. Montero, *Absorption Lengths in the Holographic Plasma*, *JHEP* **09** (2007) 057 [0706.2750].

- [83] K. Peeters, J. Sonnenschein and M. Zamaklar, *Holographic melting and related properties of mesons in a quark gluon plasma*, *Phys. Rev.* **D74** (2006) 106008 [hep-th/0606195].
- [84] M. Chernicoff, J. A. Garcia and A. Guijosa, *The energy of a moving quark-antiquark pair in an $N = 4$ SYM plasma*, *JHEP* **09** (2006) 068 [hep-th/0607089].
- [85] C. P. Herzog, A. Karch, P. Kovtun, C. Kozcaz and L. G. Yaffe, *Energy loss of a heavy quark moving through $N = 4$ supersymmetric Yang-Mills plasma*, *JHEP* **07** (2006) 013 [hep-th/0605158].
- [86] S. D. Avramis, K. Sfetsos and D. Zoakos, *On the velocity and chemical-potential dependence of the heavy-quark interaction in $N = 4$ SYM plasmas*, *Phys. Rev.* **D75** (2007) 025009 [hep-th/0609079].
- [87] E. Caceres, M. Natsuume and T. Okamura, *Screening length in plasma winds*, *JHEP* **10** (2006) 011 [hep-th/0607233].
- [88] M. Natsuume and T. Okamura, *Screening length and the direction of plasma winds*, *JHEP* **09** (2007) 039 [0706.0086].
- [89] F. Karsch, E. Laermann and A. Peikert, *The pressure in 2, 2+1 and 3 flavour QCD*, *Phys. Lett.* **B478** (2000) 447–455 [hep-lat/0002003].
- [90] F. Karsch, *Lattice results on QCD thermodynamics*, *Nucl. Phys.* **A698** (2002) 199–208 [hep-ph/0103314].
- [91] A. Karch and E. Katz, *Adding flavor to AdS/CFT*, *JHEP* **06** (2002) 043 [hep-th/0205236].
- [92] P. Breitenlohner and D. Z. Freedman, *Stability in Gauged Extended Supergravity*, *Ann. Phys.* **144** (1982) 249.
- [93] P. Breitenlohner and D. Z. Freedman, *Positive Energy in anti-De Sitter Backgrounds and Gauged Extended Supergravity*, *Phys. Lett.* **B115** (1982) 197.

- [94] J. Babington, J. Erdmenger, N. J. Evans, Z. Guralnik and I. Kirsch, *Chiral symmetry breaking and pions in non-supersymmetric gauge / gravity duals*, *Phys. Rev.* **D69** (2004) 066007 [[hep-th/0306018](#)].
- [95] D. Mateos, R. C. Myers and R. M. Thomson, *Holographic phase transitions with fundamental matter*, *Phys. Rev. Lett.* **97** (2006) 091601 [[hep-th/0605046](#)].
- [96] D. Mateos, R. C. Myers and R. M. Thomson, *Thermodynamics of the brane*, *JHEP* **05** (2007) 067 [[hep-th/0701132](#)].
- [97] C. Hoyos-Badajoz, K. Landsteiner and S. Montero, *Holographic Meson Melting*, *JHEP* **04** (2007) 031 [[hep-th/0612169](#)].
- [98] G. Policastro, D. T. Son and A. O. Starinets, *The shear viscosity of strongly coupled $N = 4$ supersymmetric Yang-Mills plasma*, *Phys. Rev. Lett.* **87** (2001) 081601 [[hep-th/0104066](#)].
- [99] M. Kruczenski, D. Mateos, R. C. Myers and D. J. Winters, *Meson spectroscopy in AdS/CFT with flavour*, *JHEP* **07** (2003) 049 [[hep-th/0304032](#)].
- [100] M. Kruczenski, D. Mateos, R. C. Myers and D. J. Winters, *Towards a holographic dual of large- $N(c)$ QCD*, *JHEP* **05** (2004) 041 [[hep-th/0311270](#)].
- [101] S. Hong, S. Yoon and M. J. Strassler, *Quarkonium from the fifth dimension*, *JHEP* **04** (2004) 046 [[hep-th/0312071](#)].
- [102] I. Kirsch, *Generalizations of the AdS/CFT correspondence*, *Fortsch. Phys.* **52** (2004) 727–826 [[hep-th/0406274](#)].
- [103] R. C. Myers and R. M. Thomson, *Holographic mesons in various dimensions*, *JHEP* **09** (2006) 066 [[hep-th/0605017](#)].
- [104] R. C. Myers, A. O. Starinets and R. M. Thomson, *Holographic spectral functions and diffusion constants for fundamental matter*, *JHEP* **11** (2007) 091 [[0706.0162](#)].

- [105] K. Peeters and M. Zamaklar, *Dissociation by acceleration*, *JHEP* **01** (2008) 038 [0711.3446].
- [106] J. Erdmenger, N. Evans, I. Kirsch and E. Threlfall, *Mesons in Gauge/Gravity Duals - A Review*, 0711.4467.
- [107] M. Abramowitz and I. A. Stegun, *Handbook of Mathematical Functions with Formulas, Graphs, and Mathematical Tables*. Dover, New York, ninth dover printing, tenth gpo printing ed., 1964.
- [108] N. Itzhaki, J. M. Maldacena, J. Sonnenschein and S. Yankielowicz, *Supergravity and the large N limit of theories with sixteen supercharges*, *Phys. Rev. D* **58** (1998) 046004 [hep-th/9802042].
- [109] D. Arean and A. V. Ramallo, *Open string modes at brane intersections*, *JHEP* **04** (2006) 037 [hep-th/0602174].
- [110] M. A. Lisa, S. Pratt, R. Soltz and U. Wiedemann, *Femtoscropy in relativistic heavy ion collisions*, *Ann. Rev. Nucl. Part. Sci.* **55** (2005) 357–402 [nucl-ex/0505014].
- [111] R. Lednicky, V. L. Lyuboshits, B. Erazmus and D. Nouais, *How to measure which sort of particles was emitted earlier and which later*, *Phys. Lett.* **B373** (1996) 30–34.
- [112] I. R. Klebanov and A. A. Tseytlin, *Entropy of Near-Extremal Black p -branes*, *Nucl. Phys.* **B475** (1996) 164–178 [hep-th/9604089].
- [113] M. Gomez-Reino, S. Naculich and H. Schnitzer, *Thermodynamics of the localized $D2$ - $D6$ system*, *Nucl. Phys.* **B713** (2005) 263–277 [hep-th/0412015].
- [114] P. K. Townsend, *The eleven-dimensional supermembrane revisited*, *Phys. Lett.* **B350** (1995) 184–187 [hep-th/9501068].

- [115] E. S. Cheb-Terrab, *Solutions for the general, confluent and biconfluent Heun equations and their connection with Abel equations*, *J. Phys. A: Math. Gen* **37** (2004) 9923–9949.
- [116] A. W. Peet, *TASI lectures on black holes in string theory*, hep-th/0008241.
- [117] R. C. Myers, *Dielectric-branes*, *JHEP* **12** (1999) 022 [hep-th/9910053].
- [118] S. Kachru and E. Silverstein, *4d conformal theories and strings on orbifolds*, *Phys. Rev. Lett.* **80** (1998) 4855–4858 [hep-th/9802183].
- [119] A. E. Lawrence, N. Nekrasov and C. Vafa, *On conformal field theories in four dimensions*, *Nucl. Phys.* **B533** (1998) 199–209 [hep-th/9803015].
- [120] A. Kehagias, *New type IIB vacua and their F-theory interpretation*, *Phys. Lett.* **B435** (1998) 337–342 [hep-th/9805131].
- [121] I. R. Klebanov and E. Witten, *Superconformal field theory on threebranes at a Calabi-Yau singularity*, *Nucl. Phys.* **B536** (1998) 199–218 [hep-th/9807080].
- [122] D. R. Morrison and M. R. Plesser, *Non-spherical horizons. I*, *Adv. Theor. Math. Phys.* **3** (1999) 1–81 [hep-th/9810201].
- [123] B. S. Acharya, J. M. Figueroa-O’Farrill, C. M. Hull and B. J. Spence, *Branes at conical singularities and holography*, *Adv. Theor. Math. Phys.* **2** (1999) 1249–1286 [hep-th/9808014].
- [124] I. R. Klebanov and M. J. Strassler, *Supergravity and a confining gauge theory: Duality cascades and chiSB-resolution of naked singularities*, *JHEP* **08** (2000) 052 [hep-th/0007191].
- [125] F. Cachazo, B. Fiol, K. A. Intriligator, S. Katz and C. Vafa, *A geometric unification of dualities*, *Nucl. Phys.* **B628** (2002) 3–78 [hep-th/0110028].
- [126] B. Fiol, *Duality cascades and duality walls*, *JHEP* **07** (2002) 058 [hep-th/0205155].

- [127] A. Hanany and J. Walcher, *On duality walls in string theory*, *JHEP* **06** (2003) 055 [[hep-th/0301231](#)].
- [128] R. Ahl Laamara, M. Ait Ben Haddou, A. Belhaj, L. B. Drissi and E. H. Saidi, *RG cascades in hyperbolic quiver gauge theories*, *Nucl. Phys.* **B702** (2004) 163–188 [[hep-th/0405222](#)].
- [129] S. Franco, Y.-H. He, C. Herzog and J. Walcher, *Chaotic duality in string theory*, *Phys. Rev.* **D70** (2004) 046006 [[hep-th/0402120](#)].
- [130] S. Franco, Y.-H. He, C. Herzog and J. Walcher, *Chaotic cascades for D-branes on singularities*, [hep-th/0412207](#).
- [131] S. Franco, A. Hanany, Y.-H. He and P. Kazakopoulos, *Duality walls, duality trees and fractional branes*, [hep-th/0306092](#).
- [132] J. P. Gauntlett, D. Martelli, J. Sparks and D. Waldram, *Supersymmetric AdS(5) solutions of M-theory*, *Class. Quant. Grav.* **21** (2004) 4335–4366 [[hep-th/0402153](#)].
- [133] J. P. Gauntlett, D. Martelli, J. Sparks and D. Waldram, *Sasaki-Einstein metrics on $S(2) \times S(3)$* , *Adv. Theor. Math. Phys.* **8** (2004) 711–734 [[hep-th/0403002](#)].
- [134] D. Martelli and J. Sparks, *Toric geometry, Sasaki-Einstein manifolds and a new infinite class of AdS/CFT duals*, *Commun. Math. Phys.* **262** (2006) 51–89 [[hep-th/0411238](#)].
- [135] S. Benvenuti, S. Franco, A. Hanany, D. Martelli and J. Sparks, *An infinite family of superconformal quiver gauge theories with Sasaki-Einstein duals*, *JHEP* **06** (2005) 064 [[hep-th/0411264](#)].
- [136] B. Feng, A. Hanany and Y.-H. He, *D-brane gauge theories from toric singularities and toric duality*, *Nucl. Phys.* **B595** (2001) 165–200 [[hep-th/0003085](#)].

- [137] M. Bertolini, F. Bigazzi and A. L. Cotrone, *New checks and subtleties for AdS/CFT and a -maximization*, *JHEP* **12** (2004) 024 [[hep-th/0411249](#)].
- [138] O. Aharony, *A note on the holographic interpretation of string theory backgrounds with varying flux*, *JHEP* **03** (2001) 012 [[hep-th/0101013](#)].
- [139] S. S. Gubser, C. P. Herzog and I. R. Klebanov, *Symmetry breaking and axionic strings in the warped deformed conifold*, *JHEP* **09** (2004) 036 [[hep-th/0405282](#)].
- [140] S. S. Gubser, C. P. Herzog and I. R. Klebanov, *Variations on the warped deformed conifold*, *Comptes Rendus Physique* **5** (2004) 1031–1038 [[hep-th/0409186](#)].
- [141] A. Butti, M. Grana, R. Minasian, M. Petrini and A. Zaffaroni, *The baryonic branch of Klebanov-Strassler solution: A supersymmetric family of SU(3) structure backgrounds*, *JHEP* **03** (2005) 069 [[hep-th/0412187](#)].
- [142] K. Intriligator and B. Wecht, *The exact superconformal R-symmetry maximizes a* , *Nucl. Phys.* **B667** (2003) 183–200 [[hep-th/0304128](#)].
- [143] R. G. Leigh and M. J. Strassler, *Exactly marginal operators and duality in four-dimensional $N=1$ supersymmetric gauge theory*, *Nucl. Phys.* **B447** (1995) 95–136 [[hep-th/9503121](#)].
- [144] D. Berenstein, C. P. Herzog and I. R. Klebanov, *Baryon spectra and AdS/CFT correspondence*, *JHEP* **06** (2002) 047 [[hep-th/0202150](#)].
- [145] C. P. Herzog, I. R. Klebanov and P. Ouyang, *D-branes on the conifold and $N = 1$ gauge / gravity dualities*, [hep-th/0205100](#).
- [146] C. P. Herzog, I. R. Klebanov and P. Ouyang, *Remarks on the warped deformed conifold*, [hep-th/0108101](#).
- [147] M. Bertolini *et. al.*, *Fractional D-branes and their gauge duals*, *JHEP* **02** (2001) 014 [[hep-th/0011077](#)].

- [148] I. R. Klebanov and N. A. Nekrasov, *Gravity duals of fractional branes and logarithmic RG flow*, *Nucl. Phys.* **B574** (2000) 263–274 [hep-th/9911096].
- [149] J. Polchinski, *$N = 2$ gauge-gravity duals*, *Int. J. Mod. Phys.* **A16** (2001) 707–718 [hep-th/0011193].
- [150] K. Dasgupta, G. Rajesh and S. Sethi, *M theory, orientifolds and G-flux*, *JHEP* **08** (1999) 023 [hep-th/9908088].
- [151] M. Grana and J. Polchinski, *Supersymmetric three-form flux perturbations on $AdS(5)$* , *Phys. Rev.* **D63** (2001) 026001 [hep-th/0009211].
- [152] S. S. Gubser, *Supersymmetry and F-theory realization of the deformed conifold with three-form flux*, hep-th/0010010.
- [153] N. Halmagyi, K. Pilch, C. Romelsberger and N. P. Warner, *The complex geometry of holographic flows of quiver gauge theories*, *JHEP* **09** (2006) 063 [hep-th/0406147].
- [154] N. Seiberg, *Electric - magnetic duality in supersymmetric nonAbelian gauge theories*, *Nucl. Phys.* **B435** (1995) 129–146 [hep-th/9411149].
- [155] J. Callan, Curtis G. and L. Thorlacius, *Sigma Models And String Theory*, . Print-89-0232 (PRINCETON).
- [156] R. M. Wald, *General Relativity*, ch. 10, in particular see (10.2.23).
- [157] M. J. Strassler, *The duality cascade*, hep-th/0505153.
- [158] P. Argyres, *Introduction to supersymmetry*.
<http://www.physics.uc.edu/~argyres/661/susy1996.pdf>, 1996.
- [159] V. A. Novikov, M. A. Shifman, A. I. Vainshtein and V. I. Zakharov, *Exact Gell-Mann-Low Function of Supersymmetric Yang-Mills Theories from Instanton Calculus*, *Nucl. Phys.* **B229** (1983) 381.

- [160] V. A. Novikov, M. A. Shifman, A. I. Vainshtein and V. I. Zakharov,
Supersymmetric instanton calculus: Gauge theories with matter, *Nucl. Phys.*
B260 (1985) 157–181.
- [161] V. A. Novikov, M. A. Shifman, A. I. Vainshtein and V. I. Zakharov, *Beta*
Function in Supersymmetric Gauge Theories: Instantons Versus Traditional
Approach, *Phys. Lett.* **B166** (1986) 329–333.